Perturbations in plant energy homeostasis alter lateral root plasticity via SnRK1-bZIP63-ARF19 signalling

****

Störungen in der pflanzlichen Energiehomöostase verändern die laterale Wurzelplastizität vermittelt durch das SnRK1-bZIP63-ARF19-Signalmodul

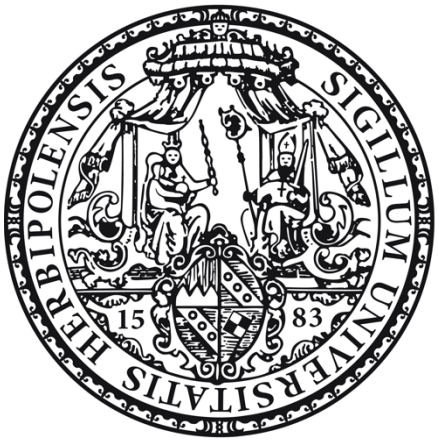

Doctoral Thesis

for the conferral of the degree “Doctor rerum naturalium” (Dr. rer. nat.)

at the Graduate School of Life Sciences, Integrative Biology Section

Julius-Maximilians-Universität

Würzburg

Submitted by

Prathibha Muralidhara

born in Bengaluru, India

Würzburg, 2020

Submitted on: ……..

Office stamp

Members of the Thesis Committee

Chairperson: **Prof. Dr. Thomas Müller**

Primary Supervisor: **Prof. Dr. Wolfgang Dröge-Laser**

Supervisor (Second): **Prof. Dr. Johannes Hanson**

Supervisor (Third): **Prof. Dr. Dirk Becker**

Supervisor (Fourth): **Dr. Christoph Weiste**

Date of Public Defence: ……

Date of Receipt of Certificates: …….

To,

My late grandmother

TABLE OF CONTENTS

SUMMARY

Photosynthetic plants have a remarkable ability to modify their metabolism and development according to ever changing environmental conditions. The root system displays continuous growth of the primary root and formation of lateral roots enabling efficient water and nutrient uptake and anchorage of the plant in soil. With regard to lateral roots, development is post-embryonic, originating from the pericycle of the primary root. Coordinated activity of several molecular signalling pathways controlled by the hormone auxin is important throughout all stages of lateral root development.At first, two adjacent Xylem Pole Pericycle (XPP) cells are activated and the nuclei of these cells migrate towards a common cell wall.This is followed by XPP cells acquiring volume thus swelling up.The XPP cells then undergo anticlinal cell division, followed by a series of periclinal and anticlinal divisions,leading to lateral root primordia.These break through the radial cell layers and emerge out the primary root.

Although root system plasticity is well-described in response to environmental cues such as ion nutrition in the soil, little is known on how root development is shaped according to the endogenous energy status of the plant.In this study, we were able to connect limited perturbations in photosynthetic energy supply to lateral root development.We established two experimental systems – treatment with low light and unexpected darkness which led to short-term energy imbalance in the plant.These short perturbations administered, showed an increase in the emerged lateral root density and decrease in root hexose availability and activation of the low energy marker gene *ASN1* (*ASPARAGINE SYNTHETASE 1*).Although not demonstrated, presumably, these disturbances in the plant energy homeostasis activates SnRK1 (SNF1 RELATED KINASE 1),an evolutionary conserved kinase mediating metabolic and transcriptional responses towards low energy conditions. In *A. thaliana*, two catalytic α-subunits of this kinase (SnRK1.α1 and SnRK1.α2) are functionally active and form ternary complexes with the regulatory β- and γ- subunits. Whereas unexpected darkness results in an increase in emerged lateral root density, the *snrk1.α1* loss-of-function mutant displayed decrease in emerged lateral root density. As this effect is not that pronounced in the *snrk1.α2* loss-of-function mutant, the α1 catalytic subunit is important for the observed lateral root phenotype under short-term energy perturbations. Moreover, root expression patterns of

SnRK1.α1:GFP supports a role of this catalytic subunit in lateral root development. Furthermore, the lateral root response during short-term perturbations requires the SnRK1 downstream transcriptional regulator bZIP63 (BASIC LEUCINE ZIPPER 63), as demonstrated here by a loss-of-function approach. Phenotypic studies showed that in comparison to wild-type, *bzip63* mutants displayed decreased lateral root density upon low-light and unexpected darkness conditions. Previous work has demonstrated that SnRK1 directly phosphorylates bZIP63 at three serine residues. Alanine-exchange mutants of the SnRK1 dependent bZIP63 phosphorylation sites behave similarly to *bzip63* loss-of-function mutants and do not display increased lateral root density upon short-term unexpected darkness. This data strongly supports an impact of SnRK1-bZIP63 signalling in mediating the observed lateral root density phenotype. Plants expressing a bZIP63:YFP fusion protein showed specific localization patterns in primary root and in all developmental stages of the lateral root. *bzip63* loss-of-function mutant lines displayed reduced early stage lateral root initiation events under unexpected darkness as demonstrated by Differential Interference Contrast microscopy (DIC) and the use of a GATA23 reporter line. This data supports a role of bZIP63 in early lateral root initiation.

Next, by employing Chromatin Immunoprecitation (ChIP) sequencing, we were able to identify global binding targets of bZIP63, including the auxin-regulated transcription factor (TF) ARF19 (AUXIN RESPONSE FACTOR 19), a well-described central regulator of lateral root development. Additional ChIP experiments confirmed direct binding of bZIP63 to an *ARF19* promoter region harboring a G-Box *cis*-element, a well-established bZIP63 binding site. We also observed that short-term energy perturbation upon unexpected darkness induced transcription of *ARF19*, which was impaired in the *bzip63* loss-of-function mutant. These results propose that bZIP63 mediates lateral root development under short-term energy perturbation via ARF19.

In conclusion, this study provides a novel mechanistic link between energy homeostasis and plant development. By employing reverse genetics, confocal imaging and high-throughput sequencing strategies, we were able to propose a SnRK1-bZIP63-ARF19 signalling module in integrating energy signalling into lateral root developmental programs.

ZUSAMMENFASSUNG

Photosynthestisch aktive Pflanzen haben die bemerkenswerte Fähigkeit, ihren Stoffwechsel und ihre Entwicklung an sich ständig ändernde Umweltbedingungen anzupassen. Das pflanzliche Wurzelsystem weist ein kontinuierliches Primärwurzelwachstum und eine Ausbildung von Seitenwurzeln auf, wodurch eine effiziente Wasser- und Nährstoffaufnahme sowie die Verankerung der Pflanze im Boden ermöglicht werden. Die Entwicklung der Seitenwurzeln verläuft post-embryonal, ausgehend vom Perizykel der Primärwurzel. Die koordinierte Aktivität mehrerer molekularer Signalwege, die durch das Hormon Auxin gesteuert werden, ist in allen Stadien der Seitenwurzelentwicklung wichtig. Bei diesem Prozess werden zunächst zwei benachbarte Xylem-Pol-Perizykel-Zellen (XPP) aktiviert, deren Zellkerne zu einer gemeinsamen Zellwand migrieren. Daraufhin schwillt das Volumen der XPP-Zellen an, bevor sich diese zunächst antiklinal teilen. Durch sukzessive periklinale und antiklinale Teilungen entstehen so Seitenwurzel-Primordien. Diese durchbrechen die radialen Zellschichten und treten aus der Primärwurzel aus.

Während die Plastizität des Wurzelsystems als Reaktion auf Umwelteinflüsse, wie z.B. die Versorgung mit Ionen aus dem Boden, bereits umfassend erforscht wurde, so ist die Abhängigkeit der Wurzelentwicklung vom endogenen Energiezustand der Pflanze weitgehend unbekannt. In dieser Arbeit konnten wir geringfügige Störungen der photosynthetischen Energieversorgung mit der Seitenwurzelentwicklung in Verbindung bringen. Pflanzen wurden Schwachlicht oder unerwarteter Dunkelheit ausgesetzt und damit ein kurzzeitiges Energieungleichgewicht erzeugt. Hierdurch zeigte sich eine Zunahme der Seitenwurzeldichte bei gleichzeitiger Abnahme der Verfügbarkeit von Hexosen in der Wurzel und Aktivierung des Energieverarmungs-Markergens *ASN1* (*ASPARAGIN-SYNTHETASE 1*). Obwohl dieser Mechanismus noch nicht geklärt ist, aktiviert die Störung der pflanzlichen Energie-Homöostase vermutlich SnRK1 (SNF1 RELATED KINASE 1), eine evolutionär konservierte Kinase, die metabolische und transkriptionelle Reaktionen auf niederenergetische Bedingungen vermittelt. In *Arabidopsis* sind zwei katalytische α-Untereinheiten dieser Kinase (*SnRK1.α1* und *SnRK1.α2*) funktionell aktiv und bilden ternäre Komplexe mit den regulatorischen β- und γ-Untereinheiten. Während eine unerwartete Dunkelheit zu einer Zunahme der Dichte der auswachsenden Seitenwurzeln führt, zeigte die *Snrk1.α1* Funktionsverlustmutante den gegenteiligen Effekt. Da dieser Effekt in der

Funktionsverlustmutante von *snrk1.α2* weniger stark ausgeprägt ist, scheint die katalytische Untereinheit α1 für den beobachteten Seitenwurzel-Phänotyp unter kurzfristigen Energiestörungen eine wichtige Rolle zu spielen. Das Expressionsmuster von SnRK1.α1:GFP in der Wurzel unterstützt die mögliche Rolle dieser katalytischen Untereinheit bei der Seitenwurzelentwicklung weiter.

Darüber hinaus erfordert die Seitenwurzelbildung während kurzfristiger Störung des pflanzlichen Energiehaushalts den SnRK1-nachgeschalteten Transkriptionsregulator bZIP63 (BASIC LEUCINE ZIPPER 63). Phänotypische Studien zeigten, dass *bzip63*-Funktionsverlust-Mutanten im Vergleich zum Wildtyp nach der Kultivierung unter Schwachlicht oder nach unerwarteter Dunkelheit eine geringere Seitenwurzeldichte aufwiesen. Frühere Arbeiten haben gezeigt, dass SnRK1 bZIP63 direkt an drei Serinresten phosphoryliert. Alanin-Austauschmutanten der SnRK1-abhängigen bZIP63-Phosphorylierungsstellen verhielten sich ähnlich wie *bzip63*-Funktionsverlustmutanten und zeigten bei kurzzeitiger unerwarteter Dunkelheit keine erhöhte Seitenwurzeldichte. Diese Daten weisen deutlich auf einen Einfluss des SnRK1-bZIP63-Signalwegs auf den beobachteten Seitenwurzeldichte Phänotyp hin. Pflanzen, die ein bZIP63:YFP-Fusionsprotein exprimieren, zeigten ein spezifisches bZIP63 Lokalisierungsmuster in der Primärwurzel, sowie in allen Entwicklungsstadien der Seitenwurzel. *bzip63*-Funktionsverlustmutantenlinien zeigten reduzierte Seitenwurzel- Initiationsereignisse bei unerwarteter Dunkelheit, wie durch Differentialinterferenzkontrast-Mikroskopie (DIC) und der Verwendung einer GATA23-Reporterlinie nachgewiesen wurde. Diese Ergebnisse deuten auf eine Rolle von *bZIP63* bei der frühen Seitenwurzel-Initiierung hin.

Durch die Anwendung der Chromatin-Immunopräzipitation (ChIP)-Sequenzierungsmethode konnten wir daraufhin globale Bindungsziele von bZIP63 identifizieren, einschließlich des auxinregulierten Transkriptionsfaktors *ARF19* (*AUXIN RESPONSE FACTOR 19*), einem gut beschriebenen zentralen Regulator der Seitenwurzelentwicklung. Zusätzliche ChIP-Experimente bestätigten die direkte Bindung von bZIP63 an eine *ARF19*-Promotorregion, die ein G-Box *cis*-Element, eine bekannte bZIP63-Bindungsstelle, beherbergt. Wir beobachteten auch, dass kurzfristige Energiestörungen bei unerwarteter Dunkelheit die Transkription von *ARF19* induzierte, die in der *bzip63*-Funktionsverlustmutante beeinträchtigt war. Diese Ergebnisse legen nahe, dass bZIP63 die Seitenwurzelentwicklung unter kurzfristiger Energiestörung über ARF19 vermittelt.

Zusammenfassend lässt sich sagen, dass diese Studie eine neuartige mechanistische Verbindung zwischen Energiehomöostase und Pflanzenentwicklung herstellt. Durch den Einsatz von reverser Genetik, konfokaler Mikroskopie und Hochdurchsatz-Sequenzierungsstrategien konnten wir einen SnRK1-bZIP63-ARF19-Signalweg zur Integration von Energiesignalen in Seitenwurzelentwicklungsprogramme aufdecken.

1. INTRODUCTION

1.1 Plant root system and architecture

Plants display a significant degree of complexity and plasticity in the underground root system (Smith and de Smet, 2012). The root system functions to provide nutrition and in addition help to anchor the plant securely in soil (Su et al., 2017).Roots serve as a major interface between the plant and the soil environment (Smith, 2007).Plants encounter several abiotic and biotic environmental stresses both separately and in combination and they respond by modifying their growth, signalling and metabolism (Ghosh and Xu, 2014; Saijo and Loo, 2020). Optimal plant root behaviour in response to biotic and abiotic conditions is essential for survival and crop yield in agriculture (Pandey et al., 2017a; Augstein and Carlsbecker, 2018)

Angiosperms or flowering plants are classified into monocots (one cotyledon in the embryo) and dicots (two cotyledons in the embryo) (Chaffey, 2014).In terms of organization of the root architecture,there are important differences between monocot and dicot plants.Monocots tend to have larger and more complex primary roots consisting of several cortical cell layer in comparison to root system of the dicot plants. Moreover, with regard to root branching (formation of lateral root system) monocots have a fibrous root system, made of numerous branching roots of the same size whereas in dicot tap root system branching takes place from/within a dominant root (primary root) (Smith and de Smet, 2012). The process of formation of the primary root and lateral roots in both monocots and dicots follow a similar pattern (Hochholdinger and Zimmermann, 2008; Smith and De Smet, 2012). This work focusses on ´the root system of the dicotyledonous model plant *Arabidopsis thaliana*, which consists of a primary root established during embryogenesis , post-embryogenic lateral roots and root hair (Petricka et al., 2012).

1.1.1 Primary root structure and development in *A. thaliana*

An adult plant primary root of *A. thaliana* consists of several well-established radial tissue layers, namely epidermis, cortex, endodermis, pericycle as well as xylem and phloem vasculature (figure 1) (Benfey and Scheres, 2000). These functionally defined tissues are organized in a concentric pattern of cell layers (Miyashima and Nakajima, 2011).The epidermis (also known as the rhizodermis) is the outermost cell layer. It acts as a protective barrier against biotic and abiotic stresses and an interface controlling exchange of water and nutrients from the environment (Javelle et al., 2011). The epidermis contains trichoblast cells, which can form a root hair and atrichoblast cells which do not develop into root hair (Ryan et al., 2001). The cortex cell layers is located below the epidermis and is responsible for the storage of food reserves in the root (Von Fircks and Sennerby-Forsse, 1998). The endodermis separates the inner vasculature from the outer cortex and epidermis. It functions as an apoplastic barrier and allows selective nutrient uptake. The endodermis contains two differentiation states, cell walls with lignin (giving rise to Casparian strips) and suberin lamella, respectively (Doblas et al., 2017). The Casparian strip acts as a diffusion barrier that prevents the apoplastic flow of water-soluble substances in and out of the cortex and stele (Miyashima and Nakajima, 2011; Grebe, 2011). The pericycle forms the outermost layer of the vasculature and lies next to the endodermis. The pericycle is known for two main functions – xylem loading through transporters present on the pericycle and in the lateral root initiation and secondary root growth (Beeckman and De Smet, 2014). The central vasculature, the innermost part of the root contains the xylem and the phloem tissues. They facilitate water, hormone and nutrient transport and provide stability to the plant body (Hellmann et al., 2018). In addition, the primary root harbours outer protective layers mainly at the root tip consisting of the lateral root cap and the columella root cap (Iijima et al., 2008; Petricka et al., 2012).

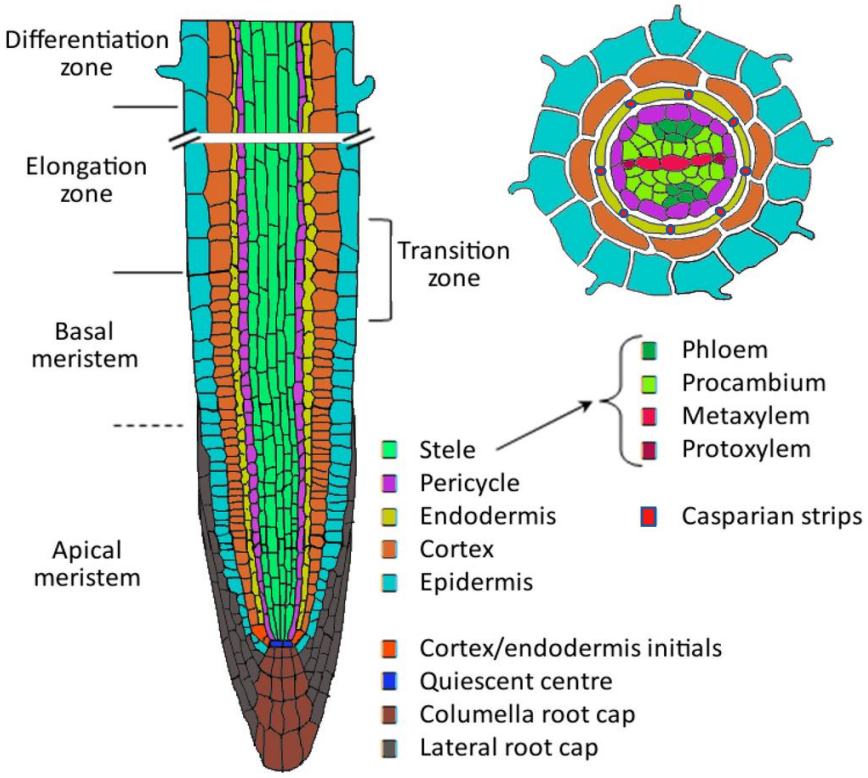

Figure 1: Pictorial representation of different developmental zones and radial cell layers in the primary root. Image adapted from (De Smet, Cuypers, Vangronsveld, & Remans, 2015).

Apart from the different radial tissue layers, the primary root has been divided into different longitudinal zones based on cellular differentiation from the root tip to the hypocotyl (figure 1). Root apical meristem (RAM), localized proximal to the root tip comprises of the stem cell niche which contains a group of lower mitotic activity cells called the Quiescent Centre (QC) (Dolan et al., 1993; Rahni et al., 2016). The QC is surrounded by four types of stem or initial cells, namely epidermis/lateral root cap, cortex/endodermal, vascular/pericycle and columella initials. Initials divide asymmetrically to give rise to daughter cells that further divide, elongate upwards and form specific root cell files (Aceves-García et al., 2016). Root cell division starts to occur at apical meristem, from which the cells are displaced into the basal meristem where division decreases and cell elongation increases (Nieuwland et al., 2009). The basal meristem is proximal to the elongation zone. Cells at the elongation zone stop to divide and expand rapidly. The zone following the elongation zone is the differentiation zone or the maturation zone. It consists of mature cells which are differentiated into specific cell types that no longer elongate (Dolan et al., 1993; Pavelescu et al., 2018). The zone also harbours

root hair (Balcerowicz et al., 2015). With regard to the lateral root development, each of these zones play an important role.

1.1.2 Lateral root structure and development in *A. thaliana*

Lateral roots develop horizontally from the primary root. A subset of pericycle cells are competent to initiate cell division to establish a new lateral root. As they are located at the xylem pole they are termed xylem pole pericycle (XPP) cells (Ram Yadav et al., 2010; De Smet, 2012). The XPP cells form the mitotically active "meristem continuum" of the primary root and are suitable to undergo cell division and differentiation to form new roots (Casimiro et al., 2003; Vilches-Barro and Maizel, 2015; Motte et al., 2019). Which XPP cells develop into the lateral root are determined at the zone above basal meristem with is characterized by oscillating auxin activity, termed oscillation zone (De Smet et al., 2007; Ram Yadav et al., 2010). Auxin is an important signal needed to induce XPP cells. The dynamics of oscillating auxin signalling can be studied using DR5:Luciferase (*DR5:Luc*) reporter. DR5 is a highly active synthetic auxin response element. It consists of tandem **D**irect **R**epeats of 11 bp including the **Aux**in-**R**esponsive TGTCTC **E**lement (AuxRE) (Ulmasov et al., 1997). After the appearance of an auxin maxima, a new root tissue is being produced and for a next new peak of auxin maxima to be observed it usually takes about 4-6 h. During this time the cells leave the meristem without being exposed to auxin-response maxima. This is a periodic process and the periodicity correlates with the reoccurring programmed cell death of the lateral root cap cells and temporary release of auxin from these cells to the root meristem (Xuan et al., 2016) Those XPP cells that encounter auxin begin to divide and develop into lateral root in the elongation and differentiation zone at the pre-branch sites (figure 2). Pre-branch sites are a region in the young primary root with strong auxin (*DR5:Luc*) activity correlated with early stages of lateral root formation (Motte et al., 2019). It is important to note that, not all XPP cells become lateral root. It's either a further cue what is required for XPP cell to continue to divide or an inhibitory effect stopping further division of XPP cell (Toyokura et al., 2019).

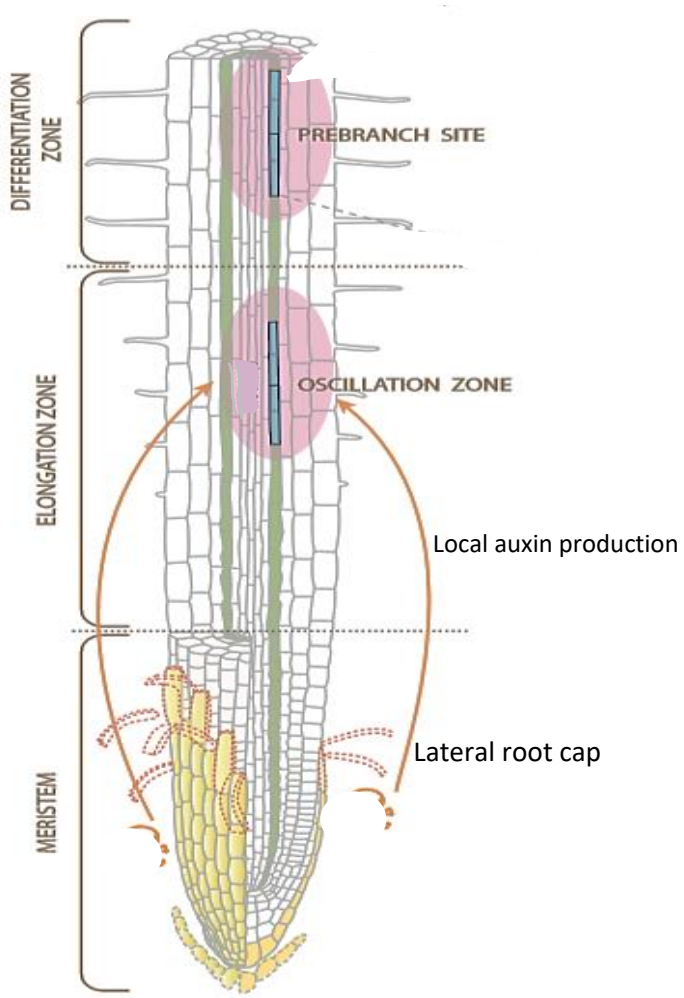

Figure 2: Lateral root initiation in the primary root. Primary root zones which are important for XPP priming, auxin oscillation and lateral root initiation. Orange arrows indicate induction of auxin signalling oscillation due to cell death at lateral root cap. Pink spots refer to auxin maxima before lateral root initiation. Blue cells indicate cell division of XPP cells and lateral root initiation. Image modified from (Motte et al 2019).

Lateral root formation from initiation to emergence is a complex developmental process. Here we have summarized below the step by step developmental events. The first visible hallmark is when nuclei of XPP cells migrate towards the common cell wall and the cells gain volume and swell up (figure 3C) (Vilches-Barro and Maizel, 2015). This is followed by an asymmetric anticlinal division resulting in stage I primordium consisting of one cell layer (figure 4A). This is the first stage in lateral root initiation and the developing lateral root is called founder cell (Van Norman et al., 2013). Then a periclinal cell division that produces a new cell layer results in a stage II primordium (figure 4B). This newly formed outer layer (OL) in stage

II primordia undergoes periclinal cell divisions and creates the three-layered primordium-stage III (figure 4C). Stage IV of the lateral root primordium (LRP) is characterized by four distinct cell layers: two inner cell layers (IL) and two outer cell layers. The LRP here surpasses the endodermis (figure 4D). During stage V of the development, a group of central cells in the outer layer, divides anticlinally to form four cuboidal cells. The cells in the inner layer continue enlarging radially and then start to divide. The growing LRP crosses the overlying tissue layer of cortex cells (figure 4E). Stage VI is characterized where the LRP acquires a cellular organization similar to that of the primary root meristem (figure 4F). In the final emergence stage (figure 4G-H), the LRP breaks through the epidermis and enters the soil (Malamy and Benfey, 1997).

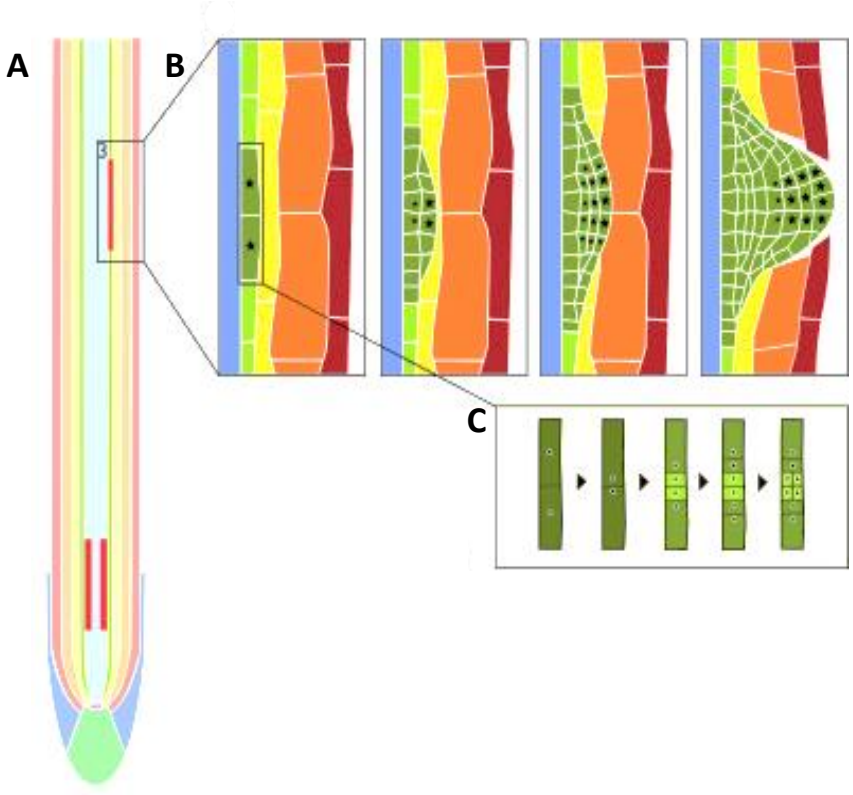

Figure 3: Horizontal branching out of the lateral root from the primary root (A) Longitudinal view of the primary root indicating lateral root initiation (marked black box) (B) Pictorial representation of lateral root stages emerging out of the primary root (C) Cell swelling and nuclear migration towards common cell wall in the XPP cells. Image adapted and modified from (Santos Teixeira and ten Tusscher, 2019)

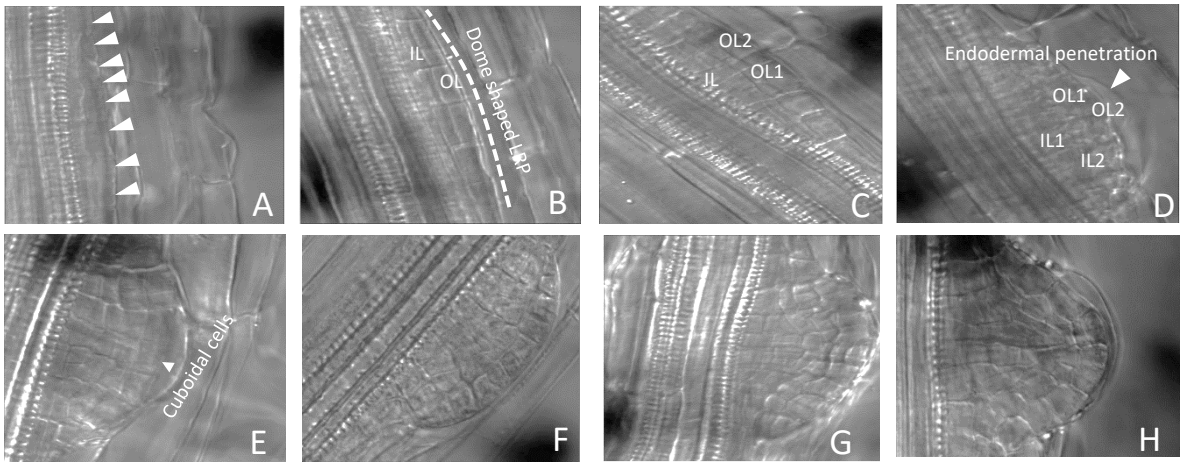

Figure 4: Stages of lateral root primordium development. Shown are DIC (Differential Interference Contrast) microscope images of cleared *A. thaliana* roots from initiation to emergence of lateral roots (Stage I to Emergence). (A) Stage I, white arrows indicate new cell wall formation after the anticlinal divisions. (B) Stage II, demarcating inner layer (IL) and outer cell layers (OL) and formation of dome-shaped LRP. (C) Stage III, periclinal divisions of outer layer, making a new cell layer. This stage has 3 cell layers marked by IL, OL1 and OL2. (D) Stage 4 contains four distinct cell layers (IL1, IL2, OL1 and OL2). A white arrow indicates the place of endodermal penetration. (E) Stage V shows OL dividing anticlinal to form cuboidal cells. (F) Stage VI is when the emerging LRP interacts with the endodermis and the cortex. (G) Stage VII is marked by the LRP through epidermis and emerging out of the parent primary root horizontally. (H) Emergence of lateral root from the primary root.

1.1.2.1 Molecular events controlling lateral root development

Coordinated gene expression and the activity of TFs along with the phytohormone auxin are important in lateral root development (Vilches-Barro and Maizel, 2015). Significant molecular networks are summarized in this section and in figure 5.

Lateral roots initiate in the pericycle at the xylem poles. Studies using marker lines for pericycle identity, analysis of mutants defective in vascular development and ultrastructural analysis shows that there are at least two different pericycle cell identities, each of them associated with either xylem or phloem (refer figure 1 for radial view of the primary root) (Motte et al., 2019). XPP and phloem pole pericycle (PPP) differ from each other but have features in common with their respective vascular tissue (Parizot et al., 2008). AHP6 (HISTIDINE PHOSPHOTRANSFERASE PROTEIN 6) is a negative regulator of cytokinin signalling and is required

for normal protoxylem formation (Mähönen et al., 2006). This marker is expressed in the developing protoxylem and in the associated pericycle cell files (Moreira et al., 2013). The marker expression suggests that the specification of XPP cells to become a lateral root is correlated with its vascular patterning. Based on *AHP6* expression, starting from the stem cell area near the QC, specification of XPP cell files to become lateral roots is predicted to happen already in the meristem (Motte et al., 2019)

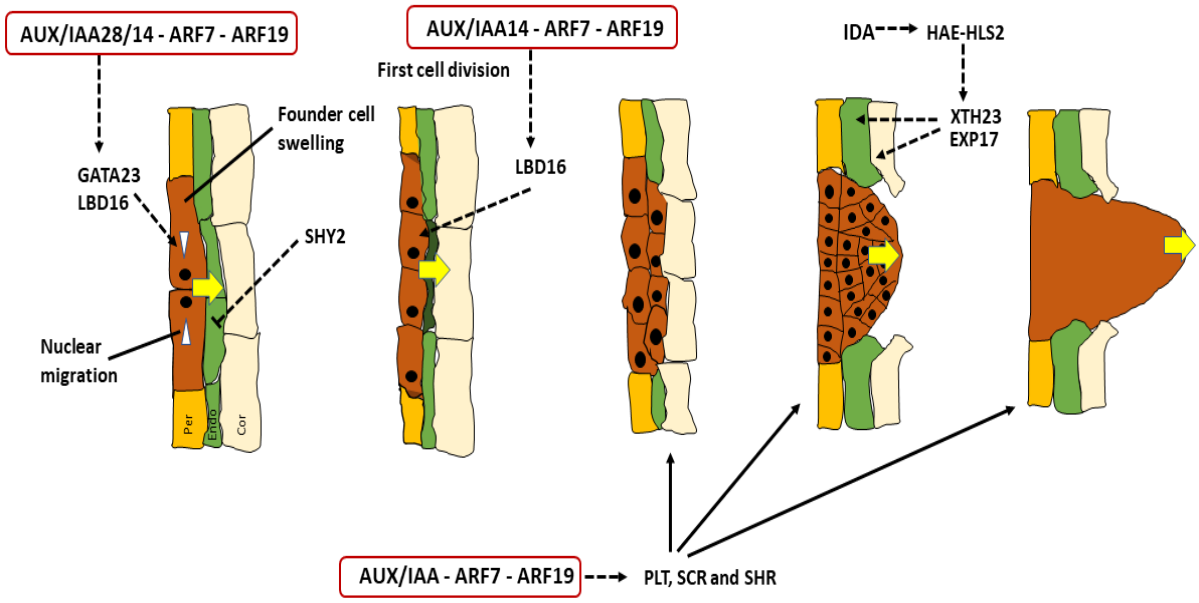

Figure 5: Molecular networks important for lateral root initiation and development. The events start with GATA TRANSCRIPTION FACTOR 23 (GATA23) and LATERAL ORGAN BOUNDARIES-DOMAIN 16 (LBD16) that control nuclear migration and founder cell swelling. LBD16 is important for first cell divisions. PLETHORA (PLT) TFs are important for LRP cell division and emergence. INFLORESCENCE DEFICIENT IN ABSCISSION (IDA) peptides and their receptors, HAESA (HAE) and HAESA-like2 (HSL2) modulate expression of the cell wall modifying proteins such as XTH23 (XYLOGLUCANENDOTRANSGLYCOSYLASE6) and EXP17 (EXPANSIN17) and help in emergence of the lateral root. Most of these networks are controlled by auxin inducible AUX/IAA – ARF7/19 (AUXIN RESPONSE FACTOR7/19) signalling. Yellow arrows indicate directional flow of auxin, important for functioning of these signalling networks. Per-Pericycle, Endo-Endodermis and Cor-Cortex.

Due to anticlinal division and cell elongation at the RAM, XPP cells leave the meristem and encounter auxin signalling maxima at the oscillation zone (figure 2). The zone is characterized by auxin maxima followed by periods of low auxin, thus creating an oscillating gene and transcriptional regulation due to the phytohormone (Moreno-Risueno et al., 2010).

The auxin-signalling dynamics at the oscillation zone can be visualized using *DR5:LUC*. The strength of the *DR5:LUC* signal can be correlated to auxin responsiveness (Moreno-Risueno et al., 2010). Auxin perception and auxin signalling, which is mediated by AUX/IAA (AUXIN/INDOLE ACETIC ACID) inhibitors and ARFs (AUXIN RESPONSE FACTORS) TF play a major role in further stages of lateral root development (Du and Scheres, 2018).

Members of Aux/IAA family repress the activity of ARF TFs in the absence of auxin, ARFs bind to Auxin Response Elements (AuxRE) (Ulmasov et al., 1999) on the promoters of auxin-responsive genes and either activates or represses it (Ulmasov et al., 1999). When auxin is present, the AUX/IAA repressors are bound by the F-box protein TRANSPORT INHIBITOR RESPONSE 1 (TIR1), or related members of a small gene family, which forms the part of the SCF^{TIR1} ubiquitin ligase complex. Via ubiquitination, the SCF^{TIR1} complex marks Aux/IAA proteins for proteolytic degradation, which releases the ARFs from Aux/IAA-mediated repression and mediates transcription of target genes (Mockaitis and Estelle, 2008; Dharmasiri et al., 2005; Gray et al., 2001). Different AUX/IAA-ARF modules are proposed to control particular stages of lateral root development (Goh et al., 2012). Once the competence to develop into a lateral root is established, the *GATA23* gene is transcriptionally induced in two adjacent XPP cells and their expression correlate the nuclear migration activity in these XPP cells. *GATA23* serves as an early lateral root initiation marker as it is expressed in early stages of lateral root development. It is controlled by IAA28-ARF7/ARF19 module (De Rybel et al., 2010; Murphy et al., 2016).Once the nuclei are migrated towards the common cell wall of the XPP cells, the cells swell up and begin the first round of anticlinal divisions.

Once the founder cell identity is established, auxin responsiveness increase and these cells undergo a set of asymmetric anticlinal divisions. Two different AUX/IAA-ARF modules control this stage: IAA14-ARF7/ARF19 and IAA12-ARF5 (Fukaki et al., 2002, 2005; de Smet, 2010). The swelling of the founder cells is dependent on the early auxin perception. There is a biochemical and mechanical interplay between the pericycle, the endodermis and auxin (Lucas et al., 2013). The endodermis undergoes changes, shrinks and deforms. The AUX/IAA repressor, SHORT HYPOCOTYL2 (SHY2)/IAA3, plays an important role in mediating the first division and interaction with the endodermis. SHY2 is well expressed in the endodermis (Vermeer et al., 2014; Tian and Reed, 1999; Swarup et al., 2008) . It has been shown that gain-of-function of *shy2-2* represses lateral root outgrowth, whereas the opposite effect is seen in *shy2-24* loss-

of-function mutant (Vermeer et al., 2014). Additionally, SHY2/IAA3 has been shown to influence primary root growth by blocking PIN transporters (Tian and Reed, 1999; Weiste et al., 2017) making this important for both primary and lateral root development. Therefore, the Auxin-SHY2 module is necessary for the pericycle cell swelling and interaction with the endodermis (figure 5).

Another important gene required for the initiation and asymmetric cell division of the lateral root founder cells is *LATERAL ORGAN BOUNDARIES-DOMAIN 16 (LBD16)* (Okushima et al., 2007a). The expression of this gene is also controlled by the IAA14-ARF7-ARF19 module. When *LBD16* is dominantly repressed using LBD16-SRDX (chimeric repressor technology where addition of SRDX peptide to C-terminal end turns a transcriptional activator into a repressor construct; (Hiratsu et al.,2003), nuclear migration and subsequent asymmetric cell division is blocked. This inhibits lateral root initiation thus making it an important regulator of early-stage development (figure 5) (Okushima et al.,2007).

PLETHORA (PLT) genes (*PLT1, PLT2*) are expressed in stage I primordia and they are responsible for the post-initiation steps of lateral root formation (Du and Scheres, 2017). They help to initiate the periclinal divisions that generate two distinct inner and outer layers during stage II of the development (Casimiro et al., 2001; Malamy and Benfey, 1997; Du and Scheres, 2017). The PLTs directly regulate the GRAS transcription factors SCR (SCARECROW) and SHR (SHORT-ROOT) and altogether, they are important in establishing the cellular patterning of the lateral root (stage III to Stage VI) (Santuari et al., 2016; Motte et al., 2019). Furthermore, during these stages LRPs undergo several periclinal and anticlinal cell divisions (figure 5) (Du and Scheres, 2017). The Casparian strip in the endodermis is locally degraded to allow the confined opening of the lignin networks helping the emerging primordia to penetrate the next layer (Robbins et al., 2014). Once crossing of the endodermis is successful, the cortex and epidermis cell layers separate from each other to make way for the emerging lateral root primordia (Vilches-Barro and Maizel, 2015). This separation of the cortex and epidermal cell layers is due to pectin degradation in these layers (Laskowski et al., 2006).

Apart from these evidences, localized auxin perception induces *INFLORESCENCE DEFICIENT IN ABSCISSION* (*IDA*) expression in endodermal cells (Aalen et al., 2013). Next IDA peptide signals through its receptors, the leucine rich repeat like kinases HAESA (HAE) and HAESA-like2 (HSL2) which are already present in the endodermal membrane (Kumpf et al., 2013). These signalling

events up-regulate the cell wall modifying proteins such as XTH23 (XYLOGLUCANENDO-TRANSGLYCOSYLASE6) and EXP17 (EXPANSIN17), POLYGALACTURONASE ABSCISSION ZONE A (PGAZAT) and PGLR belonging to pectin lyase like super family which help in remodel the cell wall in the cortex and the epidermis to open up a gateway for emerging lateral root (Kumpf et al., 2013).

1.2 Environmental and nutritional changes affecting root system architecture and development

One of the most important factors affecting crop yield and plant productivity in today´s world is the effect of environment and climatic changes on plants (Kang et al., 2009). An unfavourable environment influences gene expression in any living system (Griffiths et al., 2000).

Environmental factors could be categorized into biotic and abiotic factors. Biotic factors are bacteria, nematodes or fungi to name a few. Abiotic factors include soil composition, water deficiency, ions, toxic compounds etc (Pandey et al., 2017).

The development of the lateral root primordia is induced or repressed in response to environmental conditions and this provides a mechanism for the plant to cope with the changing environments (Malamy, 2005). Different environmental factors have been shown to influence various stages of lateral root development. Mild water stress impacts the root architecture by inducing new lateral roots for reaching asymmetric distribution of water also referred to as hydropatterning (Orman-Ligeza et al., 2018). The lateral root development is sensitive to the availability of nutrients such as nitrogen and phosphorous. To acquire more phosphate, the lateral root number and density increases, whereas the primary root system delves into deeper layers of soil in search of nitrate (York et al., 2013; Motte et al., 2019). Low phosphate condition increases local auxin accumulation (Nacry et al., 2005) and positively induces the expression of the auxin sensor *TIR1* in the lateral root primordia. This induces auxin sensitivity and enhanced lateral root formation (Pérez-Torres et al., 2008). The increased branching, in this case, leads to more root tips and thereby, more phosphate uptake (Nacry et al., 2005). It has been shown that the ARF7/ARF19 regulators are important for the observed lateral root phenotype under low phosphate conditions through PHOSPHATE STARVATION RESPONSE 1 (PHR1). ARF7 and ARF19 binds to the three auxin response elements on the *PHR1* promoter and activate its expression (Huang et al., 2018). Nitrogen is the central element in amino acids

and proteins and is of utmost importance to plant functioning. In roots, nitrogen is taken up in form of ammonium or nitrate (Kiba and Krapp, 2016). Ammonium has been shown to inhibit root elongation and gravitropism, whereas nitrate stimulates root elongation. If locally present, both nitrogen-containing ions stimulate root branching of lateral roots, thereby enabling root systems to forage for nitrogen in heterogeneous soil environments (Lima et al., 2010; Sun et al., 2017).

Sugars are a primary energy resource in plants and are important for plant growth and development (Sakr et al., 2018; Van den Ende, 2014). Cell division, expansion and cell growth largely depend on the availability of carbohydrates (Lastdrager et al., 2014). Sugars are produced in the photosynthetically active shoot and are translocated via the phloem to the root (Wang and Ruan, 2016). Once translocated and utilized in the root, some parts of sugars are extruded into the rhizosphere as root exudates which are utilized by soil microbiota (Hu et al., 2018). Sugars not only function as resources but they act as signals regulating various processes (Rosa et al., 2009). When biotic and abiotic stress affects the allocation of these sugars, it leads to homeostatic imbalance especially in the root system (Rosa et al., 2009). In recent years, several signalling pathways and signalling molecules that link plant sugar/energy status to maintaining plant growth homeostasis have been well studied (Wingler, 2018). These include:

HEXOKINASE (HXK1), which is a glucose sensor and is primary for converting glucose to glucose-6-phosphate (Moore et al., 2003; Lastdrager et al., 2014). Hexokinase mutants (*hxk1*) have severe growth defects such as reduced shoot and root growth and altered sensitivities to the growth hormones auxin and cytokinin (Lastdrager et al., 2014).

TREHALOSE-6-PHOSPHATE (T6P), which is an important signalling metabolite in plants is synthesized from glucose-6-phosphate and UDP-glucose. Starvation or low energy conditions depletes T6P levels while sucrose feeding lead to T6P accumulation and the levels of T6P correlates with the levels of sugar availability (Smeekens et al., 2010). T6P connects the sugar status to multiple physiological and developmental processes but the underlying mechanisms are yet to be elucidated (Ponnu et al., 2011).

TARGET OF RAPAMYCIN (TOR) kinase has emerged as a master regulator that is evolutionarily conserved among yeasts, plants, animals and humans (Xiong and Sheen, 2014). They are fundamental in growth processes such as embryogenesis, meristem activation, root growth, flowering and senescence (Ren et al., 2011). TOR integrates transcriptional networks that connect metabolism and biosynthesis for energy and biomass production (Xiong and Sheen, 2014).

Snf1-RELATED KINASE 1 (SnRK1) are similar to its orthologs SUCROSE NON-FERMENTING 1 (SNF1) in yeast and AMP-ACTIVATED PROTEIN KINASE (AMPK) in animals and are key metabolic regulators involved in downregulating anabolic processes and inducing catabolic processes to make sure plant resources are utilized optimally and help in stress tolerance and survival (Crepin and Rolland, 2019). SnRK1 is activated upon low energy conditions. These kinases forms a part of metabolic stress signalling networks which includes TOR kinases (Smeekens et al., 2010; Wingler, 2018; Crepin and Rolland, 2019).

SnRK1 and TOR pathways have been well studied as independent systems, but knowledge of their interconnections are less available. These central pathways are involved in growth-defence trade-offs that are associated with biotic and abiotic stress response. TOR primarily regulates growth whereas SnRK1 primarily regulates energy homeostasis (Smeekens et al., 2010).

Antagonistic to SnRK1, TOR signalling is activated in nutrient rich condition (Xiong and Sheen, 2014).Photosynthetically derived glucose and sucrose are potential activators of TOR (Rodriguez et al., 2019). Most stresses restrict carbon assimilation through photosynthesis and/or ATP production through respiration leading to decrease in overall energy levels and this leads to activation of SnRK1. During biotic stresses SnRK1 and TOR play opposite roles but when considering abiotic stresses, reports show that SnRK1 and TOR over expressors are more resistant than wild-type to abiotic stress and loss-of-function is more susceptible (Margalha et al., 2019).

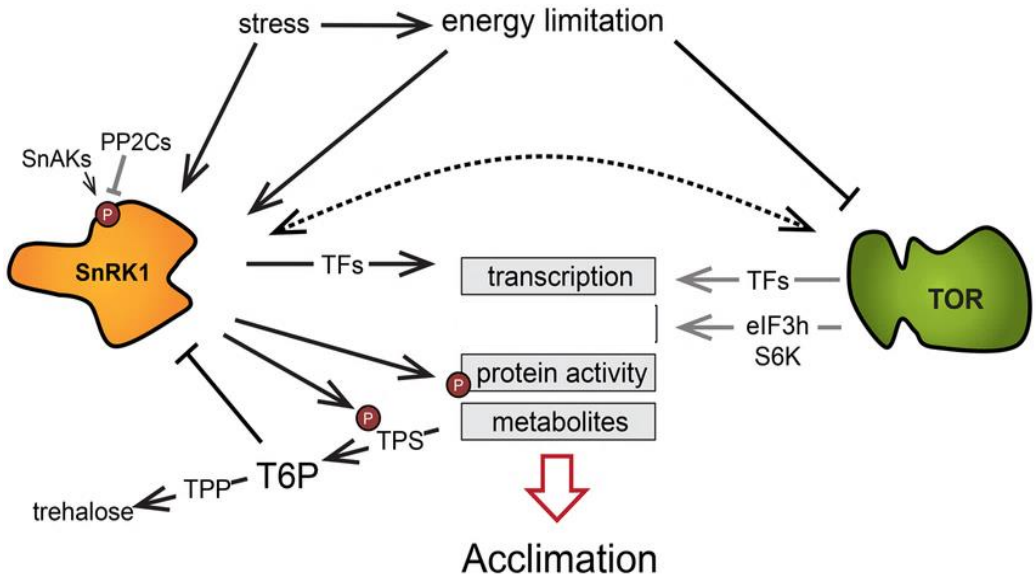

Figure 6: The energy-controlled signalling network involves TOR and SnRK1 kinases. The TOR and SnRK1 kinases are influenced by energy availability. They mediate transcription, enzyme activity and metabolic changes to help plants adapt to different environmental conditions. Due to energy limitation the TOR processes are shut down (black arrow) and SnRK1 processes are activated. There are probable interactions between these two pathways (indicated by dotted arrows). TOR, Target of Rapamycin, SnRK1, Sucrose-Non-Fermenting (SNF1) related kinase 1, TPS, Trehalose Phosphate Synthase, TPP, Trehalose Phosphate, T6P, Trehalose-6-Phosphate. Image adapted and modified from (Tomé et al., 2014).

Below we introduce SnRK1 protein kinase in detail and how it maintains energy homeostasis and impose an effect on plant development.

1.2.1 Snf1-related kinase 1 (SnRK1) and the low-energy signalling network

The SnRK1 protein kinase represents the plant ortholog of the Snf1 protein kinase in yeast and AMP activated PK (AMPK) in mammals (Crozet et al., 2014).

SnRK1/Snf1/AMPK are evolution conserved kinases, consisting of a heterotrimeric complex made of three subunits (figure 7), the catalytic α subunit and the regulatory β and γ subunit (Smeekens et al., 2010; Broeckx et al., 2016; Crepin and Rolland, 2019). The catalytic α subunits are made of an N-terminal catalytic (kinase) domain and a C-terminal regulatory domain,

involved in interactions with the β and γ regulatory subunits. In *A. thaliana* 3 catalytic subunits are described, SnRK1.α1 (AKIN10/KIN10), SnRK1.α2 (AKIN11/KIN11), and SnRK1.α3 (AKIN12/KIN12) (Broeckx et al., 2016). However, only *SnRK1.α1* and *SnRK1.α2* have been found to be functionally important. *snrk1α1/ α2* double knockout approaches are lethal and both catalytic subunits have been proposed to perform partially redundant functions (Baena-González et al., 2007). The *SnRK1.α3* is poorly expressed and seen only during early stages of development (Broeckx et al., 2016). The catalytic domain contains key residues required for kinase activity including the conserved lysine (K) important for phosphotransfer reaction (Baena-González et al., 2007). Another important aspect to remember is the phosphorylation of a conserved threonine T175 in SnRK1.α1 (T-loop) further stabilizes an activation loop in an open and extended conformation that facilitates substrate binding (Baena-González et al., 2007) Phosphorylation of this residue is required for kinase activity (Broeckx et al., 2016; Baena-González et al., 2007). This catalytic subunit is very important for phosphorylating the downstream enzymes and signalling compounds (e.g. TFs) and to regulate a multitude metabolic and cellular processes (Broeckx et al., 2016). *A. thaliana* regulatory β subunits comprises of SnRK1β1, SnRK1β2, and a plant-specific truncated SnRK1β3 (Broeckx et al., 2016). In β subunits, there is a myristoylated N-terminal domain enabling membrane association, a central carbohydrate binding (CBM) module and C-terminal α and γ subunit binding domain. The regulatory β subunits function as complex scaffolds, but also affect kinase activity, localization, and substrate specificity (Crepin and Rolland, 2019). In AMPK, the γ subunit functions as the cellular energy sensing module of the trimeric complex. In plants specifically there is a βγ hybrid subunit with an additional N-terminal CBM domain (Crepin and Rolland, 2019). Loss of SnRK1βγ subunit is lethal and shows an essential function in pollen hydration and germination defect (Broeckx et al., 2016).

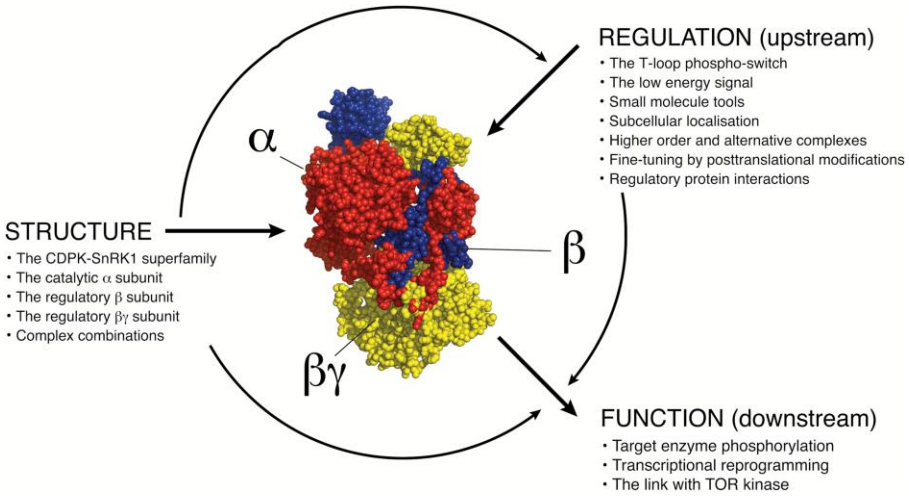

Figure 7: SnRK1 structure, function and regulation. SnRK1 is a heterotrimeric complex consisting of a catalytic α subunit, represented in red and regulatory βγ subunits, represented in yellow. This pictorial representation describes the structure, function and regulation of SnRK1 protein kinases. Image is adapted from (Broeckx et al., 2016)

Although SnRK1 shares structural and functional similarities with Snf1 and AMPK, there are some significant differences particularly with respect to its regulation. AMPK is regulated by nucleotide charge with ADP/AMP competing with ATP to bind at the regulatory subunit (Hardie et al., 2011; Hardie and Hawley, 2001; Hardie, 2011). This results in a conformational change, allosteric activation and T-loop phosphorylation. In SnRK1, a ubiquitin associated domain (UBA) promotes T-loop phosphorylation by upstream kinases and maintain catalytic activity (Crepin and Rolland, 2019). Whereas AMPK and Snf1 are activated upon energy deficit conditions, SnRK1 is under negative control and de-repressed under conditions of energy limitation (Crepin and Rolland, 2019). Confirming the above hypothesis, SnRK1 activity is inhibited by sugar phosphates such as Trehalose-6-phosphate (T6P) (Crepin and Rolland, 2019). T6P is a recently described essential signalling molecule in plants (O'Hara et al., 2013). It is synthesized from glucose 6-phosphate and UDP-glucose by TREHALOSE 6-PHOSPHATE SYNTHASE (TPS), and converted by TREHALOSE 6-PHOSPHATE PHOSPHATASE (TPP) to trehalose (Paul et al., 2008). The Sucrose-T6P nexus model proposes that T6P is both a signal and negative feedback regulator of sucrose levels, to maintain sucrose at an optimal range (Figueroa and Lunn, 2016). T6P was recently shown to bind to the catalytic domain of SnRK1 α subunit *in vitro* and to interfere with upstream kinases which are proposed to activate SnRK1 via T-loop phosphorylation (Zhai et al., 2018). Whether this mechanism is of general importance

still needs to be established. Regulation of SnRK1 is further complicated as the α subunit may function in activation of gene expression without forming a trimeric complex (Ramon et al., 2019). Recently, it has been proposed that the α subunit translocates to the nucleus in response to energy stress. Due to myristoylation, β subunits are tethered to membranes in the cytoplasm which inhibits nuclear translocation of the α subunit via protein-protein interaction. Altogether, these data suggest that plant SnRK1 regulation differs considerably form its mammalian counterpart, particularly by utilizing negative regulators, releasing SnRK1 under energy limiting conditions (Ramon et al., 2019).

With regard to SnRK1 expression, the two catalytic and regulatory subunits of SnRK1 are differentially expressed throughout the plant (Williams et al., 2014). SnRK1.α1 promoter-β-glucuronidase (GUS) analysis shows expression in meristematic and vascular tissues, SnRK1.α2 expression is more spatially and temporally restricted (Williams et al.,2014). With regard to expression of SnRK1 subunits in roots, SnRK1α1 and SnRK1βγ shows high expression in the entire root (Bitrián et al., 2011). The β1 subunit expression is dark induced. SnRK1.α2*,* but not SnRK1.α1, is also specifically induced by trehalose in the root area close to the root to shoot junction, possibly as a tissue-specific feedback effect of increased T6P levels (Schluepmann et al., 2004).

Upon energy stress, SnRK1 switches on energy saving programs using two different mode of action a) direct phosphorylation of metabolic enzymes and regulatory proteins b) extensive transcriptional reprogramming (Margalha et al., 2016). SnRK1 induces genes involved in amino acid catabolism, cell wall, sucrose, starch and polysaccharide hydrolysis (Baena-González and Sheen, 2008; Baena-González et al., 2007). With regard to growth and development, proper functioning of SnRK1 pathway is crucial. Altered SnRK1 pathways causes growth defects in many plant species (Margalha et al., 2016). With regard to inducing tolerance to abiotic stresses, SnRK1 induces hypoxia responsive genes and therefore promotes tolerance to submergence in rice (Lee et al., 2009). The kinase function has been linked to phosphate starvation (Fragoso et al., 2009) and heat stress response (Slocombe et al., 2004). Under biotic stress, it has been shown that SnRK1 is a component of the plant defense system activated by metabolic imbalances due to pathogen attack (Margalha et al., 2016). SnRK1 together with Abscisic Acid (ABA) induce salt stress tolerance in *A. thaliana* (Hartmann et al., 2015).

Studies have shown that these protein kinases phosphorylate the group C- basic leucine zipper (bZIP) TF bZIP63 (Mair et al., 2015). This post-translational modification increase the formation of group C/S_1 bZIP heterodimers to regulate several downstream processes leading to metabolic adaptation upon stress (Dröge-Laser et al., 2018; Dröge-Laser and Weiste, 2018).

1.2.2 Group C/S1-bZIP transcription factors - downstream mediators of SnRK1 signalling

bZIP TFs are characterized by a basic DNA-binding region and an adjacent leucine zipper, which aids in bZIP dimerization (figure 8) (Vinson et al., 1989; Kouzarides and Ziff, 1989). Structural model of bZIP shows that bZIP domain forms a continuous α-helical structure and dimerize via the leucine zipper (ZIP). They form a "pair-of-scissors" with other bZIP proteins (heterodimerization) and contact the major groove of double-stranded DNA via the basic DNA-binding domain. The leucine zipper domain consists of heptad repeats of leucine (L) or related hydrophobic amino acid. There are 78 bZIP TFs classified into 13 groups, designated A-M. (Dröge-Laser et al., 2018)

Members of group C (bZIP9, bZIP10, bZIP25 and bZIP63) preferentially heterodimerize with group S_1 bZIP TFs (Mair et al., 2015; Pedrotti et al., 2018; Dröge-Laser and Weiste, 2018). Group S comprises the largest bZIP cluster of 17 genes. They are generally intron less and codes for small TF proteins of 20 kD in size. A few members have been characterized in detail. This S_1 subgroup include bZIP1, bZIP2, bZIP11, bZIP44 and bZIP53 (Ehlert et al., 2006).

Studies have shown that SnRK1 protein kinases phosphorylate the group C- basic leucine zipper (bZIP) TF bZIP63 (Mair et al., 2015). This post-translational modification increase the formation of group C/S_1 bZIP heterodimers to regulate several downstream processes leading to metabolic adaptation upon stress (Dröge-Laser et al., 2018; Dröge-Laser and Weiste, 2018).

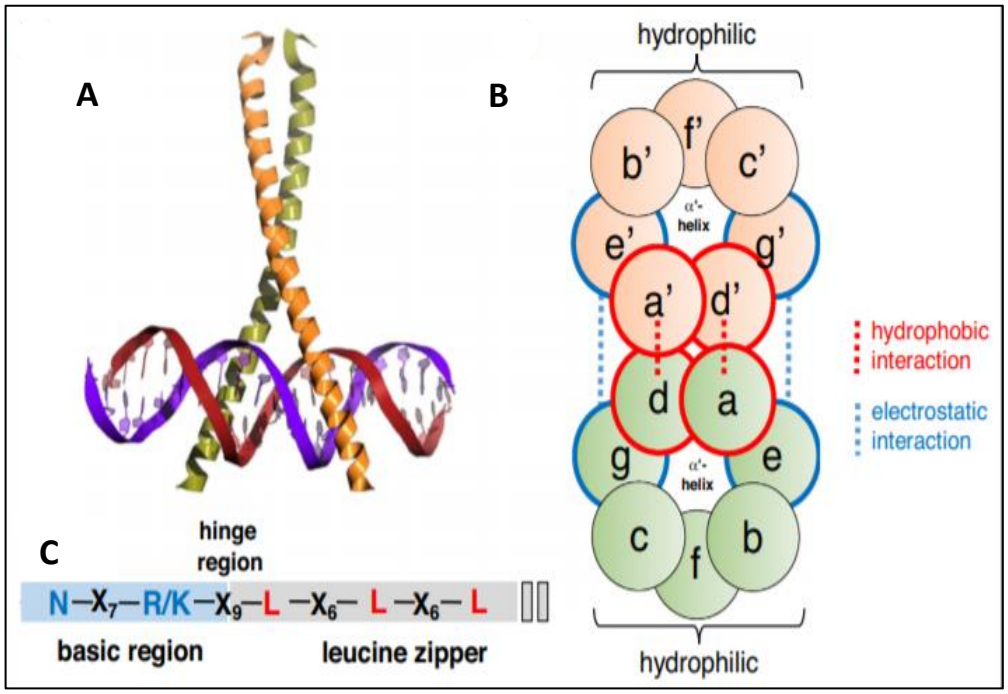

Figure 8: bZIP transcription factor structure. (A) Each bZIP domain forms continuous α-helical structure and dimerises via the so-called leucine zipper (ZIP). They form a scissor like structure and bind to the DNA. (B) Schematic representation of the bZIP dimerisation interphase. The amphipathic C-terminal zipper domain dimerises to form coiled-coils. A heptameric repeat is formed by seven aa, arranged in two turns and labelled a–g. As depicted in the scheme, the positions a–d and are hydrophobic (typically L) and expose their site-chains to form a hydrophobic face facilitating intermolecular interactions. Charged aa in positions g and e often form crosswise electrostatic interactions between helices. Deduced from these interactions, structure-based rules have been used for predictions of heterodimerisation, proposing that preferentially homodimers or dimers within related group-members (quasi-homodimers) are formed by *Arabidopsis* bZIPs. (C) Schematic representation of the bZIP domain, consisting of a basic DNA-binding region (blue) and the adjacent ZIP domain (grey). The ZIP domain consists of heptad repeats of leucine (L) or related hydrophobic aa. Image and text adapted from (Dröge-Laser et al., 2018).

Among these, the heterodimerization complex of C/S_1-bZIPs are proposed as signalling hub to facilitate reprogramming in plants, both in development and in metabolism during low energy stress (Dröge-Laser and Weiste, 2018). The C/S_1 network is activated upon nutritional starvation mediated by SnRK1 and Sucrose Induced Repression of Translation (SIRT). SIRT is described as translational control of the main open reading frame (ORF) by upstream ORF situated in the 5' end of the gene. A nascent peptide encoded by this upstream ORF (uORF) is

produced which is proposed to lead to ribosome stalling and inhibition of main ORF-translation in a sucrose dependent manner. All S_1 bZIPs share this conserved uORF system. SIRT provides a mechanism by which sucrose availability is relayed into gene expression (Rahmani et al., 2009; Wiese et al., 2004).

Data derived from transiently transformed protoplasts and plants indicate the impact of S_1 bZIPs on starvation-induced gene expression of *ASPARAGINE SYNTHETASE 1* (*ASN1*) (Hanson et al., 2007). ASN1 is central in the biosynthesis of asparagine (Asn) (Gaufichon et al., 2010). Asparagine is a major transported amino acid during low energy stress conditions and the promoter of *ASN1* contains G/Boxes (CACGTG) which are well characterized binding sites for bZIP TFs (Lea, 1997., Menkens et al., 1995). bZIP TFs (bZIP 1 and bZIP53) increases *ASN1* transcript levels during darkness. The direct promoter binding of bZIP1 and bZIP53 TFs on *ASN1* promoters has been confirmed by Chromatin Immunoprecipitation (Dietrich et al., 2011).

In another study conducted by Pedrotti et al. (2018), SnRK1 and the C/S_1 bZIP network was shown to link energy starvation to changes in gene regulation and increased survival. SnRK1 and bZIPs control the expression of genes involved in branched-chain amino acid (BCAA) catabolism, which supports ATP production under energy limiting conditions (Dietrich et al., 2011). In addition, the promoter of the ELECTRON TRANSFER FLAVOPROTEIN:UBIQUINONE OXIDOREDUCTASE – *ETFQO* gene, which encodes for a crucial electron transport protein involved in BCAA degradation (Binder, 2010; Pedrotti et al., 2018) is bound by both group C and S_1 bZIPs at their G-boxes in a SnRK1 dependent manner. This finding proved the importance of SnRK1-C/S1-bZIP network in reprogramming metabolism in plants for their survival under energy-limiting conditions.

Recent studies by Weiste et al. (2017) shows the importance of the closely related group S_1 members bZIP11, bZIP2 and bZIP44 on primary root growth. They are proposed to control auxin flow by transcriptionally repressing major auxin transport facilitator (PINs) and consequently impacting the root apical meristem (RAM) size under extended night/low energy. Via direct promoter binding, bZIP11 related TFs activate *IAA3/SHY2* transcription. IAA3/SHY2 plays a negative role in controlling root growth and repress the transcription of major auxin transport facilitators of the PIN-FORMED (PIN) gene family (PIN1 and PIN3) (Weiste et al., 2017). This study reveals a new aspect of bZIP TFs in plant's energy management by controlling meristematic root growth through modulation of auxin transport. Moreover, bZIP11-

related TFs act as strong transcriptional activator, which recruit via direct protein-protein interaction the histone acetylation machinery to target promoters (Weiste and Dröge-Laser, 2014). Although a global view of bZIP-mediated gene expression in auxin responses is missing, several auxin signalling regulators are expressed in response to starvation, suggesting a selective impact of plants limiting energy status in auxin-mediated root growth response (Weiste et al., 2017)

With regard to group C bZIPs, bZIP63 has been demonstrated to be directly phosphorylated by SnRK1 in response to extended night. In line with what we know about SnRK1 which is deactivated by sugars, bZIP63 phosphorylation was decreased in presence of sugars and increased with extended night/starvation (Mair et al., 2015). Phosphorylation by SnRK1 enhances the ability of bZIP63 to heterodimerize with S_1-bZIPs and form a SnRK1-C/S_1-bZIP complex which has been shown to be important for energy management in plants (Mair et al., 2015; Pedrotti et al., 2018). A recent study conducted by Frank A et al. (2018) showed another novel function of bZIP63 in modulating the circadian clock. bZIP63 is proposed to act downstream of T6P and SnRK1 kinases and directly bind to PSEUDO RESPONSE REGULATOR 7 (PRR7) promoter. This leads to changes in the circadian phase in response to sugars.

There is still a of information yet to be discovered with respect to how SnRK1-C/S_1-bZIP network links energy status of the plant to different aspects of development. Our study will focus on this aspect.

1.3 AIMS AND OBJECTIVES

Roots provide an excellent model system for developmental studies, as developmental changes are easy to quantify and monitor. In this study we aim to understand how root development respond to short-term energy perturbations.

First step in achieving our aim is to establish suitable experimental systems which may bring about short-term energy/metabolic perturbations and which would reflect on the root development. For this purpose, we would like to treat *A. thaliana* seedlings with low light, extended night and unexpected darkness. Lateral root development will be closely monitored as a quantifiable output.

Next aim is to establish a mechanistic link between the treatments and the response observed on the lateral roots. The SnRK1-bZIP network has been previously established as candidates important in modulating gene expression and metabolic adaptation under stress (Pedrotti et al., 2018). We aim to use reverse genetics and confocal imaging to localize target proteins to demonstrate if the SnRK1-bZIP network is important for changes in the lateral root development under short-term perturbations.

Final step will be to identify the downstream targets of the predicted SnRK1-bZIP signalling impacting lateral root development. We will employ high-throughput sequencing approaches to know the possible downstream targets.

Overall, our study will focus to provide information on a signalling pathway important for lateral root development under short-term energy perturbations.

2. MATERIALS AND METHODS

2.1 Materials

2.1.1 Plants

Table 1: *A.thaliana* wild-type and mutant lines used in this study have been listed below.

Ecotype/Mutant	Characteristic	Reference
Wassilewskija (WS)	Wildtype	
Columbia (Col-0)	Wildtype	
Landsberg	Wildtype	
XVE:amibZIP2/11/44	Col-0, Estradiol-inducible artificial microRNA over bZIP2/11/44	Weiste and Dröge-Laser, 2014
snrk1.α1	Col-0, *KIN10*-Knockout	Pedrotti et al, 2018
snrk1.α2	Col-0, *KIN11*-Knockout	Pedrotti et al, 2018
bzip63	WS, Knockout	Mair et al, 2015
bzip63-CR	Col-0, CRISPR-Cas9 induced *bzip63* loss-of-function	Muralidhara et al, Unpublished
SnRK1.α1:GFP	SnRK1.α1 with GFP-tag	Bitrian M et al, 2011
pbzip63:bZIP63:YFP	WS-2, Complementation line with C-terminal fusion of YFP-Tag	Mair et al, 2015
bZIP63 S/A	Col-0, Complementation line, in the Serine residues S29/S294/S300 were exchanged for Alanine	Mair et al, 2015
pASN1:LUC	Promoter *ASN1* tagged to Luciferase	Baena-González, Unpulished

XVE:bZIP11	Col-0, Estradiol-induced overexpression	Weiste and Dröge-Laser, 2014
*pGATA23:*NLS-GFP	GATA23 N-terminal fusion of GFP tag under the native promoter	De Rybel et al, 2010
bzip11-CR	Col-0, CRISPR-Cas9 induced bZIP11 loss-of-function	Weiste et al, Unpublished
bzip44-CR	Col-0, CRISPR-Cas9 induced bZIP44 loss-of-function	Weiste et al, Unpublished
pbZIP11:bZIP11-UTR:GFP	bZIP11 without 5' UTR tagged to GFP under native promoter	Weiste et al 2017

2.1.2 Bacteria

Table 2: Bacterial strains used in this study in cloning protocols are listed below

Strain	**Properties**
Escherichia coli DH5α	Chemical competent
Agrobacterium tumefaciens GV3101 pMP90	Electrocompetent, Resistence to Rifampicin und Gentamycin

2.1.3 Vector used in CRISPR-Cas9 cloning protocol

Egg Cell Specific Promoter (ECP) and enhancer driven Cas9 binary vector – pHEE401E which is suited for both *A. tumefaciens* and plant transformation was used in this study. They have kanamycin and hygromycin resistant cassettes.

2.1.4 Oligonucleotides

Oligonucleotides (primers) used for CRISPR-Cas9 gene editing, for sgRNA cloning and sequencing was designed according to the protocol in the published manuscript (Wang et

al.,2015). For qRT-PCR expression analysis, the primers were designed using Universal Probe Library (Roche). For ChIP-PCR binding analysis primers were designed using GeneiousR-7.0.6. All primers were obtained from Invitrogen. The lyophilized oligonucleotides were diluted to a stock-concentration of 100 µM with distilled Milli Q water. For usage, aliquots with a working concentration of 10 µM were prepared by dilution with distilled Milli Q water. Primers were stored at -20 °C.

Table 3: Primers used in this study

Gene Name	**Forward**	**Reverse**	
bZIP63	ATTGAGATTCTCCGTCGTCTGCAG	AAACCTGCAGACGACGGAGAATCT	**CRISPR-Cas9 Gene editing**
ARF19 (G-Box 1)	AAGACATCAAGTGGGGTGCC	TTGGGATCGGATACATGCGG	**ChIP-PCR**
ARF19 (G-Box 2)	GGTCAAAACCTCCCCCACTA	GGACCGGAGTAGAGTTGTTCC	**ChIP-PCR**
ARF19 (G-Box 3)	TCGTTTTGATGAGGAGTGATTTCT	GCTGCGCGTGGAGAGTATAT	**ChIP-PCR**
Actin7	CGTTTCGCTTTCCTTAGTGTTAGCT	AGCGAACGGATCTAGAGACTCACCTT	**ChIP-PCR**
Actin8	GGTTTTCCCCAGTGTTGTTG	CTCCATGTCATCCCAGTTGC	**ChIP-PCR**
EF1A	ATGCCCCAGGACATCGTGATTTCAT	TTGGCGGCACCCTTAGCTGGATCA	**qRT-PCR**
ASN1	CACGTGTACGGCTCTAAAGCA	GACCAGCTGTTTCCACGTGTT	**qRT-PCR**
ARF19	AGCTGGAGATAGGCCAAGCC	TCTGTGCGTCCTTCATCCCA	**qRT-PCR**
bZIP63	GAAGAAATCTCCGGTAACCATCAC	GATTCTCCGTCGTCTGCAGC	**qRT-PCR**

2.1.5 Antibiotics

All the antibiotics used in this work are summarized below. Stock solutions were stored at -20 °C

Table 4: Antibiotics used in this study

Antibiotic	Stock Concentration	Final Concentration
Gentamycin (Gent)	50 mg/mL	50 µg/mL
Kanamycin (Kan)	50 mg/mL	50 µg/mL
Rifampicin (Rif)	20 mg/mL	20 µg/mL
Hygromycin (Hyg)	50 mg/mL	50 µg/mL

2.1.6 Equipments

Table 5: Equipment used to perform scientific experiments

Equipment	Model	Manufacturer
Gel-Documentation system	ChemiDoc™ MP Imaging System	BIO-RAD
Vibrator Mill	MM 400	RETSCH
Heat Block	Thermomixer compact	Eppendorf
Confocal Microscope	SP8 Convocal Laser Scan-ning Microscope	Leica
Spectrophotometer	V-1200	VWR
Electrophoresis Unit	Gene Pulser™	BIO-RAD
Spectrophotometer	Nanodrop 2000	Thermo Scientific
Thermo Cycler PCR	T100™ Thermo Cycler	BIO-RAD
Thermo cycler qPCR	C1000 Thermal cycler CFX 96 RT-System	BIO-RAD
Table Centrifuge	Centrifuge 5417C	Eppendorf

Cooling Centrifuge	5417R	Eppendorf
Vortexer	Vortex Genie 2	Scientific Industries
Large Centrifuge	Rotina 420R	Hettich

2.1.7 Software

Table 6: Software used for measurements and analysis of experiments

Software	**Company/Reference**
Excel	Microsoft
Geneious R6 (6.1.6)	Biomatters
ImageJ 1.48v	National Institutes of Health
Leica Application Suite V2.6	Leica Microsystems
Origin Pro	Origin Lab Corporation
qRT-PCR- CFX Manager V3.1	Bio Rad
Nanodrop 2000/2000c	Thermo Fischer
ChIPseek- Genome Annotation	Chen et al., 2014
ShinyGo – Gene Ontology	Ge et al., 2019
Burrows Wheeler Alignment-BWA	Li and Durbin, 2010
MACS2-Peak calling	Zhang et al., 2008
Integrated Genome Viewer-IGV	Thorvaldsdóttir et al., 2013

2.1.8 Chemicals

Table 7: List of chemicals used for preparing buffers, media and reagents

Chemical	**Company**
Agar	Carl Roth GmbH & Co. KG
Antibiotics	AGS
Chloroform	Merck KGaA
DNA stain G	SERVA Electrophoresis GmbH

dNTPs	MBI Fermentas
EDTA	Fermentas
Ethanol	Merck KGaA
Formaldehyde	Carl Roth GmbH & Co. KG
Gelrite	Carl Roth GmbH & Co. KG
Glycine	Carl Roth GmbH & Co. KG
Magnesium Chloride	Carl Roth GmbH & Co. KG
β-Mercaptoethanol	Carl Roth GmbH & Co. KG
Luciferin	Synchem
MS Media	Duchefa Biochemie B.V
Sodium Hypochloride	Carl Roth GmbH & Co. KG
B-Estradiol	Carl Roth GmbH & Co. KG
Phytoagar	Duchefa Biochemie B.V
PMSF	AppliChem GmbH
Sucrose	Carl Roth GmbH & Co. KG
Glucose	Carl Roth GmbH & Co. KG
Sybr Green	Lonza
Silwet	Lehle Seeds Company
Triton X 100	Carl Roth GmbH & Co. KG
Tween 20	Sigma-Aldrich Co.
Hydrochloric Acid	Hedinger GmbH & Co. KG
Tris	Carl Roth GmbH & Co. KG
Cetyltrimethyl ammoniumbromide	Carl Roth GmbH & Co. KG
Sodium Chloride	Carl Roth GmbH & Co. KG
Dipotassium phosphate	Carl Roth GmbH & Co. KG
Monopotassium phosphate	Carl Roth GmbH & Co. KG
Glycine	Carl Roth GmbH & Co. KG
Hxyleneglycol	Carl Roth GmbH & Co. KG
Percoll	
Acetic Acid	Carl Roth GmbH & Co. KG
SDS	Carl Roth GmbH & Co. KG

Protease Inhibitor	
Hepes	Carl Roth GmbH & Co. KG
Sodium Phosphate	Carl Roth GmbH & Co. KG
Zinc Sulphate	Carl Roth GmbH & Co. KG
Sarkosyl	Roche
Trehalose	Carl Roth GmbH & Co. KG
Methanol	Carl Roth GmbH & Co. KG

2.1.9 Consumables

Table 8: List of consumables used in this study

Consumables	**Company**
Glass Material	Brand, Schott
Plastic Material	Sarstedt, Eppendorf, Greiner, Roth
Leucopore	BSN-Medical
Parafilm	BEMIS-COMPANY, INC
PVDC-Membrane	Hartenstein

2.1.10 Enzymes

Table 9: List of enzymes used in this study

Enzyme	**Concentration**	**Company**
DreamTaq™ DNA-Polymerase	5 U/µL	Thermo Scientific
BIOTAQ™ DNA-Polymerase	5 U/µL	BIOLINE
Reverse Transcriptase	200 U/µL	Thermo Scientific
DNAse I	1 U/µL	Thermo Scientific
Restriction enzyme Bsa I	10 U/µL	NEB
T_4-Ligase HF	400 U/µL	NEB

2.1.11 Molecular Biology Kits

Table 10: Kits used in DNA and RNA extraction

Kit	Company
NucleoSpin® Gel extraction and PCR Clean-up	Macherey- Nagel
NucleoSpin® Plasmid DNA purification	Macherey- Nagel
RNA extraction kit	Qiagen
DNA purification kit	Qiagen

2.1.12 Antibody

Antibody	Units	Company
Anti-GFP-ChIP grade antibody	1:1000	Abcam (Ab290)

2.1.13 Growth Chambers

Table 11: Different growth chambers used in this study to grow plants

Growth Chamber	Company
Climate Chamber	BINDER GMbH
Percival	Percival Co
Dark Box	Werkstatt University of Würzburg

2.1.14 Growth Medium

LB-Medium (Sambrook et al., 1989):

10 g/L Trypton

5 g/L Hefeextract

10 g/L NaCl

Adjust pH to 7.4 with NaOH

YEB-Medium (Sambrook et al., 1989):

10 g/L Beefextract

2 g/L Hefe-Extract

5 g/L Peptone

5 g/L Sucrose

2 mM $MgSO_4$

Adjust pH to 7

MS Medium for Plant Growth (Murashige und Skoog, 1962)

2.2 g/L MS salts

8 g/L Phytoagar

pH adjusted to 5.2

MS Gelrite Medium

2.2 g/L MS salts

8 g/L Gelrite

pH adjusted to 5.2

2.1.15 Buffers

CTAB (DNA-Extraction):

2 %	CTAB (Cetyl Trimethyl Ammonium Bromide)
100 mM	Tris-HCl pH 8.0
20 mM	EDTA pH 8.0
1.4 M	NaCl
2 %	ß-Mercaptoethanol

TAE 50X:

242 g	Tris-base
100 %	Acetic Acid
0.5 M	Sodium EDTA

35 % Percoll Bed

17.5 mL	Percoll
0.5 M	Hexylenglycol (2.98 g Hexylenglycol)
50 mM	PIPES-KOH pH7.2 (5 mL of 0.5 M Stock)
10 mM	$MgCl_2$ (500 µL aus 1 M Stock)
1 %	Triton X-100 (500 µL of 100 %)

Make up the volume with 50 mL water

5 mM β-Mercaptoethanol (17.5 µL)

Crosslinking Buffer (ChIP):

50 mM	Potassium Phosphate buffer pH 5.8
1 %	Formaldehyde

Elution Buffer (ChIP):

0.1 M	Glycin pH 2.5 mit HCl (5 mL from 1 M)
500 mM	NaCl (5 mL from 5 M)
0.05 %	Tween20 (25 µL)

Make up the volume with 50 mL water

Extraction Buffer (ChIP):

1 M	Hexylenglycol (5.968 g)
50 mM	PIPES-KOH pH 7.2 (5 mL from 0.5 M)
10 mM	$MgCl_2$ (500 µL aus 1 M)

Make up the volume with 50 mL water

5 mM	β-Mercaptoethanol (17.5 µL)

Protease Inhibitor 1 tablet for 10 mL (5 Tabs)

Glycine Buffer (ChIP):

50 mM	Potassium Phosphate Buffer pH 5.8
0.3 M	Glycine

Gradient Buffer (ChIP):

0.5 M	Hexylenglycol (2,98 g)
50 mM	PIPES-KOH pH7.2 (5 mL from 0.5 M)
10 mM	$MgCl_2$ (500 µL from 1 M)
1 %	Triton X-100 (500 µL from 100 %)

Make up the volume with 50 mL water

5 mM	β-Mercaptoethanol (17.5 µL)

RipaF (ChIP):

50 mM	Hepes/NaOH pH7.4 (50 mL from 0.5 M)
140 mM	NaCl (14 mL from 5 M)
1 mM	EDTA pH 8.0 (1 mL from 0.5 M)
1 %	Triton X-100 (5 mL from 100 %)
0.1 %	DOC (Sodium Deoxycholate) (5 mL from 10 %)
0.1 %	SDS (2.5 mL from 20%)

Make up volume with 500 mL water

RipaF -SDS (ChIP):

50 mM Hepes/NaOH pH7.4 (5 mL from 0.5 M)

140 mM NaCl (1.4 mL from 5 M)

1 mM EDTA (100 µL from 0.5 M)

1 % Triton X-100 (500 µL from 100 %)

0.1 % DOC (500 µL from 10 %)

Make up the volume with 50 mL water

Sonic Buffer -SDS (ChIP):

10 mM Tris/HCl pH 7.4 (1 mL from 0.5 M)

1 mM EDTA pH 8.0 (100 µL from 0.5 M)

Make up the volume with 50 mL water

Sonic Buffer 0.25 % SDS (ChIP):

10 mM Tris/HCl pH 7.4 (1 mL from 0.5 M)

1 mM EDTA pH 8.0 (100 µL from 0.5 M)

0.25 % SDS (625 µL from 20 %)

Make up the volume with 50 mL water

Sonic Buffer 0.5 % SDS (ChIP):

10 mM Tris/HCl pH 7.4 (1 mL from 0.5 M)

1 mM EDTA pH 8.0 (100 µL from 0.5 M)

0.5 % SDS (1.25 mL from 20 %)

Make up the volume with 50 mL water

Protease Inhibitor 1 tablet for 10ml (5 Tabs)

MC-Buffer (ChIP-Seq)

10 mM Sodium Phosphate buffer, pH 7.0 (50 mL from 0.1 M)

50 mM NaCl (5 ml from 5 M)

100 mM Sucrose (50 mL from 1 M)

Make up the volume to 500 mL with water

MC-Buffer (ChIP-Seq)

10 mM	Sodium Phosphate buffer, pH 7.0 (30 mL from 0.1 M)
100 mM	NaCl (6 mL from 5 M)
10 mM	B-Mercaptoethanol (210 µL from 14.4 M)

Make up the volume with 300 mL water

Protease Inhibitor 2 tablet for 150 mL (2 Tabs)

M1-Buffer (ChIP-Seq)

18.4 mL	Hxyleneglycol
141.6 mL	Master-M-Buffer

M2-Buffer (ChIP-Seq)

10 mM	MgCl2 (1.2 mL from 1 M)
0.5%	Triton-X-100 (6 mL from 10 %)
112.8 mL	Master-M-Buffer

Sonic Buffer (ChIP-Seq)

10 mM	Sodium Phosphate pH 7.0 (1 mL from 0.1 M)
100 mM	NaCl (200 µL from 5 M)
1 %	Sarkosyl (500 µL from 10 %)
10 mM	EDTA (1 mL from 0.1 M)
1 X	Complete protease inhibitor 25 X (400 µL from 25 X)
1 mM	PMSF (100 µL from 100 mM)
6.8 mL	Water

IP-Buffer (ChIP-Seq)

50 mM	Hepes pH 7.5 (2.5 mL from 1 M)
150 mM	KCL (2.5 mL from 3 M)
5 mM	MgCl2 (250 µL from 1 M)
10 µM	ZnSo4 (50 µL from 10 mM)
1 %	Triton-X-100 (5 mL from 10 %)
0.05 %	SDS (250 µL from 10 %)
39.4 mL	Water

Extraction solvent (LC-MS)

MeOH/Water 50:50

Internal standard mix

0.2 µg/µL 1,1-d_2-Trehalose (MW: 344.31 g mol^{-1})

0.8 µg/µL 6,6-d_2-Glucose (MW: 182.17 g mol^{-1});

Final amounts: m(d_2-Glu) = 8 µg, m(d_2-Tre) = 2 µg.

2.2 Methods

2.2.1 Plant cultivation and transformation

2.2.1.1 Plant material and culture

A.thaliana wild-type ecotypes- Col-0, WS and Ler and all transgenic lines listed in table 1 were surface sterilized by placing seeds in a 2 mL dry eppendorf tube and then in a rack. The rack is then placed in a desiccator next to the beaker containing 100 mL Sodium hypochlorite (bleach) and 6 mL 37 % Hydrochloric acid for 3 h. Seeds were then placed under the sterile fume hood for 45 minutes to evaporate the chloride gas. They were then grown on round petri dishes (8.6 cm diameter) containing half strength Murashige-Skoog (1/2 MS) medium with phyto agar and stratified for 48 h in dark and in 4 ^{o}C. They were then transferred to long day conditions (16 h Light at 23 ^{o}C /8 h dark at 16 ^{o}C) at 100 µmol m^{-1} s^{-1}, relative humidity of 60 % and grown for 5 or 8 days until different short-term darkness treatments mentioned below.

2.2.1.2 Analysing root architecture (primary root length, lateral root number and density) under low-light treatment

8-day-old seedlings were used for studying root architecture. Control seedlings were under long day conditions. Seedlings used for low-light treatment were subjected to 15 μmol m^{-2} s^{-1} intensity for different time-points -24 h to 72 h (for example: 16 h of low light during the day regime followed by 8 h of dark regime on day 1 and an additional 8 h of low light during the day regime of day 2 which constitutes to 24 h of low light – refer figure 11). After the low-light treatment, seedlings were transferred back to long day conditions and root growth (primary root length and lateral root number) was measured at day 14 (6^{th} day post treatment). Plates were scanned with a (plustek opticbook 3600 plus) scanner and images were saved in .tiff format. Primary root length of all seedlings was measured from the end of the hypocotyl to the root tip by using the free-hand tool of Fiji (Schindelin et al., 2012). The primary root length was converted to centimetre (cm) keeping diameter of the agar plate in mind. Emerged lateral roots (eLR) were carefully counted all along the primary root. eLR is calculated by dividing the number of lateral roots with the length of the primary root in cm.

2.2.1.3 Analysis of root architecture under unexpected darkness

8-day-old seedlings on new agar plate were subjected to complete darkness for different time-points (0.5 h to 4 h) (10 am to 2 pm) during the 16 h light cycle (figure 13). After the darkness treatment, seedlings were transferred back to long day conditions and root growth was measured on day 14 after germination. Primary root was measured, emerged lateral root was counted and eLR density was calculated.

2.2.1.4 Analysis of root architecture under extended night treatment

8-day-old seedlings on new agar plate were subjected to extended night for 6 h immediately after the end of the night cycle. After extended night, seedlings were transferred back to long day conditions and root growth was measured at day 14 after germination (figure 12). Primary root length was measured, emerged lateral roots were counted and eLR density was calculated.

2.2.1.5 Analysis of root architecture with supplementation of basic sugars

8-day-old seedlings transferred on to the media containing sugars. ½ MS in phyto agar was supplemented with 1 % sucrose, glucose, and mannitol (as osmotic control). Seedlings were subjected to unexpected darkness for 4 h (treatment similar to figure 13) and after the unexpected darkness treatment, seedlings were transferred back to long day conditions and root growth was measured on day 14 after germination. Primary root length was measured, emerged lateral roots were counted and eLR density was calculated.

2.2.1.6 Analysis of root architecture for measurements with β-estradiol inducible transgenic plants

8-day-old XVE-bZIP11 and XVE-amibZIP2/-11/-44 lines were transferred one day before the darkness treatment on ½ MS agar plates with 10 µM β-estradiol. 4 h of unexpected darkness was given the next day and seedlings were transferred back to long day conditions after the treatment. Primary root length was measured, emerged lateral roots were counted and eLR density was measured on day 14 after germination

2.2.1.7 Floral dip transformation of *A. thaliana*

Bacteria *A. tumefaciens* has the distinct ability to transform the Ti plasmid into the plant cell and randomly insert them into the genome. The method was adapted and modified from (Clough and Bent, 1998). For flower dip transformation 6-week-old *A. thaliana* plants grown under long-day regime (16 h light/8 h dark) were used. To ensure high transfection efficiency we utilized plants with mature floral organs but with not many developed siliques and healthy plants. To prepare the floral dip solution a 3 mL LB pre-culture of *A. tumefaciens* carrying the constructs of interest was grown at 28 °C overnight. The next day 100 µL of pre-culture were used to inoculate 250 mL YEP media and the culture was again grown overnight at 28 °C. Bacteria were pelleted and re-suspended in a solution of ½ MS media, 5% sucrose and 0,02% of Silwet L-77. Re-suspended pellet was used to dip the inflorescence for 20 seconds to avoid uptake of several T-DNA copies. Plants were kept for one night to dry outside the growth chamber and were brought back in the growing chamber the next day.

2.2.2 Bacterial cultivation and transformation

2.2.2.1 Heat-shock transformation of chemically competent *E.coli* DH5α cells

E. coli transformations were conducted using the chemical competent strain *DH5-alpha* (modified protocol from Inoue et al., 1990). For transformation, 50 µL of competent cells were thawed on ice and mixed with 100 ng of the DNA or 5 µL of a ligation mixture. Tubes containing the bacteria and DNA were swirled gently and incubated on ice for 30 minutes. After incubation, cells were heated up to 42 °C in a heat block for 90 s and then immediately transferred on ice for 2 minutes. Then, 1 mL of LB medium was added to the cells and incubated at 37 °C for 1 h with shaking at 350 rpm. 50-75 µL of transformation mixture was plated on LB agar plates containing kanamycin (50 µg/µL) and incubated at 37 °C overnight. Colonies appeared after 24 h of incubation

2.2.2.2 Transformation of electro competent *A. tumefaciens* cells

The protocol was adopted and modified from (Koncz and Schell, 1986). Binary vector containing the desired DNA were transformed into *A. tumefaciens* strain GV3101. For transformation, 50 µL of electro-competent *A. tumefaciens* cells were thawed on ice, gently mixed with 50 ng of vector DNA and incubated for 2 minutes. After incubation, the mixture was transferred into an electroporation cuvette (2 mm gap). Electroshock was performed at 25 µF, 400 Ω, 2.5 kV using a Bio-Rad electroporator. 1 mL of YEP medium was immediately added to transformed cells and they were incubated at 28 °C with shaking for 2 h. After incubation the cells were centrifuged at 11,000 g for 3 minutes. Supernatant was discarded and the cell pellet was resuspended in 100 µL YEP medium. Finally, 50 µL of the bacterial culture was plated on media plates with rifampicin (20 µg/mL), gentamycin (50 µg/mL) and kanamycin (50 µg/mL) and incubated at 28 °C for 2 days. Following incubation, colonies appearing on plates were picked and streaked on a fresh YEP agar plate. The cells were incubated overnight at 28 °C. A colony PCR was set up to screen the colonies containing vector using insert-specific primers.

2.2.3 General Molecular Biological Methods

2.2.3.1 Genomic DNA isolation from plant cells

The method was adopted and modified from (Doyle and Doyle 1987). It involves extraction of DNA using CTAB buffer and chloroform. By addition of chloroform, the DNA dissolves better leaving other residues at the bottom. *A. thaliana* leaves (2 to 3 in number) were harvested in 2 mL eppendorf tubes containing about 1-2 metal beads and were quickly frozen in liquid nitrogen. The tubes were transferred pre-cooled grinding jar and ground to homogenize the leaves.300 µL of CTAB extraction buffer was added and the sample was mixed well by vortexing. The mixture was incubated for 15 minutes at 65 ^{o}C. To this an equal volume of a chloroform/isoamyl alcohol mixture (24:1) was added and incubated at RT for 2 minutes. The samples were centrifuged down at 11,000 g for 5 minutes. 300 µL supernatant was added to 300 µL of isopropanol and mixed well. The mixture was centrifuged, and the supernatant was discarded. The obtained pellet was washed with 70 % EtOH for 5 minutes. After washing the

pellet with EtOH and discarding the supernatant completely, the samples were kept at 37 ^{o}C for 10 minutes. After drying, the pellet was dissolved in 50 µL of water and stored at -20°C.

2.2.3.2 Separation of DNA molecules by agarose gel electrophoresis

Gel electrophoresis is a technique wherein, an electrical field is used to move the negatively charged DNA through an agarose gel matrix towards a positive electrode to separate DNA by size (e.g., length in base pairs). Depending on the agarose concentration in the gel, short (up to 2 % agarose) or longer (as low as 0.8 % agarose) DNA sequences can be more efficiently separated. DNA samples were mixed with 5 X DNA loading buffer (Orange G in deionized water). Depending on the size of the DNA fragment, different concentrations (0.8 % or 2 %) of agarose powder was dissolved in 1X TAE buffer. To visualize the DNA fragments, SERVA DNA stain G was added to the gel with a final concentration of 0.05 (v/v). Besides the samples, 5 µL of the 1 Kb DNA-ladder (GENE RULER), was applied to the pockets and the agarose gel was run for 45-60 minutes at 120 V. The gel was photographed under UV light of a wavelength of 260-360 nm, using the gel imager.

2.2.3.3 Mini Scale Plasmid DNA isolation from E. coli

For plasmid isolation, 5 mL of LB-medium containing kanamycin antibiotic was inoculated with a bacterial colony from a plate using a sterile yellow pipette tip. The cultures were grown overnight at 37 °C. Plasmid DNA was isolated using the Nucleospin Plasmid DNA isolation kit (Machery Nagel).Overnight cultures were harvested by centrifugation at 11,000 g for 3 minutes, the supernatant was discarded, and plasmid isolation was performed according to the manufacture`s protocol as described below.

- The cell pellet was resuspended in **250 µL of Buffer A1** with RNAse and vortexed until the pellet was dissolved.
- **250 µL of Buffer A2** was added and mixed gently 6-8 times to avoid shearing of genomic DNA. The mix was incubated at room temperature for up to 5 minutes till the lysate became clear.

- **300 µL of Buffer A3** was added to the mixture and thoroughly mixed by inverting 6-8 times.
- The mixture was centrifuged for 5 minutes at 11,000 g at RT. Supernatant was carefully aspirated to avoid picking up impurities and added to the DNA binding column in a collection tube. The mixture was centrifuge for 1 minutes at 11,000 g.
- **600 µL of Buffer A4** supplemented with ethanol was added to the mixture. This was centrifuged for 1 minutes at 11,000 g. Supernatant was discarded.
- The empty column in a new collection tube is centrifuged for 2 minutes at 11,000 g to dry the silica membrane of the column and to remove residual ethanol.
- DNA was eluted with 50 µL clean milliQ water.

The plasmid concentrations were determined using a spectrophotometer Nanodrop (Thermo Scientific- 2000 c- UV-VIS spectrophotometer).Milli Q water (1.5 µL) was used as reference and the NanoDrop™ software was set to measure DNA.To determine the concentration,1.5 µL of each sample was carefully pipetted onto the detection surface and measured.The absorption of light by aqueous solutions of DNA was measured at 260 nm. To determine the purity of the nucleic acids the absorption of proteins at 280 nm was also measured. The ratio between OD260/OD280 always represent a measure of the degree of purity.The degree of purity of the samples was between 1.7 and 2.0.

2.2.3.4 Sanger DNA sequencing

All amplified PCR products or plasmids were sequence verified by Sanger sequencing at LGC genomics (www.lgcgenomics.com). For this purpose, 500-1000 ng of DNA was mixed with 2µL (10 µM) of sequence specific primer in a 1.5 mL Eppendorf microcentrifuge tube and was made up to 14 µL in volume with MilliQ water. The determined DNA sequences were then analysed with the help of Geneious-R7 analysis program (/www.geneious.com).

2.2.3.5 RNA isolation from *A. thaliana* roots

8-day-old wild-type and transgenic plant seedlings with and without treatments *(Time course- 1 h control/darkness, 2 h control/darkness 4 h control/darkness, 4 h dark + 8 h light recovery control/darkness, 4 h dark + 16 h light recovery control/darkness)*, were harvested carefully below the hypocotyl to obtain 5-10 mg of roots. They were harvested in 2 mL Eppendorf centrifuge tubes containing 1 metal bead and was frozen in liquid nitrogen quickly. The tubes were quickly transferred to a pre-cooled grinding jar to homogenize the tissue. The RNA was isolated using the Qiagen RNeasy Micro Kit. Isolation was performed according to manufacturer's protocol described below.

- **350 µL of RLT** buffer was added to the homogenized tissue. Mixed gently and the mix was centrifuged at 11,000 g for 2 minutes. Supernatant was carefully removed and added into a fresh 1.5 mL Eppendorf tube with equal volume of 70 % EtOH in DEPC water.
- This sample including any precipitate was transferred to an RNeasy MiniElute spin column placed in a 2 mL collection tube. This was centrifuged for 15 s at 8000 g and the flow-through was discarded.
- The spin column was placed in a new 2 mL collection tube and **500 µL of Buffer RPE** was added to the spin column. The mixture was centrifuged at 8000 g for 15 s. Flow-through was discarded.
- 500 µL of 80 % EtOH in DEPC water was added to the spin column and centrifuged for 2 minutes at 8000 g to wash the RNA. The flow-through was discarded.
- The spin column was placed in a new 2 mL collection tube and centrifuged at top speed to remove the residual EtOH and to dry the pellet.
- The spin column was placed in a new 1.5 RNA free collection tube and RNA is eluted with 20-30 µL of DEPC water.

The RNA concentrations were determined using a spectrophotometer Nanodrop (Thermo Scientific- 2000 c- UV-VIS spectrophotometer). MilliQ water (1.5 µL) was used as reference and the NanoDropTM software was set to measure RNA. To determine the concentration, 1.5 µL of each sample was carefully pipetted onto the detection surface and measured. The absorption of light by aqueous solutions of RNA was measured at 260 nm. To determine the purity

of the nucleic acids the absorption of proteins at 280 nm was also measured. The ratio between OD260/OD280 always represent a measure of the degree of purity. The degree of purity of the samples was above 2.0.

2.2.3.6 cDNA synthesis from total plant RNA

cDNA was synthesized from 1 µg of total RNA extracted from roots using the Thermofischer scientific RevertAid first strand cDNA synthesis kit. Genomic DNA from the RNA sample was removed by treating the sample with 1 µL of *DNase I* and 1 µL of 10X *DNase* buffer containing $MgCl_2$ and incubated at 37 ^oC for 30-45 minutes. To this mixture, 1 µL 50 mM EDTA was added and incubated at 65°C for 10 minutes.RNA hydrolyses during heating with divalent cations in the absence of a chelating agent,EDTA was therefore used. 0.2 µL of oligo (dT) primers and 1 µL of random nonamer primers are added and incubated for 10 minutes at 70 ^oC. The tubes were cooled for 2 minutes on ice before the reverse transcriptase reaction. A master mix containing, 5 X Reaction Buffer, 10 mM dNTPs and RevertAid M-MuLV RT (200 U/µL) was prepared and added to the treated RNA sample. The reverse transcriptase reaction below was carried out.

Table 12: Reverse transcriptase reaction protocol

	Reaction Conditions	Time
Step 1	42 ^oC	70 minutes
Step 2	70 ^oC	10 minutes
Step 3	4 ^oC	Hold

The prepared cDNA is diluted 1:10 in DEPC water and used for qRT-PCR reactions

2.2.3.7 Quantitative real-time PCR (qRT-PCR)

qRT-PCR is a technique where the amplification of DNA (PCR reaction) can be monitored or quantified in real time (Livak and Schmittgen, 2001). Mix containing 2.5 mM dNTPs, 10 x *DNA polymerase* buffer, 50 mM $MgCl_2$, 10 mM of each forward and reverse primer mix and Sybr Green and 5 U/µL of *BIOTaq DNA polymerase* was added to the cDNA sample.The following PCR amplification conditions were applied:

Table 13: Conditions for PCR amplification

	Reaction Conditions	Time
Step 1	95° C	10 minutes
Step 2	95° C	20 seconds
Step 3	57 °C	20 seconds
Step 4	72 °C	20 seconds
	Goto Step 2	40 x
Step 5	95 °C	10 seconds
Step 6	70 °C	0.5 seconds
Step 7	Increment to 95 °C	5 seconds

Relative fold change was calculated from at least three independent biological replicates and three technical replicates for each biological replicate, by using the method by (Livak and Schmittgen, 2001). ΔCT value was calculated by subtracting the CT value of reference gene from the CT value of the gene under investigation.Since all calculations are in logarithm base 2, there was twice as much DNA, the CT values decrease by 1. The 2^ ΔCT is calculated to get the relative expression. To calculate the fold change, relative expression of the control was set to 1 and the difference in fold change was measured for each treated sample.

2.2.3.8 Chromatin Immunoprecipitation (ChIP) coupled with -qRT-PCR in *A. thaliana* roots

It is a technique used to investigate the interaction between a protein and DNA. It determines whether a specific protein is associated with specific genomic region (Kim and Dekker, 2018). We utilized 2 g of root material from 10-day-old wild-type (WS) and bZIP63:YFP plants after treatment with 4 h of unexpected darkness. The root tissue was incubated with cross-linking buffer (containing 1 % formaldehyde) for 15 min under vacuum. Samples were then incubated in glycine buffer for 5 min under vacuum and washed with ice-cold water 3 times. Samples were dried with paper towels then frozen in liquid $N_{2,}$ either stored in -80 degree or grinded fine using mortar and pestle for nuclei extraction. Nuclei extraction was performed at 4 °C and cold room with pre-cooled equipment. The ground root material was resuspended in 20 mL ice-cold extraction buffer and the contents were filtered through cell strainer into a clean beaker. 800 µL of 25 % cold Triton X-100 was added dropwise to the nuclei extract. This was incubated for 15 minutes and the nuclei were isolated by density-gradient centrifugation using a 35% percoll bed in a pre-cooled centrifuge for 30 minutes at 2000 g. Supernatant was discarded and the obtained pellet was resuspended in gradient buffer. The nuclei once again isolated by density gradient centrifugation using 6 mL 35 % percoll bed. Supernatant was discarded and the pellet was resuspended in 1 mL sonication buffer with SDS and incubated for 20 minutes. Another 0.5 mL of sonication buffer without SDS was added and mixed well before sonication. Chromatin was sheared with Bioruptor (Diagenode) for 10 x 3 cycles with 30 seconds at maximum power and 60 seconds of rest. Chromatin was cleared by centrifugation for 5 min at 11,000 g at 4°C and stored at -80°C.

For each IP 15 µg chromatin, 3 µg ChIP grade anti-GFP antibody (ab290) (Abcam, Cambridge, UK) was added and incubated for 4-6 h. 70 µL of protein G-coated magnetic beads (Invitrogen, Karlsruhe, Germany) dissolved in ice-cold RIPAF buffer, supplemented with protease inhibitor (Roche, Mannheim, Germany) was added to each sample. Antibody—antigen binding was achieved during a 4 h incubation step at 4 °C on a slow rotating Intelli-Mixer. Beads were washed five times (with incubation for 5 minutes each time) with RIPAF buffer supplemented with protease inhibitor, Protein-DNA complexes was eluted using 30-70 µL elution buffer.

Chromatin was incubated with 5 µL Proteinase K (Roche) overnight and purified using Qiagen DNA purification kit the following day (refer 2.2.3.9)

Precipitated DNA was quantified by q-RT-PCR using the oligonucleotide primers summarized in table 3. Data was normalized to DNA input (not-precipitated sample), which was quantified by employing *ACTIN8* (At1g49240) specific primers. Presented mean and SD values were calculated from three independent ChIP experiments that were performed on each of three independently prepared chromatin samples from wild-type (WS) and bZIP63:YFP plants, respectively.

2.2.3.9 Chromatin-Immunoprecipitation DNA Sequencing

A modified protocol from (Kaufmann et al., 2010) was adopted. 10-day-old *bzip63* loss-of-function and bZIP63:YFP were treated with 4 h of unexpected darkness. The roots were separated from the shoot and 10 g of root material was fixed with MC buffer with 1 % formaldehyde for 20 minutes (15 minutes in vacuum and 5 minutes without vacuum). Fixation was stopped by adding 2.5 mL glycine (1.25 M stock) and was incubated for 5 minutes in vacuum. Roots were then washed 3 times with MC buffer, dried and frozen in liquid N_2. Frozen tissue was ground well with mortar and pestle, and the powder was transferred to a 50 mL falcon containing M1 buffer. The slurry was passed through two layers of miracloth and an additional of 5 mL M1 buffer was added to quantitatively collect nuclei in the filtrate. The mixture was centrifuged at 1,000 x g for 20 minutes at 4°C. The pellet obtained was washed with M2 Buffer for 5 times. The pellet was finally washed with M3 buffer and the crude nuclear pellet was resuspended in Sonic buffer. Chromatin was sheared with Covaris (Duty Cycle: 20%; Intensity: 5; Cycles per Burst: 200; Cycle time: 2 minutes). Sheared samples were centrifuged at 11,000 g for 5 minutes at 4°C. 750 µL of the supernatant was mixed with equal volumes of IP buffer and the remaining 250 µL was used as input DNA. 3 µg of ChIP grade anti-GFP antibody (Ab290) was added to the IP samples and incubated overnight on rotating wheel at 4°C. On day 2, the IP mix was centrifuged at 11,000 g for 2 minutes at 4°C. The supernatant was mixed with 40 µL protein A-agarose beads (Santa Cruz Biotechnology sc-2001). The beads and the IP mix were incubated for 6 h at 4°C. Beads were pelleted by centrifuging at 20,000 g for 2 minutes at 4°C. Supernatant was saved as post-binding fraction. The pellet was washed with 1 ml IP-buffer for 5 times (4x at 4°C, 3’ spins max; last wash at RT). Supernatant was discarded and DNA was eluted with 100 µL ice cold glycine elution buffer. The mixture was vortexed for 30 s then centrifuged at 20,000 g for 1 minute at RT. The supernatant was transferred to a fresh tube with 150 µL of TRIS. 1 µL RNase A/T_1 (10 mg/mL) was added to both IP and input

and incubated at 37°C for 15 minutes. 1.5 µL of proteinase K (Roche) was added and mixed by vortexing. This was incubated at 37 °C overnight. On day 3, a second aliquot of proteinase-k was added and incubated for 6 h at 65 °C.

The DNA from both IP and input sample were column purified using MiniElute (QIAGEN) DNA kit according to manufacturer's protocol.

- IP sample was split in half and **3x vol ERC buffer** was added
- 40 µL .2 micron filtered (Sigma112K8928) 3 M NaAc was added to ppt samples to stabilize the pH
- 700 µL of the mixture was added to the column and centrifuged at 11,000 g for 1 minute, the flow-through was discarded and the procedure was repeated for the remaining amount of sample.
- Washed once with 750 µL PE buffer and centrifuged for 1 minute at 11,000 g and the flow-through was discarded. Centrifuged for 1 more minute to dry the membrane and remove the residual ethanol.
- Eluted with 30-35 µL MilliQ water

Precipitated DNA was quantified by q-RT-PCR using the oligonucleotide primers summarized in table 3.

Library preparation and Illumina high-sequencing was carried out at Novogene Hongkong using the NEB Next Ultra II DNA Library Preparation Kit for Illumina (NEB).

For ChIP-sequencing analysis, raw data from ChIP-seq was trimmed of adapters and the reads were mapped to the *A. thaliana* (TAIR 10) genome with BWA-Burrows Wheeler Alignment (Li and Durbin, 2010) with default parameters. Mapped reads were sub sampled (**refer to pipeline in supplementary)** and peak calling for transcription factor binding was performed with MACS v2.1.1 (Zhang et al. 2008). For regular peaks the cut off value was kept at of 9.00e+07 and q value of 0.01. For visualization, read density files containing peak information in bedgraph format was generated using the BEDTools v2.26.0 (Quinlan and Hall 2010) and the Integrative Genomics Viewer (Robinson et al. 2011). Genome annotations, pie chart to predict percentage of promoter TSS binding was analysed using ChIPSeek online web tool (Chen et al., 2014).

2.2.3.10 Generation of transgenic Arabidopsis loss-of-function plants using Crispr-Cas9 technology and analysis of mutants

The technique utilizes RNA-guided DNA endonuclease Cas9 from the bacterial immune system CRISPR (clustered regularly interspaced short palindromic repeats). CRISPR/Cas9 system uses a single guide RNA (sgRNA) which has sequence specificity and forms a sgRNA/Cas9 complex to produce double-strand breaks at the genomic sites specified by these guide RNAs. These double stranded breaks are joined via non-homologous end joining (NHEJ) which is known to be error prone. This makes small deletions or insertions in the genomic sites which lead to premature stop or truncated/unfunctional protein after translation (Hsu et al., 2014).

The current approach utilizes promoter of the egg cell *EC1.2* gene to drive the Cas9 gene. Specific expression of Cas9 in egg-cells and one-cell stage embryo lead to creation of homozygous or biallelic mutants already in the first generation with high efficiency.

To obtain this, a guide RNA for *bZIP63* gene was designed using CHOP CHOP, an online sgRNA prediction tool (https://chopchop.cbu.uib.no/). This single guide RNA (sgRNA) was generated within exon-1 of the *bZIP63* gene between 120 and 140 bp from the start ATG (figure 9). The sgRNA, which exhibited a high specificity score and no off-target was selected. In order to introduce the CRISPR construct into *pGATA23*:NLS-GFP transgenic line and Col-0 wild-type , we cloned the selected sgRNA into the egg-cell promoter driven Cas9 system allowing targeted mutation of bZIP63 (figure 10).

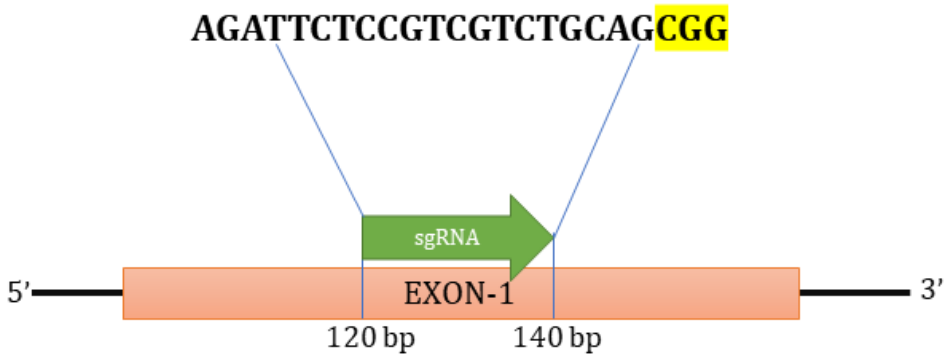

Figure 9: Schematic representation of the predicted sgRNA binding site within exon 1 of bZIP63. Predicted sgRNA for bZIP63 by CHOP CHOP tool (Labun et al., 2019). sgRNA site is between 120 and 140 bp of exon-1. Position of sgRNA is marked as green arrow on exon-1 and predicted sequence is highlighted in black. The PAM (protospacer adjacent motif), important for site recognition by sgRNA is present next to the sgRNA sequence and marked in yellow.

For single sgRNA cloning

Two complementary oligonucleotides were hybridized to generate guide RNA. After hybridization the fragment (insert) has the sticky ends for integration into pHEE401E vector. To generate an insert (sgRNA) 100 µmol/L of each forward and reverse primers were mixed and heated at 95^{o}C and cooled down at room temperature. Golden Gate reaction was carried out as follows to insert sgRNA into pHEE401E crispr-Cas9 vector.

Table 14*: Golden-gate protocol for generating sgRNA insert*

Component	**Volume**
Insert (50µMol/L)	2 µL
pHEE401E (~100ng/L)	2 µL
10x T4 DNA Ligase Buffer (NEB)	1.5 µL
10x *BsaI* buffer	1.5 µL
BsaI (NEB)	1 µL
T4 DNA Ligase (HC,NEB)	1 µL
ddH_20	5 µL
Total Volume	**15 µL**

Reaction Conditions	Time
37°C	5 h
50°C	5 minutes
80°C	10 minutes

3 µL of the golden-gate reaction mixture was transformed into *E.coli DH5a* cells. These were plated on LB agar plates containing the antibiotic *kanamycin* (50 µg/mL) as selection marker. 5 colonies were picked, and colony PCR was carried out to identify the correct colony.

Table 15: Reagents and protocol for colony PCR

Component	Volume
ddH_20	40 µL
Dreamtaq Buffer	5 µL
dNTP (10 nM)	1 µL
DreamTaq Polymerase	1 µL
U6-26p-Forward (10 mM)	1.5 µL
U6-26p-Reverse (10 mM)	1.5 µL

	Reaction Conditions	Time
Step 1	95° C	5 minutes
Step 2	95° C	30 seconds
Step 3	54° C	30 seconds
Step 4	72° C	50 seconds
	Goto Step 2	**34 x**
Step 5	72° C	5 minutes

DNA extracted from colonies with a clear amplification at 423 bp were considered positive. Plasmid was extracted from over-night culture of positive colony and was sanger sequenced. *Agrobacterium* mediated transfection of *A. thaliana* was carried out.

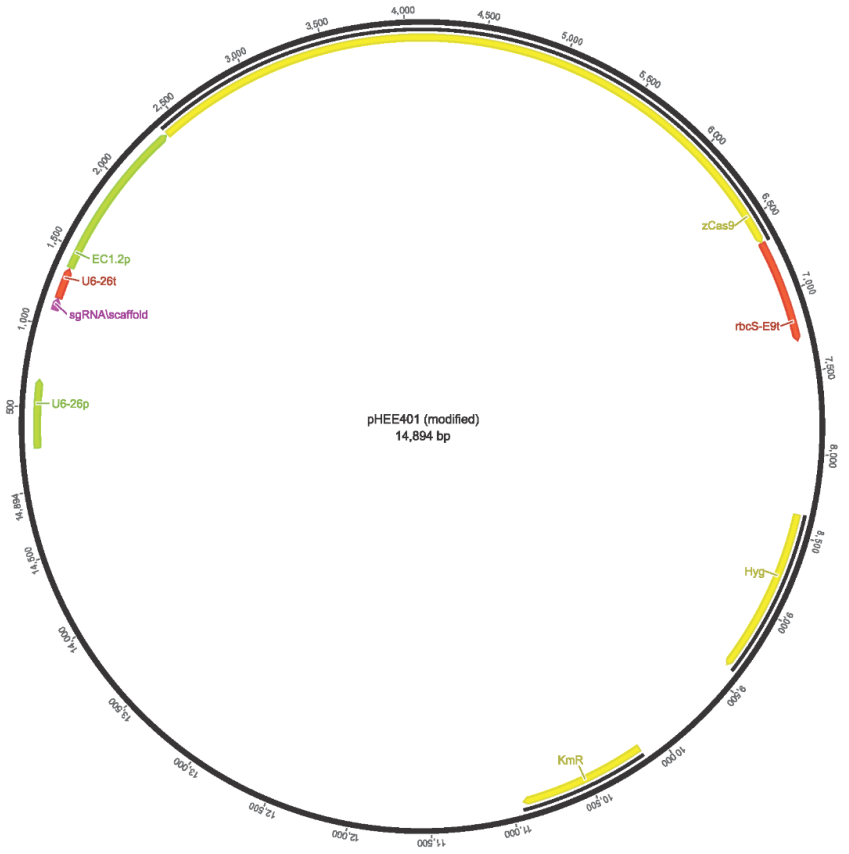

Figure 10: Diagram illustrating the assembly of sgRNA into pHEE401E vector. Presented is the CRISPR/Cas9 binary vector (pHEE401E), harbouring the zCas9 gene driven by the egg-cell specific promoter (ECP - Green) and a sgRNA (purple) driven by the Pol-III promoter U6-26p (green). The sgRNA is tagged to 76 bp scaffold RNA sequence and ends with terminator U6-29t (red). The expression module has kanamycin-Km^R for bacterial selection and Hygromycin - Hyg resistance cassette for selection of transgenic plants. The sgRNA module containing designed sgRNA sequence was inserted into destination vector pHEE401E through Golden Gate reaction.

Selection of positive transformants

The seeds collected from putative *A. thaliana* Col-0 T1 (first generation) transgenic plants were surface sterilized (refer 2.2.1.1) and were put on ½ MS medium containing hygromycin B (40 mg/L) and stratified in dark at 4 °C for 2 days. Following a stratification period seeds were incubated for 8 h at 22 °C in light, followed by incubation at 22° C in the dark for 3 days. The plants were grown until positive transformants could be distinguished by their elongated hypocotyl from non-transformants that did not grow. When green seedlings (T1) reached 3-4 leaf stage they were transferred to pots containing soil and grown until the leaves got bigger.

1-2 leaves from each plant were harvested to extract the genomic DNA, in order to PCR amplify targeted gene and check by sequencing for CRISPR mediated mutations

According to Wang et al. (2015), the specific expression of Cas9 in the egg cell can lead to the creation of mutant transgenic line already at T1 generation. In the next generation, the T1 heterozygous plants should be able to give rise to homozygous or bi-allelic mutant T2 plants or wild-type. We screened 30 plants in the T1 generation, among which two plants (figure 40), were homozygous mutants for *bZIP63*. The analyses was conducted by examining their sequencing chromatograms. The T2 progeny from self-fertilized T1 parent plant (P13) were further examined for the mutation at the same site.

2.2.4 Microscopy and Histology techniques

2.2.4.1 To study the localization pattern of *GATA23* in different stages of lateral root development

To determine *GATA23* expression from the lateral root initiation to the emergence with and without 4 h of unexpected darkness, 5-day old seedlings (grown under long-day regime: 16 h light/8 h dark) of *pGATA23*::NLS-GFP in WT or *bzip63* loss-of-function mutant background (*bzip63CR)*, respectively were treated with 4 h of unexpected darkness and transferred back to the growth cabinet under long day regime. Control (without dark treatment) was maintained under long-day growth conditions. After one-day recovery phase (16 h of light) seedlings were imaged using a Leica SP5 confocal microscope at 25x magnification for 8 individual roots. The whole root, from root tip to hypocotyl was scanned and the number of lateral roots at different stages (stage I to stage VII) of lateral root development and were counted in both control and darkness treated seedlings. Stack of individual images for each part of the seedling was obtained and the entire primary root was reconstructed using image tiles on MS PowerPoint.

2.2.4.2 To study the localization pattern of *SnRK1.α1, bZIP63* and *bZIP11* across the primary root

5-day-old seedlings grown under long-day conditions (16 h light/8 h dark) on ½ MS-phyto agar media without sugar were imaged from root tip up until 1.5 cm approximately of the primary root consisting of root apical meristem, transition zone, elongation and start of differentiation zone. Roots of 5 individual seedlings were imaged at 25 x magnification using the Leica SP5 confocal microscope. Several stacks per field was taken for each root and a 3D projection of the z-stack was obtained. Whole root was then reconstructed in tiles when required. bZIP63:YFP (*pbzip63*:bZIP63:YFP) and *bZIP11*:GFP (*pbZIP11*:bZIP11-UTR:GFP) driven under their native promoters was imaged without counter staining with propidium iodide (PI) which stains the cell wall. *SnRK1.α1*:GFP was counter stained with propidium iodide (PI) with concentration of 10 µg/mL for 1 minute. For the detection of fluorescent signals from YFP, GFP and PI, different excitation and emission wavelengths were used as described. PI fluorescence emission and excitation at 570-670nm, GFP emission at 488-507 and YFP emission and excitation at 513-527 nm.

2.2.4.3 To study localization pattern in different layers of the primary root

5-day-old seedlings grown in long day condition (16 h light/8 h dark) on ½ MS in phyto agar without sugar were imaged in the elongation zone for determining *SnRK1.α1*:GFP, *bZIP63:YFP* and *bZIP11*:GFP (driven by their native promoters) protein in different cell layers of primary root. Images were taken at 40x magnification on single sections showing xylem, pericycle, endodermis and cortex cell layers.

2.2.4.4 To study localization pattern of SnRK1.α1, bZIP63 and bZIP11 in different stages of the lateral root development

8 to 10-day-old seedlings of SnRK1.α1, *bZIP63:YFP and bZIP:GFP* (driven by their native promoters) were grown in long day condition (16 h light/8 h dark) on ½ MS in phyto agar without sugar. Entire primary root was scanned for different stages of developing lateral root (from stages II to emergence). Once located, Several stacks per stage was obtained and a 3D projection of the z-stack was obtained. *SnRK1.α1*:GFP was counter stained with propidium iodide (PI) with concentration of 10 µg/ml for 1 minute. For the detection of fluorescent signals from

YFP, GFP and PI, different the excitation and emission wavelengths were used as described. PI fluorescence emission and excitation at 570-670nm, GFP emission at 488-507 and YFP emission and excitation at 513-527 nm.

2.2.4.5 Monitoring *ASN1* activity using luciferase reporter

Luciferase reporters have been proven to be important mainly for exploring different aspects of signal transduction and gene regulation (Greer and Szalay, 2002; Southern et al, 2006.) For monitoring *ASN1* activity in shoots 8-day old transgenic *pASN1:LUC* plants were subjected to darkness for 1 h, 2 h and 4 h during the 16 h light cycle (treatment similar to figure 13). After each darkness treatment, seedlings were sprayed with luciferin and incubated for 10 minutes. The plates were placed horizontally and imaged using a CCD camera. Pictures were imported as TIFF file and Region of Interest (ROI) was generated around the shoot and integrated intensity of the observed luciferase signals for each seedling was calculated. Average value of integrated densities of the luciferase signals of all seedlings was calculated and used for statistical analysis and representation.

2.2.4.6 Differential interference contrast imaging

This protocol is beneficial to study the developmental stages of the lateral root. Roots were cleared with a modified protocol from Malamy & Benfey (1997). 5-day-old seedlings were treated with and without 4 h of unexpected darkness. After the treatment they were recovered in light for 16 h and taken for root clearing. Seedlings were incubated in a solution of 4 % HCl and 20 % methanol for 15 minutes at room temperature. Then the solution was changed to 7 % NaOH and 60 % ethanol and incubated 15 minutes at room temperature. Plants were progressively rehydrated in 40, 20 and 10 % ethanol changing the solutions every 5 minutes. The storage solution was in autoclaved water and 5 % ethanol. Plants were placed on a glass slide with a solution of 50 % glycerol and covered with a cover slide. The microscope Zeiss Axio Imager M1 equipped with an AxioCamHR3_552 cameras and DIC optics was used for imaging the cleared root.

2.2.4.7 Outlining the root architecture

8-day-old wild-type (WS) and *bzip63* loss-of-function seedlings grown on ½ MS phyto agar media were subjected to 4 h of unexpected darkness. After the darkness treatment, they were placed back in long day conditions along with the respective controls. On day 6 post-treatment, the plates were scanned to obtain images of the primary root and all the projecting lateral roots. The root architecture shape projecting the outline of the root system of 10 individual seedlings for each line was obtained as shown in the figure 26.

2.2.5 Extraction of sugars from *A. thaliana* seedlings

8-day-old wild-type Col-0 grown on ½ MS gellrite agar media were subjected to 1 h and 4 h of unexpected darkness. Control seedlings were maintained at long day conditions. After treatment roots and shoots were separated and frozen in a 2 mL Eppendorf tube containing 1 metal bead. The tubes with 290 µL of extraction solvent and 10 µL of internal standard mix were transferred to a pre-cooled grinding jar and ground to homogenize the tissues. Tissues were homogenised at 21 Hz for 5 minutes. The samples were centrifuged at 4 °C for 10 minutes at 20,000 g. Supernatant was transferred to a fresh 1.5 mL eppendorf tube. 300 µL of extraction solvent was further added and the mixture was vortexed briefly.The samples were centrifuged at 4 °C for 10 minutes at 20,000 g. Samples were dried in a speedvac for 120 minutes at 50°C. Dry tissue was resuspended in 25 µL of extraction solvent and transferred in LC vial (approximately. 20 µL) for LC-MS. LC-MS was performed at the facility in the department of Pharmaceutical biology, University of Würzburg.

3. RESULTS

3.1 Short-term perturbations in plant energy homeostasis alter root architecture

Exposure to various environmental stresses can alter plant's metabolic homeostasis and consequently its developmental plasticity. We hypothesize that, when plants encounter short-term energy changes, they reprogram their development to mitigate these changes. Here, we focus on understanding how root development is affected due to short-term perturbations in photosynthesis and energy metabolism. *A. thaliana* roots provide an excellent quantifiable system to study the effect of short-term energy perturbations on development.

3.1.1 Treatment with low light increases the lateral root density

In a first attempt seedlings were grown on ½ MS agar for 8 days (16 h light/8 h dark, 100 μmol m^{-2} s^{-1}), then transferred to new media plates and subjected to low light conditions (15 μmol m^{-2} s^{-1}) for 24 h (16 h of low light during the day regime followed by 8 h of dark regime and an additional 8 h of low light during the second day refer figure 11A). Similarly, low light was given for 36 h, 48 h and 72 h. We utilized this light level in our experiment to create a low photosynthetic activity and study changes in the root architecture. These conditions are close to the light compensation point and the cryptochrome and phytochrome signalling is still active (Lauxmann et al., 2016). Post treatment with low light, seedlings were transferred back to control conditions. Emerged LR density (eLR; number of emerged lateral root per cm of primary root) was measured on 14th day after germination (6th day post-treatment). Primary root length, number of eLR and eLR density was quantified after growth under low light and control conditions (figure 11). Primary root length of low light treated seedlings did not change in comparison to control condition at earlier time points up to 36 h, but longer low light treatment reduced the root length (figure 11C). Control seedlings had eLR density between 0.2 to 1.25 cm^{-1}, which is the observed standard for Col-0 seedlings day 14 after germination (Dubrovsky and Forde, 2012). As seen in the figure 11D, 24 h and 36 h of low light treatment had higher eLR density between 0.5 to 2.5 cm^{-1} which is significantly higher in comparison to Col-0 control. However, eLR density reduced in comparison to control with longer

treatments of 48 h and 72 h low light. These results indicate that short term low light treatment has a positive effect on the eLR density. Moreover, this response is transient as longer low light treatments decrease eLR density.

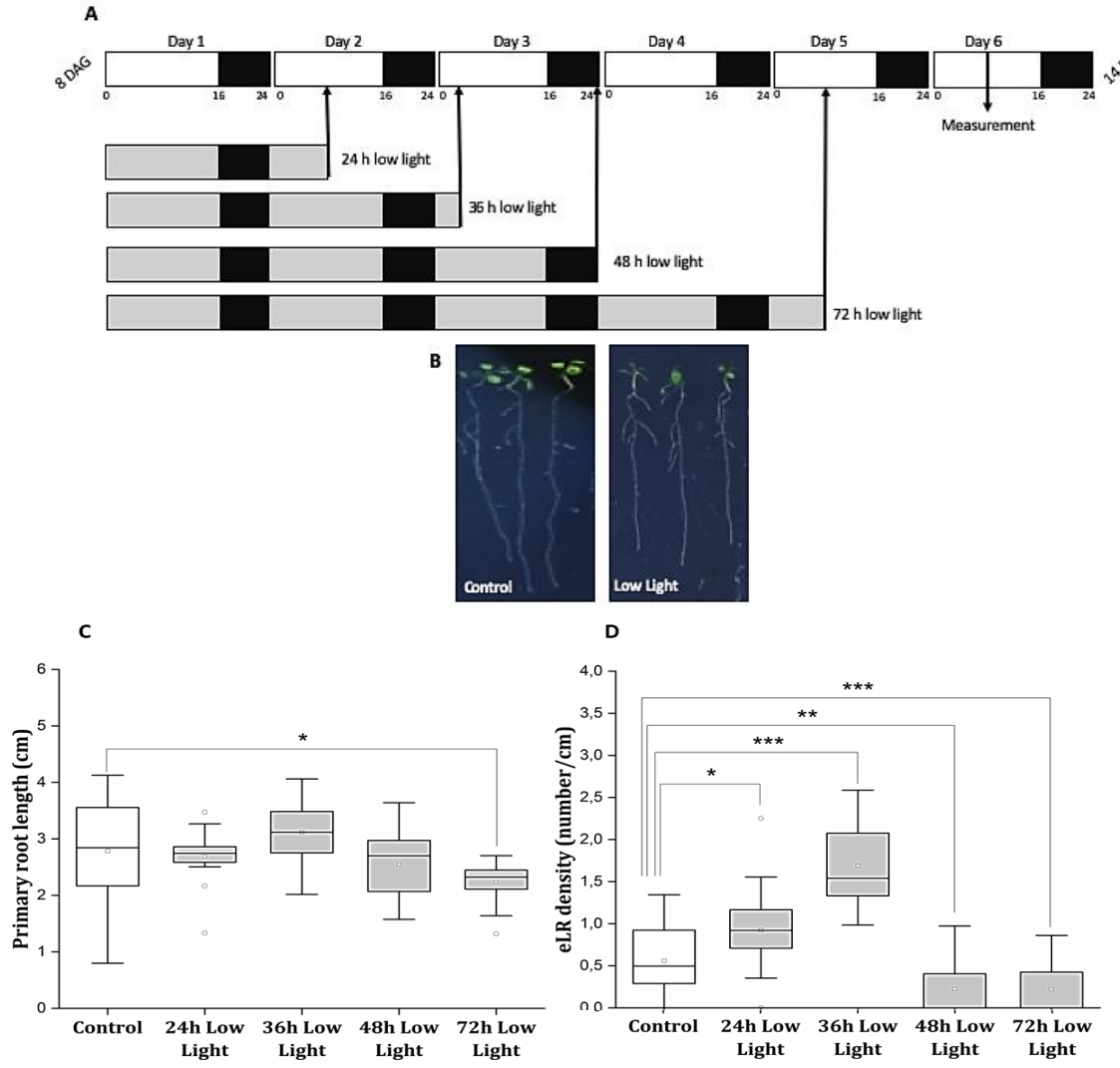

Figure 11: Short-term low light treatment increases eLR density. 8-day-old, *A. thaliana* Col-0 seedlings grown on ½ MS media in long day conditions (16 h day/8 h dark) were subjected to different hours of low light treatments. Untreated control group was maintained at long day conditions. Post treatment, all seedlings were grown until day 14 under long day conditions. Control and treated seedlings were then measured for primary root length and eLR density was calculated. (A) Treatment scheme for control and low light (B) Representative image of seedlings with and without 24 h low light treatment on 6th day post treatment (C) Primary root length of control (white bar) and low light treated seedlings (gray bars) measured from the end of hypocotyl to the root tip by using the free-hand tool of Fiji (Schindelin et al., 2012) (D) eLR density of control (white bar) and low light treated seedlings (gray bars). Normal distribution was calculated for each group. Student's *t-test* and Mann-Whitney's-*U test* was used to test significance. n=15 seedlings were analysed for each group. Asterisk indicate significance **p<0.05 **p<0.01 ***p<0.001*.

3.1.2 Extended night impacts root system by reducing the primary root length and increasing the lateral root density

As another approach to study the root system upon a metabolic perturbation, we subjected plants to extended night conditions. The amount of carbon assimilated during the day is sufficient to be utilized for the night. If night regime is extended it will create a metabolic imbalance. Like the previous experiment, we wanted to test whether extended night treatments perturb the energy balance and influence the root system architecture.

8-day-old *A. thaliana* Col-0 seedlings grown on ½ MS media were treated with extended night for 6 h after the end of night regime. Col-0 seedlings without extended night served as control. Post treatment, the seedlings were transferred back to the long day condition and on 14^{th} day after germination (6^{th} day post treatment), primary root length and lateral root number was measured and eLR density was calculated (figure 12). In contrast to what was observed in low light treatment, the primary root length significantly decreased in the extended night treated group (figure 12C). Emerged lateral root number showed no significant increase (figure 12D) but the eLR density (figure 12E) increased upon extended night treatment. Density of the control seedlings were well within the previously recorded density range of 0.5 to 3.5 cm^{-1} (Dubrovsky and Forde, 2012). The density of the extended night treated samples was increased from 1.0 to 3.75 cm^{-1}. The increase in the eLR density is due to shortening of the primary root length not because of an increase in overall lateral root number and density. To conclude, extended night shortens the primary root length, and increases lateral root density.

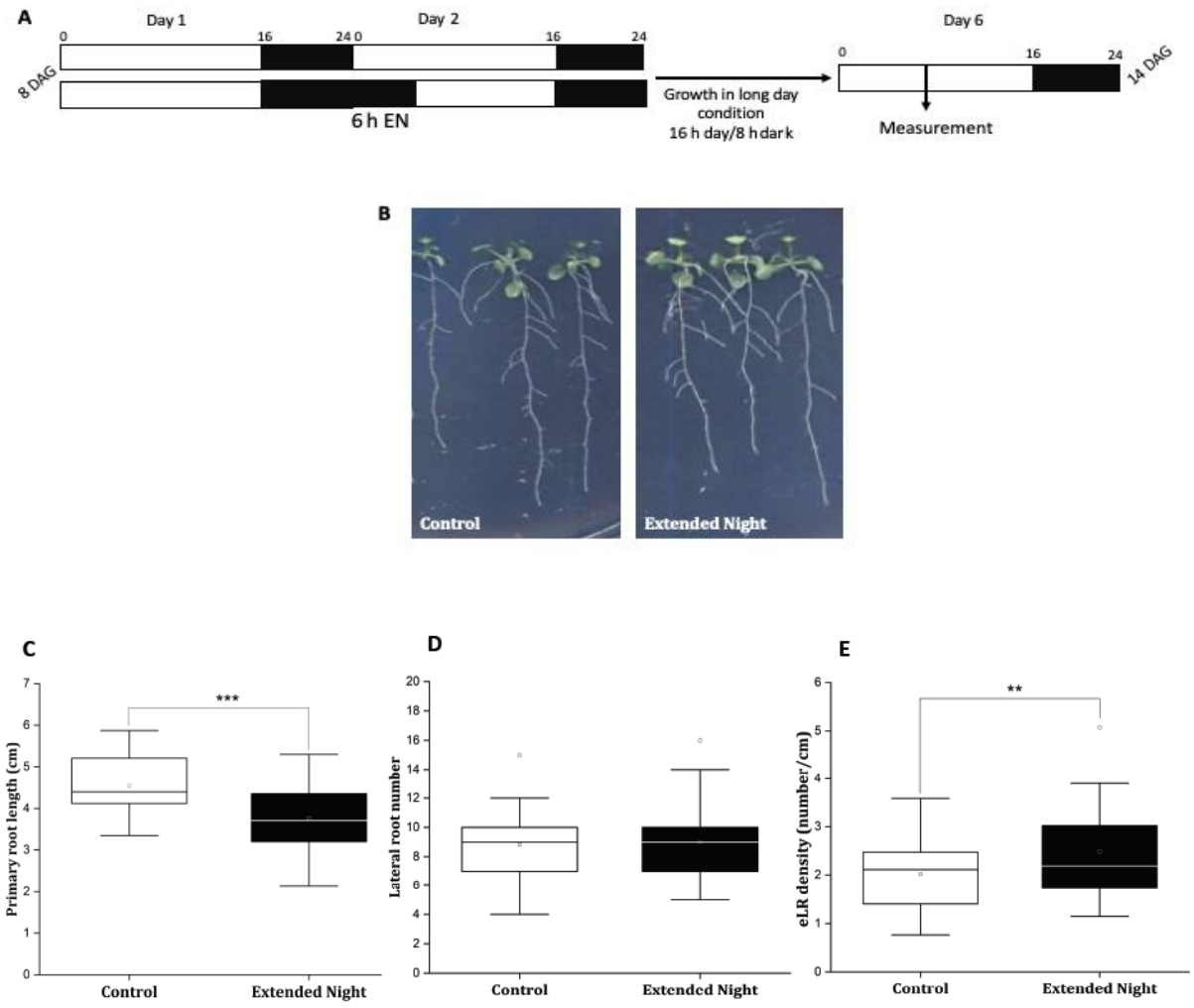

Figure 12: Extended night decreases primary root length and increases eLR density. 8-day-old, *A. thaliana* Col-0 seedlings grown on ½ MS media in long day conditions (16 h day/8 h dark) were subjected to 6 h of extended night treatment. Untreated control group was maintained at long day conditions. Post treatment, all seedlings were grown until day 14 under long day conditions. Control and treated seedlings were then measured for primary root length, lateral root number and eLR density. (A) Treatment scheme for control and extended night. Each extended night treatment group (black bars) is compared to the untreated control group (white bars) (B) Representative image of control and extended night treated seedlings on 6th day post treatment. (C) Primary Root length measured from end of the hypocotyl to the root tip. (D) eLR number and (E) eLR density. Normal distribution was calculated for each group and student's *t-test* was used to test significance. n=26 seedlings were analysed, and asterisks indicate significance **p<0.05 **p<0.01 ***p<0.001*. The experiment was repeated 3 times with similar results.

3.1.3 Unexpected darkness impacts root system architecture by increasing the lateral root density without changing the primary root length

We employed a third set-up of treating 8-day-old *A. thaliana* seedlings with "unexpected darkness" (short darkness treatment during the day).

Treatment with 0.5 h to 4 h of unexpected darkness displayed an increase in eLR density as seen in figure 13D with 4 h unexpected darkness showing the highest increase in density compared to its control group. 4 h of unexpected darkness treatment was now chosen for future experiments even though 0.5 h to 2 h of unexpected darkness showed increased eLR density but had lesser statistical significance. Unexpected darkness did not influence primary root length (figure 13C). We looked at the eLR phenotype between *A. thaliana* ecotypes Col-0, Wassilewskija (WS) and Landsberg (Ler) under 4 h of unexpected darkness to observe if the effect of short-term energy perturbation is ecotype specific. While all three ecotypes displayed higher eLR density with 4 h unexpected darkness, Col-0 and WS showed significance with the chosen sample size (n=15 and n=20), but significant increase in eLR density was not seen in Ler (n=15) (figure 32). As an attempt to test whether unspecific short-term stress have similar impact on root architecture similar to low light and 4 h unexpected darkness, we tested Col-0 seedlings with heat stress of 42 ^{o}C at two timepoints-20 minutes and 60 minutes and did not observe any change in the eLR density (figure 31).

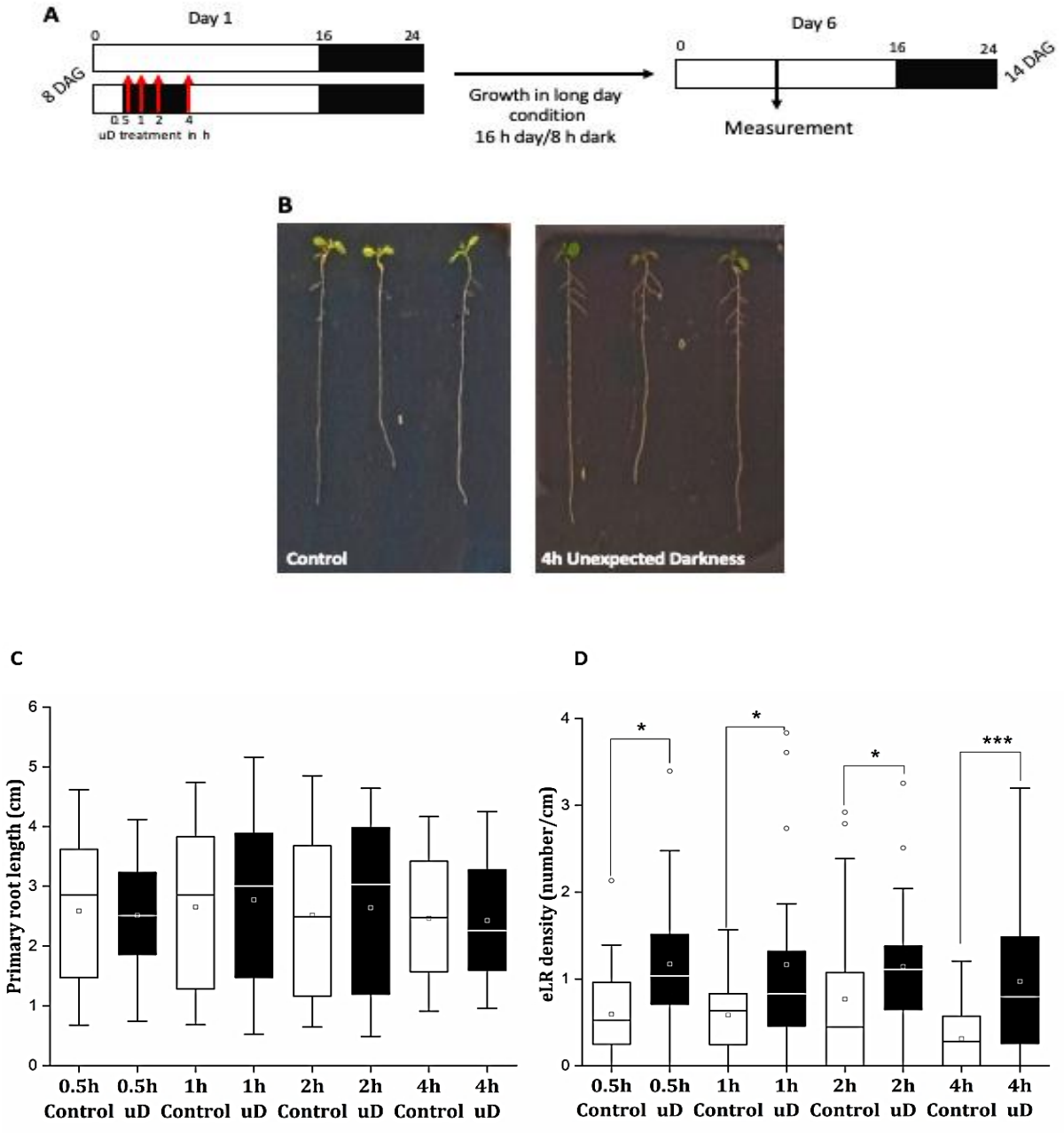

Figure 13: Unexpected darkness increases eLR density and has no effect on primary root length. 8-day-old, *A. thaliana* Col-0 seedlings grown on ½ MS media in long day conditions (16 h day/8 h dark) were subjected to 0.5 h to 4 h of unexpected darkness treatment. Untreated control group was maintained at long day conditions. Post treatment, all seedlings were grown until day 14 under long day conditions. Control and treated seedlings were then measured for primary root length and eLR density was calculated. (A) Treatment scheme for control and unexpected darkness. (B) Representative image of Col-0 seedlings with and without unexpected darkness treatment at day 6 post treatment (C) Primary Root length measured from end of the hypocotyl to the root tip. (D) eLR density of control (white bars) and unexpected darkness (black bars) treated seedlings. Normal distribution was calculated for each group. Student's *t-test* and Mann-Whitney's *U test* was used to test significance. Asterisk indicate significance *$p<0.05$ **$p<0.01$ ***$p<0.001$ for sample size n=30. The experiment was repeated 3 times with similar results.

3.1.4 Unexpected darkness results in an increase of cells showing expression of the lateral root founder cell marker *GATA23*

We have shown that short-term low light and unexpected darkness treatments, increase the eLR densities. To further understand, and to visualize early events of lateral root development, we employed a well-established lateral root initiation event marker *GATA23* (De Rybel et al., 2010). The expression of *GATA23* reduces in later stages of development.

We utilized the existing *pGATA23*::NLS-GFP (De Rybel et al., 2010) to monitor early lateral root developmental events after treatment with 4 h of unexpected darkness. Lateral root begin to develop between 3 to 5 days after germination. It has been shown that in a 3 to 5-day-old seedling more early stage lateral root initiation and primordia events are present in comparison to fewer emergence events (Kircher and Schopfer, 2016). Hence we utilized 5-day-old seedlings in this experiment to count earlier events of lateral root development. After recovery, initiation (stage I, II and III), primordia (stage IV, V and VI) and emergence with *pGATA23*::NLS-GFP expression as shown in figure 14 A-H were counted manually across the primary root using Leica confocal fluorescence microscopy software. The unexpected darkness treated seedlings contained a higher number of lateral roots (figure 14 A-H) showing *pGATA23*::NLS-GFP signal. This experiment validates the increase in lateral root number after unexpected darkness treatment (figure 14I).

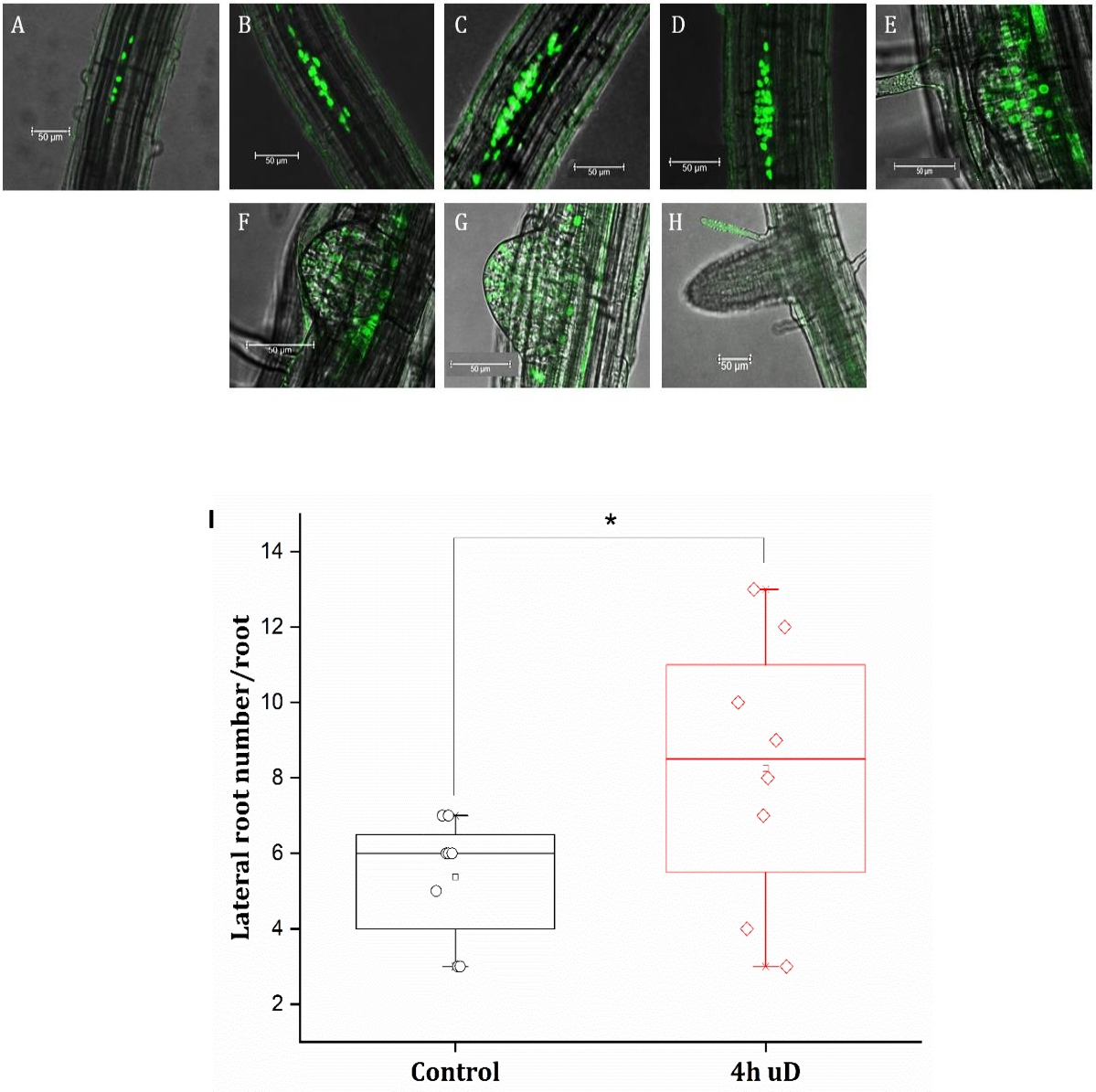

Figure 14: Unexpected darkness leads to an increase in the number of cells showing expression of the early stage lateral root marker *pGATA23*::NLS-GFP. Transgenic plants of *pGATA23*::NLS-GFP (*GATA23* expression employing a nuclear-targeted GFP reporter) were grown for 5 days on ½ MS media and treated with and without unexpected darkness (uD). They were recovered for 16 h in light and imaged to visualize and count lateral root developmental stages (A-H) between control and unexpected darkness treatment groups. (A) Stage I of the lateral root development. (B-C) Stage II and stage III, also termed as lateral root initiation events. These stages show strong *pGATA23*::NLS-GFP expression. (D-F) Stage IV, V and VI termed as lateral root primordia. Here *pGATA23*::NLS-GFP expression reduces gradually. (G-H) Emergence events and expression of *pGATA23*::NLS-GFP is reduced (I) Represented are the lateral root numbers in a box plot. Unexpected night treatment group was compared to its respective control group. Normal distribution was calculated for each group and student's *t-test* was used to test significance. Asterisk indicate significance *$p<0.05$* for n=8 seedlings.

3.1.5 Unexpected darkness increases expression of the starvation marker *ASN1,* both in shoot and root

ASN1 encodes a glutamine-dependent ASPARAGINE SYNTHETASE1 (Lam et al., 1994). Asparagine Synthetase controls the biosynthesis of amino acid asparagine. *ASN1* is expressed in several plant tissues including roots (Gaufichon et al., 2017). *ASN1* is upregulated under darkness and downregulated in light (Hanson et al., 2008). To observe changes in *ASN1* levels during unexpected darkness, we utilized the transgenic line, where promoter *ASN1* is fused to luciferase (*pASN1:LUC)* (Baena-Gonzalez, unpublished). Luciferase reporters have been proven to be very important research tools in plants, mainly for exploring different aspects of signal transduction and gene regulation (Greer and Szalay, 2002; Southern et al, 2006). In this experiment luciferase activity is assumed to reflect plant's energy status. Moreover, it is an *in vivo* measurement from intact living plant tissues. 8-day-old transgenic *A. thaliana* seedlings were treated with 1 h, 2 h and 4 h of unexpected darkness. Seedlings without unexpected darkness treatment served as the control group.

We observed that already after 1 h of unexpected darkness treatment, the *pASN1:LUC* activity in leaves of darkness treated seedlings significantly increased (figure 15A). Similar pattern was observed in the further time points of 2 h and 4 h, but they were not statistically significant and moreover 4 h time point showed a reduction in the *pASN1:LUC* levels both in control and darkness treated leaves compared to the previous two time points. This effect was only recorded in younger 8-day-old seedling (figure 15A). Similar tests were conducted on 14-day-old adult seedlings and *ASN1* induction was not detected in the shoot (figure 33) suggesting *ASN1* levels decrease in older seedlings. This also suggests that older plants are not responsive to unexpected darkness treatment.

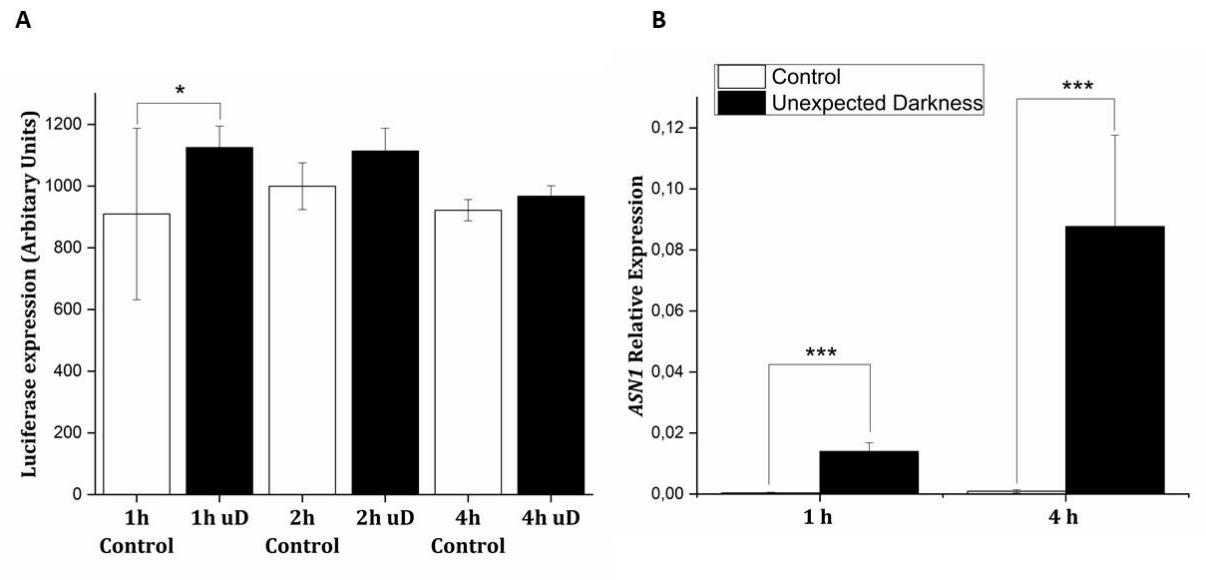

Figure 15: *ASN1* expression increases under unexpected darkness. (A) Transgenic *pASN1*:LUC seedlings were grown for 8 days under long day conditions and then treated with 1 h , 2 h and 4 h of unexpected darkness (uD in the figure). After the darkness treatment, luciferin solution was sprayed, and imaging was performed after 10 minutes with a CCD camera. *ASN1* promoter activity is shown as luciferase signal in leaves of control (white bars) and 1 h, 2 h and 4 h of unexpected darkness (black bars). Normal distribution was calculated for each group and student's *t-test* was used to check significance in normal distributed samples of n=10 seedlings. Asterisk indicate significance **p<0.05*. (B) Quantification of *ASN1* transcripts in roots of 8-day-old *A. thaliana* WT seedlings in control (white bars) and 1 h and 4 h unexpected darkness (black bars) by qRT-PCR. Relative gene expression was normalized to *EF1A* growth factor transcripts (Roberts et al., 2016). Three independent biological replicates were used for each treatment. Normal distribution was calculated for each group and student's *t-test* was used to test significance. Asterisk indicate significance ****p<0.001*

On the other hand, *ASN1:LUC* activity was only displayed in the leaves, not in roots. To quantitatively measure the *ASN1* expression upon unexpected darkness, qRT-PCR was performed. Roots from respective time point controls, 1 h and 4 h unexpected darkness treated roots were checked for *ASN1* transcript abundance (figure 15B). In contrast to what was seen in the luciferase test, 4 h time point showed a significant increase in *ASN1* transcript levels relative to the light grown control. Collectively, these data suggest that unexpected darkness may lead to a transient impairment in energy homeostasis.

3.1.6 Short-term perturbations in photosynthesis reduce the level of hexoses in shoot and root

Previous data indicate that limited perturbations in photosynthesis are perceived by the plant which responds by induction of the *ASN1* marker gene. To further assess metabolic changes upon unexpected darkness, we quantified the most important sugars in plants, namely sucrose, fructose and glucose. 8-day-old seedlings were grown on ½ MS media without sugars and treated with 1 h and 4 h of unexpected darkness. Shoot and root tissue were harvested separately and sugars levels were determined by using LC-MS. Consistent to our hypothesis that unexpected darkness induces a shift in sugar levels, we noticed a significant decrease in sugar levels in the root tissue (figure 16B). In comparison to the hexoses, sucrose levels were rather low and hence, may not add substantially to the overall sugar content. Although the sugars are not completely exhausted leading to starvation, a reduction in hexoses support a shift in energy homeostasis to occur.

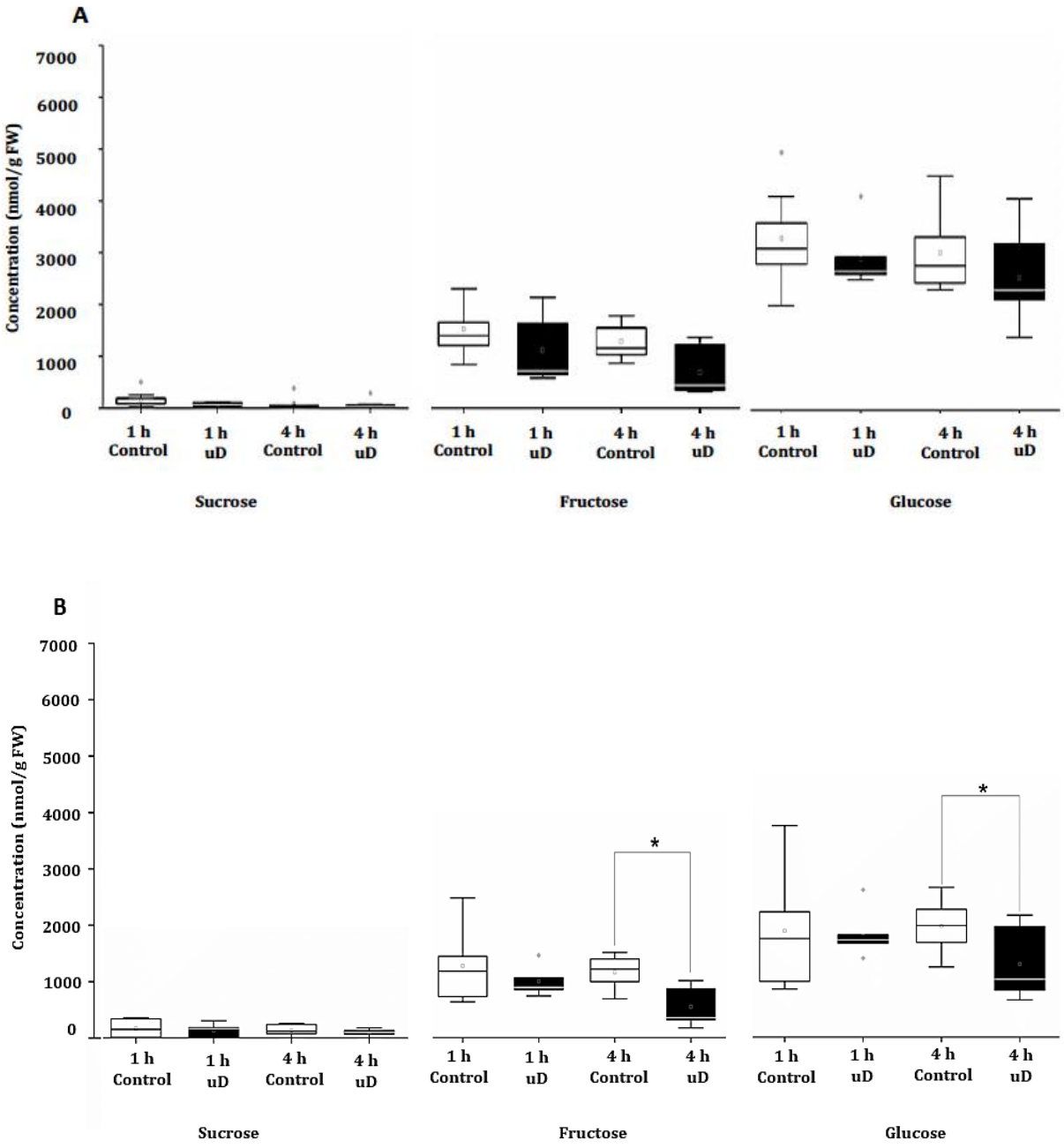

Figure 16: Hexose sugars decrease in response to unexpected darkness. 8-day-old *A. thaliana* Col-0 seedlings grown on ½ MS media were treated with 1 h and 4 h of unexpected darkness. After treatment, shoot (A) and root (B) were harvested separately of untreated control seedlings (white bars) and treated seedlings (black bars). Primary sugars were determined using LC-MS. D-Glucose and Trehalose were used as reference sugars. Normal distribution was calculated for each group and Mann-Whitney's *U test* was used to test significance. Asterisk indicate significance ** p<0.05 **p<0.001*. FW. Fresh Weight. **Measurements were performed in collaboration with Dr. Markus Krischke, Metabolic Core Facility, University of Würzburg**.

3.1.7 External sugar treatment partially rescues the unexpected darkness induced lateral root phenotype

To further characterize the effect of perturbation treatment, we were interested to see if providing external sugar would compensate the proposed impairment in energy homeostasis. We utilized the experimental procedure of unexpected darkness and supplemented the growth media with 1% sucrose, 1% glucose and 1% mannitol (as osmotic control). After the unexpected darkness treatment, they were grown for additional 6 days along with controls in long day condition and eLR density was recorded.

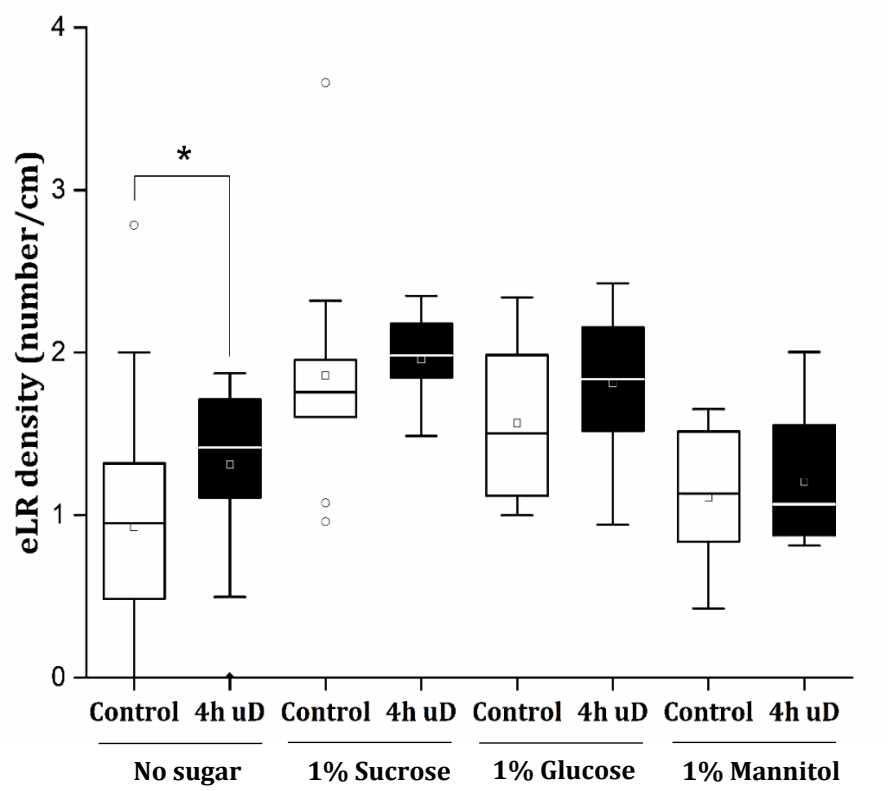

Figure 17: External sugar treatments rescues the unexpected darkness induced lateral root phenotype. 8-day-old, *A. thaliana* Col-0 seedlings grown on ½ MS media in long day conditions (16 h day/8 h dark). They were then transferred to ½ MS media containing sugars and then subjected to 4 h of unexpected darkness treatment. Untreated control group was maintained at long day conditions. eLR density was determined in wild-type Col-0 seedlings treated with 1 % of sucrose, glucose and mannitol (as osmotic control) with (black bars) and without (white bars) 4 h of unexpected darkness. Seedlings treated without sugars served as controls. Normal distribution was calculated for each group. Student's *t-test* and Mann-Whitney's *U test* was used to test significance. Asterisk indicate significance *$p<0.05$ for n=20 seedlings (no sugar) and n=10 seedlings (with sugar).

Results given in figure 17 indicate that application of external sugars such as sucrose and glucose showed no increase in eLR density under unexpected darkness treatment. However, these sugars are metabolized by the plant and aids in overall root growth. The eLR density in the "no sugar" control displayed an increase after 4 h of unexpected darkness as seen in earlier experiments. This would indicate that application of external sugars reverses the phenotype we observe without sugar in the media. Seedlings grown on media containing mannitol and 4 h unexpected darkness showed no increase in eLR density.

3.2 SnRK1 and its downstream transcription factor bZIP63 impact root plasticity upon short-term energy limitation

3.2.1 Increased lateral root density by short-term unexpected darkness requires SnRK1.α1

SnRK1 and its yeast and mammalian homologue Snf1 and AMPK have been established as central metabolic regulators (Crepin and Rolland, 2019). Besides metabolic adjustment, SnRK1 may also modulate developmental processes according to the nutrient and energy status of the plant living system. This makes SnRK1 a likely candidate to study under our short-term energy perturbation conditions. To decipher the role of SnRK1 kinases in mediating lateral root development, we treated loss-of-functions mutants of catalytic SnRK1 subunits *snrk1.α1* and *snrk1.α2* in the unexpected darkness setting described above. Apart from the no treatment controls, the wild-type ecotype was used as a second set of control. We monitored the eLR densities of Col-0 wild-type, *snrk1.α1* and *snrk1.α2* at day 14 after germination (day 6 post treatment). The eLR density (figure 18A). and number (figure 34) was decreased significantly in *snrk1.α1* during 4 h unexpected darkness, whereas eLR density in *snrk1.*α2 remained unchanged and density in Col-0 under 4 h unexpected darkness was increased like earlier experiments. The primary root length for wild-type, *snrk1.α1* and *snrk1.α2* showed no significant difference (figure 18B). These results indicate the observed changes in lateral root development during short-term energy perturbations requires SnRK1.α1. SnRK1.α2 has little or no impact on the lateral root development under these conditions as the loss-of-function mutant shows no strong reduction with unexpected darkness treatment.

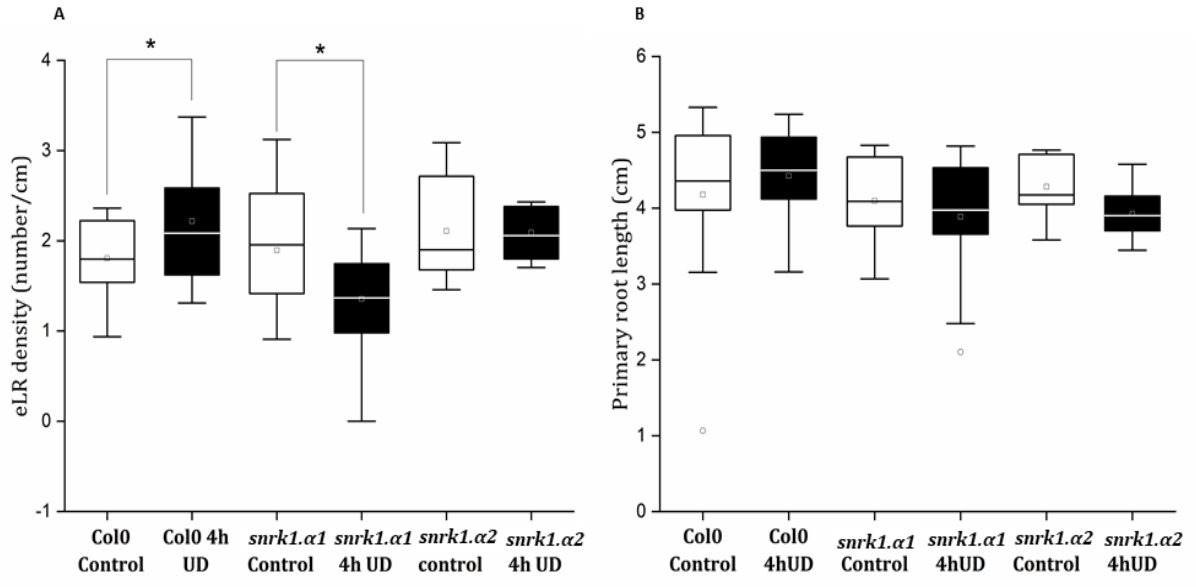

Figure 18: SnRK1.α1 is required for eLR density under short-term unexpected darkness. 8-day-old *A. thaliana* Col-0, *snrk1.α1* and *snrk1.α2* mutant seedlings grown on ½ MS media were subjected to 4 h of unexpected darkness. Post treatment they were grown until 14th day after germination under long day conditions (A) eLR density (B) primary root length of control (white bars) and 4 h unexpected darkness (black bars) treated seedlings were measured. Normal distribution was calculated for each group and student's *t-test* and Mann-Whitney's *U test* was used to test significance. Asterisk indicate significance **p<0.05* for n=15 samples (Col-0 and *snrk1.α1)* and n=10 (*snrk1.α2*).

3.2.2 SnRK1.α1-GFP is ubiquitously expressed in primary and lateral roots

Previously, we have shown that SnRK1.α1 is important for the lateral root development under short-term energy perturbations. Loss-of-function *snrk1.α1* displayed decrease in eLR density under 4 h unexpected darkness. To further confirm its proposed function in lateral root formation, we utilized a transgenic line expressing *SnRK1.α1*-GFP C-terminal translational fusion under native promoter to visualize *SnRK1.α1* expression in different parts of the primary and lateral root (figure 19) (Bitrián et al., 2011). *SnRK1.α1*-GFP is localized throughout the root. In the primary root tip, *SnRK1.α1*-GFP appears to be localized in both cytoplasm and in the nucleus (figure 19A) of actively dividing meristematic cells and in the zone proximal to the meristematic zone. *SnRK1.α1*-GFP is localized in the pericycle cell layer (figure 19B). In the lateral roots, SnRK1.α1 is localized in early initiation stage (figure 19C), LRP (figure 19E) and in the emerged lateral root (figure 19G)

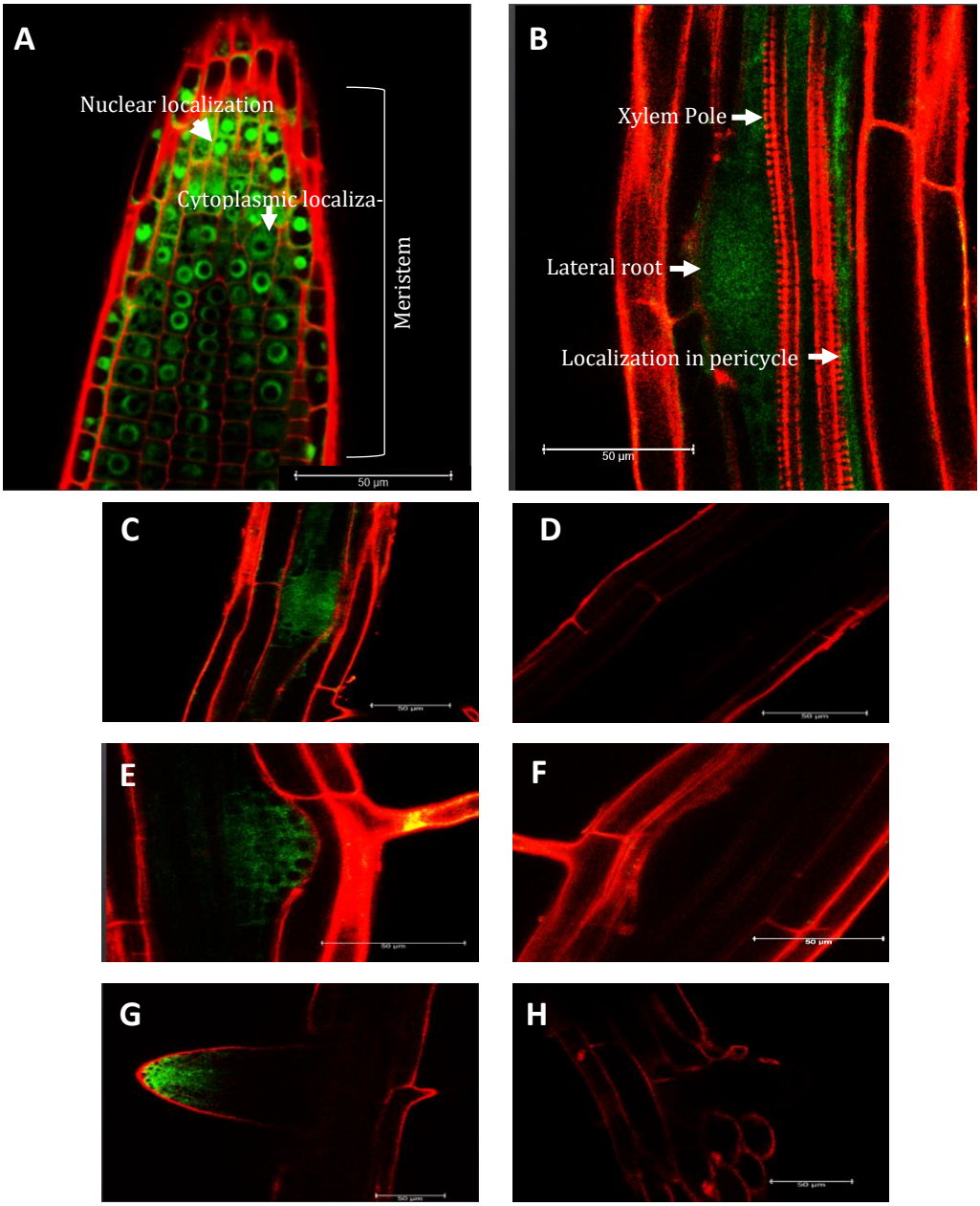

Figure 19: Sub-cellular localization of SnRK1.α1-GFP in the primary root and the lateral root: 8-day-old, *A. thaliana* transgenic line expressing *SnRK1.α1-GFP* was visualized by confocal microscope in the primary and lateral root. (A) Localization in the primary root meristematic zone. Arrows indicate nuclear and cytoplasmic localization. (B) Localization in the xylem pole pericycle cell layer with emerging lateral root (Arrow). Localization in early stage lateral root initiation (C), LRP (E) and emerged lateral root (G) along with respective wild-type controls (D, F and H). The cell wall is counter stained with propidium iodide. Scale bar is 50 µm.

3.2.3 Increased lateral root density requires SnRK1 downstream target bZIP63

SnRK1 signals are in part mediated by bZIP TFs (Mair et al., 2015; Pedrotti et al.,2018). SnRK1 phosphorylates the TF bZIP63 which modulates downstream signalling during low-energy stress.

Based on previous studies, bZIP63 would be an ideal candidate to study the impact on lateral root development under short-term energy perturbations. We analysed eLR density in a loss-of-function *bzip63* mutant upon 4 h unexpected darkness. The eLR density was reduced in comparison to WS wild-type density in unexpected darkness suggesting bZIP63 is required for the lateral root development under these conditions (figure 20A). Similar results were obtained with another transgenic loss-of-function mutant, *bzip63-CR* (figure 37). This line has been established in the work using CRISPR gene editing (Wang et al., 2015). Furthermore, the *bzip63* loss-of-function mutant phenotype was rescued by WT bZIP63 (*pbZIP63*:bZIP63:YFP - here on represented as bZIP63:YFP) as demonstrated by comparable eLR densities with WS wild-type in figure 21A. The primary root length between control and 4 h unexpected darkness in WS wild-type remained unchanged whereas the primary root length in loss-of-function *bzip63* mutant with 4 h unexpected darkness treatment was significantly reduced in comparison to the *bzip63* loss-of-function under control conditions (figure 20B). It needs to be noted, that primary root of loss-of-function *bzip63* displayed longer primary root length compared to WS wild-type under control conditions (figure 20B). Collectively our data indicate that bZIP63, is required for the lateral root development under energy limiting conditions.

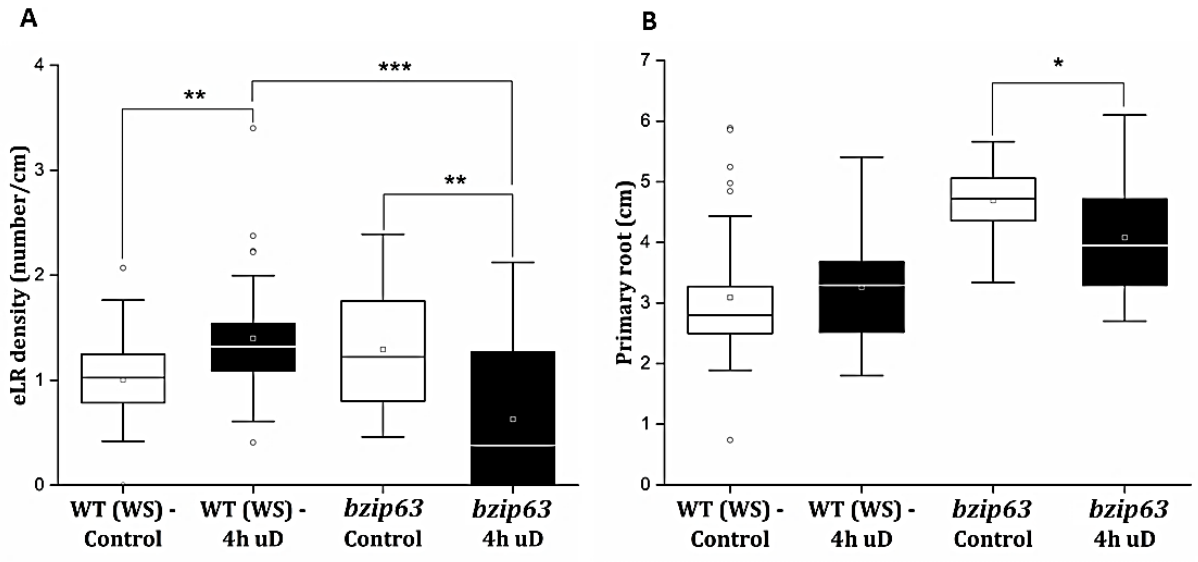

Figure 20: Loss of *bzip63* shows reduction in eLR density under short-term energy limitation. 8-day-old A*. thaliana* seedlings were treated with 4 h unexpected darkness. Post treatment they were transferred to long day conditions. The eLR density (A) and primary root length (B) in wild-type WS and loss-of-function *bzip63* with (black bars) and without (white bars) 4 h of unexpected darkness were measured at 14 days after germination. Normal distribution was calculated for each group. Student's *t-test* and Mann-Whitney's *U test* was used to test significance. Asterisk indicate significance **p<0.05 **p<0.01 ***p<0.001*. This experiment has been repeated 3 times with similar results with sample size n=35 (WT) and n=18 (*bzip63*).

3.2.4 Alanine-exchange mutants of the SnRK1 dependent bZIP63 phosphorylation sites do not display increased lateral root density upon short-term unexpected darkness

To understand whether the observed lateral root phenotype is due to SnRK1 mediated phosphorylation of bZIP63, we utilized an alanine-exchange mutant with respect to SnRK1 phosphorylation sites (bZIP63 S/A) (Mair et al., 2015). SnRK1.α1 phosphorylates 3 conserved and functionally important serine residues in bZIP63. These three serines (S29, S294 and S300) are replaced by alanine, disabling SnRK1.α1 phosphorylation of bZIP63. We treated WS wild-type, bZIP63 S/A and *pbZIP63*:bZIP63:YFP (*bzip63* loss-of-function mutant rescued with WT bZIP63) with and without 4 h unexpected darkness. We observed that the eLR density of the bZIP63

S/A mutant is significantly reduced upon 4h of unexpected darkness (figure 21A). This phenotype is similar to loss-of-function *bzip63* mutant. Wild-type WS and *pbZIP63*:bZIP63:YFP complementation lines showed similarities in their eLR density phenotype in unexpected darkness. Only the bZIP63:YFP can complement the loss-of-function *bzip63* phenotype and not the bZIP63 S/A mutant. These results collectively indicate that SnRK1 and bZIP63 TF are part of the signalling pathway and SnRK1 mediated phosphorylation is needed for conferring this lateral root phenotype under unexpected darkness. The primary root length of WS wild-type, bZIP63:YFP and bZIP63 S/A were not significantly different(figure 21B).

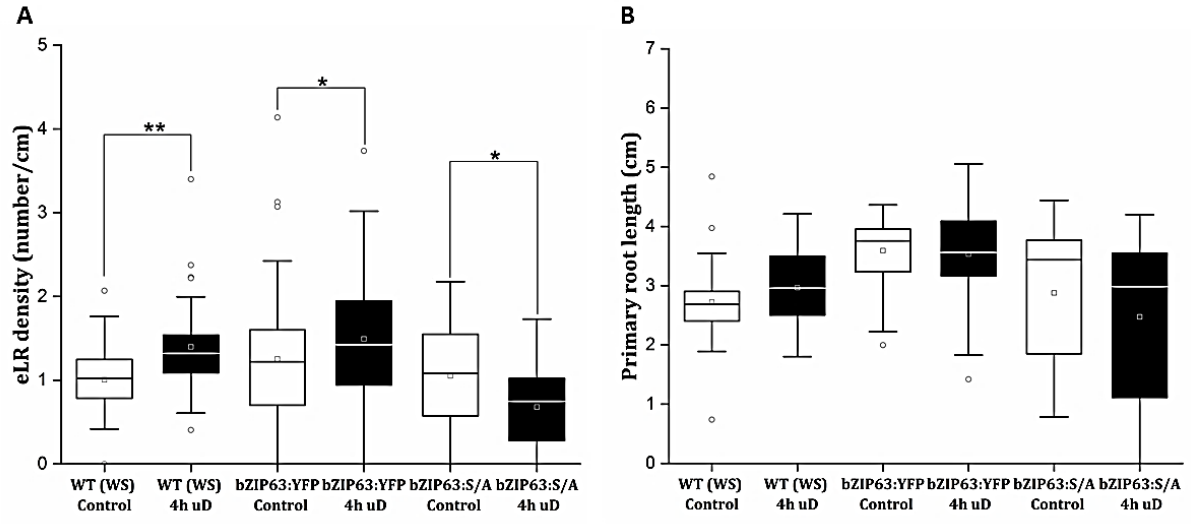

Figure 21: The SnRK1 phosphorylation mutant of bZIP63 do not display increased eLR densities under short-term energy limitation. 8-day-old *A. thaliana* seedlings grown on ½ MS plates were treated with 4 h of unexpected darkness. Post treatment they were transferred to long day conditions (A) The eLR density and (B) primary root length in wild-type WS (n=35), phosphorylation mutant bZIP63 S/A (n=30) and complemented bZIP63:YFP (n=60) with (black bars) and without (white bars) 4 h of unexpected darkness were measured at 14 day after germination. Normal distribution was calculated for each group. Student's *t-test* and Mann Whitney's *U test* was used to test significance. Asterisk indicate significance **p<0.05*. The experiment was repeated 3 times.

3.2.5 bZIP63-YFP is localized in primary root and all stages of lateral root development

Previous findings show that bZIP63 is required for the lateral root phenotype we observe upon 4 h unexpected darkness. To further understand the functional impact of bZIP63, it is necessary to observe the expression patterns of bZIP63:YFP in roots. We utilized the *bzip63* loss-of-function mutant complemented with functional bZIP63 protein tagged to YFP driven by native promoter (*pbZIP63*:bZIP63:YFP) (Mair et al., 2015) for this experiment. We utilized 10-day-old bZIP63:YFP seedlings which display lateral roots in all developmental stages. We focused the plane to visualize the xylem pole and scanned for the lateral root initiation, primordia and emergence stages for bZIP63:YFP expression (figure 22 and 23). Strong expression was determined in the root tip of the primary root (figure 22C and G). Expression reduced in the proximal transition zone where periodic clusters of cells expressing bZIP63:YFP were observed (figure 22F). The expression gradually increased in the elongation and differentiation zone (figure 22D and E). When we had a closer look at the differentiation zone, nuclear bZIP63:YFP was expressed in the epidermis, cortex, endodermis and the pericycle cell layers (figure 22B). We observed that bZIP63 was not localized at the quiescent centre in the root tip (figure 22C). bZIP63 demonstrates a wide range of localization all along the root. As shown, bZIP63:YFP is localized in meristem, transition, elongation and in differentiation zone of the primary root (figure 22A). These zones are important in XPP cells priming, lateral root initiation and development (Motte et al., 2019; De Rybel et al., 2010). Expression in elongation and differentiation zone and most importantly expression in different stages of the lateral root development (figure 23) will further support a possible function of bZIP63 in the lateral root development.

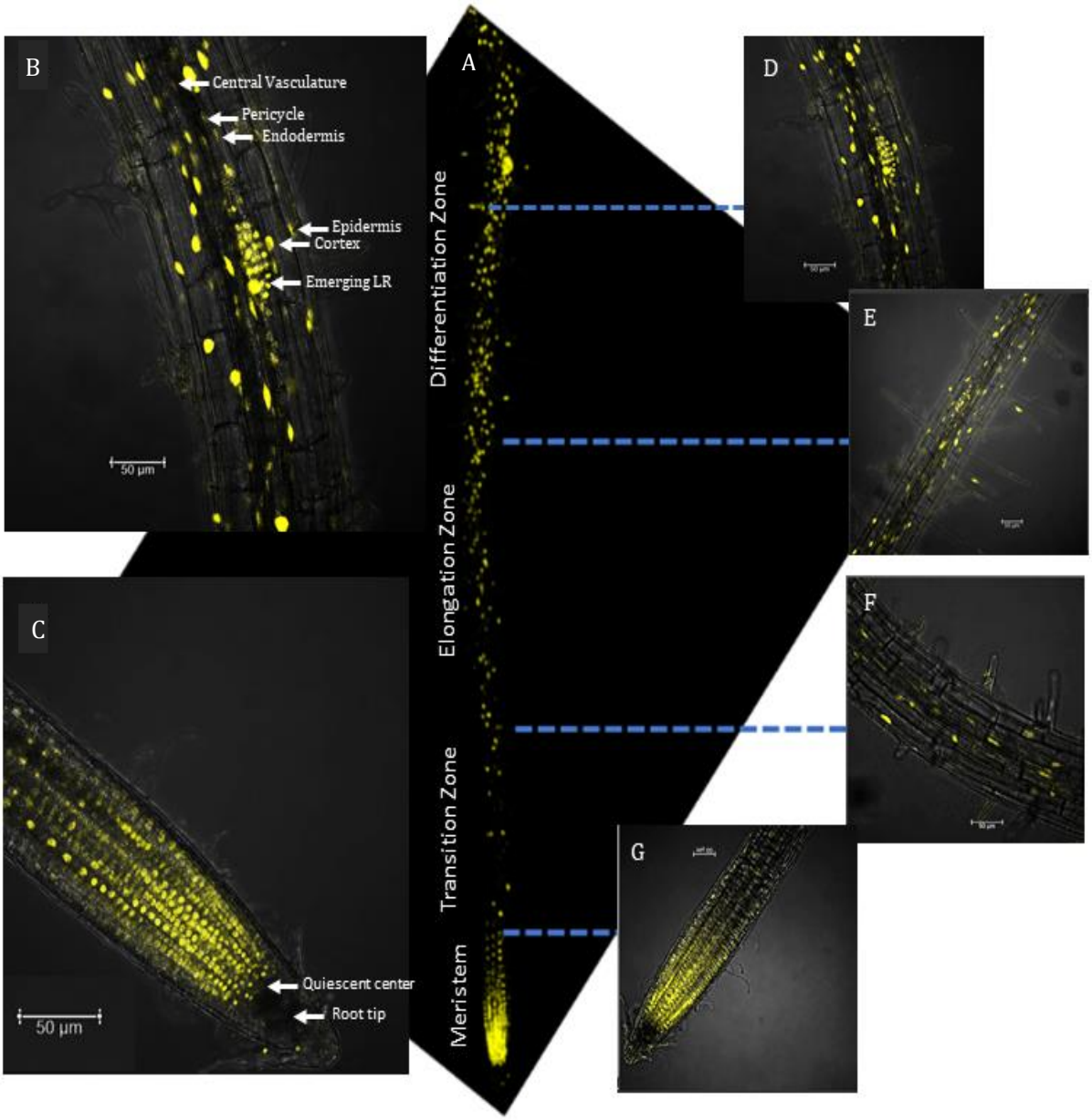

Figure 22: Expression of bZIP63:YFP in the primary root. 10-day-old, *A. thaliana* transgenic line expressing *pbZIP63*:bZIP63:YFP was visualized by confocal microscope in the primary root from root tip until the differentiation zone (approximately 1.5 cm from the root tip) (A) Fluorescent protein localization of bZIP63:YFP in the primary root developmental zones (B) Fluorescent protein localization of bZIP63:YFP in different cell layers at the differentiation zone (C) bZIP63:YFP is not localized in the quiescent centre at the root tip (D) Increase in expression of bZIP63:YFP in differentiation zone and (E) elongation zone (F) Expression considerably reduced in the proximal transition zone (G) Strongest expression at the root tip. Dotted blue line marks the corresponding zone to the image. Images are obtained under 25X (for length of primary root) and 40X water immersion objective of confocal laser scanning microscope. Representative image of several samples (n=5). Scale bar 50 µm.

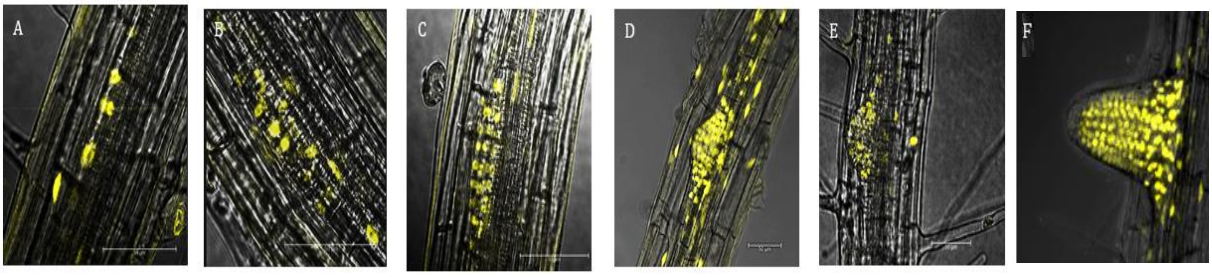

Figure 23: bZIP63:YFP is expressed in all stages of lateral root development. bZIP63:YFP expression as seen in a 10-day-old plant in different stages of the lateral root development. (A) Stage II (B) Stage III (C) Stage IV (D) Stage V (E) Stage VI and (F) Emergence of adult lateral root. Plane was adjusted to visualize xylem pole and each stage was then imaged at 40X water immersion objective. Scale bar 50 µm.

3.2.6 bZIP63 affects the lateral root initiation during short-term energy perturbations

Next, we wanted to understand in which step of lateral root development does bZIP63 play a role during short-term energy perturbations. To test this, we utilized 5-day-old wild-type WS and *bzip63* loss-of-function seedlings and treated them with and without 4 h of unexpected darkness. It has been shown that a 3 to 5-day-old seedling has more early stage lateral root initiation and primordia events and only a few emergence events (Kircher and Schopfer, 2016). Post-treatment they were recovered for 16 h in light. We presume this light recovery is important for new lateral root initiation and development to start. The roots of these seedlings were then cleared using the protocol developed by Malamy and Benfey (1997). The protocol helps in identifying early lateral root stages, which are not visible without clearing the roots. The roots were imaged using Differential Interference Contrast (DIC) imaging. The advantage of DIC imaging is that the specimen (in our case the lateral roots) appear bright in contrast to the dark background. We found that WT treated with 4 h unexpected darkness contained more lateral root initiation events of stage I, II and III in comparison to WT under control conditions (figure 24B). In *bzip63,* the initiation events of stage I, II and III is reduced upon 4 h of unexpected darkness in comparison to *bzip63* control. The lateral root primordia stages IV, V, VI showed no significant difference between WT and *bzip63* loss-of-function mutants in both control and 4 h unexpected darkness conditions (figure 24C).

Taken together, these results indicate that bZIP63 is important for early stage initiations and cell division of the lateral root under limiting energy conditions.

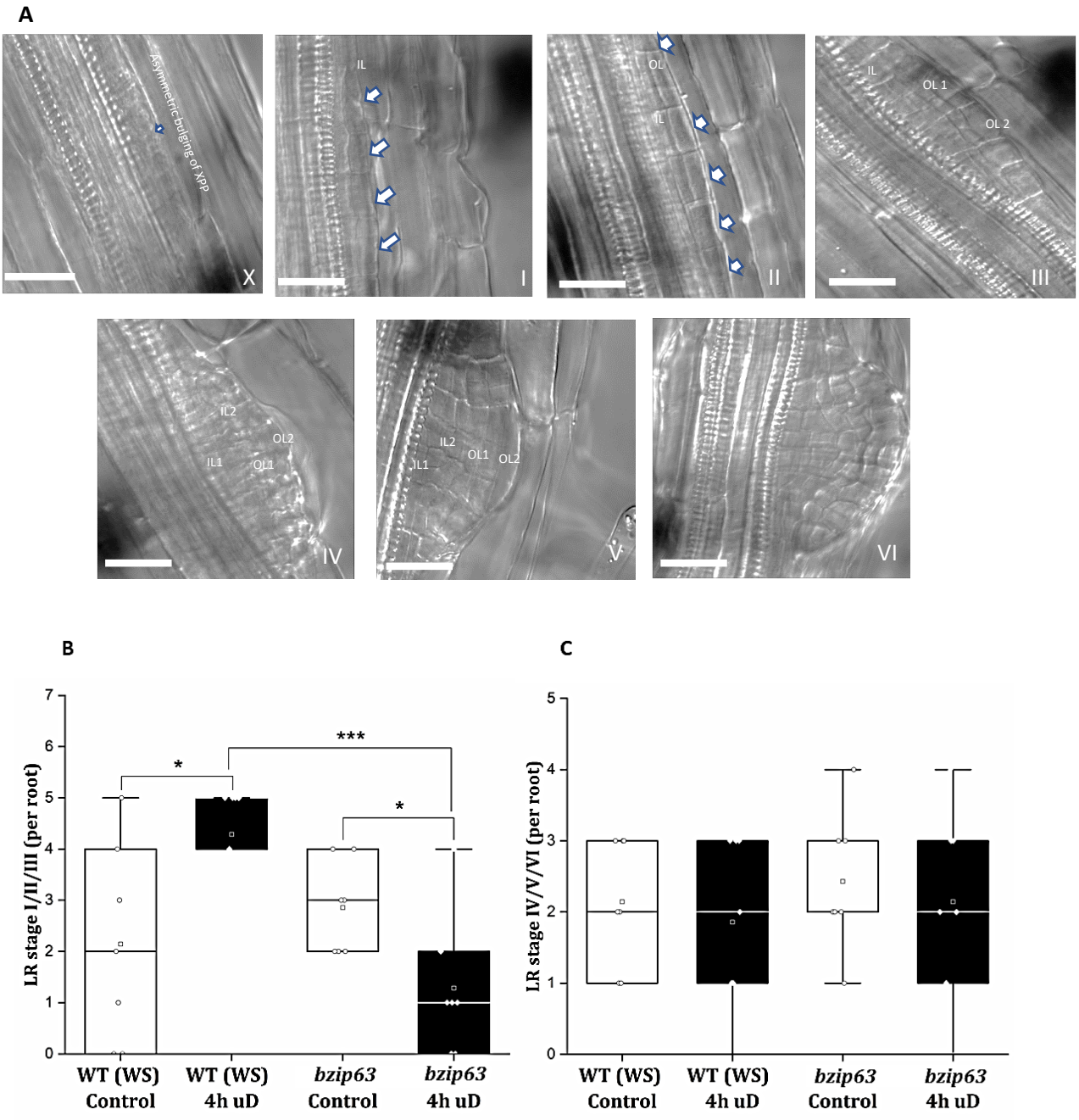

Figure 24: Quantification of the number of early and late stages in lateral root development in wild-type and *bzip63* loss-of-function mutants. (A) Shown are stages of lateral root primordia development imaged by DIC microscopy. In A (X) Refers to lateral root initiation stage where XPP are activated and bulge before their first division. (I) Arrows indicate the first anticlinal division. This is the formation of lateral root initiation (II) Arrows indicate periclinal division which differentiates layers to Inner Layer (IL) and Outer Layer (OL) (III) Second round of periclinal division in OL created a total of three layers (IV) Third round of periclinal division creating 4 layers

(V) Anticlinal division resulting in four cell layers and start of complex reorganization of LRP (VI) Each layer acquires cellular identity and forms epidermis, cortex, endodermis and vasculature. Number of lateral root at developmental stages I, II and III of LRP (B) and IV, V and VI (C) observed in 5-day-old seedlings of the wild-type WS and the *bzip63* mutant comparing control and 4 h unexpected darkness treatment. Primordia were counted and examined for developmental stages from 7 plants, and the experiments were repeated 3 times. Lateral roots are marked as LR in this figure. Normal distribution was calculated for each group. Student's *t-test* was used to test significance. Asterisk indicate significance **p<0.05, **p<0.01, ***p<0.05*

3.2.7 bZIP63 regulates early stage lateral root initiation upon short-term energy perturbation

In earlier experiments we have shown that loss-of-function of *bzip63* displays lesser lateral root initiation events. By utilizing the loss-of-function *bzip63* in *pGATA23*::NLS-GFP background *(bzip63-CR)*, we wanted to study if there are differences in the number of lateral root initiation and LRPs (marked by *GATA23* expression) upon 4 h unexpected darkness. To obtain the loss-of-function transgenic line, we utilized CRISPR-Cas9 system established by Wang et al. (2015). We utilized the previous experimental set-up of treating 5 day after germination seedlings with and without 4 h unexpected darkness and recovering in 16 h of light. We quantified the images obtained by confocal microscope of early stage lateral root initiation and primordia events manually. In transgenic line (*pGATA23*::NLS-GFP) treated with 4 h unexpected darkness, the initiation events and the LRPs were increased in number when compared to ones grown in control conditions. The initiation and primordia events in the *bzip63-CR* with 4 h unexpected darkness was reduced in comparison to *bzip63-CR* control (figure 25).

Taken together, we conclude that bZIP63 is involved in regulating early lateral root initiation upon short-term perturbation of energy homeostasis.

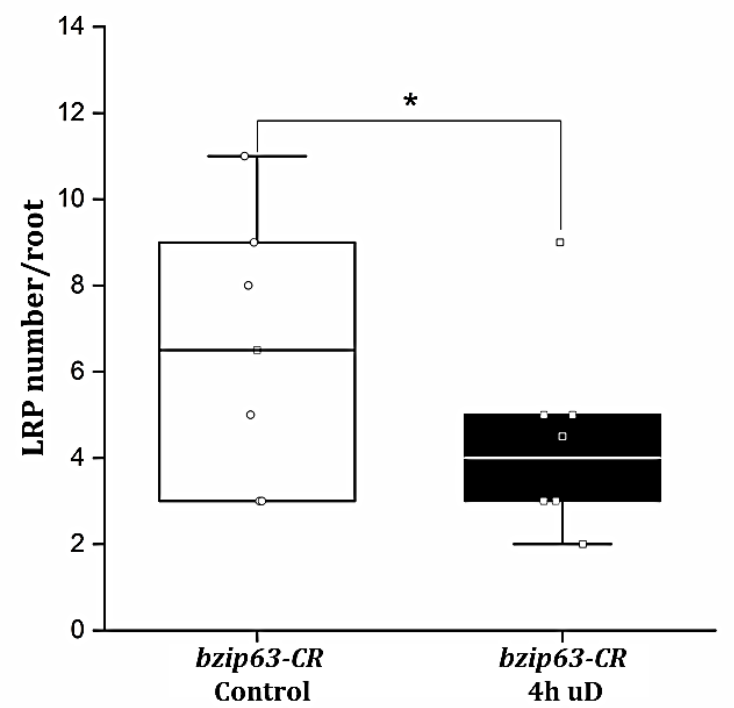

Figure 25: Short-term unexpected darkness decreases early stage lateral root events in *bzip63* loss-of-function. 5-day-old *bzip63-CR* seedlings were treated with 4 h of unexpected darkness. Post treatment the seedlings were transferred to long day conditions and were recovered under 16 h of light. All the initiation and primordia events expressing *GATA23* were quantified all along the primary root from the root tip to hypocotyl in *bzip63-CR* with and without unexpected darkness treatment. Unexpected darkness treatment group was compared to its respective control group. Normal distribution was calculated for each group and student's *t-test* was used to test significance. Asterisk indicate significance **p<0.05* for n=8 samples. The experiment was repeated 4 times with similar results.

3.2.8 Loss of bZIP63 affects the overall root architecture during unexpected darkness

Based on the previous experiments that bZIP63 affects the early lateral root formation during short-term energy perturbations, we studied the overall architecture in WS wild-type and *bzip63* loss-of-function mutant in control and in 4 h unexpected darkness conditions. We constructed outline map of the overall root system with and without 4 h of unexpected darkness (figure 26). We employed this approach to observe if loss of bZIP63 imposes an effect on the overall root architecture. We observed that there was no difference between the overall architecture of WS wildtype and *bzip63* loss-of-function seedlings under control conditions (figure 26B and D). With 4 h unexpected darkness treatment, the WS wildtype architecture (figure 26C) was similar to what is observed with control seedlings, whereas in *bzip63* loss-of-

function mutant in unexpected darkness (figure 26E) had a more compact architecture. These results indicate that loss of *bzip63* affects the overall root architecture by impacting lateral root development under energy limiting conditions.

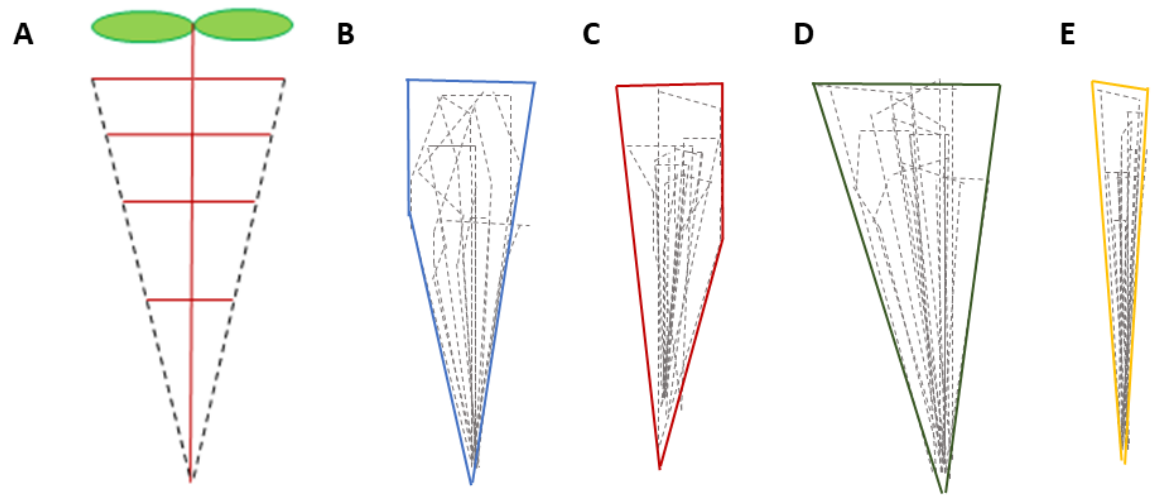

Figure 26: *bzip63* loss-of-function mutant affects the overall root architecture. (A) Representative image of the method employed to construct the root architecture. Each seedling grown on ½ MS plates was outlined from the tip of the primary root and tip of each lateral root using the straight-line tool in MS PowerPoint. An overlay of 10 seedlings was prepared and a final overlay or the maximum projection of those 10 seedlings determined the root architecture. Outline of the overall root architecture of WS wild-type (B, C) and *bzip63* (D, E) grown at control conditions (B, D) and 4 h unexpected darkness (C, E).

3.3 bZIP11, -2, -44 heterodimerization partners of bZIP63 partially impact root plasticity under short term energy limitation

3.3.1 Gain–and loss-of-function approaches of bZIP 11, -2 and -44 partially impacts lateral root development under short-term energy perturbations

Mair et al (2015) and Pedrotti et al (2018) showed that the SnRK1 mediated phosphorylation of bZIP63 enhances heterodimerization particularly with group S1 members. It is therefore tempting to speculate that heterodimers of bZIP63 with group S1 TFs such as bZIP11 would impact lateral root development upon short-term energy perturbations. In a study conducted

by Weiste et al (2017), the bZIP11 and its homologs bZIP2 and bZIP44 control the growth of the primary root during extended darkness.

To study the impact of bZIP11, -2 and -44 TFs on the lateral root development, we utilized ß-estradiol induced transgenic line ectopically expressing bZIP11 (XVE11). Unpublished results by Weiste et al showed that ß-estradiol inducible XVE11 lines displayed a higher eLR density in comparison to non-treated controls, which is similar to the results obtained in this study. We further tested this line with and without ß-estradiol induction and with and without 4 h of unexpected darkness. After 4 h of unexpected darkness, they were transferred to long day growth conditions, where control seedlings (with and without ß-estardiol) was maintained (figure 27). We noticed that with ß-estradiol and 4 h unexpected darkness, XVE11 exhibited the increased eLR density in comparison to untreated seedlings without ß-estradiol (figure 27A). This gave us a first indication that bZIP11 may impact lateral root development under unexpected darkness. However, phenotype is complex as the primary root of the ß-estradiol induced XVE11 lines were shorter in length both in control and 4 h unexpected darkness (figure 36)

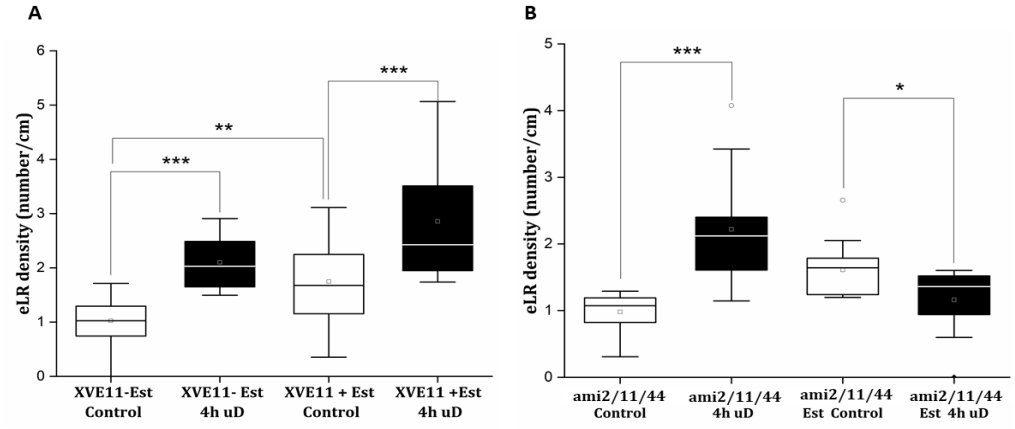

Figure 27: Ectopic expression of bZIP11 increases whereas knock-down of bZIP11, -2 and -44 reduces lateral root density under unexpected darkness. 8-day-old *A. thaliana* seedlings were grown on ½ MS media without 10µM ß-estradiol and then transferred to ½ MS containing 10µM of ß-estradiol. eLR density was recorded at 14 days after germination. (A) eLR density in β-estradiol induced ectopic bZIP11 overexpression (XVE11) with and without 4 h unexpected darkness (B) eLR density of ß-estradiol induced artificial microRNA (amiR2/11/44) knock-down of bZIP2, -11 and -44 with and without 4 h unexpected darkness. Normal distribution was calculated for each group and student's *t-test* was used to test significance. Asterisk indicate significance **p<0.05 **p<0.01 ***p<0.001* for n=14 seedlings.

Single loss-of-function mutants of *bzip11* and *bzip44* had partial impact on lateral root development in 4 h unexpected darkness (figure 35). As group S1 shows partial redundancy, we used a multiple knock-down approach to study the effect of loss-of-function mutant on lateral root development upon 4 h of unexpected darkness. We utilized the available ß-estradiol inducible artificial micro RNA (amiR) mediated knockdown lines of bZIP11, -2 and -44 (Weiste et al., 2014). Without ß-estradiol induction, there was no knockdown of bZIP11, -2 and -44 and the transgenic line behaved similarly to wildtype. In contrast, ß-estradiol induced knockdown of the TFs, the eLR density decreased in 4 h unexpected darkness, compared to the eLR density of control seedlings in light (figure 27B). This indicates that knocking down of group S_1 TFs influences the observed eLR density under 4 h unexpected darkness. Furthermore, primary root with ß-estradiol displayed similarities to what was shown earlier by Weiste et al (2017). Taken together these data suggest that bZIP11 and related TFs impact root architecture upon unexpected darkness with respect to both lateral root and primary root.

3.3.2 bZIP11 expression does not overlap with bZIP63 expression

Previous findings have established bZIP11 or related TFs as a potential heterodimerization partner of bZIP63 (Pedrotti et al., 2018). Hence, these TFs may functionally interact with bZIP63 in lateral root development under short-term energy perturbations. To further understand the functional role of bZIP11 and whether or not it overlaps with the expression pattern of bZIP63, we utilized Col-0 plants stably transformed with genomic bZIP11 including -2300bp promoter region, followed by *bZIP11* gene tagged to GFP (Weiste et al, 2017) (*pbZIP11*::bZIP11-UTR:GFP). Previous studies by Weiste et al (2017) has shown genuine bZIP11 expression at the primary root tip and in the primary root endodermis. We wanted to study the localization pattern of bZIP11 in different stages of the lateral root development. 8-day-old transgenic plant grown on ½ MS media without sugar or 4 h unexpected darkness treatment was utilized to localize the bZIP11:GFP protein. We were able to visualize bZIP11:GFP localization in the primary root tip, as seen by *Weiste et al.* (2017) (figure 28A). bZIP11:GFP was poorly expressed or absent in the early (stage I -figure 28B) and LRP (stage V and VI -figure 28C and 28D). In the emerged lateral root, bZIP11:GFP showed expression similar to the primary root. There was genuine nuclear bZIP11:GFP expression at the developed

endodermis of emerged lateral root (figure 28E). bZIP11 was not found to be expressed in the pericycle cell layer.

Taken together this result shows that it bZIP11 only partially overlaps with bZIP63 expression specifically at the endodermis of the primary root and is not localized at the early stages of lateral root development. Genuine bZIP11 expression was absent in the pericycle important for lateral root initiation. These expression patterns may not prove bZIP11 as a potential heterodimerization partner of bZIP63 in imparting lateral root development under unexpected darkness. Transgenic lines with bZIP2 and bZIP44 tagged to fluorescent protein is currently not available to check their expression patterns.

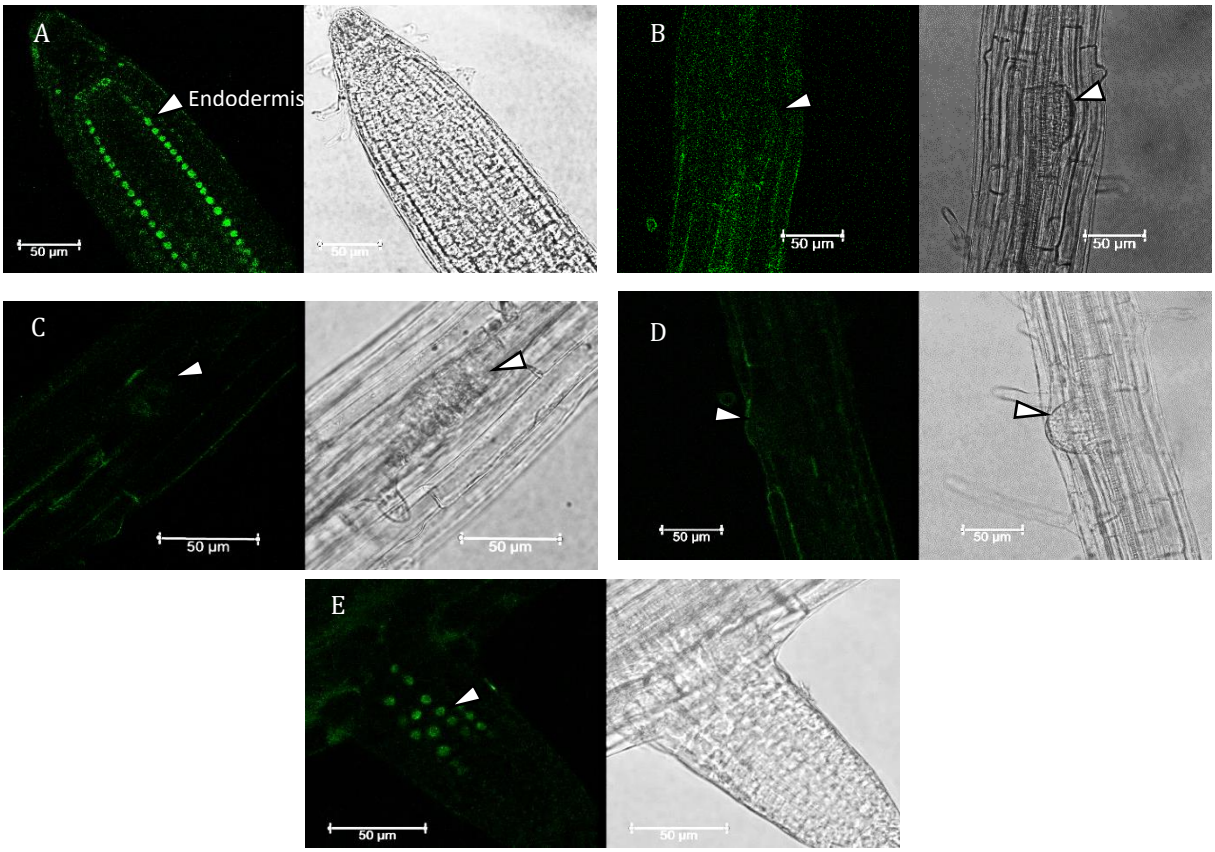

Figure 28: bZIP11:GFP is absent in stages of early lateral root development but is expressed in endodermis of adult lateral root and primary root. 8-day-old seedling of *A. thaliana* plant carrying genomic bZIP11 fused to GFP was utilized to study the expression patterns in primary and lateral root (A) bZIP11 expression in the endodermis in the primary root tip (B) Lack of bZIP11:GFP expression in the stage II – early initiation and in (C and D) stage V and VI LRP. (E) Genuine bZIP11 expression in the endodermis of adult lateral root. Endodermis and LRPs are marked with an arrow. Images were obtained at 40X water immersion objective. Scale bar 50 µm.

3.4 bZIP63 regulates important genes involved in lateral root development

3.4.1 AUXIN RESPONSE FACTOR 19 is the direct target of bZIP63

So far, we have established bZIP63 as a potential candidate important for the lateral root development under short-term energy perturbations. As a TF, bZIP63 may regulate several genes by direct binding to the cognate G-Boxes on their promoters. To identify genome-wide targets of bZIP63 and the regions bound by this TF, we employed chromatin immunoprecipitation (ChIP) followed by high-throughput DNA sequencing (ChIP-seq). This is a powerful tool to identify promoters bound by a specific TF. We utilized the *bzip63* loss-of-function mutant complemented with functional bZIP63 protein tagged to YFP driven by native promoter (*pbZIP63*:bZIP63:YFP) (Mair et al., 2015). As the promoter and coding regions were tagged to YFP, ChIP was performed using antibodies against the YFP tag (α-GFP antibody recognizes YFP tag, a genetic mutant of GFP). The background transgenic line used to complement functional bZIP63 (loss-of-function *bzip63*) served as control. Roots from 10 day-old seedlings were harvested after 4 h of unexpected darkness in control and bZIP63:YFP transgenic lines.

A total of 821 enriched peaks were identified in one working replicate. Enrichment refers to reads obtained from the ChIP of bZIP63:YFP divided by the reads from the control ChIP. The peaks were mapped to promoter region (51.2%), Intergenic (19%), Exon (15.8%), Transcription Termination Site (TTS) (11.3%) and Intron (2.7%) (figure 29A). The relative enrichment corresponding to promoter region agrees with what is known about TFs (Collani et al., 2019). Peak region showed a strong enrichment (most mapped counts) in G-Boxes which is a *cis*-element for several bZIPs (figure 29B). G-Boxes (CACGTG) are highly conserved and are bound particularly by several TFs of bHLH (basic helix-loop-helix) and bZIP families ranging from yeast to human (Ezer et al 2017). With the total of 821 direct binding regions with false discovery rate or p-value of 0.05, several direct binding targets of bZIP63 were identified. These findings are in line with described bZIP63 target genes such as *MCCA (METHYLCROTONYL-COA CARBOXYLASE)* (figure 29C), *ETFQOo* (*ELECTRON-TRANSFER FLAVOPROTEIN: UBIQUINONE OXIDO-REDUCTASE) BCAT-2 (BRANCHED CHAIN TRANSAMINASE2)* and *ProDH (PROLINE DEHYDROGENASE)* (figure 29C) which is part have been confirmed by ChIP (Pedrotti et al., 2018). This also confirms the robustness of the ChIP sequencing experiment. A complete list of traget genes is given in table 17

Only a subset of bound genes has shown to be directly involved with lateral root development table 16. Of these, ARF19 has been very well studied in different aspects of plant development. *ARF19* along with its gene family member *ARF7* regulate different aspects of the lateral root development from initiation till emergence. A double loss-of-function mutant of *arf19arf7* does not show any emerged lateral root (Okushima et al., 2007). *ARF19* possesses four G-Boxes in its promoter region and from the obtained ChIP-sequencing results, the binding region of bZIP63 corresponds to the region harbouring G-BOX 1 on *ARF19* promoter (figure 29D).

To further confirm the binding of bZIP63 to the promoter of *ARF19* and to exactly map the binding site near the G-Boxes, we employed ChIP-PCR technique. We used 10-day-old seedlings of bZIP63:YFP and treated them with 4 h of unexpected darkness. WS wild-type seedlings served as control.

Primers were designed to map bZIP63 binding in the *ARF19* promoter with respect to the G-Boxes to yield a product of 150 bp. Input controls (Chromatin without immunoprecipitation) served as the normalization control. Extracted and purified chromatin was subjected to qRT-PCR with primers spanning around G-BOX1, G-BOX2 and G-BOX3. Although the *ARF19* promoter possess a 4th G-Box, it was not predicted to be a binding region. Hence the 4th G-Box was excluded from analysing the binding around that region. We utilized *ACT7* (ACTIN 7) as non-binding control. *ACT7* promoter do not possess G-Boxes of bZIP binding regions and thus serve as a good non-target control.

We observed strong enrichment of precipitated *ARF19* promoter fragments compared to WS wild-type control (figure 29D). In contrast fragments corresponding to non-binding *ACT7* promoter was not enriched. Enrichment was significant in G-Box 1 and non-significant in G-Box 2 and G-Box 3, respectively.

These findings, which are in line with ChIP-seq studies, suggest that bZIP63 is able to directly target the *ARF19* promoter, presumably by binding to a cognate G-box 1 *cis*-element located around -300 bp apart from the translational start site. These findings support the view that the bZIP63 control ARF19 mediated LR development under unexpected darkness.

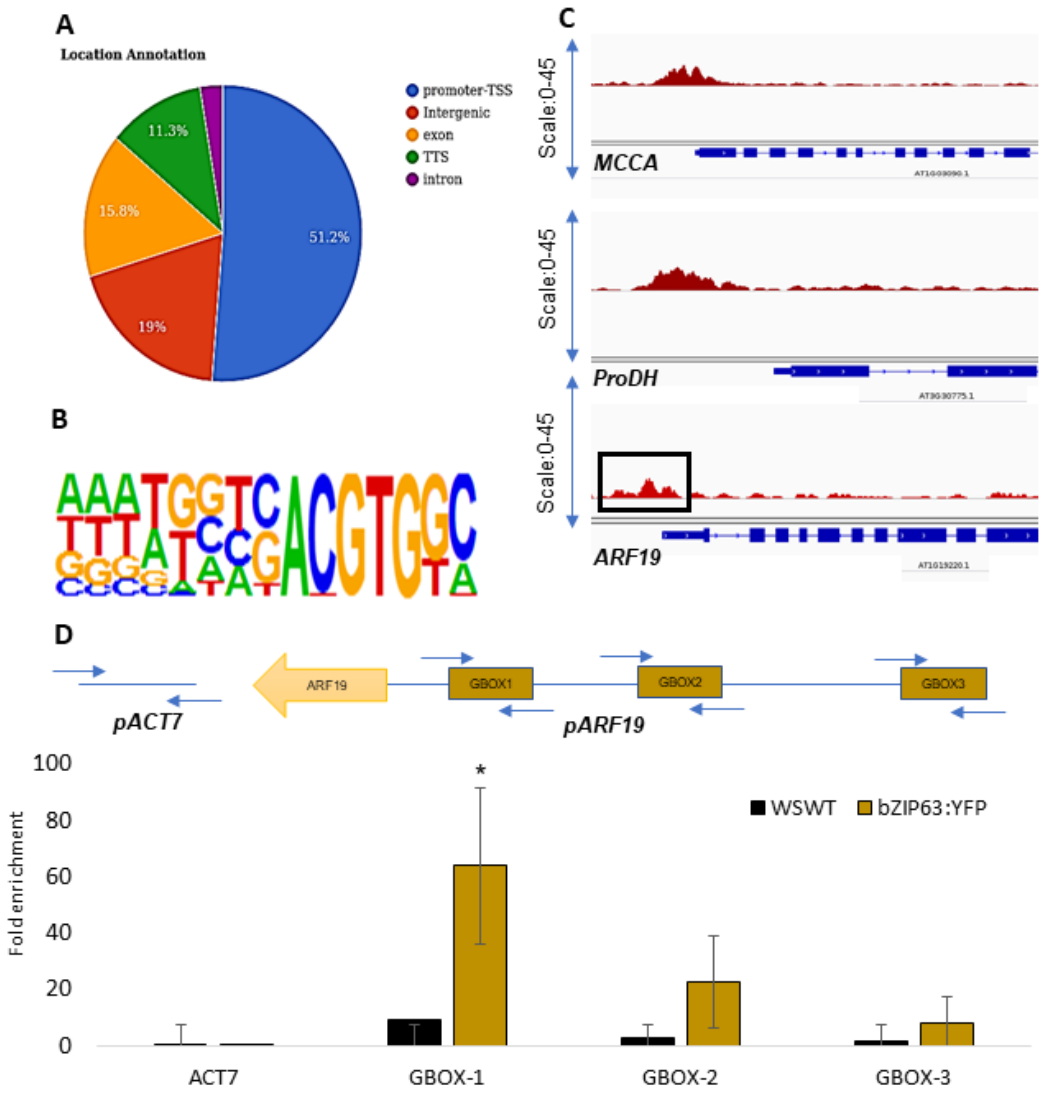

Figure 29: bZIP63 binds the ARF19 promoter, presumably to G-BOX1. For ChIP-seq roots of 10 DAG seedlings of *pbZIP63*:bZIP63:YFP and loss-of-function *bzip63* were harvested after 4 h of unexpected darkness. ChIP was performed for extracted chromatin with anti-GFP antibody. The pull-down chromatin-DNA complex was subjected to high throughput DNA sequencing. (A) Annotation of high-confidence peaks found in 1 biological replicate in YFP tagged bZIP63. TSS- transcription start site, TTS- transcription terminator site. (B) Nucleotide logo of the predicted and enriched bZIP63 binding site: the G-BOX (CACGTG). (C) Reads from bZIP63:YFP sample mapped against selected known targets as controls (*MCCA* and *ProDH*) and *ARF19*. Blue colour represents the exons of the gene. The *ARF19* promoter is marked for G-Box 1 binding region (black box). (D) For ChIP-PCR roots of 10 DAG seedlings from WS wild-type and bZIP63:YFP were harvested after 4 h of unexpected darkness. ChIP was performed for extracted chromatin with anti-GFP antibody. G-Box specific primers were used to amplify the chromatin. Direct binding of YFP tagged bZIP63 (Yellow bars) to *ARF19* promoter at three different regions each of which spans G-BOX 1, G-BOX 2 and G-BOX 3 as well as *ACT7* promoter as non-binding control was assessed by ChIP. WS wild-type served as control (Black bars). Presented are mean expression values from 3 independent plant pools per genotype (+/- SD), relative to Input *ACT8* expression. Significant differences between genotypes for each individual time-point were determined by Student's *t-test* and are labelled with asterisks *(* $p < 0.05$)*

3.4.2 The *bzip63* loss-of-function mutant shows no increased *ARF19* transcript levels upon short-term energy perturbations

Making use of Col-0 wild-type plants, we analysed *ARF19* transcript abundance in roots, at defined time-points of 1 h unexpected darkness, 2 h unexpected darkness, 4 h unexpected darkness as well as 4 h unexpected darkness plus 8 h or 16 h recovery in light with (figure 30C). Among tested treatment timepoints, *ARF19* transcripts which significantly increased during treatment with 4 h unexpected darkness in wild-type, showed no similar effect in *bzip63* loss-of-function mutant (figure 30C). This strongly indicates bZIP63 dependency on *ARF19* expression during energy limiting conditions. As a control, we confirmed that transcripts of *bZIP63* and *ASN1* also increased during 4 h of unexpected darkness, however not in *bzip63* loss-of-function mutant (figure 30A and B). During the recovery phase under light conditions, expression levels of all induced genes tested returned to normal.

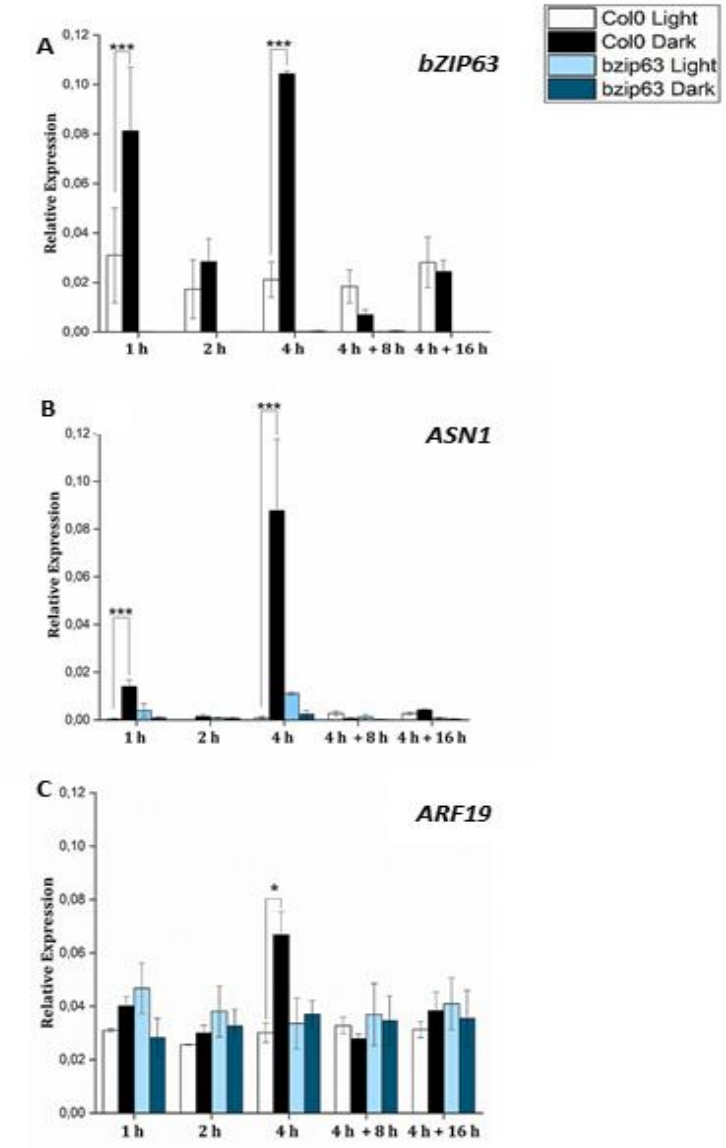

Figure 30: Loss of bZIP63 reduces expression of ARF19 during short-term unexpected darkness. 8-day-old *A. thaliana* seedlings were subjected with and without 1 h, 2 h or 4 h of unexpected darkness plus 8 h and 16 h of light recovery. Roots were harvested post-treatment and the RNA was extracted for cDNA synthesis and qRT-PCR was performed with primers amplifying *bZIP63, ASN1 and ARF19*. Expression of (A) *bZIP63* (B) *ASN1* and (C) *ARF19* was quantified in unexpected darkness time-points of 1 h, 2 h, 4 h, 4 h + 8 h light recovery and 4 h + 16 h light recovery between WS wildtype control (white bars), WS wild-type dark treatment (black bars), *bzip63* loss-of-function light control (light blue bars) and *bzip63* loss-of-function dark treatment (dark blue bars). Presented are mean expression values from 3 independent plant pools per genotype (+/- SEM), relative to *EF1A* expression. Significant differences between genotypes for each individual time-point were determined by Student's *t-test* and are labelled with asterisks (** p < 0.05, **p < 0.01, *** p < 0.001*). The experiment was repeated 3 times with similar results.

Taken together, these qRT-PCR data suggest a strong bZIP63 dependency in directly or indirectly modulating important lateral root developmental genes such as *ARF19*.

The above results unravel a novel role of SnRK1-bZIP63-ARF19 signalling in mediating lateral root development under short-term energy perturbations.

4. DISCUSSION

4.1 Short-term perturbations in plant energy homeostasis modify root architecture by increasing the lateral root density

A myriad of environmental cues is interpreted by plants and incorporated into developmental outputs. The root system have a strong phenotypic plasticity to adapt to fluctuating environmental conditions (Koevoets et al., 2016). Understanding how root system changes under different environmental conditions will prompt plant breeders to include root properties in current pipeline for stress tolerant plants (Li et al., 2016; Koevoets et al., 2016).

This work unravels a novel signalling pathway and the underlying molecular mechanism that transduces low energy conditions or metabolic limitation into changes in the root architecture, particularly focussing on lateral roots. Lateral root formation and development provides a good model for understanding how plant morphology is regulated and coordinated with changing environment (Malamy and Ryan, 2001).

So far there have been several experimental evidences on how internal metabolic nutrient imbalance in plants impact lateral root system. For example, a study conducted by Malamy and Ryan, (2001) showed that lateral root number and density decreased dramatically under high carbon (C) low nitrogen (N) levels. Another observation by Perres-Torres et al (2008) depicts that phosphate deficiency increases the lateral root number in order to acquire more phosphate from the soil. Our study provides one of the first evidences that link short-term metabolic shifts into lateral root developmental plasticity.

Treatments affecting photosynthesis lead to metabolic imbalances. Effects such as extended night, treatment with photosynthetic inhibitors, result in severe carbon/energy limitation, activation of catabolic pathways, growth inhibition and protein synthesis (Gibon et al., 2004; Smith and Stitt, 2007; Jin et al., 2017). In addition, extended night strongly affects the meristematic growth and reduces primary root length (Weiste et al., 2017; Yazdanbakhsh et al., 2011). Therefore, these treatments have a harsher effect on both primary and lateral root development and are not suitable.

Here, in this study we utilized treatments which do not impose harsh effects but still bring out changes in root architecture. We observed that short-term unexpected darkness during the day period did not interfere with primary root growth but resulted in increased lateral root density. This response was also triggered by other short-term metabolic perturbations such as low light. The low light treatment we employed here will not limit photoreceptor activity but is close to the light compensation point (Lauxmann et al., 2016). Taken together, these experimental approaches are well-suited to reproducibly study lateral root developmental outputs in response to short-term metabolic perturbations in a quantitative manner. Furthermore, longer treatments with low light negatively affected primary root length and lateral root density in comparison to short treatments. This indicates that only short-term triggers, such as 4 h unexpected darkness, 24 h and 36 h low light, bring out changes in the lateral root density.

On the other hand, it is important to know, what this short-term perturbation does and how it may impact root system architecture? We speculate that these short-term perturbations act as a cue or trigger in activating pericycle cells to divide and develop into lateral roots. Additionally, increase in lateral root density due to metabolic changes may lead to increased root biomass. Measuring root biomass after these short-term treatments both in *A. thaliana* and a model crop plant would help confirm this speculation and provide a biological relevance.

Next, we wanted to observe if short-term non-metabolic stress affect lateral root density in a similar manner to those of short-term metabolic perturbation. For this reason, we treated the seedlings with 20 minutes and 40 minutes of 42 ^{o}C heat. Although, there is not much evidence on the effect of heat stress on lateral root, a recent study by Song et al (2017) showed that long exposure (3 days) to heat reduces primary root growth and decreases emerged lateral root. Our results did not display any effect on either primary or lateral root growth. This indicates that the increased lateral root effect that we observe is specific for short-term metabolic perturbations. To further confirm this, treatment with other unspecific stresses such as cold or salinity could be another possibility.

The short-term energy/metabolic fluctuations could refer to shifts in principle energy components such as sugar/starch, ATP or C/N ratio. One recent study by Zhu et al (2017) on *Brassica campestris ssp Chinensis* Makino has shown that treatment with low light affects C/N ratio

and CO_2 fixation. On the other hand, darkness treatment led to a drop in soluble sugars in 3-week-old *Zea mays* L. leading to changes in metabolism and root growth. Therefore, it was vital for us to experimentally observe what changes the treatments we employ could have. Our treatments resulted in a transient drop in hexoses, first observed in shoot (not significant) and then significantly in roots. Sucrose levels were low in comparison to hexoses. We presume that this short-term imbalance is enough to cue developmental reprogramming.

Limitations of this approach include that the measurements are performed on overall plant organs and therefore the quantification of local sugar depletion is tedious. On the other hand, as sugar (glucose) is converted to energy (ATP) recently developed ATP sensors could be useful in measuring localized energy responses under short-term perturbations (De Col et al., 2017). In addition, we could measure ATP/ADP ratios in tissue extracts. These alternatives could be more suitable for measuring energy responses to different stress conditions at specific root regions.

Indeed, external sugars rescued the lateral root phenotype and thus, supports the view that limited carbohydrates might be the cause of the response. In the same experimental set up, mannitol was used as an osmotic control (Groenewegen and Mills, 1960). However, we did not see an increase in eLR density as expected. We utilized mannitol since it cannot be consumed and will show a similar effect to short-term perturbations on no sugar controls. Studies have shown that mannitol is indeed taken up by the root and transported to shoot but does not influence the glucose and sucrose content (Lipavská and Vreugdenhil, 1996). This may explain the no effect of mannitol on lateral root density phenotype. On the other hand, externally added sugars have a strong growth effect on overall root development. As the concentration of sugars is high, it does not say much about the small endogenous changes that may have occurred due to short-term perturbations.

We then observed that short-term perturbations activate the starvation marker *ASN1.* *ASN1* is induced by darkness and repressed by light (Lam Hon Ming et al., 1994; Lam Hon-Ming et al., 1995). Although the mechanisms of gene induction are not fully understood, *ASN1* has been a well-known target of low-energy activated SnRK1-C/S1-bZIP signalling network and the *ASN1* reporter has been used to study starvation responses (Baena-González et al., 2007; Hanson et al., 2007; Dietrich et al., 2011). In our experiments, we could demonstrate that *ASN1* responds to 1 h and 4 h of unexpected darkness by increased transcription in roots and

increased *ASN1:LUC* levels in shoots. Our data suggests that the increase in *ASN1* is due to a fluctuating energy response caused by treatment with short-term unexpected darkness. In addition, as expression of *ASN1* is under the metabolic control of the nitrogen to carbon ratio in cells (Lam Hon Ming et al., 1994), our treatments might influence this N/C ratio and *ASN1* expression is an output of that.

To summarize, although experiments to monitor energy levels are still not well developed, based on our results, we assume that the short-term perturbations used do not lead to starvation but to a limited metabolic imbalance, which results in a developmental response.

4.2 The conserved regulator of plant energy homeostasis SnRK1 plays a crucial role in modifying root architecture upon short-term metabolic perturbations

Transcriptome studies conducted by Beana-Gonzalez et al. (2007) have outlined that many catabolic or energy-saving processes are activated by SnRK1 kinases. What regulates SnRK1 remains largely elusive, as it is not regulated by the raise in ADP/AMP levels like in the mammalian AMPK counterpart (Corton et al., 1994). The SnRK1 kinases are activated upon reduced sugar levels (Crepin and Rolland, 2019; Tsai and Gazzarrini, 2014; Emanuelle et al., 2016; Smeekens et al., 2010). It is also shown that Trehalose-6-Phosphate (T6P) metabolite negatively impacts SnRK1 activity (Lunn et al., 2006; Figueroa and Lunn, 2016; Schluepmann and Paul, 2009). T6P has been recognized as a novel signal for carbohydrate status positively correlating with sugar levels (Lunn et al., 2006; Tsai and Gazzarrini, 2014). T6P levels closely follow the levels of sugar and an increase in level of sugar results in an increase in T6P which leads to metabolic shift and can accelerate growth in plants. If this is true, we could speculate that short-term unexpected darkness or low light treatments that reduce sugar levels reduce T6P levels and activate SnRK1 kinase. In addition to this, our data indicates an increase in eLR density under energy perturbations, confirming the likelihood of SnRK1 mediating this response.

Previous studies have shown the positive effects of SnRK1 on root growth. The line of plants that are overexpressing SnRK1.α1 subunit had an increased rate of primary root growth compared to the wild-type (Baena-González et al., 2007). In a recent study done by Ramon et al

(2019), low energy-stimulated translocation of SnRK1 catalytic α subunit in the nucleus is proposed to impact primary root length and root hair length positively. The plants expressing nuclear α subunit had longer primary root and root hair compared to wild-type (Ramon et al., 2019).

SnRK1 kinases consist of a catalytic subunit α and regulatory subunits β and γ. The two SnRK1 α subunits (SnRK1.α1 and SnRK1.α2) complement the yeast *snf1* mutant (Alderson et al., 1991). Although, the above information demonstrates functional redundancy of these subunits, recent studies have shown that their functions are not completely overlapping (Williams et al., 2014) and have partially redundant function (Baena-González et al., 2007). Similarly, in our study the loss-of-function of *snrk1.α2* displayed only minor to no effect whereas the loss of function of *snrk1.α1* displayed significant reduction in the eLR density after treatment with unexpected darkness. This supports that notion that SnRK1.α1 is important for lateral root development under metabolic perturbations. The primary roots of both wild-type and *snrk1.α1* and *snrk1.α2* do not show any differences under the short-term unexpected darkness. We also utilized plants with β-estradiol (*kin10:XVE:amiKIN11*) induced knockdown of *snrk1.α2* in *snrk1.α1* loss-of-function mutants to observe the combined effects of the catalytic subunits as complete loss-of-function of *snrk1.α1* and *snrk1.α2* is lethal. The *kin10;XVE:amiKIN11* transgenic line displayed severe growth defects within 3 days of β-estradiol treatment, also possibly due to loss of kinase activity. This was indicated by anthocyanin production as a sign of stress (Chalker-Scott, 1999). On the other hand, we utilized the SnRK1.α1 overexpressing transgenic line (*Pro35s:SnRK1.α1*) and noticed an increase in eLR density upon unexpected darkness. The wild-type ecotype *Ler* used for the generation of *Pro35s:SnRK1.α1* was devoid of the eLR density phenotype upon unexpected darkness. Therefore, the observed eLR density phenotype in *Pro35s:SnRK1.α1* could not be considered.

It is important to understand the expression pattern of SnRK1.α1 in the primary and the lateral roots, as we presume that it plays a role in the observed lateral root density under short-term perturbations. It has been shown that low energy stress activates SnRK1.α1 nuclear localisation and induced target gene expression (Ramon et al., 2019). In the present study, we noticed nuclear SnRK1.α1 expression at the root tip under normal growth conditions. The zone proximal to the root tip had SnRK1.α1 expression surrounding the nucleus in the cytoplasm in a ring-like manner. Based on the trigger or cue the SnRK1.α1 could translocate from

cytoplasm into the nucleus although the exact mechanism is not known. With respect to lateral roots, SnRK1.α1 is localized in the pericycle cell layer, early-stage lateral root initiation, LRP and emerged lateral root. Localization in the pericycle is indicative of a possible role of this kinase in the lateral root initiation process. Previous studies have shown highest level of SnRK1.α1 accumulation in the meristematic, elongation and differentiation zones of primary root and lateral root (Bitrián et al., 2011). This is in line with the present study, as we also observe SnRK1.α1 localization in these zones and as a ring-shaped structure around the nuclei. The SnRK1.α1, C terminal GFP fusion line does not allow more modifications to understand complex formation of SnRK1.α1 and this appears to be a limitation of this fusion line. It would be important to generate a SnRK1.α2- fluorescent fusion line to understand the localization pattern of the other catalytic subunit. Crucial understanding of how and where SnRK1 is responding to energy perturbations is important to map its downstream signalling pathways.

Furthermore, SnRK1 could respond to the energy perturbations in leaves where it phosphorylates downstream TFs which is then further transported to roots. As an example of shoot to root signalling, a study on HY5 bZIP TF provides evidence that a TF could translocate from shoot to root based on different triggers (Chen et al., 2016) and further research is needed to disclose long-distance communications in plant energy homeostasis.

Altogether, our data propose a novel function of SnRK1.α1 in mediating lateral root development under short-term energy perturbations.

4.3 Phosphorylation of bZIP63 by SnRK1 links short-term energy perturbations to early lateral root development

bzip63 loss-of-function mutants displayed a reduction in the eLR density in comparison to WS wild-type upon 4 h unexpected darkness and 24 h low light. Furthermore, we generated CRISPR-Cas9 loss-of-function mutant of *bzip63* under Col-0 wild-type background (*bzip63-CR*) and saw similar results. Lines with two independent loss-of-function transgenic lines showed that bZIP63 is required for the lateral root phenotype that can be observed under short-term energy perturbations. This was further confirmed by using *pbZIP63*:bZIP63:YFP (*bzip63* loss-of-function mutant rescued with wild-type bZIP63) (Mair et al., 2015) which displays increased eLR density upon unexpected darkness similar to wild-type. Next, it was important to understand at which stage of the lateral root development is bZIP63 involved. By combining

DIC imaging and use of lateral root developmental marker *pGATA23*::NLS-GFP, we confirmed that bZIP63 affects early stages of lateral root development.

GATA23 has an increased and correlating expression of the early stages of lateral root development and its expression decreases in adult and later stages of lateral root development. For our purpose this was a better choice than other lateral root initiation markers (MAKR4 and RALFL34) (De Rybel et al., 2010b; Murphy et al., 2016; Xuan et al., 2015). We observed an increase in early lateral root developmental stages in wild-type under short-term perturbations. On the other hand, *bzip63* loss-of-function mutant showed lesser number of early stage events under short-term energy perturbations. In addition, there were no defects seen in any stage of development in the loss-of-function mutant. We presume that our results indicate that bZIP63 TF is required for making new lateral roots. We hypothesize that this could be by triggering more XPP cells to undergo anticlinal cell division or by controlling cell-cycle progression, although this could not be more precisely identified in the present study. Future experiments using mutants defective in XPP division (Parizot et al., 2008; De Smet, 2012) or with cell-cycle (Himanen et al., 2002; Vanneste et al., 2005) along with bZIP63 can shed light in this direction.

In addition, the overall root architecture of *bzip63* loss-of-function mutant was reduced and more compact under unexpected darkness treatment. This implies that, even though the loss-of-function mutant produces lateral root, its number is lesser, and emergence is affected. The overall root architecture displayed no difference in wild-type with and without unexpected darkness treatment. This tool provides a pictorial representation of how the overall root system architecture would look and change upon unexpected darkness. It also provides an indication if emergence of lateral root is affected, which in our case holds true for *bzip63* loss-of-function mutant upon unexpected darkness.

These evidences prove that bZIP63 is an important lateral root development regulator under short-term perturbations of energy.

Although there are no previous studies showing role of bZIP63 in mediating aspects of root development under reduced energy, bZIP63 has been shown to adjust plant circadian system in response to low energy (Frank et al., 2018).bZIP63 binds and regulates the circadian clock gene *PRR7* to change the phase of the circadian clock in response to metabolic status of the

plant (Frank et al., 2018). It can be speculated, that the observed lateral root density phenotype due to short-term perturbations could also be an outcome of the input of SnRK1-bZIP63 signalling on the circadian clock. Indeed, the circadian regulation has been shown to have an impact on lateral root development (Voß et al., 2015). This study states that a fully operating circadian clock is necessary during lateral root emergence and the circadian clock modulates expression of genes which control auxin responses in cells overlying the lateral root primordia (Voß et al., 2015). Our ChIP-sequencing study showed that the promoter of *TOC1* (TIMING OF CAB EXPRESSION) is bound by bZIP63. *TOC1* transcription is auxin inducible during lateral root development and regulates rephasing of circadian clock oscillations in lateral roots (Voß et al., 2015). We could speculate that bZIP63 may exert its function on the lateral root development via regulating *TOC1. TOC1* is important for circadian regulation (Alabadí et al., 2001). To further understand this, quantifying root and shoot phenotypes of wild-type and bZIP63 dependent on day length and shift in day-night phases is important.

Besides being a target of SnRK1, another important evidence which supports the hypothesis that bZIP63 could be a possible candidate in controlling lateral root development comes from the publicly available VLRTC (Visual Lateral Root Transcriptome Compendium) database (Parizot et al., 2010). VLRTC tool provides a platform to identify the lateral root regulators which are yet to be studied. This platform combines all publicly available transcriptome data sets that provide information on regulators that are involved in the lateral root development and with additional information on tissue-specific expression of cell cycle involvement. According to this tool bZIP63 is the only bZIP TF that is expressed in the pericycle cell layer important for lateral root development (Parizot et al., 2010). We observed that bZIP63:YFP seems to be localized in the pericycle cell layer supporting the VLRTC results. This can be further substantiated using a bZIP63-promoter GUS fusion transgenic line and analysing the localization in a root cross-section as localization through microscopy provides a less easy explanation for the claim that bZIP63 is involved in lateral root initiation. Furthermore, bZIP63:YFP can be seen localized in primary root longitudinal zones in an oscillating pattern. The meristem and differentiation zone show increased localization and both of these longitudinal zones are important for XPP cell priming and lateral root initiation (De Smet et al., 2007; Xuan et al., 2018). Localization of bZIP63:YFP in different stages of lateral root is indicative of bZIP63 being important for the development of the organ.

Our next attempt was to find whether there is a possible link between SnRK1.α1-bZIP63 and the lateral root development under unexpected darkness. Extended night treatments increase phosphorylation events of bZIP63, and this supports the idea that bZIP63 plays a role in energy signalling. Recently, Mair et al (2015) found that SnRK1.α1 is the kinase responsible for the starvation-induced hyper-phosphorylation of bZIP63. We utilized the bZIP63 phosphorylation mutant, where functionally important serine residues are replaced with alanine. In these mutant lines, phosphorylation by SnRK1 is impaired (Mair et al., 2015). Upon short-term unexpected darkness, eLR density reduced showing similarities to *snrk1.α1* and *bzip63* loss-of-function transgenic lines. With these results we could postulate that when SnRK1.α1 is unable to phosphorylate bZIP63, the TF could not confer the observed lateral root phenotype under short-term unexpected darkness, thus highlighting a functional link between the kinase and the TF.

Apart from these phenotypic studies, co-localising the kinase and transcription factor in primary root and lateral root developmental stages will further confirm their role. From our data, both partners show similar expression profiles in the primary root, pericycle cells and early stage lateral root stages. Therefore, it is presumable that SnRK1-mediated phosphorylation of the bZIP63 TF occurs in cells important for lateral root initiation.

bZIP63 has emerged as an important metabolic regulator of starvation/low energy response. This is in line with energy-dependent expression of bZIP63 (Kunz et al., 2015; Matiolli et al., 2011) and that the several downstream gene targets of bZIP63 are involved in starvation response (Matiolli et al., 2011; Veerabagu et al., 2014). bZIP63 has not been shown either as an activator or repressor of transcription but studies by Pedrotti et al (2018) proposes that phosphorylation of bZIP63 by SnRK1 leads to increased heterodimerization between C/S_1 bZIPs TFs. Moreover, a ternary C/S_1-SnRK1 complex is formed on the DNA. This leads to recruitment of HAT (HISTONE ACETYL TRANSFERASE) to open up the chromatin. bZIP63 heterodimerize with group S_1 bZIP TFs such as bZIP11 which have also been linked with starvation response (Ehlert et al., 2006; Weltmeier et al., 2009). Group S_1 bZIP TFs -bZIP11, -2 and -44 influence the primary root growth under low energy (Weiste et al., 2017). Therefore, bZIP11 and related TFs bZIP2 and bZIP44 were candidates to examine their influence on the observed lateral root phenotype. Our data indicates that ectopic bZIP11 increases the lateral root density and a multiple knockdown of bZIP11, -2 and -44 reduces the lateral root density suggesting that

group S_1 members could be involved in mediating lateral root development under short-term energy perturbations. At the same time, it is important to study the role of bZIP44 and bZIP2 TFs as heterodimerization partners. Generation of single CRISPR/Cas9 loss-of-function mutants of bZIP2 and -44 and treatment with unexpected darkness would be required to study their role in this direction.

Furthermore, bZIP11:GFP is not localized in early stages of lateral root development and in pericycle cell layer. This information may not support the role of bZIP11 as a heterodimerization partner of bZIP63 in activating early lateral root events under short-term unexpected darkness. We cannot eliminate the possibility of bZIP11 playing a role in lateral root development, as it is well localized in the endodermis. Endodermis acts as a communication center of chemical, mechanical and hormonal crosstalk to allow development of new lateral roots (Augstein and Carlsbecker, 2018; Marhavý et al., 2012; Vilches-Barro and Maizel, 2015). At the same time, it acts a signalling center to perceive stressful environmental signals and regulate this lateral root growth (Robbins Ii et al., 2020; Geldner, 2013). As bZIP11 has been shown to play a role in auxin signalling and modulate root growth in primary root under low energy (Weiste et al., 2017) and the fact that it has a strong expression in endodermis, it is an important candidate to-further study its role in lateral root development confining to endodermis.

4.4 bZIP63 mediates its impact on lateral root development by directly controlling transcription of the crucial auxin dependent regulator ARF19

To identify targets mediating bZIP63 responses in facilitating lateral root development under short-term perturbations, we performed ChIP sequencing analysis. The quality of the generated ChIP-sequencing data-set is considered quite robust as several confirmed or proposed bZIP63 targets genes have been detected (e.g. *ETFQO, MCCA, BCAT2, ProDH*) (Pedrotti et al., 2018). These ChIP experiments were performed in a complemented *bzip63* mutant background expressing bZIP63:YFP under control of its own endogenous promoter. Thus, the ChIP signals obtained are reliable, since they are not due to ectopic miss-expression. Moreover, ChIP has been performed with root material harvested after 4 h unexpected darkness conditions, which provide information of the inductive condition and specific tissue of interest – root.

We identified *ARF19* promoter to be bound by bZIP63 TF in our ChIP-sequencing analysis with short-term unexpected darkness treatment. Many studies have shown that auxin rapidly alters transcript levels of genes involved in lateral root development and two such genes are *ARF7* and *ARF19.* ARF7 and ARF19 play essential roles such as regulation of downstream targets that are important for nuclear migration, cell division and emergence (Motte et al., 2019). They have strong overlapping expression at early stage lateral root initiation events (Okushima et al., 2005). The double mutant of *arf7arf19* do not show any lateral root initiation events (Okushima et al., 2007). Single *arf19* and *arf7* show lateral roots and it's been presumed that the genes redundantly regulate the other missing gene (Okushima et al., 2005). *ARF19* has been well studied as a transcriptional activator. Key roles of this ARF has been shown in mediating lateral root development under phosphate starvation where ARF19 binds to the promoter of *PHR1* phosphate response regulator (Huang et al., 2018). On the other hand, *ARF7* promoter was not bound by bZIP63 . We could speculate that the eLR density response what we observe could be independent of ARF7 or that bZIP63 may indirectly regulate ARF7 through ARF19.

To further confirm the binding on *ARF19*, we analysed the promoter for G-Box (TACGTG) binding region and found 3 G-Boxes which are in close vicinity to the transcriptional start site on the *ARF19* promoter. We found significant binding closer to the G-Box 1 on the *ARF19* promoter (we say closer to G-Box1 as ChIP PCR experiment does not provide the resolution to exactly map the binding of a TF to exact sequences on the promoters). This evidence further confirms that *ARF19* is the direct binding target of bZIP63 during short-term unexpected darkness. We also observed that unexpected darkness induces *ARF19* transcription and this induction is impaired in the *bzip63* mutant. This is indicative of bZIP63 being essential for inducing *ARF19* transcripts under unexpected darkness. We need to further confirm that the observed eLR density phenotype under unexpected darkness is dependent on ARF19. A suitable experiment for this would be to test *arf19* loss-of-function transgenic line under short-term energy perturbations. If the eLR density shows no response to short-term energy perturbations, then this would further support that the lateral root response we see depends on ARF19.

In addition, control of lateral root development involves complex regulation of auxin biosynthesis, transport and ability of the XPP cells to perceive auxin and respond to start cell division of

lateral root (Du and Scheres, 2018).Several environmental stresses alter the levels of auxin (Kazan, 2013). Auxin is the cue to stimulate ARF19. Presence of auxin degrade Aux/IAAs repressors and activate ARF TFs (Ulmasov et al., 1999). It has been recently shown that ARF19 undergoes nucleo-cytoplasmic partitioning as a mechanism for controlling auxin responsiveness in specific tissue (Powers et al., 2019). In this direction, we speculate that bZIP63 may be important to fine tune the ARF19 nuclear translocation and mediate transcription of downstream targets important for lateral root development under energy perturbations.

Apart from ARF19, our ChIP sequencing experiment identified other targets important for lateral root development namely – *PUCHI* and *MYB77*. *PUCHI* (Toyokura et al., 2019) and *MYB77* (Shin et al., 2007) have been shown to play important roles in early lateral root primordia development and emergence. *PUCHI* is regulated by a ARF7 and ARF19 TFs. *MYB77* TF modulates auxin signal transduction by interacting with other ARF TFs and is a part of combinatorial transcriptional control of lateral root development (Shin et al., 2007). This indicates that bZIP63 has several potential ways to signal into lateral root development and not just with ARF19.

5. CONCLUSIONS AND PERSPECTIVES

Our study provides novel insights on how developmental plasticity is controlled by minor changes in the plant's energy homeostasis via SnRK1-bZIP63-ARF19 signalling. We propose a model, wherein the short-term energy perturbations imposed by low-light and unexpected darkness lead to fluctuation in sugar levels. The SnRK1 kinases is proposed to be activated by these cues. The catalytic α subunit of the SnRK1 kinases, phosphorylate its downstream bZIP63 TF at three conserved serine residues. Upon phosphorylation, the bZIP63 TF may heterodimerize with group S1 bZIP TF and bind to the G-Box 1 on the promoter of ARF19 and activate its transcription. The bZIP63 heterodimerisation partners still need to be determined. ARF19 is a well-known transcriptional activator of genes important for lateral root development and is primarily regulated by the phytohormone auxin. The regulatory input of auxin in this response needs to be established. In this respect, auxin-dependent degradation of specific AUX/IAA repressors should be further studied. Moreover, future work is needed to functionally characterize other bZIP63 downstream targets involved in controlling lateral root development upon short-term energy limitation.

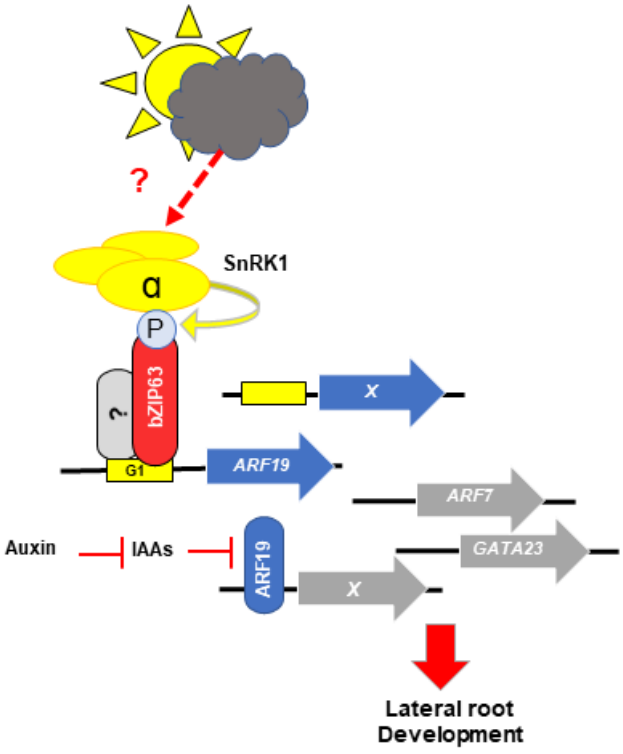

Taken together, we speculate that plants sense slight changes in metabolism and rapidly react with respect to developmental plasticity. The SnRK1-bZIP63 module provides an input to

transmit this information into transcriptional fine-tuning of *ARF19*, a central regulator of lateral root development. This increased root system might be due to overall shoot-root growth balance depending on available resources or useful for resource foraging (Tian and Doerner, 2013) and in turn survival. Yet, the biological relevance remains unclear. Nevertheless, understanding how root developmental plasticity changes due to short-term or mild stress in crop plants, may provide important information for crop survival and development.

6. REFERENCES

Aalen, R.B., Wildhagen, M., Stø, I.M., and Butenko, M.A. (2013). IDA: a peptide ligand regulating cell separation processes in Arabidopsis. J. Exp. Bot. **64**: 5253–5261.

Aceves-García, P., Álvarez-Buylla, E.R., Garay-Arroyo, A., García-Ponce, B., Muñoz, R., and Sánchez, M. de la P. (2016). Root Architecture Diversity and Meristem Dynamics in Different Populations of Arabidopsis thaliana. Front. Plant Sci. **7:** 858.

Alabadí, D., Oyama, T., Yanovsky, M.J., Harmon, F.G., Más, P., and Kay, S.A. (2001). Reciprocal regulation between TOC1 and LHY/CCA1 within the Arabidopsis circadian clock. Science. **293**: 880–883.

Alderson, A., Sabelli, P.A., Dickinson, J.R., Cole, D., Richardson, M., Kreis, M., Shewry, P.R., and Halford, N.G. (1991). Complementation of snf1, a mutation affecting global regulation of carbon metabolism in yeast, by a plant protein kinase cDNA. Proc. Natl. Acad. Sci. U. S. A. **88**: 8602–8605.

Augstein, F. and Carlsbecker, A. (2018). Getting to the roots: a developmental genetic view of root anatomy and function from arabidopsis to lycophytes. Front. Plant Sci. **9**: 1410.

Baena-González, E., Rolland, F., Thevelein, J.M., and Sheen, J. (2007). A central integrator of transcription networks in plant stress and energy signalling. Nature **448**: 938–942.

Baena-González, E. and Sheen, J. (2008). Convergent energy and stress signalling. Trends Plant Sci. **13**: 474–482.

Balcerowicz, D., Schoenaers, S., and Vissenberg, K. (2015). Cell fate determination and the switch from diffuse growth to planar polarity in arabidopsis root epidermal cells. Front. Plant Sci. **6**: 1163.

Beeckman, T. and De Smet, I. (2014). Pericycle. Curr. Biol. CB.**24**: R378-9

Benfey, P.N. and Scheres, B. (2000). Root development. Curr. Biol. **10**: R813–R815.

Binder, S. (2010). Branched-Chain Amino Acid Metabolism in Arabidopsis thaliana . Arab. B. **8**: e0137.

Bitrián, M., Roodbarkelari, F., Horváth, M., and Koncz, C. (2011). BAC-recombineering for studying plant gene regulation: Developmental control and cellular localization of SnRK1 kinase subunits. Plant J. **65**: 829–842.

Broeckx, T., Hulsmans, S., and Rolland, F. (2016). The plant energy sensor: evolutionary conservation and divergence of SnRK1 structure, regulation, and function. J. Exp. Bot. **67**: 6215–6252.

Casimiro, I., Beeckman, T., Graham, N., Bhalerao, R., Zhang, H., Casero, P., Sandberg, G., and Bennett, M.J. (2003). Dissecting Arabidopsis lateral root development. Trends Plant Sci.

8: 165–171.

Casimiro, I., Marchant, A., Bhalerao, R.P., Beeckman, T., Dhooge, S., Swarup, R., Graham, N., Inzé, D., Sandberg, G., Casero, P.J., and Bennett, M. (2001). Auxin transport promotes arabidopsis lateral root initiation. Plant Cell **13**: 843–852.

Chaffey, N. (2014). Raven biology of plants, 8th edn. Ann. Bot. **113**: vii–vii.

Chalker-Scott, L. (1999). Environmental Significance of Anthocyanins in Plant Stress Responses. Photochem. Photobiol. **70**: 1–9.

Chen, T.W., Li, H.P., Lee, C.C., Gan, R.C., Huang, P.J., Wu, T.H., Lee, C.Y., Chang, Y.F., and Tang, P. (2014). ChIPseek, a web-based analysis tool for ChIP data. BMC Genomics **15**: 539.

Chen, X., Yao, Q., Gao, X., Jiang, C., Harberd, N.P., and Fu, X. (2016). Shoot-to-Root Mobile Transcription Factor HY5 Coordinates Plant Carbon and Nitrogen Acquisition. Curr. Biol. **26**: 640–646.

Clough, S.J. and Bent, A.F. (1998). Floral dip: A simplified method for Agrobacterium-mediated transformation of Arabidopsis thaliana. Plant J. **16**: 735–743.

Collani, S., Neumann, M., Yant, L., and Schmid, M. (2019). FT modulates genome-wide DNA-binding of the bZIP transcription factor FD. Plant Physiol. **180**: 367–380.

Crepin, N. and Rolland, F. (2019). SnRK1 activation, signalling, and networking for energy homeostasis. Curr. Opin. Plant Biol. **51**: 29–36.

Crozet, P., Margalha, L., Confraria, A., Rodrigues, A., Martinho, C., Adamo, M., Elias, C.A., and Baena-González, E. (2014). Mechanisms of regulation of SNF1/AMPK/SnRK1 protein kinases. Front. Plant Sci. **5**: 190.

Dharmasiri, N., Dharmasiri, S., and Estelle, M. (2005). The F-box protein TIR1 is an auxin receptor. Nature **435**: 441–445.

Dietrich, K., Weltmeier, F., Ehlert, A., Weiste, C., Stahl, M., Harter, K., and Dröge-Lasera, W. (2011). Heterodimers of the Arabidopsis transcription factors bZIP1 and bZIP53 reprogram amino acid metabolism during Low energy stress. Plant Cell **23**: 381–395.

Doblas, V.G., Geldner, N., and Barberon, M. (2017). The endodermis, a tightly controlled barrier for nutrients. Curr. Opin. Plant Biol. **39**: 136–143.

Dolan, L., Janmaat, K., Willemsen, V., Linstead, P., Poethig, S., Roberts, K., and Scheres, B. (1993). Cellular organisation of the Arabidopsis thaliana root. Development **119**: 71–84.

Dröge-Laser, W., Snoek, B.L., Snel, B., and Weiste, C. (2018). The Arabidopsis bZIP transcription factor family — an update. Curr. Opin. Plant Biol. **45**: 36–49.

Dröge-Laser, W. and Weiste, C. (2018). The C/S1 bZIP Network: A Regulatory Hub

Orchestrating Plant Energy Homeostasis. Trends Plant Sci. **23**: 422–433.

Du, Y. and Scheres, B. (2018). Lateral root formation and the multiple roles of auxin. J. Exp. Bot. **69**: 155–167.

Du, Y. and Scheres, B. (2017). PLETHORA transcription factors orchestrate de novo organ patterning during Arabidopsis lateral root outgrowth. Proc. Natl. Acad. Sci. U. S. A. **114**: 11709–11714.

Dubrovsky, J.G. and Forde, B.G. (2012). Quantitative Analysis of Lateral Root Development: Pitfalls and How to Avoid Them. Plant Cell.**24 (1)**: 4-14

Ehlert, A., Weltmeier, F., Wang, X., Mayer, C.S., Smeekens, S., Vicente-Carbajosa, J., and Dröge-Laser, W. (2006). Two-hybrid protein-protein interaction analysis in Arabidopsis protoplasts: Establishment of a heterodimerization map of group C and group S bZIP transcription factors. Plant J. **46**: 890–900.

Emanuelle, S., Doblin, M.S., Stapleton, D.I., Bacic, A., and Gooley, P.R. (2016). Molecular Insights into the Enigmatic Metabolic Regulator, SnRK1. Trends Plant Sci. **21**: 341–353.

Van den Ende, W. (2014). Sugars take a central position in plant growth, development and, stress responses. A focus on apical dominance. Front. Plant Sci. **5**: 313.

Figueroa, C.M. and Lunn, J.E. (2016). A tale of two sugars: Trehalose 6-phosphate and sucrose. Plant Physiol. **172**: 7–27.

Von Fircks, Y. and Sennerby-Forsse, L. (1998). Seasonal fluctuations of starch in root and stem tissues of coppiced Salix viminalis plants grown under two nitrogen regimes. Tree Physiol. **18**: 243–249.

Fragoso, S., Espíndola, L., Páez-Valencia, J., Gamboa, A., Camacho, Y., Martínez-Barajas, E., and Coello, P. (2009). SnRK1 isoforms AKIN10 and AKIN11 are differentially regulated in Arabidopsis plants under phosphate starvation. Plant Physiol. **149**: 1906–1916.

Frank, A. et al. (2018). Circadian Entrainment in Arabidopsis by the Sugar-Responsive Transcription Factor bZIP63. Curr. Biol. **28**: 2597-2606.

Fukaki, H., Nakao, Y., Okushima, Y., Theologis, A., and Tasaka, M. (2005). Tissue-specific expression of stabilized SOLITARY-ROOT/IAA14 alters lateral root development in Arabidopsis. Plant J. **44**: 382–395.

Fukaki, H., Tameda, S., Masuda, H., and Tasaka, M. (2002). Lateral root formation is blocked by a gain-of-function mutation in the *SOLITARY-ROOT/IAA14* gene of *Arabidopsis*. Plant J. **29**: 153–168.

Gaufichon, L. et al. (2017). *ASN1* -encoded asparagine synthetase in floral organs contributes to nitrogen filling in Arabidopsis seeds. Plant J. **91**: 371–393.

Gaufichon, L., Reisdorf-Cren, M., Rothstein, S.J., Chardon, F., and Suzuki, A. (2010). Biological functions of asparagine synthetase in plants. Plant Sci. **179**: 141–153.

Ge, S.X., Jung, D., and Yao, R. (2019). ShinyGO: a graphical gene-set enrichment tool for animals and plants. Bioinformatics. **btz931**: 1367-4803

Geldner, N. (2013). The Endodermis. Annu. Rev. Plant Biol. **64**: 531–558.

Ghosh, D. and Xu, J. (2014). Abiotic stress responses in plant roots: A proteomics perspective. Front. Plant Sci. **5**. 6.

Gibon, Y., Blaesing, O.E., Hannemann, J., Carillo, P., Höhne, M., Hendriks, J.H.M., Palacios, N., Cross, J., Selbig, J., and Stitt, M. (2004). A robot-based platform to measure multiple enzyme activities in Arabidopsis using a set of cycling assays: Comparison of changes of enzyme activities and transcript levels during diurnal cycles and in prolonged darkness. Plant Cell **16**: 3304–3325.

Goh, T., Kasahara, H., Mimura, T., Kamiya, Y., and Fukaki, H. (2012). Multiple AUX/IAA-ARF modules regulate lateral root formation: The role of Arabidopsis SHY2/IAA3-mediated auxin signalling. Philos. Trans. R. Soc. B Biol. Sci. **367**: 1461–1468.

Gray, W.M., Kepinski, S., Rouse, D., Leyser, O., and Estelle, M. (2001). Auxin regulates SCFTIR1-dependent degradation of AUX/IAA proteins. Nature **414**: 271–276.

Grebe, M. (2011). Plant biology: Unveiling the Casparian strip. Nature **473**: 294–295.

Greer, L.F. and Szalay, A.A. (2002) Imaging of light emission from the expression of luciferases in living cells and organisms: a review. Luminescence **17**: 43–74.

Griffiths AJF, Miller JH, Suzuki DT, et al. An Introduction to Genetic Analysis. 7th edition. New York: W. H. Freeman; (2000). Genes, the environment, and the organism. Available from: https://www.ncbi.nlm.nih.gov/books/NBK21842/.

Groenewegen, H. and Mills, J. (1960). Uptake of Mannitol Into the Shoots of Intact Barley Plants. Aust. J. Biol. Sci. **13**: 1.

Hanson, J., Hanssen, M., Wiese, A., Hendriks, M.M.W.B., and Smeekens, S. (2007). The sucrose regulated transcription factor bZIP11 affects amino acid metabolism by regulating the expression of ASPARAGINE SYNTHETASE1 and PROLINE DEHYDROGENASE2. Plant J. **53**: 935–949.

Hardie, D.G. (2011). AMP-activated protein kinase-an energy sensor that regulates all aspects of cell function. Genes Dev. **25**: 1895–1908.

Hardie, D.G., Carling, D., and Gamblin, S.J. (2011). AMP-activated protein kinase: Also regulated by ADP? Trends Biochem. Sci. **36**: 470–477.

Hardie, D.G. and Hawley, S.A. (2001). AMP-activated protein kinase: the energy charge hypothesis revisited. BioEssays **23**: 1112–1119.

Hartmann, L. et al. (2015). Crosstalk between two bZIP signalling pathways orchestrates salt-induced metabolic reprogramming in arabidopsis roots. Plant Cell **27**: 2244–2260.

Hellmann, E., Ko, D., Ruonala, R., and Helariutta, Y. (2018). Plant vascular tissues—connecting tissue comes in all shapes. Plants **7**:109.

Himanen, K., Boucheron, E., Vanneste, S., De Almeida Engler, J., Inzé, D., and Beeckman, T. (2002). Auxin-mediated cell cycle activation during early lateral root initiation. Plant Cell **14**: 2339–2351.

Hiratsu, K., Matsui, K., Koyama, T., and Ohme-Takagi, M. (2003). Dominant repression of target genes by chimeric repressors that include the EAR motif, a repression domain, in *Arabidopsis*. Plant J. **34**: 733–739.

Hochholdinger, F. and Zimmermann, R. (2008). Conserved and diverse mechanisms in root development. Curr. Opin. Plant Biol. **11**: 70–74.

Hsu, P.D., Lander, E.S., and Zhang, F. (2014). Development and applications of CRISPR-Cas9 for genome engineering. Cell **157**: 1262–1278.

Hu, L., Robert, C.A.M., Cadot, S., Zhang, X., Ye, M., Li, B., Manzo, D., Chervet, N., Steinger, T., Van Der Heijden, M.G.A., Schlaeppi, K., and Erb, M. (2018). Root exudate metabolites drive plant-soil feedbacks on growth and defense by shaping the rhizosphere microbiota. Nat. Commun. **9**. 2738

Huang, K.L., Ma, G.J., Zhang, M.L., Xiong, H., Wu, H., Zhao, C.Z., Liu, C. Sen, Jia, H.X., Chen, L., Kjorven, J.O., Li, X.B., and Ren, F. (2018). The ARF7 and ARF19 transcription factors positively regulate PHOSPHATE STARVATION RESPONSE1 in Arabidopsis roots. Plant Physiol. **178**: 413–427.

Iijima, M., Morita, S., and Barlow, P.W. (2008). Structure and Function of the Root Cap. Plant Prod. Sci. **11**: 17–27.

Inoue, H., Nojima, H., and Okayama, H. (1990). High efficiency transformation of Escherichia coli with plasmids. Gene **96**: 23–28.

Javelle, M., Vernoud, V., Rogowsky, P.M., and Ingram, G.C. (2011). Epidermis: the formation and functions of a fundamental plant tissue. New Phytol. **189**: 17–39.

Jin, Y., Chen, S., Fan, X., Song, H., Li, X., Xu, J., and Qian, H. (2017). Diuron treatment reveals the different roles of two cyclic electron transfer pathways in photosystem II in Arabidopsis thaliana. Pestic. Biochem. Physiol. **137**: 15–20.

Kang, Y., Khan, S., and Ma, X. (2009). Climate change impacts on crop yield, crop water productivity and food security - A review. Prog. Nat. Sci. **19**: 1665–1674.

Kaufmann, K., Muiño, J.M., Østerås, M., Farinelli, L., Krajewski, P., and Angenent, G.C. (2010). Chromatin immunoprecipitation (ChIP) of plant transcription factors followed by

sequencing (ChIP-SEQ) or hybridization to whole genome arrays (ChIP-CHIP). Nat. Protoc. **5**: 457–472.

Kazan, K. (2013). Auxin and the integration of environmental signals into plant root development. Ann. Bot. **112**: 1655–1665.

Kiba, T. and Krapp, A. (2016). Plant Nitrogen Acquisition Under Low Availability: Regulation of Uptake and Root Architecture. Plant Cell Physiol. **57**: 707–714.

Kim, T.H. and Dekker, J. (2018). ChIP–quantitative polymerase chain reaction (ChIP-qPCR). Cold Spring Harb. Protoc: 354–355.

Kircher, S. and Schopfer, P. (2016). Priming and positioning of lateral roots in Arabidopsis. An approach for an integrating concept. J. Exp. Bot. **67**: 1411–1420.

Koevoets, I.T., Venema, J.H., Elzenga, J.T.M., and Testerink, C. (2016). Roots withstanding their environment: Exploiting root system architecture responses to abiotic stress to improve crop tolerance. Front. Plant Sci. **7**. 1335

Koncz, C. and Schell, J. (1986). The promoter of TL-DNA gene 5 controls the tissue-specific expression of chimaeric genes carried by a novel type of Agrobacterium binary vector. MGG Mol. Gen. Genet. **204**: 383–396.

Kouzarides, T. and Ziff, E. (1989). Leucine zippers of fos, jun and GCN4 dictate dimerization specificity and thereby control DNA binding. Nature **340**: 568–571.

Kumpf, R.P., Shi, C.-L., Larrieu, A., Stø, I.M., Butenko, M.A., Péret, B., Bennett, M.J., and Aalen, R.B. (2013). Floral organ abscission peptide IDA and its HAE/HSL2 receptors control cell separation during lateral root emergence. PNAS **110**. 5235-5240

Labun, K., Montague, T.G., Krause, M., Torres Cleuren, Y.N., Tjeldnes, H., and Valen, E. (2019). CHOPCHOP v3: expanding the CRISPR web toolbox beyond genome editing. Nucleic Acids Res. **47**: W171–W174.

Lam, H.M., Peng, S., and Coruzzi, G.M. (1994). Metabolic Regulation of the Gene Encoding Glutamine-Dependent Asparagine Synthetase in Arabidopsis thaliana. Plant Physiol. **106**: 1347–1357.

Lam Hon-Ming, Coschigano, K., Schultz, C., Melo-Oliveira, R., Tjaden, G., Oliveira, I., Ngai, N., Hsieh Ming-Hsiun, and Coruzzi, G. (1995). Use of Arabidopsis mutants and genes to study amide amino acid biosynthesis. Plant Cell **7**: 887–898.

Lam Hon Ming, Peng, S.S.Y., and Coruzzi, G.M. (1994). Metabolic regulation of the gene encoding glutamine-dependent asparagine synthetase in Arabidopsis thaliana. Plant Physiol. **106**: 1347–1357.

Laskowski, M., Biller, S., Stanley, K., Kajstura, T., and Prusty, R. (2006). Expression profiling of auxin-treated Arabidopsis roots: Toward a molecular analysis of lateral root

emergence. Plant Cell Physiol. **47**: 788–792.

Lastdrager, J., Hanson, J., and Smeekens, S. (2014). Sugar signals and the control of plant growth and development. J. Exp. Bot. **65**: 799–807.

Lauxmann, M.A. et al. (2016). Reproductive failure in Arabidopsis thaliana under transient carbohydrate limitation: Flowers and very young siliques are jettisoned and the meristem is maintained to allow successful resumption of reproductive growth. Plant Cell Environ. **39**: 745–767.

Lea, P.J. (1997). Primary Nitrogen Metabolism. In Plant Biochemistry (Elsevier), pp. 273–313.

Lee, K.W., Chen, P.W., Lu, C.A., Chen, S., David Ho, T.H., and Yu, S.M. (2009). Coordinated responses to oxygen and sugar deficiency allow rice seedlings to tolerate flooding. Sci. Signal. **2**: ra61–ra61.

Li, H. and Durbin, R. (2010). Fast and accurate long-read alignment with Burrows–Wheeler transform. Bioinformatics **26**: 589–595.

Li, X., Zeng, R., and Liao, H. (2016). Improving crop nutrient efficiency through root architecture modifications. J. Integr. Plant Biol. **58**: 193–202.

Lima, J.E., Kojima, S., Takahashi, H., and von Wirén, N. (2010). Ammonium triggers lateral root branching in Arabidopsis in an AMMONIUM TRANSPORTER1;3-dependent manner. Plant Cell **22**: 3621–3633.

Lipavská, H. and Vreugdenhil, D. (1996). Uptake of mannitol from the media by in vitro grown plants. Plant Cell. Tissue Organ Cult. **45**: 103–107.

Livak, K.J. and Schmittgen, T.D. (2001). Analysis of relative gene expression data using real-time quantitative PCR and the 2-ΔΔCT method. Methods **25**: 402–408.

Lucas, M. et al. (2013). Lateral root morphogenesis is dependent on the mechanical properties of the overlaying tissues. Proc. Natl. Acad. Sci. U. S. A. **110**: 5229–5234.

Lunn, J.E., Feil, R., Hendriks, J.H.M., Gibon, Y., Morcuende, R., Osuna, D., Scheible, W.R., Carillo, P., Hajirezaei, M.R., and Stitt, M. (2006). Sugar-induced increases in trehalose 6-phosphate are correlated with redox activation of ADPglucose pyrophosphorylase and higher rates of starch synthesis in Arabidopsis thaliana. Biochem. J. **397**: 139–148.

Mähönen, A.P., Bishopp, A., Higuchi, M., Nieminen, K.M., Kinoshita, K., Törmäkangas, K., Ikeda, Y., Oka, A., Kakimoto, T., and Helariutta, Y. (2006). Cytokinin signalling and its inhibitor AHP6 regulate cell fate during vascular development. Science. **311**: 94–98.

Mair, A. et al. (2015). SnRK1-triggered switch of bZIP63 dimerization mediates the low-energy response in plants. Elife **4**. e05828

Malamy, J.E. (2005). Intrinsic and environmental response pathways that regulate root

system architecture. Plant, Cell Environ. **28**: 67–77.

Malamy, J.E. and Benfey, P.N. (1997). Organization and cell differentiation in lateral roots of Arabidopsis thaliana. Development **124**.33-44

Malamy, J.E. and Ryan, K.S. (2001). Environmental regulation of lateral root initiation in Arabidopsis. Plant Physiol. **127**: 899–909.

Margalha, L., Confraria, A., and Baena-González, E. (2019). SnRK1 and TOR: Modulating growth–defense trade-offs in plant stress responses. J. Exp. Bot. **70**: 2261–2274.

Margalha, L., Valerio, C., and Baena-González, E. (2016). Plant SnRK1 Kinases: Structure, Regulation, and Function. In AMP-activated Protein Kinase, M.D. Cordero and B. Viollet, eds (Springer International Publishing: Cham), pp. 403–438.

Marhavý, P., Vanstraelen, M., De Rybel, B., Zhaojun, D., Bennett, M.J., Beeckman, T., and Benková, E. (2012). Auxin reflux between the endodermis and pericycle promotes lateral root initiation. EMBO J. **32**: 149–158.

Menkens, A.E., Schindler, U., and Cashmore, A.R. (1995). The G-box: a ubiquitous regulatory DNA element in plants bound by the GBF family of bZIP proteins. Trends Biochem. Sci. **20**: 506–510.

Miyashima, S. and Nakajima, K. (2011). The root endodermis: A hub of developmental signals and nutrient flow. Plant Signal. Behav. **6**: 1954–1958.

Mockaitis, K. and Estelle, M. (2008). Auxin Receptors and Plant Development: A New Signalling Paradigm. Annu. Rev. Cell Dev. Biol. **24**: 55–80.

Moore, B., Zhou, L., Rolland, F., Hall, Q., Cheng, W.H., Liu, Y.X., Hwang, I., Jones, T., and Sheen, J. (2003). Role of the Arabidopsis glucose sensor HXK1 in nutrient, light, and hormonal signalling. Science . **300**: 332–336.

Moreira, S., Bishopp, A., Carvalho, H., and Campilho, A. (2013). AHP6 Inhibits Cytokinin Signalling to Regulate the Orientation of Pericycle Cell Division during Lateral Root Initiation. PLoS One **8**: e56370.

Moreno-Risueno, M.A., Van Norman, J.M., Moreno, A., Zhang, J., Ahnert, S.E., and Benfey, P.N. (2010). Oscillating gene expression determines competence for periodic Arabidopsis root branching. Science. **329**: 1306–1311.

Motte, H., Vanneste, S., and Beeckman, T. (2019). Molecular and Environmental Regulation of Root Development. Annu. Rev. Plant Biol. **70**: 465–488.

Murphy, E. et al. (2016). RALFL34 regulates formative cell divisions in Arabidopsis pericycle during lateral root initiation. J. Exp. Bot. **67**: 4863–4875.

Nacry, P., Canivenc, G., Muller, B., Azmi, A., Van Onckelen, H., Rossignol, M., and Doumas,

P. (2005). A role for auxin redistribution in the responses of the root system architecture to phosphate starvation in Arabidopsis. Plant Physiol. **138**: 2061–2074.

Nieuwland, J., Maughan, S., Dewitte, W., Scofield, S., Sanz, L., and Murray, J.A.H. (2009). The D-type cyclin CYCD4;1 modulates lateral root density in Arabidopsis by affecting the basal meristem region. Proc. Natl. Acad. Sci. U. S. A. **106**: 22528–22533.

Van Norman, J.M., Xuan, W., Beeckman, T., and Benfey, P.N. (2013). To branch or not to branch: The role of pre-patterning in lateral root formation. Dev. **140**: 4301–4310.

O'Hara, L.E., Paul, M.J., and Wingler, A. (2013). How do sugars regulate plant growth and development? new insight into the role of trehalose-6-phosphate. Mol. Plant **6**: 261–274.

Okushima, Y. et al. (2005). Functional genomic analysis of the AUXIN RESPONSE FACTOR gene family members in Arabidopsis thaliana: Unique and overlapping functions of ARF7 and ARF19. Plant Cell **17**: 444–463.

Okushima, Y., Fukaki, H., Onoda, M., Theologis, A., and Tasaka, M. (2007). ARF7 and ARF19 regulate lateral root formation via direct activation of LBD/ASL genes in Arabidopsis. Plant Cell **19**: 118–130.

Orman-Ligeza, B. et al. (2018). The Xerobranching Response Represses Lateral Root Formation When Roots Are Not in Contact with Water. Curr. Biol. **28**: 3165-3173.

Pandey, P., Irulappan, V., Bagavathiannan, M. V., and Senthil-Kumar, M. (2017). Impact of combined abiotic and biotic stresses on plant growth and avenues for crop improvement by exploiting physio-morphological traits. Front. Plant Sci. **8**: 537.

Parizot, B. et al. (2008). Diarch symmetry of the vascular bundle in arabidopsis root encompasses the pericycle and is reflected in distich lateral root initiation. Plant Physiol. **146**: 140–148.

Paul, M.J., Primavesi, L.F., Jhurreea, D., and Zhang, Y. (2008). Trehalose Metabolism and Signalling. Annu. Rev. Plant Biol. **59**: 417–441.

Pavelescu, I., Vilarrasa-Blasi, J., Planas-Riverola, A., González-García, M., Caño-Delgado, A.I., and Ibañes, M. (2018).A Sizer model for cell differentiation in Arabidopsis thaliana root growth . Mol. Syst. Biol. **14**. (1): e7687

Pedrotti, L., Weiste, C., Nägele, T., Wolf, E., Lorenzin, F., Dietrich, K., Mair, A., Weckwerth, W., Teige, M., Baena-González, E., and Dröge-Laser, W. (2018). Snf1-RELATED KINASE1-controlled C/S1-bZIP signalling activates alternative mitochondrial metabolic pathways to ensure plant survival in extended darkness. Plant Cell **30**: 495–509.

Pérez-Torres, C.-A., López-Bucio, J., Cruz-Ramírez, A., Ibarra-Laclette, E., Dharmasiri, S., Estelle, M., and Herrera-Estrella, L. (2008).Phosphate Availability Alters Lateral Root

Development in Arabidopsis by Modulating Auxin Sensitivity via a Mechanism Involving the TIR1 Auxin Receptor . Plant Cell **20**: 3258–3272.

Petricka, J.J., Winter, C.M., and Benfey, P.N. (2012).Control of Arabidopsis Root Development . Annu. Rev. Plant Biol. **63**: 563–590.

Ponnu, J., Wahl, V., and Schmid, M. (2011). Trehalose-6-phosphate: Connecting plant metabolism and development. Front. Plant Sci. **2**.70

Powers, S.K. et al. (2019). Nucleo-cytoplasmic Partitioning of ARF Proteins Controls Auxin Responses in Arabidopsis thaliana. Mol. Cell **76**: 177-190.

Rahmani, F., Hummel, M., Schuurmans, J., Wiese-Klinkenberg, A., Smeekens, S., and Hanson, J. (2009). Sucrose control of translation mediated by an upstream open reading frame-encoded peptide. Plant Physiol. **150**: 1356–1367.

Rahni, R., Efroni, I., and Birnbaum, K.D. (2016). Developmental Cell Perspective A Case for Distributed Control of Local Stem Cell Behavior in Plants. Dev. Cell **38**: 635–642.

Ram Yadav, S., Bishopp, A., and Helariutta, Y. (2010). Plant Development: Early Events in Lateral Root Initiation. Curr. Biol. **20**, R843-845

Ramon, M., Dang, T.V.T., Broeckx, T., Hulsmans, S., Crepin, N., Sheen, J., and Rolland, F. (2019). Default Activation and Nuclear Translocation of the Plant Cellular Energy Sensor SnRK1 Regulate Metabolic Stress Responses and Development. Plant Cell **31**: 1614–1632.

Ren, M., Qiu, S., Venglat, P., Xiang, D., Feng, L., Selvaraj, G., and Datla, R. (2011). Target of rapamycin regulates development and ribosomal RNA expression through kinase domain in Arabidopsis. Plant Physiol. **155**: 1367–1382.

Robbins Ii, N.E., Trontin, C., Duan, L., and Dinneny, J.R. (2020). Title: Beyond the barrier: communication in the root through the endodermis.**166 (2)**. 551-559

Robbins, N.E., Trontin, C., Duan, L., and Dinneny, J.R. (2014). Beyond the barrier: Communication in the root through the endodermis. Plant Physiol. **166**: 551–559.

Roberts, I. et al. (2016). CEP5 and XIP1/CEPR1 regulate lateral root initiation in Arabidopsis. J. Exp. Bot. **67**: 4889–4899.

Rodriguez, M., Parola, R., Andreola, S., Pereyra, C., and Martínez-Noël, G. (2019). TOR and SnRK1 signalling pathways in plant response to abiotic stresses: Do they always act according to the “yin-yang” model? Plant Sci. **288**: 110220

Rosa, M., Prado, C., Podazza, G., Interdonato, R., González, J.A., Hilal, M., and Prado, F.E. (2009). Soluble sugars-metabolism, sensing and abiotic stress a complex network in the life of plants. Plant Signal. Behav. **4**: 388–393.

Ryan, E., Steer, M., and Dolan, L. (2001). Cell biology and genetics of root hair formation in

Arabidopsis thaliana. Protoplasma **215**: 140–149.

De Rybel, B. et al. (2010). A novel Aux/IAA28 signalling cascade activates GATA23-dependent specification of lateral root founder cell identity. Curr. Biol. **20**: 1697–1706.

Saijo, Y. and Loo, E.P. (2020). Plant immunity in signal integration between biotic and abiotic stress responses. New Phytol. **225**: 87–104.

Sakr, S., Wang, M., Dédaldéchamp, F., Perez-Garcia, M.D., Ogé, L., Hamama, L., and Atanassova, R. (2018). The sugar-signalling hub: Overview of regulators and interaction with the hormonal and metabolic network. Int. J. Mol. Sci. **19**: 2506.

Santos Teixeira, J.A. and ten Tusscher, K.H. (2019). The Systems Biology of Lateral Root Formation: Connecting the Dots. Mol. Plant **12**: 784–803.

Santuari, L. et al. (2016). The PLETHORA gene regulatory network guides growth and cell differentiation in Arabidopsis roots. Plant Cell **28**: 2937–2951.

Schindelin, J. et al. (2012). Fiji: An open-source platform for biological-image analysis. Nat. Methods **9**: 676–682.

Schluepmann, H., Van Dijken, A., Aghdasi, M., Wobbes, B., Paul, M., and Smeekens, S. (2004). Trehalose mediated growth inhibition of arabidopsis seedlings is due to trehalose-6-phosphate accumulation. Plant Physiol. **135**: 879–890.

Schluepmann, H. and Paul, M. (2009). Trehalose Metabolites in Arabidopsis—elusive, active and central. Arab. B. **7**: e0122.

Shin, R., Burch, A.Y., Huppert, K.A., Tiwari, S.B., Murphy, A.S., Guilfoyle, T.J., and Schachtman, D.P. (2007). The Arabidopsis transcription factor MYB77 modulates auxin signal transduction. Plant Cell **19**: 2440–2453.

Slocombe, S.P., Beaudoin, F., Donaghy, P.G., Hardie, D.G., Dickinson, J.R., and Halford, N.G. (2004). SNF1-related protein kinase (SnRK1) phosphorylates class I heat shock protein. Plant Physiol. Biochem. **42**: 111–116.

Smeekens, S., Ma, J., Hanson, J., and Rolland, F. (2010). Sugar signals and molecular networks controlling plant growth. Curr. Opin. Plant Biol. **13**: 273–278.

de Smet, I. (2010). Multimodular auxin response controls lateral root development in Arabidopsis. Plant Signal. Behav. **5**: 580–582.

De Smet, I. et al. (2007). Auxin-dependent regulation of lateral root positioning in the basal meristem of Arabidopsis. Development **134**: 681–690.

De Smet, I. (2012). Lateral root initiation: one step at a time. New Phytol. **193**: 867–873.

De Smet, S., Cuypers, A., Vangronsveld, J., and Remans, T. (2015). Gene Networks Involved in Hormonal Control of Root Development in Arabidopsis thaliana: A Framework for

Studying Its Disturbance by Metal Stress. Int. J. Mol. Sci. **16**: 19195–19224.

SMITH, A.M. and STITT, M. (2007). Coordination of carbon supply and plant growth. Plant. Cell Environ. **30**: 1126–1149.

Smith, F.A. (2007). Plant roots. Growth, activity and interaction with soils. Ann. Bot. **100**: 151–152.

Smith, S. and de Smet, I. (2012). Root system architecture: Insights from Arabidopsis and cereal crops. Philos. Trans. R. Soc. B Biol. Sci. **367**: 1441–1452.

Smith, S. and De Smet, I. Root system architecture: insights from Arabidopsis and cereal crops.**367(1595)**:1441-1452

Song, J., Liu, Q., Hu, B., and Wu, W. (2017). Photoreceptor phyB involved in Arabidopsis temperature perception and heat-tolerance formation. Int. J. Mol. Sci. **18**.1194

Southern, M.M., Brown, P.E., and Hall, A. (2006) Luciferases as Reporter Genes. In Arabidopsis Protocols (Humana Press: New Jersey), pp. 293–306.

Su, S.H., Gibbs, N.M., Jancewicz, A.L., and Masson, P.H. (2017). Molecular Mechanisms of Root Gravitropism. Curr. Biol. **27**: R964–R972.

Sun, C.H., Yu, J.Q., and Hu, D.G. (2017). Nitrate: A crucial signal during lateral roots development. Front. Plant Sci. **8**. 485

Swarup, K. et al. (2008). The auxin influx carrier LAX3 promotes lateral root emergence. Nat. Cell Biol. **10**: 946–954.

Thorvaldsdóttir, H., Robinson, J.T., and Mesirov, J.P. (2013). Integrative Genomics Viewer (IGV): High-performance genomics data visualization and exploration. Brief. Bioinform. **14**: 178–192.

Tian, Q. and Reed, J.W. (1999). Control of auxin-regulated root development by the Arabidopsis thaliana SHY2/IAA3 gene. **126**: 711-721

Tian, X. and Doerner, P. (2013). Root resource foraging: does it matter? Front. Plant Sci. **4**: 303.

Tomé, F., Nägele, T., Adamo, M., Garg, A., Marco-Llorca, C., Nukarinen, E., Pedrotti, L., Peviani, A., Simeunovic, A., Tatkiewicz, A., Tomar, M., and Gamm, M. (2014). The low energy signalling network. Front. Plant Sci. **5**.353

Toyokura, K. et al. (2019). Lateral Inhibition by a Peptide Hormone-Receptor Cascade during Arabidopsis Lateral Root Founder Cell Formation. Dev. Cell **48**: 64-75.

Tsai, A.Y.L. and Gazzarrini, S. (2014). Trehalose-6-phosphate and SnRK1 kinases in plant development and signalling: The emerging picture. Front. Plant Sci. **5**. 119

Ulmasov, T., Hagen, G., and Guilfoyle, T.J. (1999). Activation and repression of transcription by auxin-response factors. Proc. Natl. Acad. Sci. U. S. A. **96**: 5844–5849.

Ulmasov, T., Murfett, J., Hagen, G., and Guilfoyle, T.J. (1997). Aux/IAA proteins repress expression of reporter genes containing natural and highly active synthetic auxin response elements. Plant Cell **9**: 1963–1971.

Vanneste, S. et al. (2005). Cell cycle progression in the pericycle is not sufficient for SOLITARY ROOT/IAA14-mediated lateral root initiation in Arabidopsis thaliana. Plant Cell **17**: 3035–3050.

Vermeer, J.E.M., Von Wangenheim, D., Barberon, M., Lee, Y., Stelzer, E.H.K., Maizel, A., and Geldner, N. (2014). A spatial accommodation by neighboring cells is required for organ initiation in arabidopsis. Science . **343**: 178–183.

Vilches-Barro, A. and Maizel, A. (2015). Talking through walls: Mechanisms of lateral root emergence in Arabidopsis thaliana. Curr. Opin. Plant Biol. **23**: 31–38.

Vinson, C.R., Sigler, P.B., and McKnight, S.L. (1989). Scissors-grip model for DNA recognition by a family of leucine zipper proteins. Science . **246**: 911–916.

Voß, U. et al. (2015). The circadian clock rephases during lateral root organ initiation in Arabidopsis thaliana. Nat. Commun. **6**: 1–9.

Wang, L. and Ruan, Y.L. (2016). Shoot-root carbon allocation, sugar signalling and their coupling with nitrogen uptake and assimilation. Funct. Plant Biol. **43**: 105–113.

Wang, Z.P., Xing, H.L., Dong, L., Zhang, H.Y., Han, C.Y., Wang, X.C., and Chen, Q.J. (2015). Egg cell-specific promoter-controlled CRISPR/Cas9 efficiently generates homozygous mutants for multiple target genes in Arabidopsis in a single generation. Genome Biol. **16**. 144

Weiste, C. and Dröge-Laser, W. (2014). The Arabidopsis transcription factor bZIP11 activates auxin-mediated transcription by recruiting the histone acetylation machinery. Nat. Commun. **5**.3883

Weiste, C., Pedrotti, L., Selvanayagam, J., Muralidhara, P., Fröschel, C., Novák, O., Ljung, K., Hanson, J., and Dröge-Laser, W. (2017). The Arabidopsis bZIP11 transcription factor links low-energy signalling to auxin-mediated control of primary root growth. PLoS Genet. **13**. 2

Wiese, A., Elzinga, N., Wobbes, B., and Srneekens, S. (2004). A conserved upstream open reading frame mediates sucrose-induced repression of translation. Plant Cell **16**: 1717–1729.

Williams, S.P., Rangarajan, P., Donahue, J.L., Hess, J.E., and Gillaspy, G.E. (2014). Regulation of Sucrose non-Fermenting Related Kinase 1 genes in Arabidopsis thaliana. Front. Plant

Sci. **5**. 324

Wingler, A. (2018). Transitioning to the next phase: The role of sugar signalling throughout the plant life cycle. Plant Physiol. **176**: 1075–1084.

Xiong, Y. and Sheen, J. (2014). The role of target of rapamycin signalling networks in plant growth and metabolism. Plant Physiol. **164**: 499–512.

Xuan, W. et al. (2016). Cyclic programmed cell death stimulates hormone signalling and root development in Arabidopsis. Science. **351**: 384–387.

Xuan, W., Audenaert, D., Parizot, B., Möller, B.K., Njo, M.F., De Rybel, B., De Rop, G., Van Isterdael, G., Mähönen, A.P., Vanneste, S., and Beeckman, T. (2015). Root cap-derived auxin pre-patterns the longitudinal axis of the arabidopsis root. Curr. Biol. **25**: 1381–1388.

Xuan, W., Opdenacker, D., Vanneste, S., and Beeckman, T. (2018). Long-term in vivo imaging of luciferase-based reporter gene expression in Arabidopsis roots. In Methods in Molecular Biology (Humana Press Inc.), pp. 177–190.

YAZDANBAKHSH, N., SULPICE, R., GRAF, A., STITT, M., and FISAHN, J. (2011). Circadian control of root elongation and C partitioning in *Arabidopsis thaliana*. Plant. Cell Environ. **34**: 877–894.

York, L.M., Nord, E.A., and Lynch, J.P. (2013). Integration of root phenes for soil resource acquisition. Front. Plant Sci. **4**. 355

Zhai, Z., Keereetaweep, J., Liu, H., Feil, R., Lunn, J.E., and Shanklin, J. (2018). Trehalose 6-phosphate positively regulates fatty acid synthesis by stabilizing wrinkled1[open]. Plant Cell **30**: 2616–2627.

Zhang, Y., Liu, T., Meyer, C.A., Eeckhoute, J., Johnson, D.S., Bernstein, B.E., Nussbaum, C., Myers, R.M., Brown, M., Li, W., and Liu, X.S. (2008). Model-based Analysis of ChIP-Seq (MACS). Genome Biol. **9**: R137.

Zhu, H., Li, X., Zhai, W., Liu, Y., Gao, Q., Liu, J., Ren, L., Chen, H., and Zhu, Y. (2017). Effects of low light on photosynthetic properties, antioxidant enzyme activity, and anthocyanin accumulation in purple pak-choi (Brassica campestris ssp. Chinensis Makino). PLoS One **12**. 6

7. SUPPLEMENTARY INFORMATION

7.1 Supplementary Figures

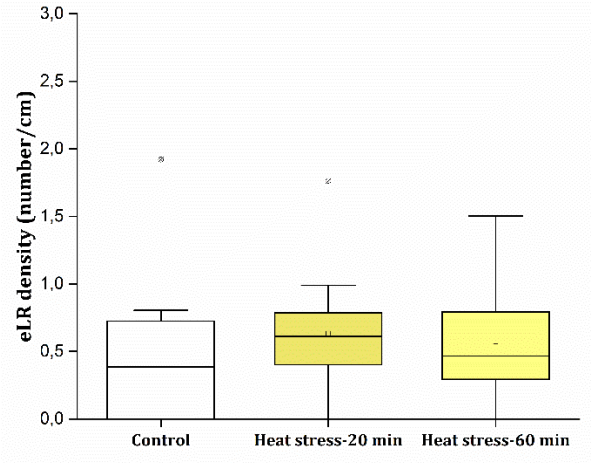

Figure 31: Lateral root density is not affected by short-term treatment with heat. 8-day-old *A. thaliana* Col-0 seedlings grown on ½ MS media were treated with 42 °C for 20 and 60 minutes. After the treatment they were transferred back to the long day (16 h light/8 h dark) conditions. eLR density was calculated on day 14 after germination. Each heat treatment group was compared to the control group. Control is represented in white bar and heat-treated sample group are represented in yellow bars. Normal distribution was calculated for each group and Mann-Whitney's *U test* was used to test significance.

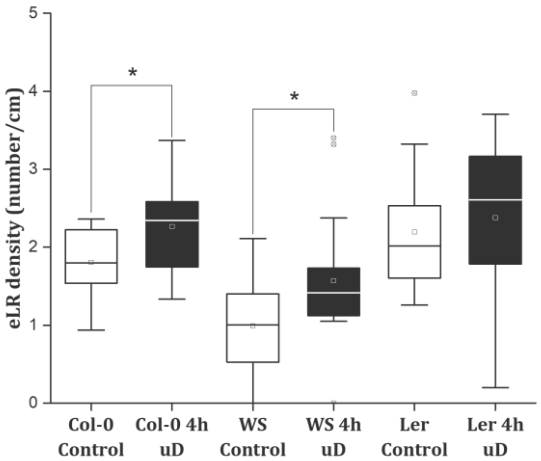

Figure 32: Ecotype comparison of lateral root densities between Col 0, WS and Ler under unexpected darkness. 8-day-old *A. thaliana* Col-0, WS and Ler seedlings grown on ½ MS media were subjected to 4 h of unexpected darkness (uD). Post treatment they were grown until 14-day after germination under long day conditions of 16 h day/8 h dark. These were then measured for primary root length and eLR density. eLR density of control (white bars) and unexpected darkness (black bars) treated seedlings. Normal distribution was calculated for each group. Mann-Whitney's *U test* was used to test significance. Asterisk indicate significance **p<0.05 **p<0.01 ***p<0.001* for sample size n=15 (Col-0 and Ler), n=20 (WS).

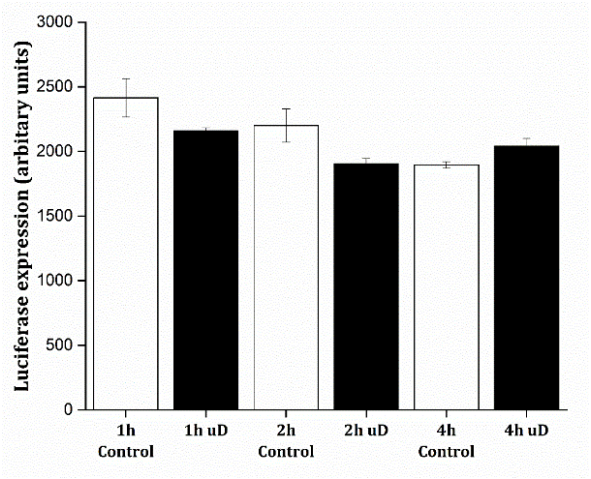

Figure 33: *ASN1* expression displays no significant changes after unexpected darkness in older seedlings. Transgenic *ASN1:LUC* seedlings were grown for 14 days under long day conditions and then treated with 1 h , 2 h and 4 h of unexpected darkness (uD in the figure). On 14th day, luciferin solution was sprayed, and imaging was performed after 10 minutes with a CCD camera. *ASN1* promoter activity is shown as luciferase signal in leaves of control (white bars) and 1 h, 2 h and 4 h of unexpected darkness (black bars). Normal distribution was calculated for each group and student's *t-test* was used to check significance in normal distributed samples of n=10 seedlings.

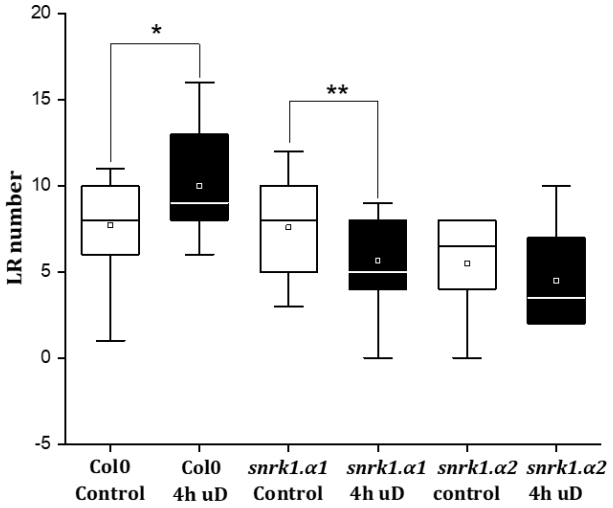

Figure 34: Unexpected darkness leads to a decrease in lateral root number in *snrk1.α1* loss-of-function mutant. 8-day-old *A. thaliana* Col-0, *snrk1.α1* and *snrk1.α2* mutant seedlings grown on ½ MS media were subjected to 4 h of unexpected darkness. Post treatment they were grown until 14th day after germination under long day conditions. Emerged lateral root number of control (white bars) and 4 h unexpected darkness (black bars) treated seedlings were counted. Normal distribution was calculated for each group and Mann-Whitney's *U test* was used to test significance. Asterisk indicate significance **p<0.05 **p<0.01* for n=15 samples.

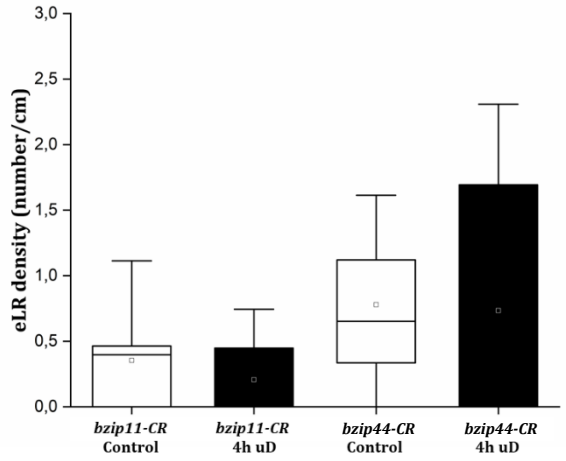

Figure 35: Single loss-of-function mutants of group S_1 bZIP TF do not display changes in the eLR density under unexpected darkness. 8-day-old *A. thaliana bzip11-CR* and *bzip44-CR* mutant seedlings grown on ½ MS media were subjected to 4 h of unexpected darkness. Post treatment they were grown until 14th day after germination under long day conditions. Emerged lateral root number of control (white bars) and 4 h unexpected darkness (black bars) treated seedlings were counted. Normal distribution was calculated for each group and Mann-Whitney's *U test* was used to test significance.

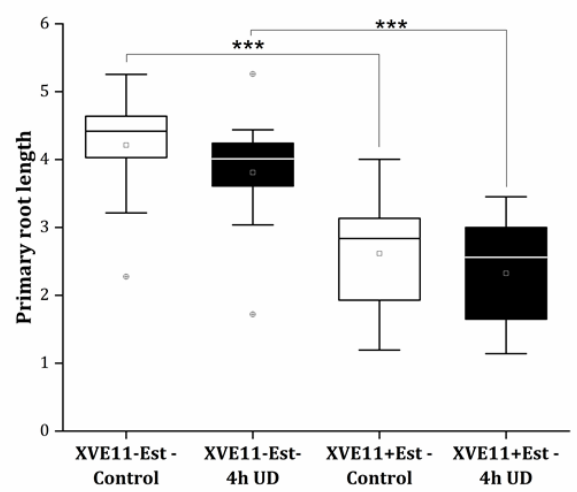

Figure 36: Ectopic overexpression of bZIP11 leads to reduction in primary root length even with short-term unexpected darkness. 8-day-old *A. thaliana* seedlings were grown on ½ MS media without 10µM ß-estradiol and then transferred to ½ MS containing 10µM of ß-estradiol. These seedlings were then subjected to 4 h of unexpected darkness. Post treatment they were grown until 14th day after germination under long day conditions. Primary root length of control (white bars) and 4 h unexpected darkness (black bars) treated seedlings were measured from root tip until hypocotyl. Normal distribution was calculated for each group and pair wise student's *t-test* and Mann-Whitney's *U test* was used to test significance. Asterisk indicate significance **p<0.05 **p<0.01 ***p<0.001* for sample size n=15.

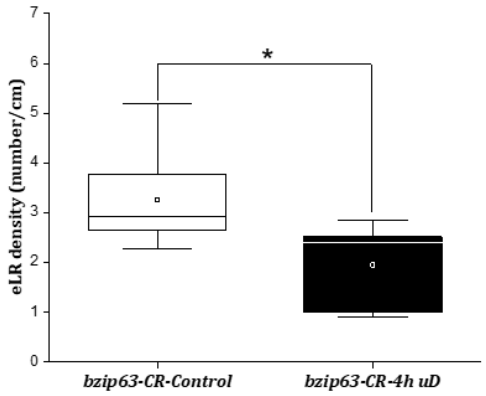

Figure 37: CRISPR/Cas9 generated loss-of-function *bzip63* mutant displays reduced lateral root density upon unexpected darkness. 8-day-old *bzip63* loss-of-function seedlings generated using CRISPR/Cas9 system grown on ½ MS media were subjected to 4 h of unexpected darkness (uD). Post treatment they were grown until 14-day after germination under long day conditions of 16 h day/8 h night. These were then measured for primary root length and eLR density. eLR density of control (white bars) and unexpected darkness (black bars) treated seedlings. Normal distribution was calculated for each group. Mann-Whitney's U test was used to test significance. Asterisk indicate significance **p<0.05* for sample size n=10.

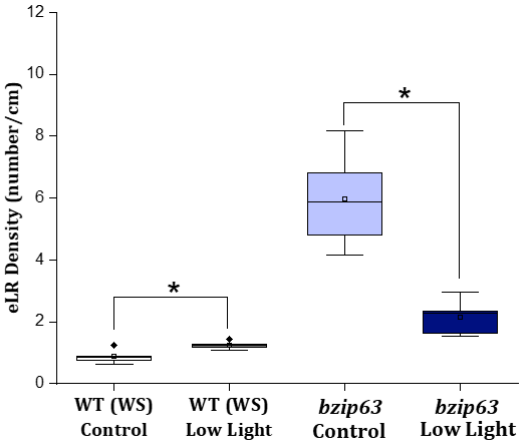

Figure 38: Loss of *bzip63* decreases lateral root density upon low light treatment. 8-day-old, *A.thaliana* wild-type WS and loss-of-function *bzip63* seedlings grown on ½ MS media were subjected to 24 h of low light treatment. Untreated control group was maintained at long day conditions (16 h day/8 h dark). Post treatment low light treated seedlings were grown until 14th day after germination under long day conditions. eLR density of control and low light treated seedlings were measured. Normal distribution was calculated for each group. Mann-Whitney's *U test* was used to test significance. n=5 (WS) and n=10 (*bzip63*) seedlings were analysed. Asterisk indicate significance **p<0.05.*

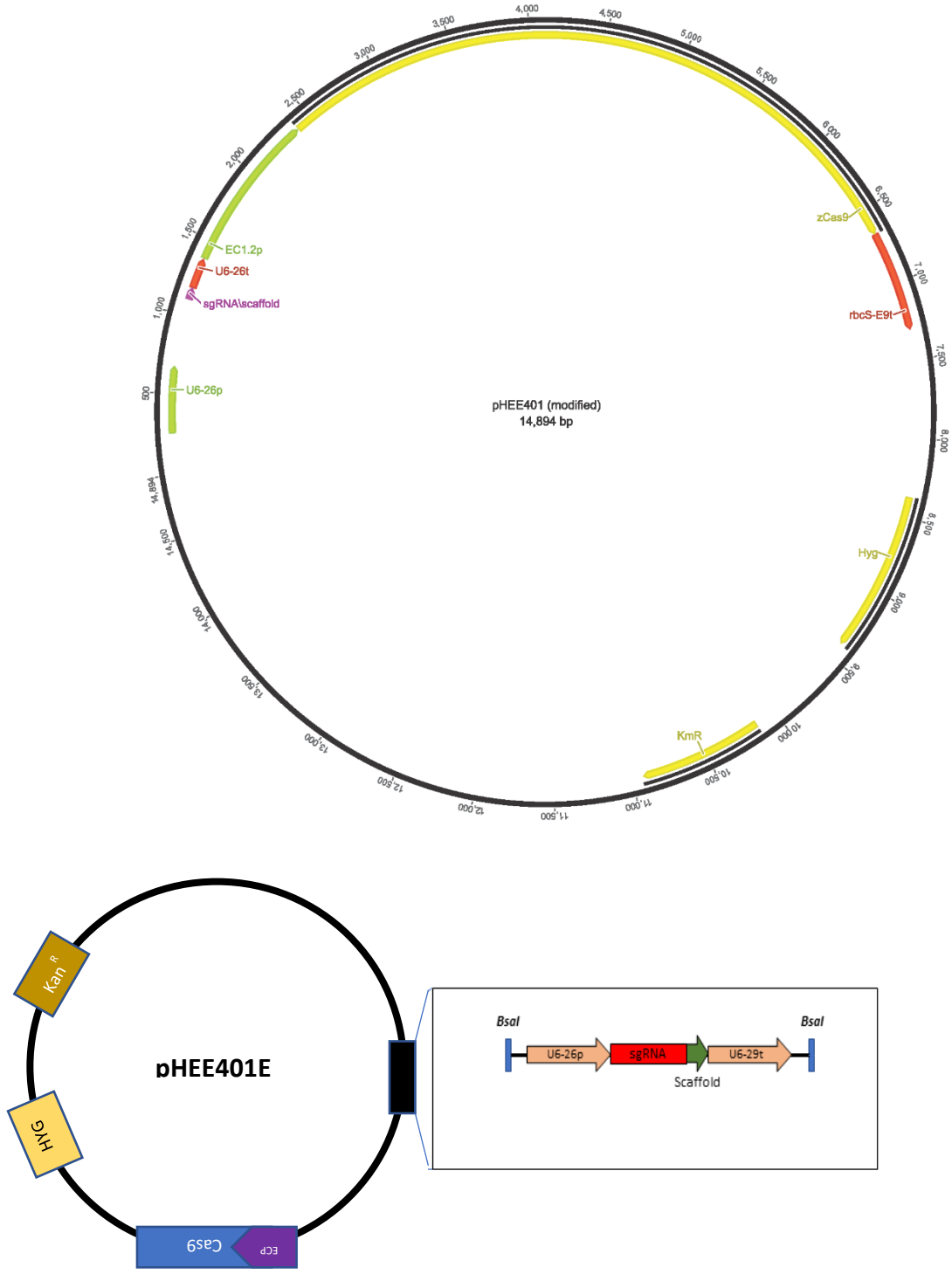

Figure 39: Diagram illustrating the assembly of sgRNA into pHEE401E vector. (A) pHEE401E vector map constructed on Geneious R6 (6.1.6) (B) Simplified illustration of CRISPR/Cas9 binary vector (pHEE401E), harbouring the Cas9 gene (Blue) driven by the egg-cell specific promoter (name) (ECP - purple) and a sgRNA (red) driven by the Pol-III promoter U6-26p (chrome). The sgRNA is tagged to 76 bp scaffold RNA sequence and ends with terminator U6-29t (chrome). The expression module has kanamycin (brown) for bacterial selection and Hygromycin (yellow) resistance cassette for selection of transgenic plants. The sgRNA module containing designed sgRNA sequence was inserted into destination vector pHEE401E through Golden Gate reaction.

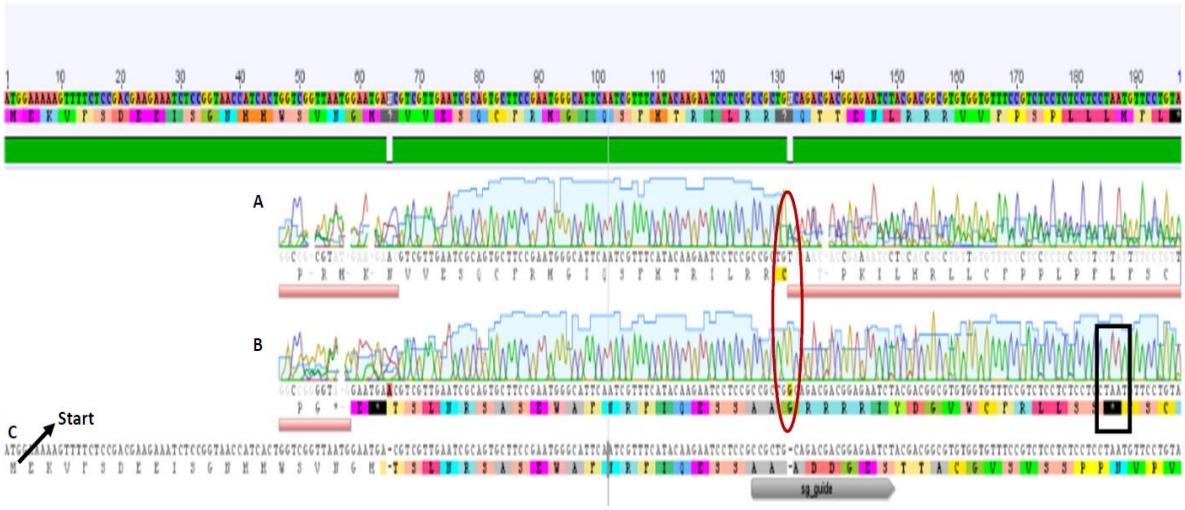

Figure 40: Sanger sequencing of PCR amplified *bZIP63* gene from T1 transgenic plants carrying CRISPR induced mutation. (A) Sequences of PCR amplified *bZIP63* exon 1 of plant number 1. Upper panel is base pair sequences of the gene. Lower panel is corresponding amino acid sequence. (B) Sequences of PCR amplified *bZIP63* exon 1 of plant number 2, prospective mutant. Upper panel indicates gene sequences and lower panel corresponds to amino acid sequences. (C) DNA sequence of *bZIP63* exon1with sgRNA (grey). Above panel indicates gene sequences and below panel corresponds to amino acid sequences. Premature stop is marked with black box. C and G insertions in plant 1 and plant 2 is marked with red circle.

7.2 Supplementary tables

Table 16: Subset of target genes known to be involved in lateral root development

Gene Name	Function (as per TAIR website)
ARF19 (AT1G19220)	Encodes an auxin response factor that contains the conserved VP1-B3 DNA-binding domain at its N-terminus and the Aux/IAA-like domains III and IV present in most ARFs at its C-terminus. The protein interacts with IAA1 (yeast two hybrid) and other auxin response elements such as ER7 and ER9 (yeast one hybrid). ARF19 protein can complement many aspects of the arf7 mutant phenotype and, together with ARF7, is involved in the response to ethylene. In the arf7 arf19 double mutant, several auxin-responsive genes (e.g. IAA5, LBD16, LBD29 and LBD33) are no longer upregulated by auxin.
NRT2.6 (AT3G45060)	member of High affinity nitrate transporter family
MYB77 (AT3G50060)	Encodes a member of the R2R3 transcription factor gene family. Expressed in response to potassium deprivation and auxin. Involved in lateral root development. Interacts with ARF7 and regulates the expression of some auxin responsive genes.
ARF2 (AT5G62000)	Encodes an auxin response factor. Mutants have many defects including enlarged rosette leaves, reduced fertility, later senescence, hypocotyl elongation defects, enlarged seeds and enlarged cotyledons. May not mediate auxin effects. Increase in seed size due to increased cell proliferation. The mRNA is cell-to-cell mobile.

TOC1 (AT5G61380)	Pseudo response regulator involved in the generation of circadian rhythms. TOC1 appears to shorten the period of circumnutation speed. TOC1 contributes to the plant fitness (carbon fixation, biomass) by influencing the circadian clock period. PRR3 may increase the stability of TOC1 by preventing interactions between TOC1 and the F-box protein ZTL. Expression of TOC1 is correlated with rhythmic changes in chromatin organization. The mRNA is cell-to-cell mobile.
PUCHI AT5G18560	Encodes PUCHI, a member of the ERF (ethylene response factor) subfamily B-1 of ERF/AP2 transcription factor family. The protein contains one AP2 domain. There are 15 members in this subfamily including ATERF-3, ATERF-4, ATERF-7, and leafy petiole. PUCHI is required for morphogenesis in the early lateral root primordium of Arabidopsis. Expressed in early floral meristem (stage 1 to 2). Required for early floral meristem growth and for bract suppression. Triple mutant with bop1 and bop2 displays a strong defect in the determination of floral meristem identity with reduced LFY expression and the lack of AP1 expression.

Table 17: Global binding targets of bZIP63 generated by ChIP sequencing

Attached at the end

7.3 Pipeline ChIPseq analysis

1- Map against Arabidopsis genome

   a. bwa aln -n 2 -e 1 -l 25 -t 4 genome.fa file-trimmed.fastq > file-trimmed.aln

2- Conversion in formats

   a. from aln to sam: bwa samse -f file-trimmed.sam genome.fa file-trimmed.aln file-trimmed.fastq

   b. from sam to bam: samtools view -b -S file-trimmed.sam > file-trimmed.bam

3- Generation of “bedgraph” files

   a. from bam to bed: bedtools bamtobed -bed12 -i file-trimmed.bam > file.bed

   b. sorting: sort -k 1,1 file-trimmed.bed > file-trimmed.sorted.bed

   c. from sorted.bed to bedgraph: bedtools genomecov -bg -i file-trimmed.sorted.bed -g arabidopsis_genome.txt > file-trimmed.bedgraph

4- Call peaks with MACS2

   a. regular peaks: macs2 callpeak --SPMR -t file_target.bam -c file_ctrl.bam --outdir destinaction_directory -f BAM -g 9.00e+07 -n name -B -q 0.01

   b. broad peaks: macs2 callpeak --SPMR -t file_target.bam -c file_ctrl.bam --outdir destinaction_directory -f BAM --broad -g 9.00e+07 -n name -B --broad-cutoff 0.1

7.4 GENERAL ABBREVIATIONS

ABA	Abscissic Acid
amiRNA	Artificial Micro RNA
AMPK	AMP-activated protein kinase
ARF	Auxin response factor
A. tumefaciens	Agrobacterium tumefaciens
ASN1	Asparagine synthase 1 gene
At	Arabidopsis thaliana
AuxRE	Auxin response factor
BCAA	Branched chain amino acid
BD	Binding domain
Bp	base pair
bZIP	basic leucine zipper
cDNA	complementary DNA
ChIP	Chromatin Immunoprecipitation
Col-0	Columbia-0 wildtype
CRISPR	Clustered regularly interspaced short palindromic repeats
Cas9	Caspase 9
DNA	Deoxyribonucleic acid
dNTPs	Deoxynucleotide triphosphate
E. coli	Eschericia coli
GRE	G-box related element
GUS	Beta glucoronidase
h	hour
HAT	Histone acetyltransferase
IAA	Indole acetic acid
kDa	kilo dalton
ko	knock-out
M	Molar
Oex	Overexpressor
PCR	Polymerase chain reaction
PIN	Pin formed mutant phenotype

Pro	Promoter
ProDH	Proline Dehydrogenase
qRT-PCR	Quantitative real time PCR
RNA	Ribonucleic acid
SCF	Skp-cullin-F box complez
SIRT	Sucrose induced repression of translation
SnRK1	Snf related kinase I
Snf I	Sucrose non-fermenting I
TDNA	Transfer DNA
TF	Transcription factor
TSS	Transcriptional start site
TTS	Transcription termination site
uORF	Upstream open reading frame
UTR	Untranslated region
WT	wild-type
XVE	Estradiol inducible expression system

ACKNOWLEDGEMENTS

My doctoral thesis wouldn't have been possible without so many of them contributing to my journey so far and standing strong by my side.

First and foremost, my deepest gratitude to my supervisor **Prof. Dr. Wolfgang Dröge-Laser**. He has been the best supervisor and mentor one could ask for. Firstly, in giving me an opportunity to work under his guidance, helping me to establish myself well into a new career in plant science, help my scholarship applications, provide me valuable tips on scientific writing, oral presentations and arranging funds for this promising project. He has been solid support not just in my professional growth but also in my personal life, during the dark days of the visa process for my husband. I will always remember and cherish my time here in your research group!

I express my sincere appreciation and gratitude to **Dr. Christoph Weiste**, for being my biggest support and a good friend in the lab. I thoroughly enjoyed our scientific discussions and certainly learned so much from you. Thank you for training me in many scientific techniques. Thank you for all the phone calls you helped me with and for being there all along to fight bureaucracy!

I am extremely thankful to Prof. **Dr. Johannes Hanson** and **Prof. Dr. Dirk Becker** for mentoring this project and providing valuable suggestions during the thesis committee meetings. Thank you **Dr. Silvio Collani**, for helping me with ChIP-Seq in Umea. I learned a lot of bioinformatics from you!

I would like to thank **Bayer AG** for providing me the Jeff-Schell Scholarship and an opportunity to do a research stay in Sweden.

Thank you, **Gabi, Stephan** and the **GSLS** for your endless support during my Ph.D. Thank you for your encouragement and providing me travel grants.

Thank you to everyone from **AG Dröge-Laser**, **Christian**, **Jan, Philip, Marcus, Alex, Christoph, Vanessa, Tobi, Christian W, Sarah,** and **Theresa.** We had a great time during our summer symposiums and weekly Wednesday lunch sessions. Thank you, **Daniel**, **Markus** and **AG Müller** for your support. Thank you, **Khusbhu**, **Kalechi**, and **Sohail** for

being my coffee buddies and the biggest support system in the department. I will miss you guys very much!!

Thank you, **Sarah** and **Nicole**. You guys were super awesome girl power when I started my Ph.D. I am very happy that we have still stayed in touch after all these years.

A big heartfelt thank you to my FOKUS family! Surviving in Germany was only possible because of you guys! Look where we started and where we have come! My heartfelt thank you to **Moataz, Passant, Gayatri, Diego, Ashley, Manuel, Diyaa, Ana, Manju, Manli, Sarina** and **Pedrina**. I have had the best time here because of all you guys. Thank you, **Andrea**, for being my best friend and cheering me up every time I was in doubt. Thank you, **Cheek** for being so encouraging throughout this journey. Thank you, **Ramon**, for your support, encouragement, not just in science but to travel around the world.

A big thank you for my extended Indian family, **Aravind, Sowmya, Rohini, Ayesha, Yasir, Zeenu** and **Ravish**. Your constant care and support made me less homesick! A special thank you to **Rohini** and **Gayatri** for being so patient and proofreading my thesis.

My friends back home **Swetha, Tinu**, and **Dwarak**, thank you for pushing me every time, for motivating me, for being that rock-solid support during these though Ph.D. years and every time I was anxious. **TOD, Dhanya**, and **Ramya** you guys have been such awesome support from the very beginning.

Last but most important, thank you **Amma** and **Appa**. You guys are the best parents one could ask for. Thank you, Amma, for imbibing that love for science at a very young age and for making me meet big scientists for my small school projects. For you, none of my projects was less important. Thank you, Appa for working so hard to arrange finances tosend me to Germany to study! I hope I have made you both proud! Thank you, **Sachin**, you are my most favorite person in the world and I have learned so much from you. Thank you Amma Shyla **Damodaran**, for your constant support, encouragement, and strength!

My biggest thank you to this one person, without whom my Ph.D. was not possible. Thank you, my then-boyfriend and now husband **Alok**. You literally moved your entire life for me from Oman. You are my biggest strength. Thank you for lifting me up every time I fell. Thank you for always being positive. Thank you for so many sacrifices. You are the best and I love you very much!

Curriculum Vitae

First Name, Surname	Prathibha Muralidhara
Address	Schiestlstraβe 30, 97080, Würzburg
Mobile Phone	+49 1736974468
E-Mail	prathibhamuralidhara88@gmail.com
Date/Place of Birth	30th December 1988, Bangalore
Nationality	Indian

Scientific Work Experience

03/2015 – Present	Department of Pharmaceutical Biology, University of Würzburg *PhD Student.* Research topic: SnRK1-bZIP signaling in incorporating energy and root development in *Arabidopsis thaliana*
06/2016 – 10/2016	Umeå Plant Science Centre (UPSC), Umeå University *Guest Researcher, Jeff-Schell Fellowship – Bayer AG* Technology transfer: ChIP-Sequencing and analysis
04/2014 – 12/2016	Institute of Molecular Infection Biology (IMIB), University of Würzburg *Master Thesis,* Research topic- Virulence control by *Candida Albicans* regulator *ZCF21*
01/2013 – 10/2013	Astrazeneca India Research and Development, Bangalore *Assistant Research Scientist I* Research topic: Understanding molecular mechanisms of *Mycobacterium tuberculosis* granuloma and pre-clinical drug testing

Academic Qualifications

03/2015 – Present	Graduate School of Life Sciences, University of Würzburg *Doctoral Programme in Life Sciences, parallel with Master FOKUS program* Thesis supervised by Prof. Dr. Wolfgang Dröge-Laser
10/2013 – 11/2015	Graduate School of Life Sciences, University of Würzburg *Master of Science in Life Sciences (FOKUS Programme)* Overall grade: 1.3 Thesis supervised by Dr. Christian Perez, IMIB-HIRI Würzburg
06/2010 – 07/2012	School of Biosciences and Technology, VIT University *Master of Science (Applied Microbiology)* Overall grade: 9.17 Thesis supervised by Dr. Raghunand Tirumalai, CCMB Hyderabad
06/2006- 06/2009	Mount Carmel College, Bangalore University *Bachelor of Science (Chemistry, Zoology and Microbiology)* Overall grade: 83 Percentage

Scientific and Technical Competencies

Molecular Biology:	Crispr-Cas9 gene editing, Recombinant cloning and screening in bacteria, yeast and plant, RNA and DNA isolation, Chromatin Immunoprecipitation
Genomics:	RNA Sequencing library preparation, RNA sequencing analysis, ChIP sequencing and analysis
Bioinformatics:	Programming language R (basic), MACS2- differential peak calling on Linux platform
Microscopy:	Confocal Imaging, Fluorescence Imaging, Transmission Electron Microscopy (basic)
Protein Biochemistry:	SDS-Page, Western Blot, Kinase activity assay and measurement
Analytical Chemistry:	Sugar and Carbohydrate measurement
Image processing:	ImageJ

Publications

Perturbations in plant energy homeostasis alter lateral root plasticity via SnRK1-bZIP63-ARF19 signalling
First author publication *(in preparation)*

The Arabidopsis bZIP11 transcription factor links low-energy signaling to auxin-mediated control of primary root growth.
Weiste C, Pedrotti L, Selvanayagam J, **Muralidhara P**, Fröschel C, Novák O, Ljung K, Hanson J, Dröge-Laser W. PLoS Genet. 2017 Feb 3;13(2):e1006607. doi: 10.1371/journal.pgen.1006607. eCollection 2017 Feb.

A Candida albicans regulator of disseminated infection operates primarily as a repressor and governs cell surface remodeling.
Böhm L, **Muralidhara P**, Pérez JC. Mol Microbiol. 2016 Apr;100(2):328-44. doi: 10.1111/mmi.13320. Epub 2016 Feb 19.

Awards and Fellowships

Bayer Foundation "Jeff-Schell Scholarship" 2015-2016
Prize money awarded for the outstanding Ph.D. projects in the field of Plant Science and Agriculture and an opportunity to perform experiments in reputed institutions across the globe.

Graduate School of Life Sciences (GSLS) Travel Fellowship 2016, Julius Maximillian Universität Würzburg
Prize money for stay at Umeå Plant Science Center (UPSC), Sweden

Merit Award for Academic Excellence, Vellore Institute of Technology University
Top 5% of the master's program are awarded with prize money for their excellent performance.

Scientific Presentations

Poster Presentation: bZIP transcription factors linking low energy to auxin-mediated control of primary root growth.
ISRR (International Society for Root Research) meeting, July 2018, Israel.

Poster Presentation: SnRK1-bZIP network in root development in Arabidopsis thaliana. Eureka 2017, Graduate school of Life Sciences (GSLS), University of Würzburg.

Selected for scientific talk at “PhD school in plant development 2019”, Retzbach, Würzburg

Skill Set

Languages:	English (Native Proficiency), German (B1- Limited working proficiency)
Productivity:	Extensive experience with Microsoft office and Libre Office products
	Elected Member of Doctoral Research Council (DRC), 2017-2019
Courses:	Good scientific practices, scientific image processing and analysis, scientific writing and publishing

AFFIDAVIT

I hereby declare that my thesis entitled, "**Perturbations in plant energy homeostasis alter lateral root plasticity via SnRK1-bZIP63-ARF19 signalling"** is the result of my own work. I did not receive any help or support from commercial consultants. All sources and/or materials applied are listed and specified in the thesis. Furthermore, I confirm that this thesis has not yet been submitted as part of another examination process neither in identical nor in similar form.

Würzburg, February 2020 _____

EIDESSTATTLICHE ERKLÄRUNG

Hiermit erkläre ich an Eides statt, die Dissertation „**Störungen in der pflanzlichen Energiehomöostase verändern die laterale Wurzelplastizität vermittelt durch das SnRK1-bZIP63-ARF19-Signalmodul**" eigenständig, d.h. insbesondere selbstständig und ohne Hilfe eines kommerziellen Promotionsberaters, angefertigt und keine anderen als die von mir angegebenen Quellen und Hilfsmittel verwendet zu haben.

Ich erkläre außerdem, dass die Dissertation weder in gleicher noch in ähnlicher Form bereits in einem anderen Prüfungsverfahren vorgelegen hat.

Würzburg, February 2020 _____

AT Numbers	Strand	Binding location	Function	Description
AT5G67411.1	-	835	GRAS family transcription factor;(source:Araport11)	
AT5G67370.1	-	-35	DUF1230 family protein (DUF1230);(source:Araport11)	CONSERVED IN THE GREEN LINEAGE AND DIATOMS 27 (CGLD27)
AT5G67300.1	+	-1143	Member of the R2R3 factor MYB gene family involved in mediating plant responses to a variety of abiotic stimiuli. The mRNA is cell-to-cell mobile.	(MYB44); (ATMYBR1);ARABIDOPSIS THALIANA MYB DOMAIN
AT5G67290.1	-	-2038	FAD-dependent oxidoreductase family protein;(source:Araport11)	
AT5G66880.1	+	-557	encodes a member of SNF1-related protein kinases (SnRK2) whose activity is activated by ionic (salt) and non-ionic (mannitol) osmotic stress. Enzyme involved in the ABA signaling during seed germination, dormancy and seedling growth. The mRNA is cell-to-cell mobile.	SUCROSE NONFERMENTING 1(SNF1)-RELATED PROTEIN KINASE 2.3 (SNRK2.3); (SRK2I);SUCROSE NONFERMENTING 1 (SNF1)-
AT5G66650.1	-	-625	Chloroplast localized mitochondrial calcium uniporter.	CHLOROPLAST-LOCALIZED MITOCHONDRIAL CALCIUM
AT5G66052.1	+	-88	transmembrane protein;(source:Araport11)	
AT5G65690.1	+	-1007	Encodes a putative phosphoenolpyruvate carboxykinase (ATP-dependent). The mRNA is cell-to-cell mobile.	PHOSPHOENOLPYRUVATE CARBOXYKINASE
AT5G65683.1	+	1913	Zinc finger (C3HC4-type RING finger) family protein;(source:Araport11)	WAV3 HOMOLOG 2 (WAVH2)
AT5G65630.1	-	-295	This gene is predicted to encode a bromodomain-containing protein. Plant lines expressing RNAi constructs targeted against GTE7 show some resistance to agrobacterium-mediated root transformation.	GLOBAL TRANSCRIPTION FACTOR GROUP E7 (GTE7)
AT5G65430.3	-	-1	member of 14-3-3 proteins. This protein is reported to interact with the BZR1 transcription factor involved in brassinosteroid signaling and may affect the nucleocytoplasmic shuttling of BZR1	(ATMIN10);GENERAL REGULATORY FACTOR 8 (GRF8)
AT5G65280.1	-	-678	Encodes a protein with reported similarity to GCR2 a putative G protein coupled receptor thought to be an ABA receptor. Loss of function mutations in GCL1 show no ABA response defects based on assays of seed germination and seedling development.GCL1 also has similarity to LANCL1 and LANCL2, human homologs of bacterial lanthionine synthetase.	GCR2-LIKE 1 (GCL1)
AT5G65110.1	-	-87	Encodes an acyl-CoA oxidase presumably involved in long chain fatty acid biosynthesis.	ACYL-COA OXIDASE 2 (ACX2); (ATACX2)
AT5G65050.3	+	4278	Originally published as Agamous like MADS-box protein AGL31. One of a group of MADS box genes involved in control of flowering time. Four variant sequences have been identified for this locus but have not been characterized for differences in expression pattern and/or function.	AGAMOUS-LIKE 31 (AGL31);MADS AFFECTING FLOWERING 2 (MAF2)
AT5G64850.1	+	-127	sorbin/SH3 domain protein;(source:Araport11)	
AT5G64510.1	+	-74	Encodes Tunicamycin Induced 1(TIN1), a plant-specic ER stress-inducible protein. TIN1 mutation affects pollen surface morphology. Transcriptionally induced by treatment with the N-linked glyclsylation inhibitor tunicamycin.	TUNICAMYCIN INDUCED 1 (TIN1)
AT5G64260.1	+	1000	EXORDIUM like 2;(source:Araport11)	EXORDIUM LIKE 2 (EXL2)
AT5G63790.1	-	-138	Encodes a member of the NAC family of transcription factors. ANAC102 appears to have a role in mediating response to low oxygen stress (hypoxia) in germinating seedlings. Its expression can be induced by beta-cyclocitral, an oxidized by-product of beta-carotene generated in the chloroplasts, mediates a protective retrograde response that lowers the levels of toxic peroxides and carbonyls, limiting damage to intracellular components.	NAC DOMAIN CONTAINING PROTEIN 102 (ANAC102);NAC DOMAIN CONTAINING PROTEIN 102 (NAC102)
AT5G63520.1	-	-1621	F-box/LRR protein;(source:Araport11)	
AT5G62320.1	-	872	Encodes a putative transcription factor (MYB99).	MYB DOMAIN PROTEIN 99 (ATMYB99);MYB DOMAIN PROTEIN 99
AT5G62090.1	-	-111	Encodes a protein that functions with LUH to promote Al binding to the root cell wall.	SEUSS-LIKE 2 (SLK2)
AT5G62000.1	+	-682	Encodes an auxin response factor. Mutants have many defects including enlarged rosette leaves, reduced fertility, later senescence, hypocotyl elongation defects, enlarged seeds and enlarged cotyledons. May not mediate auxin effects. Increase in seed size due to increased cell proliferation. The mRNA is cell-to-cell mobile.	(ATARF2);ORESARA 14 (ORE14);AUXIN RESPONSE FACTOR 2 (ARF2);ARF1-BINDING PROTEIN (ARF1-BP);HLS1 SUPPRESSOR
AT5G61440.1	+	-339	Encodes a member of the thioredoxin family protein. Located in the chloroplast. The mRNA is cell-to-cell mobile.	ATYPICAL CYS HIS RICH THIOREDOXIN 5 (ACHT5)
AT5G61380.1	+	-163	Pseudo response regulator involved in the generation of circadian rhythms. TOC1 appears to shorten the period of circumnutation speed. TOC1 contributes to the plant fitness (carbon fixation, biomass) by influencing the circadian clock period. PRR3 may increase the stability of TOC1 by preventing interactions between TOC1 and the F-box protein ZTL. Expression of TOC1 is correlated with rhythmic changes in chromatin organization. The mRNA is cell-to-cell mobile.	TIMING OF CAB EXPRESSION 1 (ATTOC1);PSEUDO-RESPONSE REGULATOR 1 (PRR1);TIMING OF CAB EXPRESSION 1 (TOC1); (APRR1)
AT5G60680.1	+	-1717	transcription initiation factor TFIID subunit (Protein of unknown function, DUF584);(source:Araport11)	
AT5G59960.1	-	-47	K-stimulated pyrophosphate-energized sodium pump protein;(source:Araport11)	
AT5G59740.1	-	-91	UDP-N-acetylglucosamine (UAA) transporter family;(source:Araport11)	
AT5G59670.1	+	4619	Leucine-rich repeat protein kinase family protein;(source:Araport11)	
AT5G59570.1	+	-90	Encodes BOA (BROTHER OF LUX ARRHYTHMO), a component of the circadian clock. The mRNA is cell-to-cell mobile.	BROTHER OF LUX ARRHYTHMO (BOA)
AT5G58720.1	-	-108	smr (Small MutS Related) domain-containing protein;(source:Araport11)	
AT5G58650.1	-	-224	Encodes PSY1, an18-aa tyrosine-sulfated glycopeptide that promotes cellular proliferation and expansion. PSY1 is widely expressed in various tissues, including shoot apical meristem, and is highly up-regulated by wounding. Perception of PSY1 depends on At1g72300, a leucine-rich repeat receptor kinase (LRR-RK).	PLANT PEPTIDE CONTAINING SULFATED TYROSINE 1 (PSY1)
AT5G58620.1	+	-275	zinc finger (CCCH-type) family protein;(source:Araport11)	TANDEM ZINC FINGER PROTEIN 9 (TZF9)
AT5G58160.1	+	-55	actin binding protein;(source:Araport11)	FORMIN HOMOLOGY 13 (FH13)
AT5G58090.1	-	-106	O-Glycosyl hydrolases family 17 protein;(source:Araport11)	
AT5G57910.1	-	1491	ribosomal RNA small subunit methyltransferase G;(source:Araport11)	
AT5G57655.2	+	-95	xylose isomerase family protein;(source:Araport11)	
AT5G56550.1	-	-660	Encodes OXIDATIVE STRESS 3 (OXS3)， involved in tolerance to heavy metals and oxidative stress.	OXIDATIVE STRESS 3 (OXS3);OXIDATIVE STRESS 3 (ATOXS3)
AT5G55840.1	+	-201	PPR superfamily protein;(source:Araport11)	
AT5G54300.1	-	957	cotton fiber-like protein (DUF761);(source:Araport11)	
AT5G53450.1	+	-267	OBP3-responsive protein 1;(source:Araport11)	OBP3-RESPONSIVE GENE 1 (ORG1)
AT5G52960.1	+	-85	tRNA dimethylallyltransferase;(source:Araport11)	
AT5G51460.3	+	-605	homologous to the C-terminal part of microbial trehalose-6-phosphate phosphatases	(ATTPPA);TREHALOSE-6-PHOSPHATE PHOSPHATASE A (TPPA)
AT5G51390.1	-	222	hypothetical protein;(source:Araport11)	
AT5G50375.2	+	93	Converts pentacyclic cyclopropyl sterols to conventional tetracyclic sterols. CPI1 function during and just after division and support gravitropism by establishing polar PIN2 localization. Required for endocytosis of PIN2	CYCLOPROPYL ISOMERASE (CPI1)
AT5G47200.1	+	1748	AtRabD2b encodes a Rab GTPase, which plays important roles in pollen development, germination and tube elongation. The mRNA is cell-to-cell mobile.	RAB GTPASE HOMOLOG 1A (RAB1A);RAB GTPASE HOMOLOG 1A
AT5G47230.1	+	1062	encodes a member of the ERF (ethylene response factor) subfamily B-3 of ERF/AP2 transcription factor family (ATERF-5). The protein contains one AP2 domain. There are 18 members in this subfamily including ATERF-1, ATERF-2, AND ATERF-5. The mRNA is cell-to-cell mobile.	(ERF102);ETHYLENE RESPONSIVE ELEMENT BINDING FACTOR 5 (ATERF5);ETHYLENE RESPONSIVE ELEMENT BINDING FACTOR- 5
AT5G47180.1	-	-4	Plant VAMP (vesicle-associated membrane protein) family protein;(source:Araport11)	
AT5G46880.1	+	4027	homeobox-7;(source:Araport11)	HOMEODOMAIN GLABROUS 5 (HDG5);HOMEOBOX-7 (HB-7)
AT5G46390.2	+	51	Peptidase S41 family protein;(source:Araport11)	
AT5G45660.1	+	-86	adenine phosphoribosyltransferase;(source:Araport11)	
AT5G44060.1	+	429	embryo sac development arrest protein;(source:Araport11)	
AT5G43540.1	+	175	C2H2 and C2HC zinc fingers superfamily protein;(source:Araport11)	
AT5G41310.1	-	-1406	P-loop nucleoside triphosphate hydrolases superfamily protein with CH (Calponin Homology) domain-containing protein;(source:Araport11)	
AT5G41080.1	+	-86	Encodes a member of the glycerophosphodiester phosphodiesterase (GDPD) family.	(AtGDPD2);GLYCEROPHOSPHODIESTER PHOSPHODIESTERASE 2
AT5G40890.1	-	-1468	Encodes a member of the voltage-dependent chloride channel. Also functions as a NO3-/H+ exchanger that serves to accumulate nitrate nutrient in vacuoles. Mutants homozygous for the T-DNA insertion mutation have reduced nitrate uptake capacity in high nitrate environment and exhibit hypersensitivity to chlorate.	CHLORIDE CHANNEL A (CLCA);CHLORIDE CHANNEL-A (CLC-A); (ATCLCA);CHLORIDE CHANNEL A (CLC-A);CHLORIDE CHANNEL A
AT5G40720.1	+	607	C3H4 type zinc finger protein (DUF23);(source:Araport11)	
AT5G40470.1	-	2656	RNI-like superfamily protein;(source:Araport11)	
AT5G40390.1	+	1760	Encodes a protein which might be involved in the formation of verbascose. A T-DNA insertion mutant was shown to have a decreased amount of verbascose (as well as mannitol) whereas the levels of raffinose and stachyose remained unchanged.	RAFFINOSE SYNTHASE 5 (RS5);SEED IMBIBITION 1-LIKE (SIP1)
AT5G40340.1	-	-336	PWWP domain protein involved in regulation of FLC and flowering time.	PWWP DOMAIN PROTEIN 3 (PDP3)
AT5G39660.1	+	-37	Dof-type zinc finger domain-containing protein, identical to H-protein promoter binding factor-2a GI:3386546 from (Arabidopsis thaliana). Interacts with LKP2 and FKF1, but its overexpression does not change flowering time under short or long day conditions.	CYCLING DOF FACTOR 2 (CDF2)
AT5G37540.1	+	1056	Eukaryotic aspartyl protease family protein;(source:Araport11)	
AT5G37260.1	-	31	Encodes a MYB family transcription factor Circadian 1 (CIR1). Involved in circadian regulation in Arabidopsis.	CIRCADIAN 1 (CIR1);REVEILLE 2 (RVE2)

AT5G28770.2	-	-188	BASIC LEUCINE ZIPPER protein which regulates the circadian oscillator gene PSEUDO RESPONSE REGULATOR7 (PRR7) to change the circadian phase in response to sugars. It upregulates PRR7 in response to low energy. bZIP63 and PRR7 are required for correct oscillator phase under light/dark cycles. bZIP protein BZO2H3 mRNA, partial cds	(BZO2H3)
AT5G28460.1	+	2665	Pentatricopeptide repeat (PPR) superfamily protein;(source:Araport11)	
AT5G27945.1	+	2171	Transducin/WD40 repeat-like superfamily protein;(source:Araport11)	
AT5G24670.2	+	2873	A protein coding gene with unknown function. The 5?UTR of this gene overlaps with a RNA coding gene TER2. TER2 (GenBank accession no. HQ401285) encodes a putative template sequence corresponding to 1.5 copies of the Arabidopsis telomere repeat (PNAS 2011, 108:73-78). Natural epiallele in Nok-1, transmission of the epiallele over generations depends only on the selfreinforcing loop between CHROMOMETHYLASE 3 and KRYPTONITE, involving DNA methylated in the CHG context and histone H3 lysine 9 methylation.	(ATTAD3);TRNA ADENOSINE DEAMINASE 3 (TAD3);EMBRYO DEFECTIVE 2820 (EMB2820)
AT5G24660.1	-	355	response to low sulfur 2;(source:Araport11)	RESPONSE TO LOW SULFUR 2 (LSU2)
AT5G24655.1	-	-95	response to low sulfur 4;(source:Araport11)	RESPONSE TO LOW SULFUR 4 (LSU4)
AT5G24470.1	-	-77	Encodes a pseudo-response regulator whose mutation affects various circadian-associated biological events such as flowering time in the long-day photoperiod conditions, red light sensitivity of seedlings during early photomorphogenesis, and the period of free-running rhythms of certain clock-controlled genes including CCA1 and APRR1/TOC1 in constant white light. Acts as transcriptional repressor of CCA1 and LHY.	PSEUDO-RESPONSE REGULATOR 5 (PRR5);PSEUDO-RESPONSE REGULATOR 5 (APRR5)
AT5G23940.1	-	2259	Encodes PERMEABLE LEAVES3 (PEL3), a putative acyl-transferase. Mutation in this locus results in altered trichome phenotype (trcichomes become tangled during leaf expansion). Additional phenotype includes altered cuticle layer.	PERMEABLE LEAVES3 (PEL3);EMBRYO DEFECTIVE 3009 (EMB3009);DEFECTIVE IN CUTICULAR RIDGES (DCR)
AT5G23350.1	-	-352	GRAM domain protein/ABA-responsive-like protein;(source:Araport11)	
AT5G22940.1	+	2059	Homolog of FRA8 (AT2G28110), a member of a member of glycosyltransferase family 47; exhibits high sequence similarity to tobacco (Nicotiana plumbaginifolia) pectin glucuronyltransferase.	FRA8 HOMOLOG (F8H)
AT5G22920.1	+	6	Encodes a protein with sequence similarity to RING, zinc finger proteins. Loss of function mutations show reduced (15%) stomatal aperture under non stress conditions.	RING ZINC-FINGER PROTEIN 34 (RZPF34);CHY ZINC-FINGER AND
AT5G22890.1	-	-927	An unique homologue of STOP1 (AT1G34370) in Arabidopsis genome. Transformation to the stop1-mutant activated several genes that are regulated by STOP1, and conferred proton sensitive phenotype.	SENSITIVE TO PROTON RHIZOTOXICITY 2 (STOP2)
AT5G22250.1	-	1112	Encodes one of the homologs of the yeast CCR4-associated factor 1: AT3G44260 (CAF1a), AT5G22250 (CAF1b). Has mRNA deadenylation activity. Also plays a role in plant defense responses.	CCR4- ASSOCIATED FACTOR 1B (CAF1b);CCR4- ASSOCIATED
AT5G21940.1	-	-710	hybrid signal transduction histidine kinase M-like protein;(source:Araport11)	
AT5G20250.4	+	-450	encodes a member of glycosyl hydrolase family 36. Expression is induced within 3 hours of dark treatment, in senescing leaves and treatment with exogenous photosynthesis inhibitor. Induction of gene expression was suppressed in excised leaves supplied with sugar. The authors suggest that the gene's expression pattern is responding to the level of sugar in the cell. The mRNA is cell-to-cell mobile.	RAFFINOSE SYNTHASE 6 (RS6);DARK INDUCIBLE 10 (DIN10)
AT5G19120.1	+	-60	Eukaryotic aspartyl protease family protein;(source:Araport11)	
AT5G19040.1	-	1103	Encodes cytokinin synthase.	ISOPENTENYLTRANSFERASE 5 (IPT5);ARABIDOPSIS THALIANA
AT5G18670.1	+	-909	putative beta-amylase BMY3 (BMY3)	BETA-AMYLASE 3 (BMY3);BETA-AMYLASE 9 (BAM9)
AT5G18630.1	+	-198	alpha/beta-Hydrolases superfamily protein;(source:Araport11)	
AT5G18440.1	+	-77	Encodes NUFIP that directs assembly of C/D snoRNP (small nucleolar ribonucleoprotein).	(AtNUFIP);NUCLEAR FMRP-INTERACTING PROTEIN (NUFIP)
AT5G17350.1	+	385	hypothetical protein;(source:Araport11)	
AT5G16370.1	-	-159	acyl activating enzyme 5;(source:Araport11)	ACYL ACTIVATING ENZYME 5 (AAE5)
AT5G16120.2	+	-320	alpha/beta-Hydrolases superfamily protein;(source:Araport11)	(MAGL15)
AT5G15500.2	-	-227	Ankyrin repeat family protein;(source:Araport11)	
AT5G14820.1	-	-2950	Pentatricopeptide repeat (PPR) superfamily protein;(source:Araport11)	
AT5G14800.1	-	-255	Delta 1-pyrroline-5-carboxylate reductase, catalyzes the final step in proline biosynthesis from glutamate and ornithine.In situ hybridization indicated that under normal growth conditions, the highest concentration of P5CR transcripts occurs in the cortical parenchyma, phloem, vascular cambium and pith parenchyma in the vicinity of the protoxylem. Single gene in Arabidopsis.	PYRROLINE-5- CARBOXYLATE (P5C) REDUCTASE (P5CR);PYRROLINE-5- CARBOXYLATE (P5C) REDUCTASE (AT-
AT5G14730.1	+	294	Unknown protein, expression induced by IDL7 and stress.	
AT5G13760.1	+	-183	Plasma-membrane choline transporter family protein;(source:Araport11)	
AT5G13170.1	-	-1106	Encodes a member of the SWEET sucrose efflux transporter family proteins.	(AtSWEET15); (SWEET15);SENESCENCE-ASSOCIATED GENE 29
AT5G11700.2	-	-20	ephrin type-B receptor;(source:Araport11)	
AT5G11520.1	-	-18	Encodes the chloroplastic isozyme of aspartate aminotransferase. Involved in aspartate biosynthesis and nitrogen metabolism. mRNA is expressed in senescing leaves.	YELLOW-LEAF-SPECIFIC GENE 4 (YLS4);ASPARTATE
AT5G11470.1	-	5877	SG1 is a Bromo-Adjacent Homology (BAH) domain containing protein involved in CHG methylation within genebodies. Loss of function results in pleiotrophic developmental effects that increase after 4 generations.	INCREASE IN BONSAI METHYLATION 2 (IBM2);ANTI-SILENCING 1
AT5G11090.1	+	1870	serine-rich protein-like protein;(source:Araport11)	
AT5G10560.1	-	3171	Glycosyl hydrolase family protein;(source:Araport11)	
AT5G10550.1	-	-48	This gene is predicted to encode a bromodomain-containing protein. A plant line expressing RNAi constructs targeted against GTE7 shows some resistance to agrobacterium-mediated root transformation.	GLOBAL TRANSCRIPTION FACTOR GROUP E2 (GTE2)
AT5G10450.4	-	-112	Encodes a member of the 14-3-3 gene family that is a lambda isoform (14-3-3λ). Interacts with APX3 (ascorbate peroxidase) and AKR2 , suggesting a role in mediating oxidative metabolism in stress response. This protein was shown to colocalize and interact with SERK1 by which it is phosphorylated. This protein is also reported to interact with the phosphorylated form of the BZR1 transcription factor involved in brassinosteroid signaling and may affect the nucleocytoplasmic shuttling of BZR1. Interacts with JAZ10.4 which lacks the Jas motif. It is also phosphorylated by CRPK1 as part of the response to cold and translocates to the nucleus after phosphorylation.	G-BOX REGULATING FACTOR 6 (GRF6)
AT5G10340.1	+	67	F-box family protein;(source:Araport11)	
AT5G08350.1	-	-231	Mutants have decreased tolerance to cold and oxidative stress. Gene expression induced by drought and ABA.	
AT5G07440.1	+	-646	Encodes the beta-subunit of the glutamate dehydrogenase. The enzyme is almost exclusively found in the mitochondria of stem and leaf companion cells.	GLUTAMATE DEHYDROGENASE 2 (GDH2)
AT5G07430.1	+	2312	Pectin lyase-like superfamily protein;(source:Araport11)	
AT5G06980.4	+	-250	hypothetical protein;(source:Araport11)	NIGHT LIGHT-INDUCIBLE AND CLOCK-REGULATED 4 (LNK4)
AT5G06820.1	+	-109	STRUBBELIG-receptor family 2;(source:Araport11)	STRUBBELIG-RECEPTOR FAMILY 2 (SRF2)
AT5G06220.2	+	-30	LETM1-like protein;(source:Araport11)	
AT5G05600.1	+	1125	Encodes a protein with similarity to flavonol synthases that is involved in the detoxifcation polycyclic aromatic hydrocarbons.One of 4 paralogs encoding a 2-oxoglutarate/Fe(II)-dependent oxygenases that hydroxylates JA to 12-OH-JA.	JASMONATE-INDUCED OXYGENASE2 (JAO2);JASMONIC ACID OXIDASE 2 (JOX2)
AT5G05250.1	-	-459	hypothetical protein;(source:Araport11)	
AT5G05140.1	+	-1814	Transcription elongation factor (TFIIS) family protein;(source:Araport11)	
AT5G04340.1	-	646	Encodes a C2H2 zinc finger transcription factor that coordinately activates phytochelatin-synthesis related gene expression and directly targets GSH1 by binding to its promoter to positively regulate Cd accumulation and tolerance.	COLD INDUCED ZINC FINGER PROTEIN 2 (CZF2); (ATZAT6);ZINC FINGER OF ARABIDOPSIS THALIANA 6 (ZAT6); (C2H2)
AT5G04040.1	+	446	Encodes a triacylglycerol lipase that is involved in storage lipid breakdown during seed germination. The mutant plant exhibits a much slower rate of postgerminative growth than the wild type.	SUGAR-DEPENDENT1 (SDP1)
AT5G03370.1	-	-1718	acylphosphatase family;(source:Araport11)	
AT5G03220.1	-	1655	Encodes together with its paralog MED7B a subunit of the middle module of the transcriptional co-regulator Mediator complex. Regulates genes required for normal development of etiolated seedlings.	MED7A (MED7A)
AT5G02580.1	+	-582	argininosuccinate lyase;(source:Araport11)	
AT5G02260.1	+	-585	member of Alpha-Expansin Gene Family. Naming convention from the Expansin Working Group (Kende et al, 2004. Plant Mol Bio)	EXPANSIN A9 (EXPA9); (ATHEXP ALPHA 1.10);EXPANSIN A9
AT5G02220.1	-	-217	cyclin-dependent kinase inhibitor;(source:Araport11)	SIAMESE-RELATED 4 (SMR4)
AT5G02160.1	+	-47	Zinc-finger domain containing protein involved in abiotic stress response. Possesses an N-terminal transit peptide followed by a hydrophobic domain and a zinc-finger domain. Despite the presence of a zinc-finger domain (C4-type) with two CXXCXGXG conserved repeats, characteristic of DNAJ protein, the conserved J domain is absent in FIP. Interacts with FtsH5. Gene expression levels are reduced and negatively regulates stress response genes during stress conditions.	FTSH5 INTERACTING PROTEIN (FIP)
AT5G01800.1	+	2022	saposin B domain-containing protein;(source:Araport11)	
AT5G01720.1	-	3788	RAE1 is an F-box protein component of a SCF-type E3 ligase complex. It is part of an alumium induced regulatory loop: its activity is induced by STOP1 and it in turn ubiquitinates STOP1 which is then targeted for degradation.	REGULATION OF ATALMT1 EXPRESSION 1 (RAE1)
AT4G40011.1	-	170	hypothetical protein;(source:Araport11)	
AT4G39990.1	+	-33	GTP-binding protein ATGB3	RAB GTPASE HOMOLOG A4B (RABA4B);ARABIDOPSIS THALIANA
AT4G39840.1	+	1622	cell wall integrity/stress response component-like protein;(source:Araport11)	
AT4G39660.1	+	-262	alanine:glyoxylate aminotransferase 2 homolog (AGT2). The mRNA is cell-to-cell mobile.	ALANINE:GLYOXYLATE AMINOTRANSFERASE 2 (AGT2)
AT4G39120.1	-	7501	Encodes a chloroplast-localized member of the myo-inositol monophosphatase family, IMPL2 (myo-Inositol monophosphatase like 2) that seems to have multiple enzymatic activities. It contributes to histidine biosynthesis based on it histidinol-phosphate phosphatase activity. In addition, the protein can act as an inositol monophosphatase and an L-galactose-1-phosphate phosphatase in vitro.	MYO-INOSITOL MONOPHOSPHATASE LIKE 2 (IMPL2);HISTIDINE BIOSYNTHESIS 7 (HISN7)
AT4G39100.1	-	51	Encodes a plant-specific histone reader capable of recognizing both H3K27me3 and H3K4me3 via its bromo-adjacent homology (BAH) and plant homeodomain (PHD) domains, respectively. Detailed biochemical and structural studies suggest a binding mechanism that is mutually exclusive for either H3K4me3 or H3K27me3. SHL plays a role in the repression of flowering.	SHORT LIFE (SHL)

AT4G38930.2	+	2587	Ubiquitin fusion degradation UFD1 family protein;(source:Araport11)	
AT4G38810.2	-	-727	Calcium-binding EF-hand family protein;(source:Araport11)	CALCIUM SENSOR (SCS)
AT4G38680.1	-	179	Encodes a glycine-rich protein that binds nucleic acids and promotes DNA melting. Its transcript and protein levels are up-regulated in response to cold treatment with protein levels peaking earlier in shoots (~10-14 days) than in roots (~21 days). It is normally expressed in meristematic regions and developing tissues where cell division occurs. RNAi and antisense lines with lower levels of CSP2/GRP2 transcripts flower earlier than wild type plants and have some defects in anther and seed development.	ARABIDOPSIS THALIANA COLD SHOCK PROTEIN 2 (ATCSP2);COLD SHOCK PROTEIN 2 (CSP2);COLD SHOCK DOMAIN PROTEIN 2 (CSDP2);GLYCINE RICH PROTEIN 2 (GRP2)
AT4G38470.1	+	-335	ACT-like protein tyrosine kinase family protein;(source:Araport11)	SERINE/THREONINE/TYROSINE KINASE 46 (STY46)
AT4G38401.1	-	-102	hypothetical protein;(source:Araport11)	
AT4G38330.1	+	-379	hemolysin-III integral membrane-like protein;(source:Araport11)	
AT4G37890.1	-	1839	Zinc finger (C3HC4-type RING finger) family protein;(source:Araport11)	EMBRYO SAC DEVELOPMENT ARREST 40 (EDA40)
AT4G37610.1	-	-130	BTB and TAZ domain protein. Located in cytoplasm and expressed in fruit, flower and leaves.	BTB AND TAZ DOMAIN PROTEIN 5 (bt5)
AT4G37540.1	-	-506	LOB domain-containing protein 39;(source:Araport11)	LOB DOMAIN-CONTAINING PROTEIN 39 (LBD39)
AT4G37480.1	+	-70	Chaperone DnaJ-domain superfamily protein;(source:Araport11)	
AT4G37420.1	+	1590	glycosyltransferase family protein (DUF23);(source:Araport11)	
AT4G37390.1	+	-154	Encodes an IAA-amido synthase that conjugates Asp and other amino acids to auxin in vitro. Lines carrying insertions in this gene are hypersensitive to auxin. May function as a negative component in auxin signaling by regulating auxin activity.	YADOKARI 1 (YDK1);AUXIN UPREGULATED 3 (AUR3); (GH3-2); (BRU6); (GH3.2)
AT4G37240.1	+	-117	HTH-type transcriptional regulator;(source:Araport11)	
AT4G36710.1	+	1695	GRAS family transcription factor;(source:Araport11)	SCARECROW-LIKE 15 (SCL15);ARABIDOPSIS THALIANA HAIRY
AT4G36040.1	-	-124	Chaperone DnaJ-domain superfamily protein;(source:Araport11)	DNA J PROTEIN C23 (DJC23);DNAJ11 (J11)
AT4G35900.1	+	509	bZIP protein required for positive regulation of flowering. Mutants are late flowering. FD interacts with FT to promote flowering.Expressed in the shoot apex in floral anlagen, then declines in floral primordia.	(atbzip14); (FD); (FD-1)
AT4G35770.1	+	-113	Senescence-associated gene that is strongly induced by phosphate starvation. Transcripts are differentially regulated at the level of mRNA stability at different times of day. mRNAs are targets of the mRNA degradation pathway mediated by the downstream (DST) instability determinant.	DARK INDUCIBLE 1 (DIN1);SENESCENCE 1 (SEN1);SENESCENCE ASSOCIATED GENE 1 (SEN1);ARABIDOPSIS THALIANA
AT4G35250.1	-	-4	HCF244 is a member of the atypical short-chain dehydrogenase/reductase superfamily, a modified group, which has lost enzyme activity.HCF244 interacts with unknown partners in a 200-400 kD membrane associated complex.	HIGH CHLOROPHYLL FLUORESCENCE PHENOTYPE 244 (HCF244)
AT4G35170.1	+	1024	Late embryogenesis abundant (LEA) hydroxyproline-rich glycoprotein family;(source:Araport11)	COMPANION OF CELLULOSE SYNTHASE 4 (CC4)
AT4G34138.1	-	-358	UDP-glucosyl transferase 73B1;(source:Araport11)	UDP-GLUCOSYL TRANSFERASE 73B1 (UGT73B1)
AT4G33980.2	-	-67	hypothetical protein;(source:Araport11)	COLD-REGULATED GENE 28 (COR28)
AT4G33430.2	-	-23	Leu-rich receptor Serine/threonine protein kinase. Component of BR signaling that interacts with BRI1 in vitro and in vivo to form a heterodimer. Brassinolide-dependent association of BRI1 and BAK1 in vivo. Phosphorylation of both BRI1 and BAK1 on Thr residues was BR dependent. Although BAK1 and BRI1 alone localize in the plasma membrane, when BAK1 and BRI1 are coexpressed, the heterodimer BAK1/BRI1 they form is localized in the endosome.	BRI1-ASSOCIATED RECEPTOR KINASE (BAK1)
AT4G32950.1	-	1672	Protein phosphatase 2C family protein;(source:Araport11)	
AT4G32890.1	+	1013	Encodes a member of the GATA factor family of zinc finger transcription factors.	GATA TRANSCRIPTION FACTOR 9 (GATA9)
AT4G32480.1	+	-247	sugar phosphate exchanger, putative (DUF506);(source:Araport11)	
AT4G32410.1	-	-10	Encodes a cellulose synthase isomer. CESA1 mutants have cellulose defect in the primary cell wall. Multiple lines of evidence suggest that CESA1, along with CESA3 and CESA6 are present in the same plasma membrane complex for cellulose biosynthesis. lasma membrane complex for cellulose biosynthesis. As inferred from the null role of secondary wall-type CesAs, included in a set of five primary wall-type CesAs that may support trichome cell wall thickening.	ANISOTROPY1 (ANY1);CELLULOSE SYNTHASE 1 (CESA1);RADIALLY SWOLLEN 1 (RSW1);CELLULOSE SYNTHASE 1 (AtCESA1)
AT4G31510.1	-	-397	major centromere autoantigen B-like protein;(source:Araport11)	
AT4G30490.1	-	-530	AFG1-like ATPase family protein;(source:Araport11)	
AT4G29950.1	+	-825	Ypt/Rab-GAP domain of gyp1p superfamily protein;(source:Araport11)	
AT4G29780.1	+	1052	Expression of the gene is affected by multiple stresses. Knockout and overexpression lines show no obvious phenotypes.	
AT4G28860.1	+	-119	Member of CKL gene family (CKL-A group)	CASEIN KINASE I-LIKE 4 (ckl4)
AT4G27950.1	-	-624	Encodes a member of the ERF (ethylene response factor) subfamily B-5 of ERF/AP2 transcription factor family. The protein contains one AP2 domain. There are 7 members in this subfamily. CRF proteins relocalize to the nucleus in response to cytokinin.	CYTOKININ RESPONSE FACTOR 4 (CRF4)
AT4G26450.1	+	-680	hypothetical protein;(source:Araport11)	WPP DOMAIN INTERACTING PROTEIN 1 (WIP1)
AT4G26260.2	+	-735	Encodes a myo-inositol oxygenase, which is the first enzyme in the inositol route to ascorbate (L‐ascorbic acid, AsA, vitamin C). Overexpression results in enhanced biomass and abiotic stress tolerance.	MYO-INOSITOL OXYGENASE 4 (MIOX4)
AT4G24231.1	+	81	This gene encodes a small protein and has either evidence of transcription or purifying selection.	
AT4G24190.1	-	-254	encodes an ortholog of GRP94, an ER-resident HSP90-like protein and is involved in regulation of meristem size and organization. Single and double mutant analyses suggest that SHD may be required for the correct folding and/or complex formation of CLV proteins. Lines carrying recessive mutations in this locus exhibits expanded shoot meristems, disorganized root meristems, and defective pollen tube elongation. Transcript is detected in all tissues examined and is not induced by heat. Endoplasmin supports the protein secretory pathway and has a role in proliferating tissues.	HEAT SHOCK PROTEIN 90-7 (AtHsp90-7);SHEPHERD (SHD);HEAT SHOCK PROTEIN 90.7 (HSP90.7);HEAT SHOCK PROTEIN 90.7 (AtHsp90.7)
AT4G22590.1	-	-686	Haloacid dehalogenase-like hydrolase (HAD) superfamily protein;(source:Araport11)	TREHALOSE-6-PHOSPHATE PHOSPHATASE G (TPPG)
AT4G22350.2	-	-237	Ubiquitin C-terminal hydrolases superfamily protein;(source:Araport11)	
AT4G21930.1	+	628	senescence regulator (Protein of unknown function, DUF584);(source:Araport11)	
AT4G21540.1	+	-96	Encodes a sphingosine kinase, also has enzyme activity towards other plant long-chain sphingoid bases. Involved in guard cell ABA signalling and seed germination.	SPHINGOSINE KINASE 1 (SPHK1)
AT4G21530.1	+	5511	Transducin/WD40 repeat-like superfamily protein;(source:Araport11)	ANAPHASE PROMOTING COMPLEX 4 (APC4)
AT4G21320.1	+	-13	Encodes heat-stress-associated 32-kD protein. Up-regulated by heat shock. Thermotolerance in a knockout mutant was compromised following a long recovery period (> 24 h) after acclimation heat shock treatment.	HEAT-STRESS-ASSOCIATED 32 (HSA32)
AT4G19140.1	+	-87	exopolysaccharide production negative regulator;(source:Araport11)	
AT4G18340.1	-	-4179	Glycosyl hydrolase superfamily protein;(source:Araport11)	
AT4G18020.1	-	3941	Encodes pseudo-response regulator 2 (APRR2) that interacts with a calcium sensor (CML9).	(APRR2);PSEUDO-RESPONSE REGULATOR 2 (PRR2)
AT4G17530.1	-	-49	AtRabD2c encodes a Rab GTPase, which plays important roles in pollen development, germination and tube elongation.	RAB GTPASE HOMOLOG 1C (RAB1C); (RAB1C);RAB GTPASE
AT4G17080.1	+	-1192	Histone H3 K4-specific methyltransferase SET7/9 family protein;(source:Araport11)	
AT4G16820.1	+	1352	Encodes a lipase that hydrolyzes phosphatidylcholine, glycolipids as well as triacylglycerols.	PHOSPHOLIPASE A I BETA 2 (PLA-I{beta]2);DAD1-LIKE LIPASE 1
AT4G16640.1	-	490	Matrixin family protein;(source:Araport11)	(AT1-MMP)
AT4G16500.1	-	56	Cystatin/monellin superfamily protein;(source:Araport11)	(ATCYS4);PHYTOCYSTATIN 4 (CYS4)
AT4G16110.1	+	-1704	Encodes a pollen-specific transcription factor involved in the expression of nuclear genes for components of mitochondrial complex I in Arabidopsis. Acts in concert with other type-B ARRs in the cytokinin signaling pathway. AHK3 mediates cytokinin-induced phosphorylation of ARR2 on the Asp-80 residue. This phosphorylation plays a positive role of ARR2 in cytokinin-mediated control of leaf longevity. Also involved in cytokinin-dependent inhibition of hypocotyl elongation.	RESPONSE REGULATOR 2 (ARR2);RESPONSE REGULATOR 2 (RR2)
AT4G14713.1	-	-181	PPD1 (and its paralog, PPD2) encode plant-specific putative DNA-binding proteins. PPD1 and PPD2 are not found in grasses. Overexpression of PPD reduces lamina size by promoting the early arrest of dispersed meristematic cells DMC proliferation during leaf and silique development. Deletion of the PPD locus increases leaf lamina size and results in dome-shaped rather than flat leaves. Siliques are also altered in shape because of extra lamina growth. The curvature of a deltappd leaf reflects the difference between excess growth of the lamina and a limitation to the extension capacity of its perimeter.	PLANT-SPECIFIC PUTATIVE DNA-BINDING PROTEIN 1 (PPD1);PEAPOD 1 (PPD1); (TIFY4A)
AT4G14620.1	-	-46	hypothetical protein (DUF506);(source:Araport11)	
AT4G14500.1	+	-165	Polyketide cyclase/dehydrase and lipid transport superfamily protein;(source:Araport11)	
AT4G12430.1	-	-1030	Haloacid dehalogenase-like hydrolase (HAD) superfamily protein;(source:Araport11)	TREHALOSE-6-PHOSPHATE PHOSPHATASE F (TPPF)
AT4G10500.1	+	2129	2-oxoglutarate (2OG) and Fe(II)-dependent oxygenase superfamily protein;(source:Araport11)	DMR6-LIKE OXYGENASE 1 (DLO1)
AT4G08980.1	+	-231	Encodes an F-box gene that is a novel negative regulator of AGO1 protein levels and may play a role in ABA signalling and/or response. It is a F-box subunit of the SCF E3 ubiquitin ligase complex that mediates the degradation of 14-3-3 proteins.	F-BOX WITH WD-40 2 (FBW2);SKP1/ASK-INTERACTING PROTEIN 18 (SKIP18)
AT4G08150.1	-	640	A member of class I knotted1-like homeobox gene family (together with KNAT2). Similar to the knotted1 (kn1) homeobox gene of maize. Normally expressed in the peripheral and rib zone of shoot apical meristem but not in the leaf primordia. It is also expressed in the fourth floral whorl, in the region that would become style, particularly in the cell surrounding the transmitting tissue. No expression was detected in the first three floral whorls. Expression is repressed by auxin and AS1 which results in the promotion of leaf fate.	BREVIPEDICELLUS 1 (BP1);KNOTTED-LIKE FROM ARABIDOPSIS THALIANA (KNAT1);BREVIPEDICELLUS (BP)

AT4G05071.1	-	-65	This gene encodes a small protein and has either evidence of transcription or purifying selection.	
AT4G03510.1	-	-168	RMA1 encodes a novel 28 kDa protein with a RING finger motif and a C-terminal membrane-anchoring domain that is involved in the secretory pathway. Has E3 ubiquitin ligase activity.	(ATRMA1);RING MEMBRANE-ANCHOR 1 (RMA1)
AT4G03010.1	+	-578	RNI-like superfamily protein;(source:Araport11)	
AT4G02670.1	-	2030	indeterminate(ID)-domain 12;(source:Araport11)	INDETERMINATE(ID)-DOMAIN 12 (IDD12);INDETERMINATE(ID)-
AT4G01870.1	-	1802	tolB protein-like protein;(source:Araport11)	
AT4G01690.1	+	-1817	Encodes protoporphyrinogen oxidase (PPOX).	(PPO1); (PPOX); (HEMG1)
AT4G01245.1	+	-1100	hypothetical protein;(source:Araport11)	
AT4G01130.1	+	-674	GDSL-motif esterase/acyltransferase/lipase. Enzyme group with broad substrate specificity that may catalyze acyltransfer or hydrolase reactions with lipid and non-lipid substrates.	
AT4G01120.1	-	-267	bZIP (basic leucine zipper) transcription factor that binds to the G-box regulatory element found in many plant promoters. GBF2 nuclear localization is increased by blue light	BASIC REGION/LEUCINE ZIPPER MOTIF 5 (ATBZIP54);G-BOX
AT4G00570.1	-	-223	Encodes an NAD-dependent malic enzyme (NAD-ME) that does not act on oxaloacetate, indicating that it belongs to EC 1.1.1.39. It is a member of the beta family of NAD-MEs in plants. It appears to function as a homodimer or as a heterodimer with the alpha-type NAD-ME2 (At2g13560). NAD-ME2 transcript and protein levels are higher during the night than during the day.	NAD-DEPENDENT MALIC ENZYME 2 (NAD-ME2)
AT4G00490.1	+	-159	Encodes a chloroplast beta-amylase. The enzyme activity is very weak compared to BAM1 and BAM3. It forms a tetramer whose activity requires K+ and exhibits sigmoidal kinetics Mutants of BAM2 have no visible phenotype.	BETA-AMYLASE 2 (BAM2);BETA-AMYLASE 9 (BMY9)
AT4G00360.1	+	938	Encodes a member of the CYP86A subfamily of cytochrome p450 genes. Expressed at moderate levels in flowers, leaves, roots and stems.	CYTOCHROME P450, FAMILY 86, SUBFAMILY A, POLYPEPTIDE 2
AT4G00150.1	-	1588	Belongs to one of the LOM (LOST MERISTEMS) genes: AT2G45160 (LOM1), AT3G60630 (LOM2) and AT4G00150 (LOM3). LOM1 and LOM2 promote cell differentiation at the periphery of shoot meristems and help to maintain their polar organization.	LOST MERISTEMS 3 (LOM3); (SCL6-IV);HAIRY MERISTEM 3 (HAM3);ARABIDOPSIS THALIANA HAIRY MERISTEM 3 (ATHAM3)
AT4G00080.1	+	34	Plant invertase/pectin methylesterase inhibitor superfamily protein;(source:Araport11)	UNFERTILIZED EMBRYO SAC 11 (UNE11)
AT3G63200.1	+	806	PATATIN-like protein 9;(source:Araport11)	PATATIN-LIKE PROTEIN 9 (PLP9); (PLA IIIB)
AT3G62650.2	+	1049	hypothetical protein;(source:Araport11)	
AT3G62260.2	-	-220	Protein phosphatase 2C family protein;(source:Araport11)	
AT3G61910.1	-	1144	NAC transcription factor NST2. NST1 and NST2 are redundant in regulating secondary wall thickening in anther walls. NST2 promoter was particularly strong in anther tissue.	NAC DOMAIN PROTEIN 66 (NAC066);NAC SECONDARY WALL
AT3G61826.1	-	91	This gene encodes a small protein and has either evidence of transcription or purifying selection.	
AT3G61740.1	-	-163	Encodes SET domain containing protein that acts redundantly with ATX4/5 to regulate histone H3-K4 methylation.	(ATX3);SET DOMAIN PROTEIN 14 (SDG14)
AT3G61680.1	+	3346	PLIP1 encodes a plastid localized phospholipase A1 involved in seed oil biosynthesis.	PLASTID LIPASE1 (PLIP1)
AT3G61260.1	-	-237	Lipid raft regulatory protein, crucial for plasma membrane nanodomain assembly to control plasmodesmata aperture and functionality. Negatively regulates the cell-to-cell movement of TuMV via competition with PCaP1 for binding actin filaments.	REMORIN 1.2 (REM1.2)
AT3G61050.1	+	4618	Encodes a novel transcriptional regulator, a calcium-dependent lipid-binding protein containing a C2 domain, that binds specifically to the promoter of THAS1 (thalianol synthase 1). It can bind ceramide and is involved in drought and salt tolerance.	(NTMC2T4);CALCIUM-DEPENDENT LIPID-BINDING PROTEIN (AtCLB);SYNAPTOTAGMIN 7 (SYT7); (NTMC2TYPE4)
AT3G60620.1	+	-197	cytidinediphosphate diacylglycerol synthase 5;(source:Araport11)	CYTIDINEDIPHOSPHATE DIACYLGLYCEROL SYNTHASE 5 (CDS5)
AT3G57540.1	-	-382	Remorin family protein;(source:Araport11)	(ATREM4.1);REMORIN GROUP 4 1 (REM4.1)
AT3G57520.1	-	-124	SIP2 encodes a raffinose-specific alpha-galactosidase that catalyzes the breakdown of raffinose into alpha-galatose and sucrose. This enzyme may function in unloading raffinose from the phloem as part of sink metabolism. Although it was originally predicted to act as a raffinose synthase (RS), that activity was not observed for recombinant SIP2.	RAFFINOSE SYNTHASE 2 (RS2);SEED IMBIBITION 2 (SIP2);SEED IMBIBITION 2 (AtSIP2)
AT3G57460.1	-	-1538	catalytic/ metal ion binding / metalloendopeptidase/ zinc ion binding protein;(source:Araport11)	
AT3G56810.1	-	-133	hypothetical protein;(source:Araport11)	
AT3G56360.1	-	1977	hypothetical protein;(source:Araport11)	
AT3G56140.1	+	-110	DUF399 family protein, putative (DUF399 and DUF3411);(source:Araport11)	RETICULATA-RELATED 6 (RER6)
AT3G56130.1	+	81	biotin/lipoyl attachment domain-containing protein;(source:Araport11)	BCCP-LIKE PROTEIN 3 (BLP3);BIOTIN/LIPOYL ATTACHMENT
AT3G55870.1	+	2353	ADC synthase superfamily protein;(source:Araport11)	
AT3G54880.1	+	3701	zinc finger protein;(source:Araport11)	
AT3G54680.1	-	-25	proteophosphoglycan-like protein;(source:Araport11)	
AT3G54500.3	-	-48	Member of a small family (4 proteins) in Arabidopsis that have some overlap in function. LNK2 along with LNK1 functions in the integration of light signaling and circadian clock. It is regulated by the clock TOC1 complex. Functions as a transcriptional coactivator.	NIGHT LIGHT-INDUCIBLE AND CLOCK-REGULATED 2 (LNK2)
AT3G54440.3	-	57	glycoside hydrolase family 2 protein;(source:Araport11)	
AT3G53950.1	+	673	glyoxal oxidase-related protein;(source:Araport11)	
AT3G53620.1	+	-131	Encodes a soluble protein with inorganic pyrophosphatase activity that is highly specific for Mg-inorganic pyrophosphate. The mRNA is cell-to-cell mobile.	PYROPHOSPHORYLASE 4 (AtPPa4);PYROPHOSPHORYLASE 4 (PPa4)
AT3G53420.1	-	-1878	a member of the plasma membrane intrinsic protein subfamily PIP2. localizes to the plasma membrane and exhibits water transport activity in Xenopus oocyte. expressed specifically in the vascular bundles and protein level increases slightly during leaf dev. When expressed in yeast cells can conduct hydrogen peroxide into those cells.	(ATPIP2;1);PLASMA MEMBRANE INTRINSIC PROTEIN 2;1 (PIP2;1);PLASMA MEMBRANE INTRINSIC PROTEIN 2
AT3G52880.2	-	-316	Encodes a peroxisomal monodehydroascorbate reductase, involved in the ascorbate-glutathione cycle which removes toxic H2O2	MONODEHYDROASCORBATE REDUCTASE 1
AT3G51910.1	+	584	member of Heat Stress Transcription Factor (Hsf) family The mRNA is cell-to-cell mobile.	ARABIDOPSIS THALIANA HEAT SHOCK TRANSCRIPTION FACTOR
AT3G51890.1	-	-85	Clathrin light chain protein;(source:Araport11)	CLATHRIN LIGHT CHAIN 3 (CLC3)
AT3G51730.1	+	120	saposin B domain-containing protein;(source:Araport11)	
AT3G50970.1	+	325	Belongs to the dehydrin protein family, which contains highly conserved stretches of 7-17 residues that are repetitively scattered in their sequences, the K-, S-, Y- and lysine rich segments. LTI29 and LTI30 double overexpressors confer freeze tolerance. Located in membranes. mRNA upregulated by water deprivation and abscisic acid. The mRNA is cell-to-cell mobile.	LOW TEMPERATURE-INDUCED 30 (LTI30); (XERO2)
AT3G50280.1	+	1294	HXXXD-type acyl-transferase family protein;(source:Araport11)	
AT3G50260.1	+	160	Encodes a member of the DREB subfamily A-5 of ERF/AP2 transcription factor family. The protein contains one AP2 domain. Involved in defense and freezing stress responses. There are 16 members in this subfamily including RAP2.1, RAP2.9 and RAP2.10. The mRNA is cell-to-cell mobile.	DREB AND EAR MOTIF PROTEIN 1 (DEAR1); (ATERF#011);COOPERATIVELY REGULATED BY ETHYLENE AND
AT3G50060.1	-	-90	Encodes a member of the R2R3 transcription factor gene family. Expressed in response to potassium deprivation and auxin. Involved in lateral root development. Interacts with ARF7 and regulates the expression of some auxin responsive genes.	MYB DOMAIN PROTEIN 77 (MYB77)
AT3G49940.1	+	-1162	LOB domain-containing protein 38;(source:Araport11)	LOB DOMAIN-CONTAINING PROTEIN 38 (LBD38)
AT3G49796.1	+	134	This gene encodes a small protein and has either evidence of transcription or purifying selection.	
AT3G49790.1	-	1752	Carbohydrate-binding protein;(source:Araport11)	
AT3G48360.1	-	-1235	Encodes a protein (BT2) that is an essential component of the TAC1-mediated telomerase activation pathway. Acts redundantly with BT3 and BT1 during female gametophyte development and with BT3 during male gametophyte development. BT2 also mediates multiple responses to nutrients, stresses, and hormones.	BTB AND TAZ DOMAIN PROTEIN 2 (bt2); (ATBT2)
AT3G47820.1	+	1268	PLANT U-BOX 39;(source:Araport11)	PLANT U-BOX 39 (PUB39)
AT3G47610.1	+	2159	transcription regulator/ zinc ion binding protein;(source:Araport11)	
AT3G47341.1	+	-18	transmembrane protein;(source:Araport11)	
AT3G45060.1	-	-2442	member of High affinity nitrate transporter family	ARABIDOPSIS THALIANA HIGH AFFINITY NITRATE TRANSPORTER
AT3G44260.1	-	801	Encodes one of the homologs of the yeast CCR4-associated factor 1: AT3G44260 (CAF1a), AT5G22250 (CAF1b). Has mRNA deadenylation activity. Also plays a role in plant defense responses.	CCR4- ASSOCIATED FACTOR 1A (AtCAF1a);CCR4- ASSOCIATED
AT3G41762.1	-	1541	hypothetical protein;(source:Araport11)	
AT3G30775.1	-	-653	Encodes a proline oxidase that is predicted to localize to the inner mitochondrial membrane, its mRNA expression induced by high levels of Al and by osmotic stress. The promoter contains an L-proline-inducible element.	(ATPDH);PROLINE DEHYDROGENASE 1 (PDH1);
AT3G29160.1	-	86	encodes a SNF1-related protein kinase that physically interacts with SCF subunit SKP1/ASK1 and 20S proteosome subunit PAD1. It has also been shown to interact with the WD protein PDL1.	SNF1 KINASE HOMOLOG 11 (ATKIN11);SNF1 KINASE HOMOLOG
AT3G27330.1	-	888	zinc finger (C3HC4-type RING finger) family protein;(source:Araport11)	
AT3G25717.1	-	-1597	ROTUNDIFOLIA like 16;(source:Araport11)	DEVIL 6 (DVL6);ROTUNDIFOLIA LIKE 16 (RTFL16)
AT3G24180.1	-	265	Beta-glucosidase, GBA2 type family protein;(source:Araport11)	
AT3G22970.1	+	-242	hypothetical protein (DUF506);(source:Araport11)	
AT3G21420.1	+	2553	LATERAL BRANCHING OXIDOREDUCTASE (LBO), encodes an oxidoreductase-like enzyme of the 2-oxoglutarate and Fe(II)-dependent dioxygenase superfamily. It is involved in the biosynthesis of strigolactones.	LATERAL BRANCHING OXIDOREDUCTASE 1 (LBO1)
AT3G20898.1	+	401	hypothetical protein;(source:Araport11)	
AT3G20340.1	-	-196	Expression of the gene is downregulated in the presence of paraquat, an inducer of photoxidative stress.	

AT3G19680.1	+	1924	hypothetical protein (DUF1005);(source:Araport11)	
AT3G18980.1	+	-286	EIN2 targeting protein1;(source:Araport11)	EIN2 TARGETING PROTEIN1 (ETP1)
AT3G18290.1	+	-182	Encodes BRUTUS (BTS), a putative E3 ligase protein with metal ion binding and DNA binding domains, which negatively regulates the response to iron deficiency. The mRNA is cell-to-cell mobile.	EMBRYO DEFECTIVE 2454 (EMB2454);BRUTUS (BTS)
AT3G16690.1	-	708	Nodulin MtN3 family protein;(source:Araport11)	(SWEET16); (AtSWEET16)
AT3G16140.1	-	-89	Encodes subunit H of photosystem I reaction center subunit VI.	PHOTOSYSTEM I SUBUNIT H-1 (PSAH-1)
AT3G15630.1	-	-241	plant/protein;(source:Araport11)	
AT3G15500.1	+	2213	Encodes an ATAF-like NAC-domain transcription factor that doesn't contain C-terminal sequences shared by CUC1, CUC2 and NAM. Note: this protein (AtNAC3) is not to be confused with the protein encoded by locus AT3G29035, which, on occasion, has also been referred to as AtNAC3. The mRNA is cell-to-cell mobile.	(ANAC55);NAC DOMAIN CONTAINING PROTEIN 3 (NAC3);NAC DOMAIN CONTAINING PROTEIN 3 (ATNAC3);NAC DOMAIN
AT3G15450.1	+	-42	aluminum induced protein with YGL and LRDR motifs;(source:Araport11)	
AT3G15020.1	+	3025	Lactate/malate dehydrogenase family protein;(source:Araport11)	MITOCHONDRIAL MALATE DEHYDROGENASE 2 (mMDH2)
AT3G14990.1	+	-338	Encodes a homolog of animal DJ-1 superfamily protein. In the A. thaliana genome, three genes encoding close homologs of human DJ-1 were identified AT3G14990 (DJ1A), AT1G53280 (DJ1B) and AT4G34020 (DJ1C). Among the three homologs, DJ1C is essential for chloroplast development and viability. It exhibits glyoxalase activity towards glyoxal and methylglyoxal. The mRNA is cell-to-cell mobile.	(DJ-1A);DJ-1 HOMOLOG A (DJ1A);DJ-1 HOMOLOG A (AtDJ1A)
AT3G14205.1	-	-2902	Phosphoinositide phosphatase family protein;(source:Araport11)	SUPPRESSOR OF ACTIN 2 (SAC2)
AT3G14180.1	-	73	sequence-specific DNA binding transcription factor;(source:Araport11)	ARABIDOPSIS 6B-INTERACTING PROTEIN 1-LIKE 2 (ASIL2)
AT3G14160.1	+	-105	2-oxoglutarate-dependent dioxygenase family protein;(source:Araport11)	
AT3G14050.1	-	-1128	RELA/SPOT homolog 2;(source:Araport11)	RELA/SPOT HOMOLOG 2 (ATRSH2);RELA-SPOT HOMOLOG 2 (AT-
AT3G13740.1	+	2667	Encodes one of two chloroplast Mini-RNase III-like enzymes in Arabidopsis. Double mutants display imprecise maturation of 23S rRNA and other rRNAs.	(RNC4)
AT3G13700.1	-	882	RNA-binding (RRM/RBD/RNP motifs) family protein;(source:Araport11)	
AT3G13450.1	-	-103	branched chain alpha-keto acid dehydrogenase E1 beta	DARK INDUCIBLE 4 (DIN4)
AT3G13310.1	-	-538	Chaperone DnaJ-domain superfamily protein;(source:Araport11)	DNA J PROTEIN C66 (DJC66)
AT3G12920.1	-	1912	Encodes one of the BRGs (BOI-related gene) involved in resistance to Botrytis cinerea.	BOI-RELATED GENE 3 (BRG3)
AT3G12510.1	+	-125	MADS-box family protein;(source:Araport11)	
AT3G12380.2	-	50	Encodes a gene similar to actin-related proteins in other organisms. Member of nuclear ARP gene family.	ACTIN-RELATED PROTEIN 5 (ARP5)
AT3G12320.1	+	-270	hypothetical protein;(source:Araport11)	NIGHT LIGHT-INDUCIBLE AND CLOCK-REGULATED 3 (LNK3)
AT3G11630.1	+	-41	Encodes a 2-Cys peroxiredoxin (2-Cys PrxA) that contains two catalytic Cys residues. Functions in redox cascade with TrxL2 via the ferredoxin-thioredoxin reductase (FTR)/thioredoxin (Trx) pathway to mediate the light-responsive reductive control of target proteins. Continuously transfers reducing power from TrxL2 to H2O2.	2-CYS PEROXIREDOXIN A (2CPA)
AT3G11560.2	+	-47	LETM1-like protein;(source:Araport11)	
AT3G11410.1	-	-160	Encodes protein phosphatase 2C. Negative regulator of ABA signalling. Expressed in seeds during germination. mRNA up-regulated by drought and ABA.	PROTEIN PHOSPHATASE 2CA (PP2CA);ARABIDOPSIS THALIANA
AT3G09690.1	+	-248	alpha/beta-Hydrolases superfamily protein;(source:Araport11)	
AT3G07680.1	+	-174	Encodes an Golgi-localized p24 protein. Interacts with p24delta5 at ER export sites for ER exit and coupled transport to the Golgi apparatus. The mRNA is cell-to-cell mobile.	P24 SUBFAMILY BETA 2 (P24BETA2)
AT3G07350.1	+	1567	sulfate/thiosulfate import ATP-binding protein, putative (DUF506);(source:Araport11)	
AT3G07250.1	-	-442	RNA-binding (RRM-RBD-RNP motif) domain nuclear transport factor 2 family protein;(source:Araport11)	
AT3G06850.1	-	-122	dihydrolipoamide branched chain acyltransferase	DARK INDUCIBLE 3 (DIN3); (BCE2); (LTA1)
AT3G03790.3	+	-360	ankyrin repeat family protein / regulator of chromosome condensation (RCC1) family protein;(source:Araport11)	
AT3G02460.1	+	3138	Ypt/Rab-GAP domain of gyp1p superfamily protein;(source:Araport11)	
AT3G02140.1	-	-485	Encodes a protein that acts in the nucleus and is an important negative regulator of ABA and salt stress responses, and could play a critical role in controlling root elongation, floral initiation and starch degradation.	TWO OR MORE ABRES-CONTAINING GENE 2 (TMAC2);ABI FIVE
AT3G02040.1	-	-95	Encodes a member of the glycerophosphodiester phosphodiesterase (GDPD) family. Has glycerophosphodiester phosphodiesterase activity. Functions in maintaining cellular phosphate homeostasis under phosphate starvation. The mRNA is cell-to-cell mobile.	(AtGDPD1);GLYCEROPHOSPHODIESTER PHOSPHODIESTERASE 1 (GDPD1);SENESCENCE-RELATED GENE 3 (SRG3)
AT3G01990.1	+	-105	Member of a small family of ACT domain containing proteins in Arabidopsis. ACT domains are involved in amino acid binding.	ACT DOMAIN REPEAT 6 (ACR6)
AT3G01290.1	-	1340	SPFH/Band 7/PHB domain-containing membrane-associated protein family;(source:Araport11)	HYPERSENSITIVE INDUCED REACTION 2 (HIR2); (AtHIR2)
AT3G01100.1	-	3844	unknown protein, has cDNAs and ESTs associated to it	HYPOTHETICAL PROTEIN 1 (HYP1); (OSCA2.3);ARABIDOPSIS
AT2G48160.1	-	-1337	HUA and HUA-LIKE (HULK) genes act redundantly to regulate a subset of essential genes, with some (or all) family members also having specific functions.	HUA2 LIKE 2 (HULK2); (SL3)
AT2G47570.1	-	2121	60S ribosomal protein L18;(source:Araport11)	
AT2G47550.1	+	1792	Plant invertase/pectin methylesterase inhibitor superfamily;(source:Araport11)	
AT2G47220.1	+	3041	Member of the plant-specific DUF724 protein family. Arabidopsis has 10 DUF724 proteins. Loss of function mutant has a WT phenotype	DOMAIN OF UNKNOWN FUNCTION 724 5 (ATDUF5);DOMAIN OF
AT2G46630.1	+	226	serine/arginine repetitive matrix protein;(source:Araport11)	
AT2G46500.1	-	12	Phosphoinositide kinase which undergo autophosphorylation and phosphorylate serine/threonine residues of protein substrates. Contains phosphoinositide 3/4-kinase and ubiquitin-like domains. Phosphorylates PUFD1 and RPN10 in vitro.	UBIQUITIN-LIKE DOMAIN KINASE GAMMA 4 (UBDK GAMMA 4);PHOSPHOINOSITIDE 4-KINASE GAMMA 4 (PI4K GAMMA
AT2G46260.1	+	2998	Involvement in protein ubiquitylation is predicted based on physical interaction with CULLIN 3 proteins.	LIGHT-RESPONSE BTB 1 (LRB1)
AT2G46225.2	+	-488	Encodes a subunit of the WAVE complex. The WAVE complex is required for activation of ARP2/3 complex which functions in actin microfilament nucleation and branching. One of four ABI-like proteins.	ABI-1-LIKE 1 (ABIL1)
AT2G46170.1	+	-215	Reticulon family protein;(source:Araport11)	RETICULON-LIKE B 5 (RTNLB5)
AT2G45970.1	-	1471	Encodes a member of the CYP86A subfamily of cytochrome p450 genes. Expressed at moderate levels in flowers, leaves, roots and stems.	CYTOCHROME P450, FAMILY 86, SUBFAMILY A, POLYPEPTIDE 8
AT2G45920.1	+	-80	U-box domain-containing protein;(source:Araport11)	
AT2G45910.1	+	-125	U-box domain-containing protein kinase family protein;(source:Araport11)	
AT2G45820.1	-	-154	Lipid raft regulatory protein, crucial for plasma membrane nanodomain assembly to control plasmodesmata aperture and functionality.	REMORIN 1.3 (Rem1.3)
AT2G45740.1	+	-200	member of the peroxin11 (PEX11) gene family, integral to peroxisome membrane, controls peroxisome proliferation. The mRNA is cell-to-cell mobile.	PEROXIN 11D (PEX11D)
AT2G45590.1	+	-251	Protein kinase superfamily protein;(source:Araport11)	
AT2G44790.1	-	1190	Encodes a uclacyanin, a protein precursor that is closely related to precursors of stellacyanins and a blue copper protein from pea pods.	UCLACYANIN 2 (UCC2)
AT2G44660.1	-	-652	ALG6, ALG8 glycosyltransferase family;(source:Araport11)	
AT2G44500.1	+	-2555	O-fucosyltransferase family protein;(source:Araport11)	
AT2G43540.1	+	182	transmembrane protein;(source:Araport11)	
AT2G43400.1	+	14	Encodes a unique electron-transfer flavoprotein:ubiquinone oxidoreductase that is localized to the mitochondrion. Mutants are more sensitive to sugar starvation when plants are kept in the dark for long periods.	ELECTRON-TRANSFER FLAVOPROTEIN:UBIQUINONE
AT2G43060.1	+	-2268	ILI1 binding bHLH 1;(source:Araport11)	(ATIBH1);ILI1 BINDING BHLH 1 (IBH1)
AT2G42900.1	+	765	Plant basic secretory protein (BSP) family protein;(source:Araport11)	
AT2G42750.1	+	-105	DNAJ heat shock N-terminal domain-containing protein;(source:Araport11)	DNA J PROTEIN C77 (DJC77)
AT2G42620.1	+	193	The mutations at MAX2 cause increased hypocotyl and petiole elongation in light-grown seedlings. Positional cloning identifies MAX2 as a member of the F-box leucine-rich repeat family of proteins. MAX2 is identical to ORE9, a proposed regulator of leaf senescence. Involved in positive regulation of light responses. The mRNA is cell-to-cell mobile.	(ATMAX2);MORE AXILLARY BRANCHES 2 (MAX2);ORESARA 9 (ORE9);PLEIOTROPIC PHOTOSIGNALING (PPS)
AT2G41900.1	+	-289	AtOXS2 specifcally entered the nuclear under salt stress. Te specifc nuclear localization of AtOXS2 could play a role in salt tolerance at the molecular level. Tese results implied that AtOXS2 might target some downstream cis-elements which are required for salt stress responses	(DEG9);OXIDATIVE STRESS 2 (OXS2);TANDEM ZINC FINGER PROTEIN 7 (TZF7)
AT2G40490.1	+	-125	Uroporphyrinogen decarboxylase;(source:Araport11)	(HEME2)
AT2G40400.1	+	45	Encodes a chloroplast localized protein of unknown function that is involved in regulation of chloroplast development.	RETICULATA-RELATED 5 (RER5);BRZ-INSENSITIVE-PALE GREEN 3
AT2G40330.1	-	424	Encodes a member of the PYR (pyrabactin resistance)/PYL(PYR1-like)/RCAR (regulatory components of ABA receptor) family proteins with 14 members. PYR/PYL/RCAR family proteins function as abscisic acid sensors. Mediate ABA-dependent regulation of protein phosphatase 2Cs ABI1 and ABI2.	PYR1-LIKE 6 (PYL6);REGULATORY COMPONENTS OF ABA RECEPTOR 9 (RCAR9)
AT2G39950.1	-	-189	flocculation protein;(source:Araport11)	
AT2G39865.1	-	-581	transmembrane protein;(source:Araport11)	
AT2G39570.1	+	-348	Encodes a ACT domain-containing protein. The ACT domain, named after bacterial aspartate kinase, chorismate mutase and TyrA (prephenate dehydrogenase), is a regulatory domain that serves as an amino acid-binding site in feedback-regulated amino acid metabolic enzymes.	ACT DOMAIN REPEATS 9 (ACR9)

AT2G39460.1	+	-133	Encodes a 60S ribosomal protein L23aA (AtrpL23aA). Paralog of RLPL23aB.	RIBOSOMAL PROTEIN L23A1 (RPL23A1);ARABIDOPSIS THALIANA
AT2G38820.2	+	-304	DNA-directed RNA polymerase subunit beta-beta protein, putative (DUF506);(source:Araport11)	
AT2G38310.1	+	627	Encodes a member of the PYR (pyrabactin resistance)/PYL(PYR1-like)/RCAR (regulatory components of ABA receptor) family proteins with 14 members. PYR/PYL/RCAR family proteins function as abscisic acid sensors. Mediate ABA-dependent regulation of protein phosphatase 2Cs ABI1 and ABI2. The mRNA is cell-to-cell mobile.	(ATPYL4);PYR1-LIKE 4 (PYL4);REGULATORY COMPONENTS OF ABA RECEPTOR 10 (RCAR10)
AT2G38060.1	-	-166	Encodes an inorganic phosphate transporter (PHT4;2).	PHOSPHATE TRANSPORTER 4;2 (PHT4;2)
AT2G37180.1	+	-1369	a member of the plasma membrane intrinsic protein PIP2. functions as aquaporin and is involved in desiccation.	PLASMA MEMBRANE INTRINSIC PROTEIN 2C (PIP2C);RESPONSIVE
AT2G36950.1	+	1629	Heavy metal transport/detoxification superfamily protein;(source:Araport11)	
AT2G36680.1	-	2082	Modifier of rudimentary (Mod(r)) protein;(source:Araport11)	
AT2G36220.1	+	1077	hypothetical protein;(source:Araport11)	
AT2G35910.1	-	657	RING/U-box superfamily protein;(source:Araport11)	ARABIDOPSIS T??XICOS EN LEVADURA 70 (ATL70)
AT2G35880.1	-	-463	TPX2 (targeting protein for Xklp2) protein family;(source:Araport11)	
AT2G35000.1	-	1092	ATL9 is an E3 ligase-like protein that is induced by chitin oligomers and contributes to fungal resistance.It differs from other members of the ATL family in that it has a PEST domain. It is a short lived protein that is subject to proteosome mediated degradation. It is expressed in many aerial tissues in a pattern that varies with developmental stage.	ARABIDOPSIS TOXICOS EN LEVADURA 9 (ATL9); (ATL2G)
AT2G34180.1	-	-466	Encodes CBL-interacting protein kinase 13 (CIPK13).	WPL4-LIKE 2 (ATWL2);CBL-INTERACTING PROTEIN KINASE 13
AT2G33830.2	-	-532	Dormancy/auxin associated family protein;(source:Araport11)	(ATDRM2);DORMANCY ASSOCIATED GENE 2 (DRM2)
AT2G32320.2	+	-88	Interacts genetically with its homolog ICA1; alters growth and flowering time plasticity in relation to temperature. Mutants display effects on growth, flowering and plant development, and ploidy level depending on ambient temperature (effects specific at >27C).	ICARUS2 (ICA2)
AT2G32270.1	+	-1548	A member of Zrt- and Irt-related protein (ZIP) family. transcript is induced in response to zinc deficiency in the root. also response to iron deficiency.	ZINC TRANSPORTER 3 PRECURSOR (ZIP3)
AT2G32150.1	+	-44	Haloacid dehalogenase-like hydrolase (HAD) superfamily protein;(source:Araport11)	
AT2G31810.1	+	-164	ACT domain-containing small subunit of acetolactate synthase protein;(source:Araport11)	ALS-INTERACTING PROTEIN1 (AIP1);ACETOLACTATE SYNTHASE
AT2G30600.5	+	19	BTB/POZ domain-containing protein;(source:Araport11)	
AT2G30200.1	-	96	Malonyl-ACP expressed in developing seeds. Loss of function mutants are embryo lethal and over expression in seeds leads to increased seed oil content.	MALONYL COA-ACP MALONYLTRANSFERASE (MCAMT);EMBRYO
AT2G29760.1	+	4	Encodes a chloroplast RNA editing factor.	(QED1);ORGANELLE TRANSCRIPT PROCESSING 81 (OTP81)
AT2G29530.3	-	-62	Encodes a small zinc finger-like protein that is a component of the mitochondrial protein import apparatus. Together with AtTIM9, AtTIM10 is non-redundantly essential for maintaining mitochondrial function of early embryo proper cells and endosperm free-nuclei.	(ATTIM10);TRANSLOCASE OF THE INNER MEMBRANE 10 (TIM10)
AT2G28920.1	+	237	RING/U-box superfamily protein;(source:Araport11)	ARABIDOPSIS T??XICOS EN LEVADURA 84 (ATL84)
AT2G27330.1	-	0	RNA-binding (RRM/RBD/RNP motifs) family protein;(source:Araport11)	
AT2G27090.1	-	176	bZIP transcription factor (DUF630 and DUF632);(source:Araport11)	
AT2G24540.1	+	547	Galactose oxidase/kelch repeat superfamily protein;(source:Araport11)	ATTENUATED FAR-RED RESPONSE (AFR)
AT2G23790.1	-	-226	calcium uniporter (DUF607);(source:Araport11)	
AT2G22790.1	+	736	hypothetical protein;(source:Araport11)	
AT2G22680.1	+	2073	Zinc finger (C3HC4-type RING finger) family protein;(source:Araport11)	WAV3 HOMOLOG 1 (WAVH1)
AT2G22500.1	-	768	Encodes one of the mitochondrial dicarboxylate carriers (DIC): DIC1 (AT2G22500), DIC2 (AT4G24570), DIC3 (AT5G09470).	DICARBOXYLATE CARRIER 1 (DIC1);UNCOUPLING PROTEIN 5
AT2G22450.1	+	-6	riboflavin biosynthesis protein;(source:Araport11)	HOMOLOG OF RIBA 2 (RIBA2); (ATRIBA2)
AT2G22080.1	+	-90	transmembrane protein;(source:Araport11)	
AT2G22010.2	-	-235	Encodes a protein predicted to act as a RING E3 ubiquitin ligase. It appears to regulate the stability of the KRP1/ICK1 cyclin dependent kinase inhibitor. Induced by beet severe curly virus (BSCTV) C4 protein.	RELATED TO KPC1 (RKP)
AT2G21960.1	+	-97	transmembrane protein;(source:Araport11)	
AT2G21060.1	-	-102	Glycine-rich protein (AtGRP2b). Also named as CSP4 (cold shock domain protein 4) containing a well conserved cold shock domain (CSD) and glycine-rich motifs interspersed by two retroviral-like CCHC zinc fingers. AtCSP4 is expressed in all tissues but accumulates in reproductive tissues and those undergoing cell divisions. Overexpression of AtCSP4 reduces silique length and induces embryo lethality.	GLYCINE-RICH PROTEIN 2B (GRP2B);COLD SHOCK DOMAIN PROTEIN 4 (ATCSP4);GLYCINE-RICH PROTEIN 2B (ATGRP2B)
AT2G20260.1	+	-68	Encodes subunit E of photosystem I. The mRNA is cell-to-cell mobile.	PHOTOSYSTEM I SUBUNIT E-2 (PSAE-2)
AT2G19802.1	-	-4754	transmembrane protein;(source:Araport11)	
AT2G19800.1	-	-844	Encodes a myo-inositol oxygenase family gene.	MYO-INOSITOL OXYGENASE 2 (MIOX2)
AT2G17990.1	+	2037	Calcium-dependent protein kinase 1 adaptor protein involved in vacuolar transport and lytic vacuole biogenesis.	CALCIUM-DEPENDENT PROTEIN KINASE 1 ADAPTOR PROTEIN 2
AT2G17870.1	-	61	Encodes COLD SHOCK DOMAIN PROTEIN 3 (CSP3), involved in the acquisition of freezing tolerance.	ARABIDOPSIS COLD SHOCK DOMAIN PROTEIN 3 (ATCSP3);COLD
AT2G16640.1	-	-118	multimeric translocon complex in the outer envelope membrane 132;(source:Araport11)	ARSENATE INDUCED CHLOROSIS 1 (AIC1);MULTIMERIC
AT2G16586.1	+	199	transmembrane protein;(source:Araport11)	
AT2G12905.1	+	125	hypothetical protein;(source:Araport11)	
AT2G08986.1	+	62	hypothetical protein;(source:Araport11)	
AT2G07981.1	+	2777	hypothetical protein;(source:Araport11)	
AT2G07768.1	+	1208	Cytochrome C assembly protein;(source:Araport11)	
AT2G07727.1	+	-220	cytochrome b;(source:Araport11)	
AT2G07725.1	+	-25	Ribosomal L5P family protein;(source:Araport11)	
AT2G07722.1	+	-776	transmembrane protein;(source:Araport11)	
AT2G07721.1	-	-1411	hypothetical protein;(source:Araport11)	
AT2G07713.1	+	-1668	hypothetical protein;(source:Araport11)	
AT2G07706.1	-	3600	hypothetical protein;(source:Araport11)	
AT2G05160.1	-	-380	CCCH-type zinc fingerfamily protein with RNA-binding domain-containing protein;(source:Araport11)	
AT2G03750.1	-	1680	P-loop containing nucleoside triphosphate hydrolases superfamily protein;(source:Araport11)	
AT2G02800.1	-	-250	Encodes protein kinase APK2b.	PBS1-LIKE 3 (PBL3);PROTEIN KINASE 2B (APK2B);KINASE 2 (KIN2)
AT2G02710.1	-	-1040	Encodes a putative blue light receptor protein.	PAS/LOV PROTEIN (PLP);PAS/LOV PROTEIN B (PLPB)
AT2G02640.1	+	-1818	Cysteine/Histidine-rich C1 domain family protein;(source:Araport11)	
AT2G02180.1	+	-202	Necessary for the efficient multiplication of tobamoviruses. The mRNA is cell-to-cell mobile.	TOBAMOVIRUS MULTIPLICATION PROTEIN 3 (TOM3)
AT2G01023.1	-	658	hypothetical protein;(source:Araport11)	
AT2G01021.1	+	737	hypothetical protein;(source:Araport11)	
AT2G01008.1	+	348	maternal effect embryo arrest protein;(source:Araport11)	
AT1G80820.1	+	1343	Encodes an cinnamoyl CoA reductase isoform. Involved in lignin biosynthesis.	CINNAMOYL COA REDUCTASE (CCR2); (ATCCR2)
AT1G80555.1	+	80	Isocitrate/isopropylmalate dehydrogenase family protein;(source:Araport11)	
AT1G80440.1	+	706	Encodes a member of a family of F-box proteins, called the KISS ME DEADLY (KMD) family, that targets type-B ARR proteins for degradation and is involved in the negative regulation of the cytokinin response. Also named as KFB20, a member of a group of Kelch repeat F-box proteins that negatively regulate phenylpropanoid biosynthesis by targeting the phenypropanoid biosynthesis enzyme phenylalanine ammonia-lyase. The mRNA is cell-to-cell mobile.	KISS ME DEADLY 1 (KMD1);KELCH REPEAT F-BOX 20 (KFB20)
AT1G80380.2	+	55	encodes a glycerate kinase which catalyzes the last step of photorespiration C2 cycle.	GLYCERATE KINASE (GLYK)
AT1G79540.1	-	2982	Pentatricopeptide repeat (PPR) superfamily protein;(source:Araport11)	
AT1G78995.1	-	-101	hypothetical protein;(source:Araport11)	
AT1G78860.1	-	2055	curculin-like (mannose-binding) lectin family protein, low similarity to Ser/Thr protein kinase (Zea mays) GI:2598067; contains Pfam profile PF01453: Lectin (probable mannose binding) but not the protein kinase domain of the Z. mays protein	LOW-BORON TOLERANCE (LBT);APPLE DOMAIN LECTIN-2 (GAL2)
AT1G78580.1	-	5927	Encodes an enzyme putatively involved in trehalose biosynthesis. The protein has a trehalose synthase (TPS)-like domain but no trehalose phosphatase (TPP)-like domain. ATTPS1 is able to complement yeast tps1 mutants in vivo. The gene product modulates cell growth but not cell differentiation by determining cell wall deposition and cell division.	TREHALOSE-6-PHOSPHATE SYNTHASE (TPS1);TREHALOSE-6-PHOSPHATE SYNTHASE (ATTPS1);TREHALOSE-6-PHOSPHATE

AT1G77280.1	-	298	kinase with adenine nucleotide alpha hydrolases-like domain-containing protein;(source:Araport11)	
AT1G76600.1	+	-125	poly polymerase;(source:Araport11)	
AT1G75810.1	+	-27	transmembrane protein;(source:Araport11)	
AT1G75800.1	+	1703	Pathogenesis-related thaumatin superfamily protein;(source:Araport11)	
AT1G75730.1	-	-90	hypothetical protein;(source:Araport11)	
AT1G75450.1	-	2755	This gene used to be called AtCKX6. It encodes a protein whose sequence is similar to cytokinin oxidase/dehydrogenase, which catalyzes the degradation of cytokinins.	CYTOKININ OXIDASE 6 (ATCKX6);CYTOKININ OXIDASE 5
AT1G75000.1	+	818	ELO family protein.	ELO HOMOLOG 3 (ELO3)
AT1G74840.1	-	-164	Homeodomain-like superfamily protein;(source:Araport11)	
AT1G74780.1	+	-393	Nodulin-like / Major Facilitator Superfamily protein;(source:Araport11)	
AT1G73880.1	+	1307	UDP-glucosyl transferase 89B1;(source:Araport11)	UDP-GLUCOSYL TRANSFERASE 89B1 (UGT89B1)
AT1G73020.1	-	-77	anoctamin-like protein;(source:Araport11)	TRANS MEMBRANE PROTEIN 16 (TMEM16)
AT1G72820.1	+	-552	Mitochondrial substrate carrier family protein;(source:Araport11)	
AT1G71980.1	+	12	RMR2 is a secretory pathway protein localized to the trans-golgi network. It belongs to a family of vacuolar sorting receptors. If forms heterodimers with RMR1.	(RMR2)
AT1G70370.1	-	2054	polygalacturonase 2;(source:Araport11)	POLYGALACTURONASE 2 (PG2)
AT1G69910.1	+	1919	Protein kinase superfamily protein;(source:Araport11)	
AT1G69890.1	-	-191	actin cross-linking protein (DUF569);(source:Araport11)	
AT1G69410.1	+	-16	Encodes eIF5A-2, a putative eukaryotic translation initiation factor. There are three eIF5A coding genes in Arabidopsis: eIF5A-1/At1g13950, eIF5A-2/At1g26630 and eIF5A-3/At1g69410.	EUKARYOTIC ELONGATION FACTOR 5A-3 (ELF5A-3);EUKARYOTIC
AT1G69030.1	-	-2582	BSD domain-containing protein;(source:Araport11)	
AT1G68440.1	+	-92	Transmembrane protein;(source:Araport11). Expression induced by abiotic stressors such as ABA, drought, heat, light, NaCl, osmotic stress and wounding.	
AT1G68300.1	-	50	Adenine nucleotide alpha hydrolases-like superfamily protein;(source:Araport11)	
AT1G68050.1	+	-359	Encodes FKF1, a flavin-binding kelch repeat F box protein, is clock-controlled, regulates transition to flowering. Forms a complex with GI on the CO promoter to regulate CO expression.	(ADO3);FLAVIN-BINDING, KELCH REPEAT, F BOX 1 (FKF1)
AT1G67810.1	+	752	Encodes a protein capable of stimulating the cysteine desulfurase activity of CpNifS (AT1G08490) in vitro. SufE2:GFP localizes to the chloroplasts where it is likely to play a role in iron-sulfur cluster assembly. Transcript levels for this gene are high in the pollen relative to other organs based on RT-PCR analysis. The mRNA is cell-to-cell mobile.	SULFUR E2 (SUFE2)
AT1G66350.1	+	332	Negative regulator of GA responses, member of GRAS family of transcription factors. Also belongs to the DELLA proteins that restrain the cell proliferation and expansion that drives plant growth. RGL1 may be involved in reducing ROS accumulation in response to stress by up-regulating the transcription of superoxide dismutases. Rapidly degraded in response to GA. Involved in flower and fruit development.	RGA-LIKE 1 (RGL1); (RGL)
AT1G66160.1	+	672	CYS, MET, PRO, and GLY protein 1;(source:Araport11)	CYS, MET, PRO, AND GLY PROTEIN 1 (CMPG1); (ATCMPG1)
AT1G66130.1	+	561	NAD(P)-binding Rossmann-fold superfamily protein;(source:Araport11)	
AT1G64380.1	-	-3743	encodes a member of the DREB subfamily A-6 of ERF/AP2 transcription factor family. The protein contains one AP2 domain. There are 8 members in this subfamily including RAP2.4.	
AT1G63420.1	+	881	O-glucosyltransferase-like protein (DUF821);(source:Araport11)	
AT1G62480.1	+	-2220	Vacuolar calcium-binding protein-like protein;(source:Araport11)	
AT1G62360.1	-	96	Class I knotted-like homeodomain protein that is required for shoot apical meristem (SAM) formation during embryogenesis and for SAM function throughout the lifetime of the plant. Functions by preventing incorporation of cells in the meristem center into differentiating organ primordia. It has also been shown to have a role in the specification of flower meristem identity.	WALDMEISTER (WAM);BUMBERSHOOT (BUM);WALDMEISTER 1 (WAM1);SHOOTLESS (SHL);BUMBERSHOOT 1 (BUM1);SHOOT
AT1G61340.2	+	-292	Encodes a F-box protein induced by various biotic or abiotic stress.	(ATFBS1);F-BOX STRESS INDUCED 1 (FBS1)
AT1G61215.1	+	3356	Bromodomain protein with a DNA binding motif	BROMODOMAIN 4 (BRD4)
AT1G58180.2	-	-85	beta carbonic anhydrase 6;(source:Araport11)	BETA CARBONIC ANHYDRASE 6 (BCA6);A. THALIANA BETA
AT1G57680.1	-	-56	plasminogen activator inhibitor;(source:Araport11)	CANDIDATE G-PROTEIN COUPLED RECEPTOR 1 (CAND1)
AT1G56340.1	-	-114	Encodes one of three Arabidopsis calreticulins. In CRT-deficient mouse fibroblasts, this protein restores ER Ca2+ levels. Post-transcriptionally regulates together with CRT2 VAMP721/722 levels under ER stress.	CALRETICULIN 1 (CRT1); (AtCRT1a);CALRETICULIN 1A (CRT1a)
AT1G56220.3	+	-276	Dormancy/auxin associated family protein;(source:Araport11)	
AT1G55810.1	+	-172	One of the homologous genes predicted to encode proteins with UPRT domains (Uracil phosphoribosyltransferase). Five of these genes (At5g40870, At3g27190, At1g55810, At4g26510 and At3g27440) show a high level of identity, and are annotated as also containing a N-terminal uracil kinase (UK) domain. These genes are referred to as UKL1 (UK-like 1), UKL2, UKL3, UKL4 and UKL5, respectively.	URIDINE/CYTIDINE KINASE 3 (UCK3);URIDINE KINASE-LIKE 3 (UKL3)
AT1G54130.1	+	-792	This gene appears to be at least partially redundant with RSH2 (At3g14050). Guanosine tetraphosphate synthesized by RSH2/RSH3 (and CRSH At3g17470) to an unknown extent can repress chloroplast gene expression, and also reduce chloroplast size.	RELA/SPOT HOMOLOG 3 (ATRSH3);RELA/SPOT HOMOLOG 3 (RSH3); (AT-RSH3)
AT1G53830.1	+	2530	encodes a pectin methylesterase	PECTIN METHYLESTERASE 2 (ATPME2);PECTIN METHYLESTERASE
AT1G53430.1	+	1186	Leucine-rich repeat transmembrane protein kinase;(source:Araport11)	NEMATODE-INDUCED LRR-RLK 2 (NILR2)
AT1G52600.1	+	-8	Peptidase S24/S26A/S26B/S26C family protein;(source:Araport11)	
AT1G52590.1	-	-32	Putative thiol-disulfide oxidoreductase DCC;(source:Araport11)	
AT1G52330.2	+	165	Late embryogenesis abundant (LEA) hydroxyproline-rich glycoprotein family;(source:Araport11)	
AT1G51680.1	-	220	encodes an isoform of 4-coumarate:CoA ligase (4CL), which is involved in the last step of the general phenylpropanoid pathway. In addition to 4-coumarate, it also converts ferulate. The catalytic efficiency was in the following (descending) order: p-coumaric acid, ferulic acid, caffeic acid and 5-OH-ferulic acid. At4CL1 was unable to use sinapic acid as substrate.	ARABIDOPSIS THALIANA 4-COUMARATE:COA LIGASE 1 (AT4CL1);4-COUMARATE:COA LIGASE 1 (4CL1);4-
AT1G48830.1	-	-11	Ribosomal protein S7e family protein;(source:Araport11)	
AT1G48410.2	-	-37	Encodes an RNA Slicer that selectively recruits microRNAs and siRNAs. There is currently no evidence that AGO1 Slicer is in a high molecular weight RNA-induced silencing complex (RISC). Mutants are defective in post-transcriptional gene silencing and have pleiotropic developmental and morphological defects. Through its action on the regulation of ARF17 expression, the protein regulates genes involved at the cross talk between auxin and light signaling during adventitious root development. AGO1 seems to be targeted for degradation by silencing suppressor F-box-containing proteins from Turnip yellow virus and Cucurbit aphid-borne yellow virus.	(ATAGO1);ARGONAUTE 1 (AGO1); (ICU9)
AT1G43670.1	+	-31	Encodes a fructose-1,6-bisphosphatase. This enzyme, in addition to catalyzing the formation of fructose-6-phosphate for sucrose biosynthesis, appears to play a role in fructose-mediated signaling that is independent of its enzymatic activity. atcfbp-1/fins1 mutants have reduced photosynthetic rates, elevated levels of starch and reduced levels of sucrose during the day. Although the protein is expected to be cytosolic, a GFP-tagged version localizes to the cytoplasm and the nucleus. The mRNA is cell-to-cell mobile.	(CYFBP);FRUCTOSE INSENSITIVE 1 (FINS1);ARABIDOPSIS THALIANA CYTOSOLIC FRUCTOSE-1,6-BISPHOSPHATASE (AtcFBP);FRUCTOSE-1,6-BISPHOSPHATASE (FBP)
AT1G40104.1	+	186	hypothetical protein;(source:Araport11)	
AT1G35670.1	+	-1738	Encodes a Ca(2+)-dependent, calmodulin-independent protein kinase that is rapidly induced by drought and high-salt stress but not by low-temperature stress or heat stress. Positive regulator of ABA signaling. Phosphorylates ABA responsive transcription factors ABF1 and ABF4.	CALCIUM-DEPENDENT PROTEIN KINASE 2 (CDPK2);CALCIUM-DEPENDENT PROTEIN KINASE 2 (ATCDPK2); (CPK11); (ATCPK11)
AT1G32460.1	+	18	hypothetical protein;(source:Araport11)	
AT1G31480.1	+	-127	encodes a novel protein that may be part of a gene family represented by bovine phosphatidic acid-preferring phospholipase A1 (PA-PLA1)containing a putative transmembrane domain. SGR2 is involved in the formation and function of the vacuole.	SHOOT GRAVITROPISM 2 (SGR2)
AT1G30840.1	+	1400	Member of a family of proteins related to PUP1, a purine transporter. May be involved in the transport of purine and purine derivatives such as cytokinins, across the plasma membrane.	PURINE PERMEASE 4 (PUP4);PURINE PERMEASE 4 (ATPUP4)
AT1G30825.1	+	-1910	Involved in trichome maturation. mutant displays enlarged trichomes	DISTORTED TRICHOMES 2 (DIS2);ACTIN-RELATED PROTEIN C2A
AT1G30640.1	+	-129	Protein kinase family protein;(source:Araport11)	
AT1G30500.2	-	-296	nuclear factor Y, subunit A7;(source:Araport11)	NUCLEAR FACTOR Y, SUBUNIT A7 (NF-YA7)
AT1G29390.1	-	-21	Integral membrane protein in the inner envelope of chloroplasts. Provide freezing tolerance.	COLD REGULATED 314 INNER MEMBRANE 2 (COR413IM2);COLD
AT1G29330.1	-	31	Encodes a protein similar in sequence to animal and yeast endoplasmic reticulum retention signal receptor. This protein can functionally complement the yeast homologue. Transcript is detected in flower buds, stems, root, and leaves.	ENDOPLASMIC RETICULUM RETENTION DEFECTIVE 2 (ERD2);ARABIDOPSIS ENDOPLASMIC RETICULUM RETENTION
AT1G28760.1	+	-295	Encodes an orthlog of the Xenopus inner nuclear membrane (INM) protein Nemp1/TMEM194A.	INNER NUCLEAR MEMBRANE PROTEIN A (NEMP_A)
AT1G28680.1	+	67	Catalyses trans-cis isomerization and lactonization in the biosynthesis of coumarins in roots.	COUMARIN SYNTHASE (COSY)
AT1G28330.5	-	-408	dormancy-associated protein (DRM1)	(ATDRM1);DORMANCY-ASSOCIATED PROTEIN-LIKE 1
AT1G27100.1	-	3509	Actin cross-linking protein;(source:Araport11)	
AT1G26800.1	-	-136	MPSR1 is cytoplasmic E3 ligase that senses misfolded proteins independently of chaperones and targets those proteins for degradation via the 26S proteasome.	MISFOLDED PROTEIN SENSING RING E3 LIGASE 1 (MPSR1)
AT1G25550.1	+	-215	myb-like transcription factor family protein;(source:Araport11)	HRS1 HOMOLOG3 (HHO3);NITRATE-INDUCIBLE, GARP-TYPE
AT1G25400.1	-	80	transmembrane protein;(source:Araport11)	

AT1G23870.1	+	-1243	Encodes an enzyme putatively involved in trehalose biosynthesis. The protein has a trehalose synthase (TPS)-like domain that may or may not be active as well as a trehalose phosphatase (TPP)-like domain. The mRNA is cell-to-cell mobile.	TREHALOSE-PHOSPHATASE/SYNTHASE 9 (ATTPS9);TREHALOSE-PHOSPHATASE/SYNTHASE 9 (TPS9);TREHALOSE -6-PHOSPHATASE
AT1G23710.1	+	-459	hypothetical protein (DUF1645);(source:Araport11)	
AT1G23040.1	+	-88	hydroxyproline-rich glycoprotein family protein;(source:Araport11)	
AT1G22400.1	-	-1769	UDP-Glycosyltransferase superfamily protein;(source:Araport11)	ARABIDOPSIS THALIANA UDP-GLUCOSYL TRANSFERASE 85A1
AT1G21680.1	+	-105	DPP6 N-terminal domain-like protein;(source:Araport11)	
AT1G21000.1	+	-1318	PLATZ transcription factor family protein;(source:Araport11)	
AT1G20890.1	-	-139	caveolin-1 protein;(source:Araport11)	
AT1G20030.2	+	815	Pathogenesis-related thaumatin superfamily protein;(source:Araport11)	
AT1G19960.1	+	-466	Unknown gene, expression decreased in response to Mn and increased by cytokinin.	
AT1G19660.1	-	-40	Wound-responsive family protein;(source:Araport11)	(ATBBD2);BIFUNCTIONAL NUCLEASE IN BASAL DEFENSE
AT1G19520.1	+	3237	Ribosomal pentatricopeptide repeat protein	NUCLEAR FUSION DEFECTIVE 5 (NFD5);RIBOSOMAL
AT1G19220.1	-	-200	Encodes an auxin response factor that contains the conserved VP1-B3 DNA-binding domain at its N-terminus and the Aux/IAA-like domains III and IV present in most ARFs at its C-terminus. The protein interacts with IAA1 (yeast two hybrid) and other auxin response elements such as ER7 and ER9 (yeast one hybrid). ARF19 protein can complement many aspects of the arf7 mutant phenotype and , together with ARF7, is involved in the response to ethylene. In the arf7 arf19 double mutant, several auxin-responsive genes (e.g. IAA5, LBD16, LBD29 and LBD33) are no longer upregulated by auxin.	INDOLE-3-ACETIC ACID INDUCIBLE 22 (IAA22);AUXIN RESPONSE FACTOR11 (ARF11);AUXIN RESPONSE FACTOR 19 (ARF19)
AT1G19000.1	-	102	Homeodomain-like superfamily protein;(source:Araport11)	
AT1G18460.1	+	-141	Alpha/beta hydrolase	(ALPHA/BETA-HYDROLASE)
AT1G18330.2	-	-55	EARLY-PHYTOCHROME-RESPONSIVE1	REVEILLE 7 (RVE7);EARLY-PHYTOCHROME-RESPONSIVE1 (EPR1)
AT1G18280.1	+	406	Bifunctional inhibitor/lipid-transfer protein/seed storage 2S albumin superfamily protein;(source:Araport11)	GLYCOSYLPHOSPHATIDYLINOSITOL-ANCHORED LIPID PROTEIN
AT1G18270.3	-	130	ketose-bisphosphate aldolase class-II family protein;(source:Araport11)	
AT1G16730.1	-	-143	hypothetical protein;(source:Araport11)	UNKNOWN PROTEIN 6 (UP6)
AT1G15670.1	+	989	Encodes a member of a family of F-box proteins, called the KISS ME DEADLY (KMD) family, that targets type-B ARR proteins for degradation and is involved in the negative regulation of the cytokinin response. Also named as KFB1, a member of a group of Kelch repeat F-box proteins that negatively regulate phenylpropanoid biosynthesis by targeting the phenypropanoid biosynthesis enzyme phenylalanine ammonia-lyase.	KELCH REPEAT F-BOX 1 (KFB01);KISS ME DEADLY 2 (KMD2)
AT1G15380.1	+	-510	Glyoxalase which affects ABA?JA crosstalk.	GLYOXYLASE I 4 (GLYI4)
AT1G15040.1	+	-132	Encodes a nitrogen regulated putative glutamine amidotransferase that represses shoot branching.	GLUTAMINE AMIDOTRANSFERASE 1_2.1 (GAT1_2.1);GLUTAMINE
AT1G14900.1	-	-47	Encodes a protein belonging to the subgroup of HMGA (high mobility group A) proteins that interact with A/T-rich stretches of DNA.	HIGH MOBILITY GROUP A (HMGA)
AT1G14860.1	-	-45	nudix hydrolase homolog 18;(source:Araport11)	NUDIX HYDROLASE HOMOLOG 18 (NUDT18);NUDIX HYDROLASE
AT1G13260.1	+	958	Encodes an AP2/B3 domain transcription factor which is upregulated in response to low temperature. It contains a B3 DNA binding domain. It has circadian regulation and may function as a negative growth regulator. The mRNA is cell-to-cell mobile.	(ATRAV1);ETHYLENE RESPONSE DNA BINDING FACTOR 4 (EDF4);RELATED TO ABI3/VP1 1 (RAV1)
AT1G13250.1	-	-3031	Encodes a protein with putative galacturonosyltransferase activity.	GALACTURONOSYLTRANSFERASE-LIKE 3 (GATL3)
AT1G12500.1	-	452	Nucleotide-sugar transporter family protein;(source:Araport11)	
AT1G11970.1	+	10	Ubiquitin-like superfamily protein;(source:Araport11)	
AT1G11380.1	+	-276	PLAC8 family protein;(source:Araport11)	
AT1G10070.1	+	-420	Encodes a chloroplast branched-chain amino acid aminotransferase. Complements the yeast leu/iso-leu/val auxotrophy mutant. Involved in cell wall development.	BRANCHED-CHAIN AMINO ACID TRANSFERASE 2
AT1G10060.2	+	2976	encodes a mitochondrial branched-chain amino acid aminotransferase. Complements the yeast leu/iso-leu/val auxotrophy mutant.	BRANCHED-CHAIN AMINO ACID TRANSFERASE 1
AT1G08990.1	+	395	plant glycogenin-like starch initiation protein 5;(source:Araport11)	PLANT GLYCOGENIN-LIKE STARCH INITIATION PROTEIN 5
AT1G08630.1	-	31	Encodes a threonine aldolase, involved in threonine degradation to glycine. Primarily expressed in seeds and seedlings.	THREONINE ALDOLASE 1 (THA1)
AT1G07870.2	-	-263	Protein kinase superfamily protein;(source:Araport11)	
AT1G07670.1	-	-317	TPLATE complex protein involved in clathrin-mediated endocytosis.	ENDOMEMBRANE-TYPE CA-ATPASE 4 (ECA4); (ATECA4)
AT1G07150.1	-	1179	member of MEKK subfamily	MITOGEN-ACTIVATED PROTEIN KINASE KINASE KINASE 13
AT1G07040.1	-	2351	plant/protein;(source:Araport11)	
AT1G07030.1	-	26	Mitochondrial substrate carrier family protein;(source:Araport11)	MITOCHONDRIAL IRON TRANSPORTER 2 (MIT2)
AT1G06570.1	-	-178	Mutation of the PDS1 locus disrupts the activity of p-hydroxyphenylpyruvate dioxygenase (HPPDase), the first committed step in the synthesis of both plastoquinone and tocopherols in plants.	4-HYDROXYPHENYLPYRUVATE DIOXYGENASE (HPPD);4-
AT1G05370.1	-	2712	Sec14p-like phosphatidylinositol transfer family protein;(source:Araport11)	
AT1G05000.2	+	-1452	Encodes an atypical dual-speciﬁcity phosphatase.	PLANT AND FUNGI ATYPICAL DUAL-SPECIﬁCITY
AT1G04980.1	-	-29	Encodes a protein disulfide isomerase-like (PDIL) protein, a member of a multigene family within the thioredoxin (TRX) superfamily. Transcript levels for this gene are up-regulated in response to three different chemical inducers of ER stress (dithiothreitol, beta-mercaptoethanol, and tunicamycin). AtIRE1-2 does not appear to be required for this response, but the atbzip60 mutant has a diminished response.	PDI-LIKE 2-2 (PDIL2-2);PDI-LIKE 2-2 (ATPDIL2-2);ARABIDOPSIS THALIANA PROTEIN DISULFIDE ISOMERASE 10
AT1G04420.1	+	-57	NAD(P)-linked oxidoreductase superfamily protein;(source:Araport11)	
AT1G04410.1	-	46	predicted to encode a cytosolic malate dehydrogenase.	CYTOSOLIC-NAD-DEPENDENT MALATE DEHYDROGENASE 1 (c-
AT1G04000.1	-	506	hypothetical protein;(source:Araport11)	
AT1G03905.1	+	1	P-loop containing nucleoside triphosphate hydrolases superfamily protein;(source:Araport11)	ATP-BINDING CASSETTE I19 (ABCI19);NON-INTRINSIC ABC
AT1G03290.1	+	-74	ELKS/Rab6-interacting/CAST family protein;(source:Araport11)	
AT1G03270.1	+	-107	CBS domain protein with a domain protein (DUF21);(source:Araport11)	
AT1G03090.2	+	-60	MCCA is the biotinylated subunit of the dimer MCCase, which is involved in leucine degradation. Both subunits are nuclear coded and the active enzyme is located in the mitochondrion.	(MCCA)
AT1G02670.1	+	-503	P-loop containing nucleoside triphosphate hydrolases superfamily protein;(source:Araport11)	
AT1G01720.1	+	-104	Belongs to a large family of putative transcriptional activators with NAC domain. Transcript level increases in response to wounding and abscisic acid. ATAF1 attentuates ABA signaling and sythesis. Mutants are hyposensitive to ABA. The mRNA is cell-to-cell mobile.	(ANAC2); (ATAF1);ARABIDOPSIS NAC DOMAIN CONTAINING PROTEIN 2 (ANAC002)
AT1G01600.1	+	1230	Encodes a member of the CYP86A subfamily of cytochrome p450 genes. Expressed significantly at highest level in mature stems and flowers.	CYTOCHROME P450, FAMILY 86, SUBFAMILY A, POLYPEPTIDE 4
AT1G01490.1	-	-141	Heavy metal transport/detoxification superfamily protein;(source:Araport11)	
AT1G01060.1	-	-236	LHY encodes a myb-related putative transcription factor involved in circadian rhythm along with another myb transcription factor CCA1	LATE ELONGATED HYPOCOTYL 1 (LHY1);LATE ELONGATED